UNIVERSITY OF SOUTHAMPTON

A STUDY OF SPECIES CONTAINING Si-O BONDS IN LOW TEMPERATURE MATRICES AND IN THE GAS PHASE

By

Sarah-Jane Bowes

A thesis submitted for the Degree of Doctor of Philosophy

Department of Chemistry

Faculty of Science

May 2001

UNIVERSITY OF SOUTHAMPTON

ABSTRACT

FACULTY OF SCIENCE

CHEMISTRY

Doctor of Philosophy

A STUDY OF SPECIES CONTAINING Si-O BONDS IN LOW TEMPERATURE MATRICES AND IN THE GAS PHASE

By Sarah-Jane Bowes

The work conducted for this thesis involved investigating reactions of species containing Si-O bonds.

Various cyclic and linear siloxanes were pyrolysed in an attempt to isolate and identify dimethylsilanone ($Me_2Si{=}O$) – a molecule of fundamental importance in silicone chemistry. It was observed that these experiments produced products such as CH_4, C_2H_2, C_2H_4 and C_2H_6, as well as the methyl radical. It was also seen that both octamethylcyclotetrasiloxane and decamethylcyclopentasiloxane produce bands due to hexamethylcyclotrisiloxane. This suggested that interconversion reactions were occurring upon pyrolysis, indicating the involvement of dimethylsilanone. It was also found that 1,1,3,3,5,5-hexamethyltrisiloxane and 3H, 5H-octamethyltetrasiloxane was not observed upon pyrolysing any of the two sets of siloxanes.

The reactions of species producing compounds containing Si-O bonds were also studied. Silylene was reacted with oxygen, nitric oxide and oxetane and the reactions followed using the technique of Laser Resonance Absorption Flash Kinetics Spectroscopy.

In both cases, *ab initio* and semi-emperical calculations were carried out in order to help understand the reaction pathways occurring. As a result of a number of energy and frequency calculations, the most feasible products and in some cases mechanisms, were able to be deduced.

Chapter 6. Cyclic Siloxanes.....103
1. Introduction.....104
2. Preliminary Results.....108
3. Preliminary Conclusions.....116
4. A Comparison of the Unknown Bands Produced as a Result of the Pyrolysis of the Three Cyclic Siloxanes: D4, D3 and D5.....134
5. Minimum Energy Calculations.....136
6. Frequency Calculations.....145
7. Conclusion.....149
8. References.....151

Chapter 7. Linear Siloxanes.....153
1. Introduction.....154
2. Preliminary Results.....156
3. Preliminary Conclusions.....165
4. A comparison of the results of the three linear siloxanes: L1, L2 and L3.....170
5. Conclusion.....175
6. Energy Calculations.....176
7. Frequency calculations of the parent compounds.....182
8. Frequency calculations of the possible products.....184
9. A comparison of the frequency calculations between the parent compound and the possible products.....187
10. Conclusion.....191
11. Future Work.....192
12. References.....193

Acknowledgements

I would like to thank my supervisor, Steve Ogden for his guidance throughout my PhD. I am also grateful to Robin Walsh and Matthew Almond from the University of Reading for their support and advice.

I would also like to thank Dow Corning for their valuable input and financial support, especially to Pat Cannady and Ian Mackinnon for making it possible for me to visit the various Dow Corning sites.

Finally, I am thankful to the EPSRC for funding.

CHAPTER ONE

INTRODUCTION

1. Silicon Chemistry

Silicon and more significantly, its compounds are of great importance both in the natural world and in industry. Their commercial uses range from concrete to electronic devices.
Silicon is the second most abundant element after oxygen[1] and is found after carbon in group IV in the periodic table. Some aspects of its chemistry can be inferred from what is known about carbon chemistry. Silicon is essentially non-metallic. After the C–C bond, the Si–Si bond is the second strongest bond in this group. Like carbon, silicon forms strong covalent bonds with other atoms. However, its most important characteristic is heterocatenation with oxygen. Silicon is found in the form of chains and polymers and is abundant in natural materials, such as rocks and minerals[2].

2. Siloxane Chemistry

Siloxanes are neutral organosilicon compounds containing Si-O bonds. They exist in cyclic, linear or polymeric forms and below are examples of the structures of both a cyclic and a linear siloxane. The polymers of siloxanes are of commercial importance in the manufacture of oils and rubbers.

The Si-O single bond is stronger than the corresponding C-O bond and may involve some double-bond character with evidence of d-orbital overlap to form dπ-pπ bonding. The bond energies are 464 and 358 kJ mol^{-1} respectively. This results in strong covalent interactions and is the reason for both the stability and occurrence of the wide range of Si-O compounds.

Figure 1. Cyclic siloxane - hexamethylcycloctrisiloxane (D3)

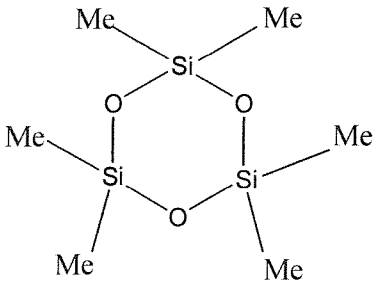

Figure 2. Linear siloxane - 1,1,3,3-tetramethyldisiloxane

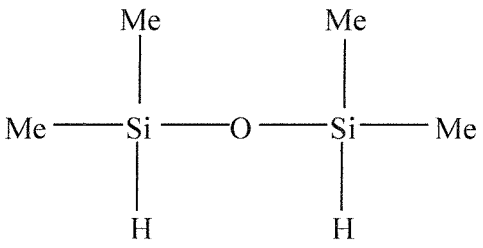

2.1. Preparation of Siloxanes

The most common process of producing both cyclic and linear siloxanes involves the hydrolysis of dimethylsilicon dichloride under carefully controlled conditions[3]. This reaction can be seen in Figure 3. Product A is a cyclic siloxane compound and may be produced in terms of D3, D4, D5 or D6. The letter D represents a $(CH_3)_2SiO$ unit. Product B is known as a silanol. Since the terminal –OH group of silanol is active, this compound is unstable and so further polymerisation is likely to occur. It is usual that high chain polymers are produced from this process.

Figure 3. Hydrolysis reaction to produce siloxanes

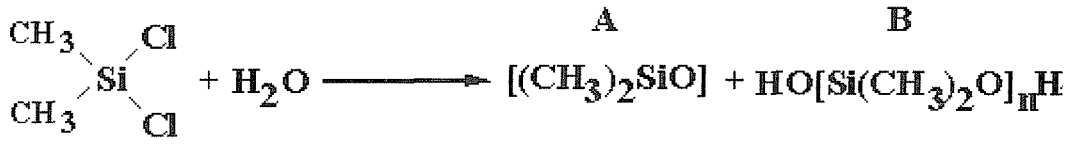

Examples of the structures of both products A and B can be seen in Figure 4 (a)-(b).

Figure 4. Structures of the products produced from the hydrolysis reaction

a). Product A – cyclic siloxane octamethylcyclotetrasiloxane

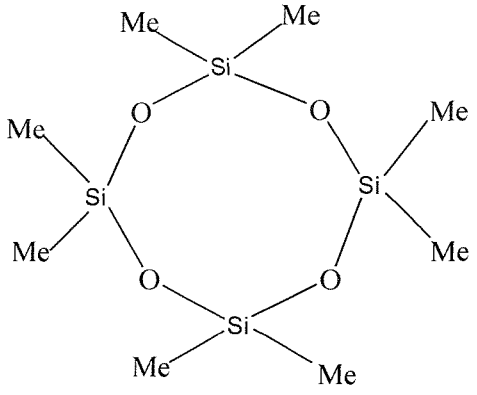

b). Product B – silanol polymer

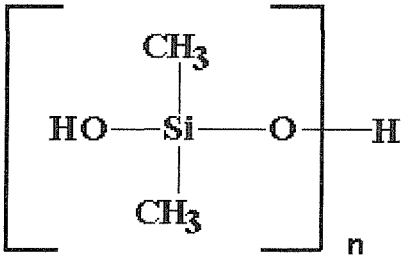

The addition of water to dimethylsilicon dichloride leads to the formation of a chain-forming group, found present in both of the above products. This group is seen as the product in the reaction below.

Figure 5. Hydrolysis reaction of dimethylsilicon dichloride

Dimethylsilicon dichloride is therefore often referred to as a chain unit, as it has the potential to form chains of siloxanes.

However, silanols (such as product B produced from the reaction in Figure 3), may also be converted to form cyclic siloxanes[4]. Upon gently heating the silanol product, a mixture of both hexamethylcyclotrisiloxane (Figure 1) and octamethylcyclotetrasiloxane (Figure 4 (a)) are produced.

If either of the above mentioned cyclic siloxanes are then further mixed with a small amount of hexamethylsiloxane, $(CH_3)_3$-Si-O-Si-$(CH_3)_3$ and H_2SO_4, a rearrangement reaction will take place resulting in the formation of linear siloxanes[5]. This is thought to occur via the cleavage of the Si-O bonds of the cyclic siloxanes to form sulfate esters and silanols that then recondense. The resultant linear siloxanes are usually polymers, known as silicones. The end groups of these species are often $(CH_3)_3$Si- and compounds with these end groups are often known as silicone oils.

Linear siloxanes may also be produced by the addition of $(CH_3)_3SiCl$ to the reaction in Figure 5. This species acts as a chain-stopping group by blocking any active terminal –OH groups. Therefore, no polymerisation of these linear siloxanes will occur. The ratio of $(CH_3)_2SiCl_2$ to $(CH_3)_3SiCl$ will determine the chain length of the product.

2.2. The Steric Nature of Siloxanes

Hexamethylcyclotrisiloxane, D3 is shown in Figure 1. A puckered ring would normally be predicted for this species, due to steric requirements as demonstrated in the analogous carbon compound. However, a planar structure actually exists[6]. This is thought to be due to the maximisation of the dπ-pπ bond between a lone pair on the oxygen atom and an empty d-orbital

on the silicon atom. As the size of the cyclic siloxanes increase, there is a greater tendency for puckering to occur. This does not, however, result in the total loss of π-bonding. A D4 ring, octamethylcyclotetrasiloxane, is puckered with a Si-O-Si bond angle of 142.5° in the crystalline structure.

The smallest linear siloxane is the disiloxane, 1,1,3,3-tetramethyldisiloxane and its structure is shown below.

Figure 6. Structural parameters of 1,1,3,3-tetramethyldisiloxane

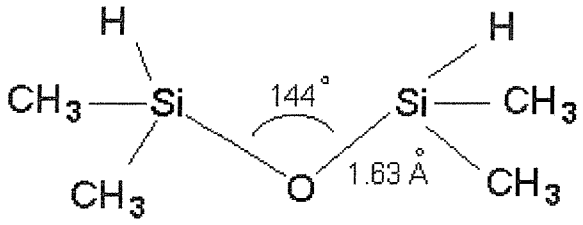

The above structural parameters have been obtained in the vapour state. However, structural data is also known from the crystalline state. Both sets of data can be obtained from electron diffraction studies. It is known that the bond angle of Si-O-Si is between 142-156° in the vapour state and 180° in the crystalline state. The bond length of Si-O is 1.63Å.

3. Silicone Chemistry

Silicones are neutral organosilicon polymers based on a backbone of rings, chains or three-dimensional networks[7] of alternating silicon and oxygen atoms with organic groups bonded to the silicon atom. These compounds have high thermal and chemical stability due to stable Si-O bonds and strong Si-C bonds. The high thermal stability of silicones allows them to withstand temperatures of up to 250-300 °. Oxidation of the adjoining organic groups first occurs at around 200-250°. These temperatures lead to cross-linking in the silicone structures. Mild chemical reagents such as weak acids and alkali or salt solutions will leave silicones unaffected. Like silicon, these compounds have a great scope of commercial use, for example, in the production of oils, fluids, rubbers and resins. These products are manufactured by companies such as Dow Corning. Silicones may be grouped according to their physical properties. Oils are usually the result of siloxane polymers. Silicones with a controlled amount of cross-linking are used for

both resins and rubbers[8]. Due to the cross-linking, the degree of polymerisation is much higher for rubbers and resins than for oils. A commercially useful rubber usually has more than eight thousand units in a silicone chain. The basis for silicone chemistry is the formation of one or more of the four fundamental building units[9]. The units represented below are widely used in industry. A number is given after each letter to represent the number of these units present in the compound and therefore the size of the silicone structure.

Figure 7. Building units of silicones

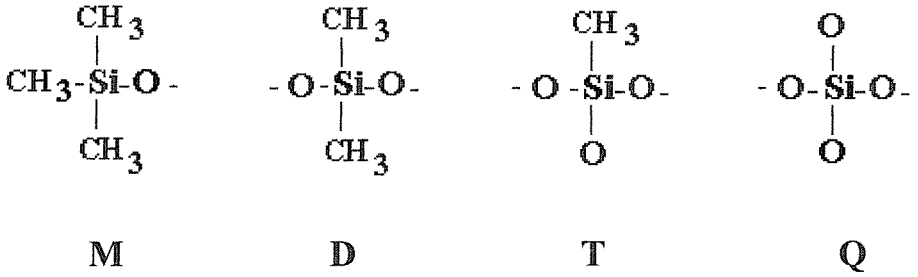

Unit **D** in Figure 7 has already been mentioned in this chapter, for explaining the nomenclature of the cyclic siloxanes. Linear siloxanes containing terminal **D** groups are unstable compounds and polymerisation is likely to result to form rings or longer chains. Therefore, in order to prevent polymerisation, the introduction of **M** units is required. The **M** unit is often found at the end of a siloxane chain and defines a silicone oil. The Cross-linking effect in silicones (Figure 10) can be represented by the unit **Q.** Compounds containing this unit are often used to produce rubbers or resins. Cross-linking may also be achieved by compounds containing the unit **T** but to a lesser extent.

3.1. Preparation of Silicones

Silicone compounds are now produced on a greater scale than any other group of organometallic species. Their production is estimated at three hundred thousand tonnes per year. A production process for the formation of silicones was first recorded by Kipping, between the period of 1901-1940. These investigations into organosilicon chemistry had intended to produce the silicon analogue to a ketone by the hydrolysis of alkyl substituted chlorosilanes[8]. However, Kipping concluded that the internuclear elimination of water from molecules containing Si-OH bonds had led to the formation of silicones. This process can be seen below in Figure 8.

Figure 8. The first process for producing silicones – developed by Kipping

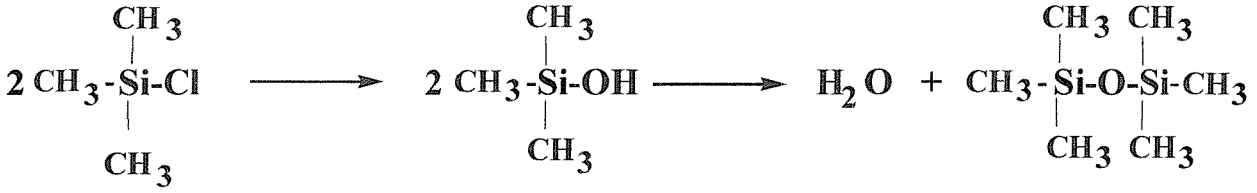

The hydrolysis of silicon trimethylmonochloride yields trimethylsilanol, as an intermediate (Step 1 in Figure 9). Silanol intermediates are very reactive and so it is impossible to isolate this compound. Therefore, a condensation reaction usually follows to produce a silicone polymer. The condensation of the latter species then yields hexamethyldisiloxane, a linear siloxane (Step 2 in Figure 9). This siloxane is the smallest silicone polymer. This process can be seen in two stages in Figure 9 below.

Figure 9. Process for the formation of silicones

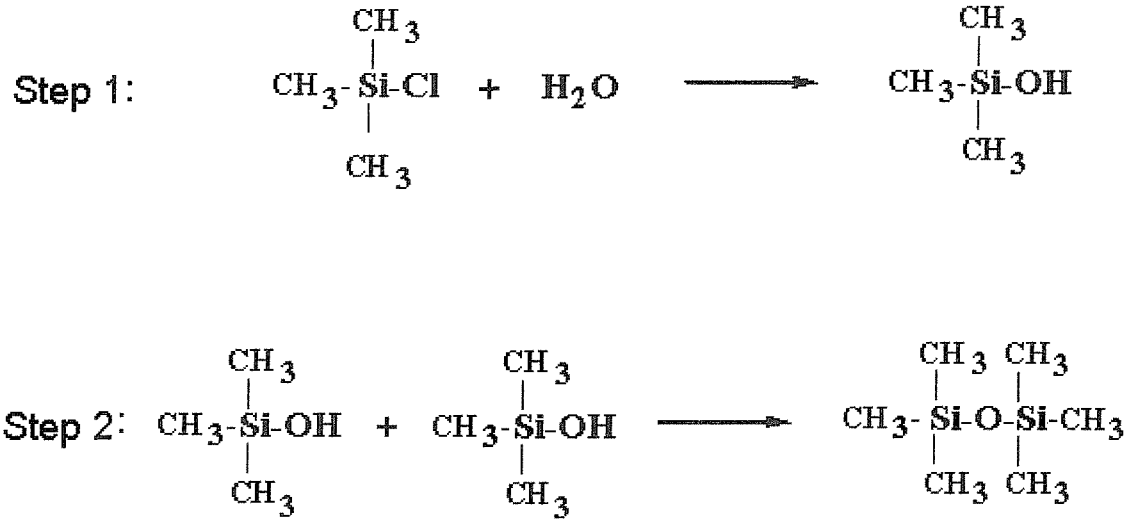

Trimethylsilanol therefore also forms hexamethyldisiloxane as a result of a condensation reaction as seen in Figure 10.

Figure 10. Condensation reaction of Trimethylsilanol

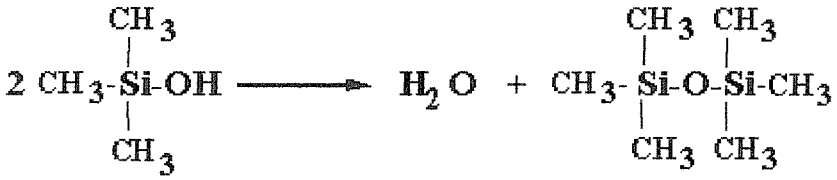

If the trimethylsilanol is formed at the same time as the diol, $(CH_3)_2Si(OH)_2$, then it can condense with one of the –OH groups of the diol and terminate the polymeric chain.

However, since no terminal –OH groups are present in hexamethyldisiloxane, there is no chance of any further polymerisation occurring.

The cross-linking of silicones to produce resins and rubbers can also be achieved by the hydrolysis of $SiCl_4$. A resultant cross-linking group can be seen below in Figure 11.

Figure 11. Cross-linking groups

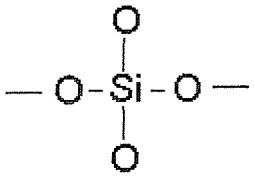

These cross-linking groups have been seen to produce resins and rubbers due to an increase in the viscosity property of the polymer.

3.2. Reactions of Silicones

One of the areas of interest in this thesis is the interconversion reactions of the siloxane polymers at high temperatures. These reactions were first reported by Khabashesku *et al.* [10] in 1989, who upon pyrolysing the cyclic siloxane, octamethylcyclotetrasiloxane, (D4), noticed that both D3 and D5 were produced as pyrolysis products. This interconversion reaction can be seen in the reaction scheme shown below.

Figure 12.

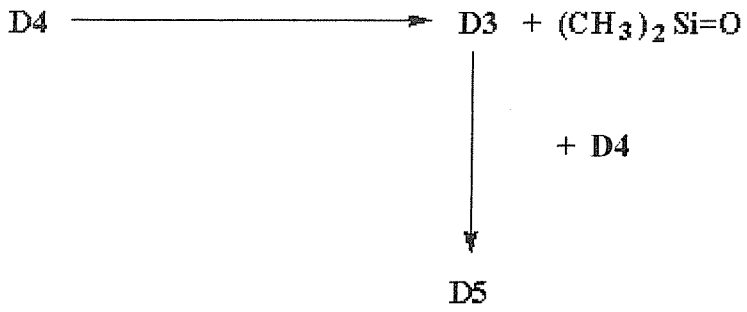

Further research has indicated that this trend is also found as a result of the pyrolysis of various linear siloxanes.

4. Silanone Chemistry

Silanones are believed to be of great industrial importance as intermediates within silicon chemistry. They are reactive species and the silicon analogues to ketones ($R_2Si=O$). The extreme reactivity of these compounds can be explained by the high polarity[11] of the Si=O π-bond, leading to dimerisation and trimerisation which proceeds with no barrier.

Figure 13. Dimerisation of silanones

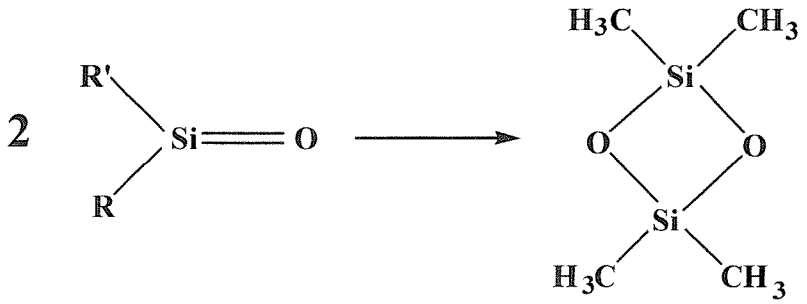

Withnall and Andrews[12] first identified the parent silanone compound ($H_2Si=O$) using the direct spectroscopic characterisation technique of infrared spectroscopy matrix isolation in the 1980's. Also around this time, Schnöckel[13] produced the first spectra of inorganic silanones, such as $F_2Si=O$ and $Cl_2Si=O$ which were synthesised within a matrix. This was followed by the

publication of work by Arrington *et al.* [14] in 1983 of spectra of organic silanones, such as dimethylsilanone, ($(CH_3)_2Si=O$). Below is a reaction reported by Arrington *et al.* showing the formation of dimethylsilanone.

Figure 14. A reaction for the formation of dimethylsilanone

The oxygen atoms in the above equation are produced photochemically from precursors such as O_3, N_2O and C_2H_4O. This reaction produced dimethylsilanone in a low yield and was identified by a weak band at 1204 cm^{-1}. This band is at a frequency expected for the Si-O stretch in silanones. Although Khabashesku *et al.*[10] did not observe this band in their pyrolysis spectra, it is reported that the band present in spectra at 1210 cm^{-1} is due to the Si=O stretch in silanone, therefore, supporting its formation. Later work by Withnall and Andrews[15] agrees with these findings as observed in the published spectra of methylsilanone ($CH_3(H)Si=O$) produced by the photo-oxidation of methylsilanes.

5. Silylene Chemistry

A second area of importance in silicon chemistry is silane chemistry. This area also has great commercial interest. Silanes are especially used within chemical vapour deposition (CVD) processes to produce silicon-containing electronic materials. Reactions of silanes often involve silylenes as reactive intermediates. These intermediates are divalent silicon compounds and exist only in the singlet ground state. The term silylene refers to silicon species that are either unsubstituted or partially substituted. As these species are very unstable, it has not as yet been possible to isolate silylene in the solid form.

5.1. Preparation of Silylenes

Silylene was first recorded as being isolated in 1969 by Atwell and Weyenberg[16]. These authors stated that the reactions used in the preparation of silylene can be divided into two classes: reduction reactions and thermal decomposition reactions.

(a). Reduction Reactions

The formation of silylene can be achieved by the pyrolysis of silane at temperatures of approximately 400 °C[17].

Figure 15. Reduction of silane

$$SiH_4\,(g) + Si\,(s) \rightleftharpoons 2SiH_2\,(g)$$

The reduction of silicon tetrahalides has been achieved by a reaction with silicon at high temperatures of above 800 °C to produce divalent silicon halides (silylenes).

Figure 16. Reduction of halosilanes

$$SiX_4\,(g) + Si\,(s) \rightleftharpoons 2SiX_2\,(g)$$

The reduction of halosilanes to produce silylene has been achieved with a number of silicon halides, where X = F, Cl, Br or I. The reaction of silicon with other metal halides[18] to produce divalent silicon halides has also been reported by Atwell and Weyenberg[16] for example, copper (I) chloride can be reacted with silicon to produce silylene as seen in Figure 17 below.

Figure 17.

$$2CuCl + Si \longrightarrow 2Cu + SiCl_2$$

The species produced from this reaction is dichlorosilylene.

(b). Thermal Deposition

The thermal decomposition of hexahalodisilanes at temperatures of about 700 ° to yield silylene was first reported by Friedel and Ladenburg[19] in 1880.

Figure 18.

$$Si_2F_6 \longrightarrow SiF_4 + SiF_2$$

In the above reaction hexafluorodisilane has been thermally decomposed to produce difluorosilylene. More recently, organosilylenes have been able to be produced at much lower temperatures of between 170 – 300 ° C, by the thermolysis of alkoxydisilanes[16].

Figure 19.

There is evidence to suggest that the thermolysis of disilane during the reaction in Figure 19 produces both a silane and a silylene. This reaction is looked at in more detail in Figure 20.

Figure 20.

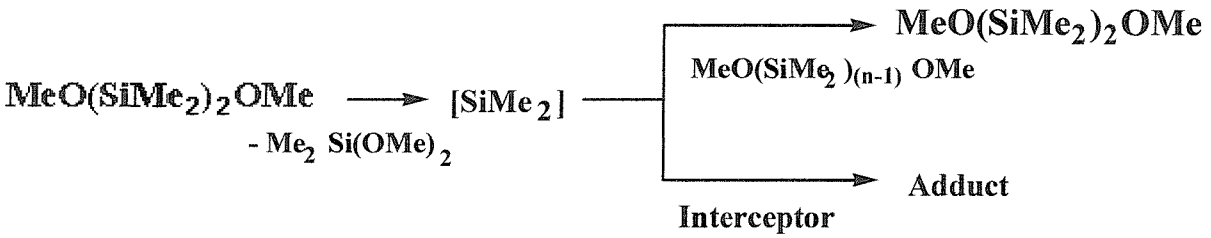

5.2. Structures of Silylenes

The most stable of the silylene species with a half-life of 150 seconds is difluorosilylene (See Figure 21).

Figure 21.

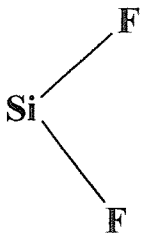

This species was studied extensively by Thompson and Margrave [20] in 1967 using both microwave and ultraviolet absorption. Silylene itself was studied by a number of research groups using infrared spectroscopy[21] and matrix isolation infrared spectroscopy[22]. Dubois *et al.*[23] were able to determine its structure.

Figure 22.

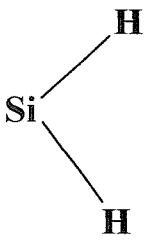

For the ground state of silylene, the Si-H bond length is known to be 1.52Å and has a H-Si-H bond angle of 92.8°. This information was obtained from experimental studies based on the visible vibronic absorption spectrum[23]. A greater H-Si-H bond angle for the excited state of silylene has been calculated as 118.5°.

5.3. Reactions of Silylene

There are three main types of reactions which silylenes undergo. These are addition, polymerisation and insertion.

(a). Addition Reactions

There are many known addition reactions of silylenes to σ-bonds. The addition reaction of SiH_2 and H_2 was first recorded with rate constants in 1985 by Inoue and Suzuki[24]. These reactions were repeated for differing temperatures and pressures by Jasinski[25]. The resultant SiH_4 adduct produced can be seen below in Figure 23. *Ab initio* calculations together with additional calculations using the RRKM theory gave a structure with a C_s symmetry for this species.

Figure 23. SiH_4 adduct

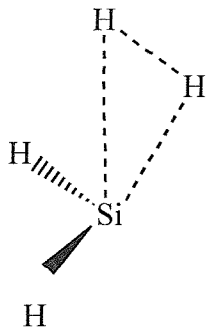

The formation of this structure suggests an electrophilic reaction[26], where the bonding electrons of an atom from the hydrogen molecule interact with the empty p-orbital of silylene.

A well known addition reaction of a silylene to a halogenated species is shown in Figure 24[27] [28].

Figure 24.

Silylenes also react with alkyloxy-substituted polysilanes. This can be seen below. Again, these reactions are well established[16].

Figure 25.

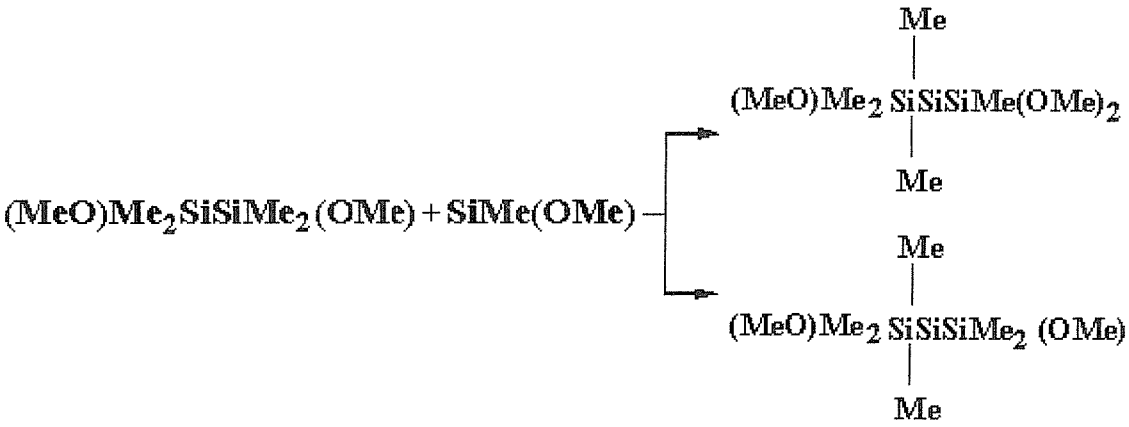

However, Atwell and Weyenberg[16] report that reactions of silylene with monosilanes have not been as successful.

Silylenes are also known to react with compounds containing π-bonds. The addition of silylene to alkenes produces unstable, strained cyclic compounds, called siliranes. The simplest of these reactions is the reaction of silylene with ethene. Following the results of the *ab initio* calculations by Anwan and Gordon[29], it was suggested that this insertion reaction takes place in two stages. Stage one involves an electrophilic attack, with the π-electrons from the carbon-carbon double bond of ethene being donated to the 3p orbital of silicon in silylene. Stage two then involves a nucleophilic σ-attack via the donation of the lone pair of electrons of silylene to the C=C anti-bonding π-orbital. These interactions can be seen in Figure 26 below.

Figure 26.

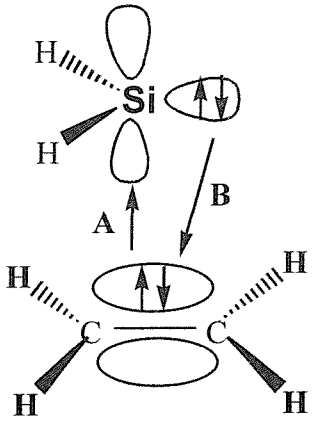

A = Stage 1; electrophilic interaction

B = Stage 2; nucleophilic interaction

(b). <u>Polymerisation Reactions</u>

A second set of reactions that may be noted here, are the polymerisation reactions. Polymerisation reactions involving silylenes often occur in the absence of other reagents[16].

Figure 27.

$$n\,SiX_2 \longrightarrow (SiX_2)_n$$

These reactions are known to occur for X = F, Cl, Br & I.

(c). <u>Insertion Reactions</u>

The importance of silylenes in chemical vapour deposition (CVD) processes has already been mentioned. It has been found that most insertion reactions of silylene involve the insertion of SiH_2 into a XY species, where either X or Y is a hydrogen, halogen or alkoxy group[16]. It is also known that the most important of these processes is the insertion of silylene into a Si-H bond. Silylene is known to readily insert into Si-H bond, therefore forming a new Si-Si bond on the surface. The most fundamental of these reactions is the insertion of silylene into a Si-H bond of

SiH_4. *Ab initio* calculations[29] support the resultant formation of the structure shown in Figure 28 and its structural parameters.

Figure 28.

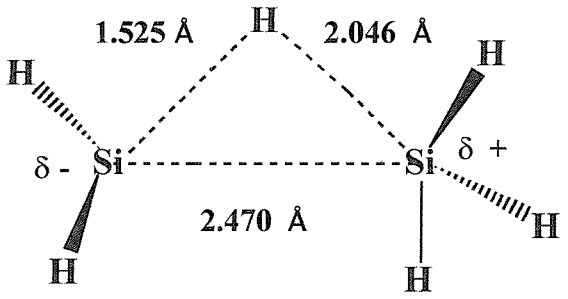

This reaction again supports an electrophilic insertion reaction, as it appears from the geometry of the product in Figure 28 that a hydrogen from SiH_4 has shown significant transfer to SiH_2.

5.4. Reactions and Formation of Si-O Containing Compounds

The research conducted for this thesis has been concerned with the reactions of compounds containing Si-O bonds. A large part of the work has been concerned with the study of pyrolysis reactions of various siloxanes (Si-O containing compounds) to produce smaller species with Si-O bonds and other secondary products. This has then been followed by a study into the formation of compounds containing Si-O bonds from a laser kinetics study of silylene with oxygen containing compounds. Once the experiments were complete, the aim was to identify any unknown species produced and then attempt to calculate the reaction mechanisms through obtaining an understanding of the potential energy surface.

(a). Pyrolysis Reactions of Species Containing Si-O bonds

Dimethylsilanone ($Me_2Si{=}O$) is an important reactive intermediate within silicon chemistry. It was hoped that the pyrolysis of various cyclic and linear siloxane compounds would lead to the formation of this transient species which could then be isolated using the technique of matrix isolation. A variety of inexpensive and easily accessible siloxane compounds were chosen for these experiments. After the reactions were complete and the spectra had been collected, it was noted that there were a number of unknown bands produced. Using previous knowledge, possible products were suggested. However, to confirm or reject these suggested products, a

number of molecular modelling calculations were carried out. These calculations were able to yield both the energies of these species and their calculated frequencies. Using both the experimental and the theoretical data, it was possible to deduce from the results of the pyrolysis experiments that a degree of interconversion had occurred. This was especially prominent for the cyclic siloxanes. It was also concluded that a number of hydrocarbons were produced as secondary products.

(b). Laser Kinetics Experiments to Produce Species Containing Si-O Bonds.

It is known that silicon has a large affinity for oxygen. Therefore, it was predicted that Si-O containing compounds would be formed by the reaction of silicon compounds with oxygen containing species. The reactive intermediate, silylene was chosen as the subject of these experiments and was formed from the photolysis of phenylsilane. Silylene was then reacted with easily accessible oxygen containing compounds namely oxygen, nitric oxide and oxetane. These experiments were conducted at a variety of temperatures and pressures and the rate constants were calculated from Linear-Least-Square fittings. A number of molecular modelling calculations were again carried out in order to attempt to predict possible reaction mechanisms. This was made possible by studying the obtained data of the possible products and estimating the potential energy surface for each reaction.

6. References

1). F. A. Cotton, G. Wilkinson, C. A. Murillo and M. Bochmann, Advanced Inorganic Chemistry, John Wiley and sons, Inc., sixth edition, **(1999)**

2). D. Thompson, Insights into Speciality Inorganic Chemicals, The Royal Society of Chemistry, **(1995)**

3). N. N. Greenwood and A. Earnshaw, Chemistry of the Elements, Butterworth Heinemann, second edition, **(1997)**

4). W. W. Porterfield, Inorganic Chemistry, Academic Press Inc., second edition, **(1993)**

5). B. Douglas, D. McDaniel and J. Alexandra, Concepts and Models of Inorganic Chemistry, John Wiley and sons, Inc., third edition, **(1994)**

6). S. M. Owen and A. T. Brooker, A Guide to Modern Inorganic Chemistry, Longman Group Ltd., fifth edition, **(1997)**

7). J. D. Lee, Concise Inorganic Chemistry, Chapman and Hall, fifth edition, **(1996)**

8). H. J. Emeleus and A. G. Sharpe, Modern Aspects of Inorganic Chemistry, Routledge, fourth edition, **(1973)**

9). A. F. Wells, Structural Inorganic Chemistry, A. F. Wells, Clarendon Press, fifth edition, **(1984)**

10). V. N. Khabashesku, Z. A. Kerzina, A. K. Maltsev and O. M. Nefedov, J. Organomet. Chem., 364, **(1989)**, 301-312

11). V. N. Khabashesku, Z. A. Kerzina, K. N. Kudin and O. M. Nefedov, J. Organomet. Chem., 566, **(1998)**, 45-59

12). R. Withnall & L. Andrews, J. Am. Chem. Soc., 107, **(1985)**, 2567

13). H. Schnöckel, J. Mol. Struct., 65, **(1980)**, 115

14). C. A. Arrington, R. West and J. Michl, J. Am. Chem. Soc., 105, **(1983)**, 6176

15). R. Withnall and L. Andrews, J. Am. Chem. Soc., 108, **(1986)**, 8118

16). W. H. Atwell and D. R. Weyenberg, Angew. Chem. Int. Ed. Engl., 8, **(1969)**, 469

17). J. H. Purnell and R. Walsh, Proc. Roy. Soc. (London), Ser. A. 293, **(1966)** , 543

18). V. I. Zubkov, M. V. Tikhomirov, K. A. Andrianov and S. A. Golubtsov, Proc. Acad. Sci. USSR, Chem. Sect., (English Translation), 159, **(1964)**, 599

19). C. Friedel and A. Ladenburg, Liebigs Ann. Chem, 203, **(1880)**, 241

20). J. C. Thompson and J. L. Margrave, Science (Washington), 155, **(1967)**, 669

21). V. M. Khanna, R. Hauge, R. F. Curl Jr. and J. L. Margrave, J. Chem. Phys., 47, **(1967)**, 5031

22). J. M. Bassler, P. J. Timms and J. L. Margrave, Inorg. Chem., 5, **(1966)**, 729

23). I. Dubois, G. Herzberg and R. D. Verma, J. Chem. Phys., 47, **(1967)**, 2462

24). G. Inoue and M. Suzuki, Chem. Phys. Letts., 122, **(1985)**, 361

25). J. M. Jasinski, J. Phys. Chem., 90, **(1986)**, 555

26). M. S. Gorgon, D. R. Gano, J. S. Binkley and M. J. Frisch, J. Am. Chem. Soc., 108, **(1986)**, 2191

27). P. Timms, Chem. Eng. News, 45, 39, **(1967)**, 57

28). P. Timms, Inorg. Chem., 7, **(1968)**, 387

29). F. Anwari and M. S. Gordon, Israeli J. Chem., 23, **(1983)**, 129

30). R. Becerra, H. M. Frey, B.P. Mason, R. Walsh and M. S. Gordon, J. Am. Chem. Soc., 114, **(1992)**, 2751

CHAPTER TWO

EXPERIMENTAL

1. Introduction

Infrared spectroscopy is a technique used for chemical analysis and determination of molecular structure. This technique can be used for all but the simplest molecules, and is capable of high sensitivity, due to the cumulative scanning procedure. Information can therefore also be obtained on molecular symmetry and thermodynamic properties.

When a species undergoes a vibrational or rotational motion, a displacement of atoms occurs which can lead to a change in dipole moment[1]. The species is then excited when it absorbs energy from a source of infrared radiation. Different species will absorb radiation at characteristic wavelengths and the range of radiation is known as the *electromagnetic spectrum*[2]. The infrared spectrometer used for this work was able to detect radiation absorption in the *mid infrared* region (4000-400 cm^{-1}).

Figure 1. The electromagnetic spectrum

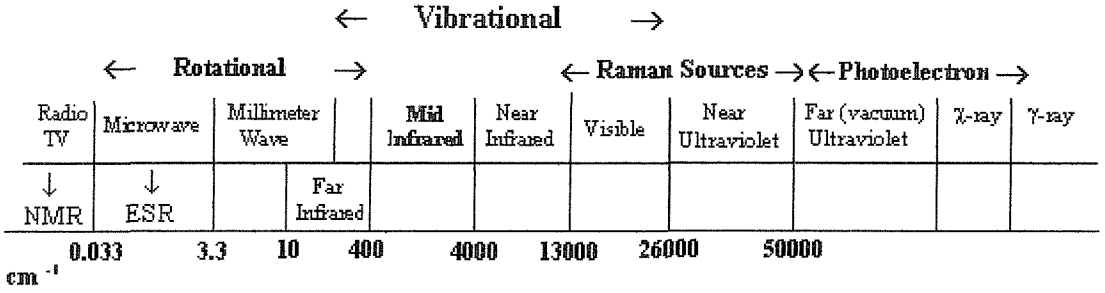

The type of detector and source equipped within the spectrometer dictate the area of the electromagnetic radiation spectrum that can be observed. There are two main different types of infrared spectrometers: *Fourier transform* and *dispersion*[13]. A dispersion spectrometer was used for this work.

1.1. Fourier Transform Spectrometers

Fourier transform spectroscopy is a procedure that can be used for a wide range of techniques. In IR spectroscopy the *Interferometer* is an important part of a Fourier transform spectrometer. It contains no dispersing element, as wavelength separation is not necessary within this technique. This technique has therefore replaced the use of monochromators, such as those used in conventional spectrometers. The first recorded design of the interferometer was by

Michelson. The Michelson interferometer is a two-beam operation. This can be seen below in Figure 2.

Figure 2. A Michelson interferometer

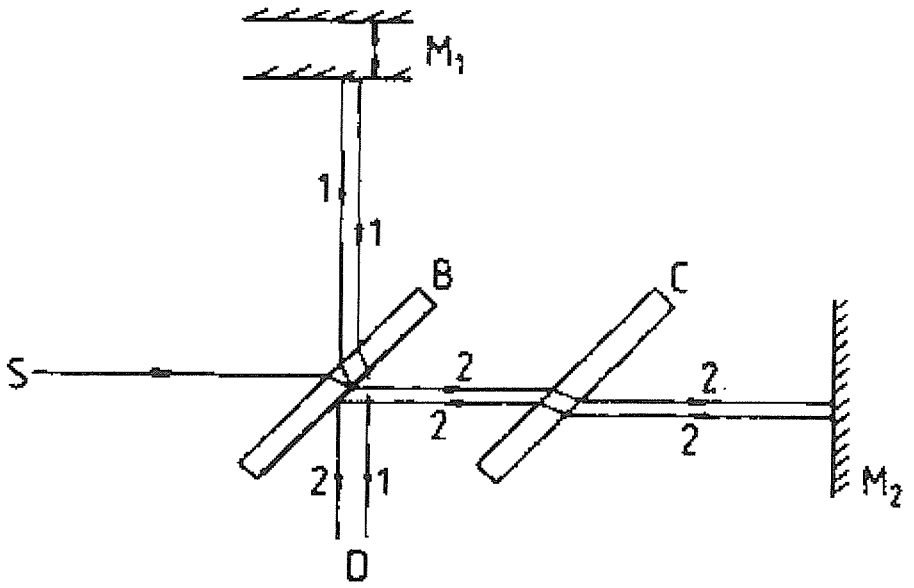

1 = Beam 1

2 = Beam 2

S = Source of radiation

B = Beam splitter

C = Compensating plate

M_1 = Movable mirror

M_2 = Fixed mirror

D = Detector

An interferometer consists of a beam splitter, composed of suitably transparent material and two mirrors, one of which is movable while the other is fixed. The beam of radiation from the source is first split by the beam splitter. The latter transmits beam 2 and reflects beam 1, therefore enabling half of the radiation to travel to each mirror then recombine into a single beam on reflection. A compensating plate is inserted into the path of beam 2 to insure that each beam has passed through the same amount of material. By moving one of the mirrors, the detector is able to detect the radiation alternating in intensity, due to many cosine waves of differing intensity. The original frequencies and intensities emitted by the source can be obtained by computing the fourier transform of the resultant signal. The equation below yields the detected intensity.

Figure 3.

$$I(\delta) = \int_0^{\infty} B(\tilde{\nu}) \cos 2\pi \tilde{\nu} \delta \, d\tilde{\nu}$$

$I(\delta)$ = Signal intensity

$\tilde{\nu}$ = Wavenumber of the source

$B(\tilde{\nu})$ = Source intensity

The resolution of the resultant spectra is high as is the speed of the data acquision, which accounts for the sensitivity of this technique. However, it is also expensive and complex, and requires a high speed computer in order to modulate the signal from the source. A complicated mathematical operation is needed to be performed in order to separate the various wavelengths that have been detected simultaneously.

1.2. Dispersion Spectrometers

Dispersion spectrometers contain a prism or a grating monochromator which selects radiation of the desired wavelength. There are two main types of dispersion spectrometers. These are *double-beam* or *single-beam* operations. In a *double-beam* operation, light from the source is split by two toroidal mirrors, producing two beams of continuum radiation. Both beams then hit the rotating mirror, which transmits the sample beam and reflects the reference beam therefore, sampling the beam through the reference and the sample cells alternately. A detector, which is tuned to detect only ac current, detects this change. The parabolic mirror reflects the beam to a diffraction grating, which ensures that only monochromatic radiation reaches the detector. The detector used is usually a thermocouple, which detects the amount of incident light. The signal is then amplified and filtered of electrical noise. This operation enables scanning to proceed without the need to frequently reset the conditions. This method is the most common of the two operations and the one that is used here.

In a *single-beam* operation, the radiation is passed through a smaller number of mirrors and so is less attenuated than radiation in a double-beam spectrometer. The resolution and the purity of the spectrum produced by a single-beam operation are lower, due to increased radiation scatter.

Figure 4. Schematic diagram of a double-beam spectrometer

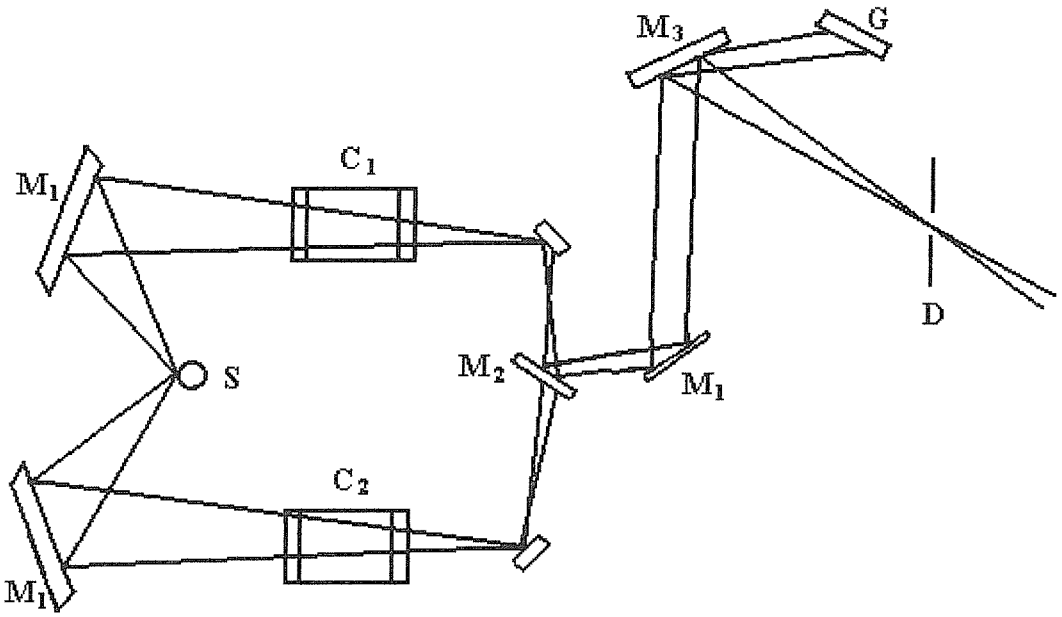

S = Radiation source

M_1 = Toroid mirror

M_2 = Rotating mirror

M_3 = Parabolic mirror

C_1 = Sample cell

C_2 = Reference cell

G = Grating

Figure 5. Schematic diagram of a single-beam spectrometer

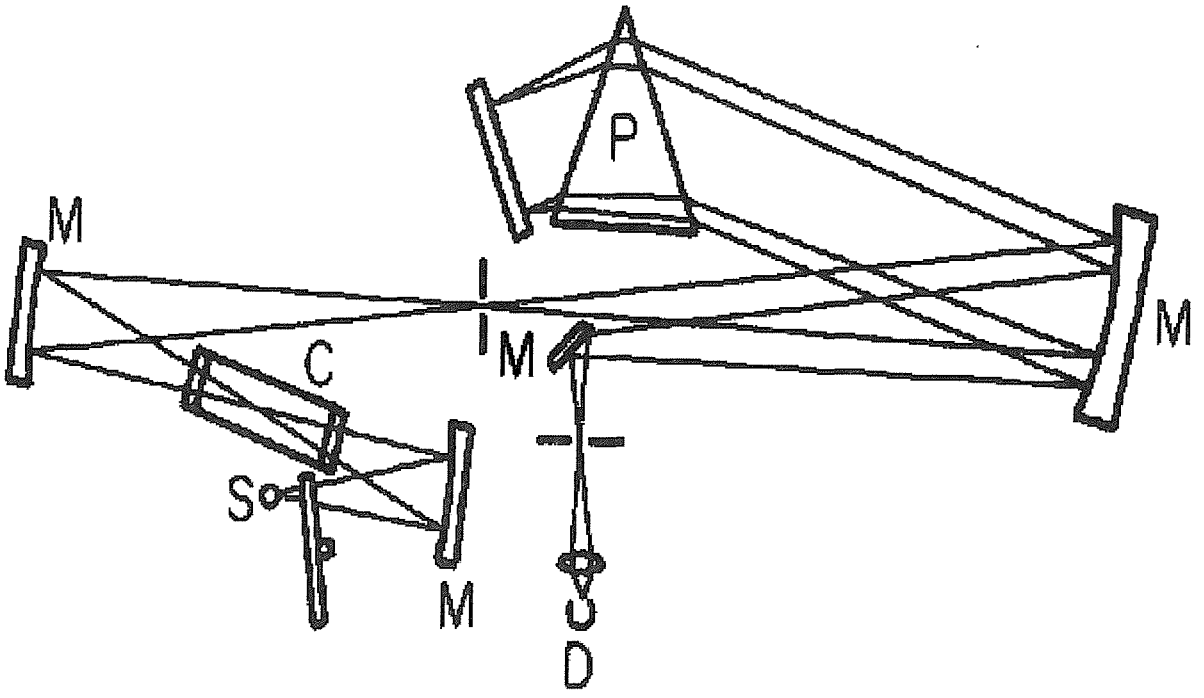

S = Radiation source

M = Mirror

C = Sample cell

P = Prism

D = Detector

2. Matrix Isolation

Matrix isolation is a technique used to trap and isolate reactive intermediates within a matrix cage in order to study their properties. It enables the lifetime of reactive species to be extended almost indefinitely. These species would otherwise be non-existent and go undetected under normal conditions. This technique was initially utilised by Lewis and then further developed by Porter[4]. It can now be employed combined with spectroscopic techniques such as, I.R., U.V. / vis, Raman, E.S.R., mass spectrometry, and Mössbauer[5]. *Infrared spectroscopy* is the most common spectroscopic technique used in conjunction with matrix isolation, as it can be easily applied.

Once the reactive species are trapped within a matrix cage, immobilisation occurs and so rotation of the species is usually denied. This results in a simplification of the obtained spectra, as rotational fine structure is lost. This leads to the formation of sharp bands from vibrational transitions. These narrow vibrational bands allow high resolution to be effectively employed. However, this technique results in the loss of information concerning moments of inertia. Diffusion experiments are also possible, where the matrix cage becomes less rigid by allowing the deposition window to warm to temperatures of ~ 27 K. These experiments yield further information on the mechanism of polymerisation.

Reactive intermediates, produced by co-condensation reactions in matrix isolation IR spectroscopy, need to be placed initially in a non-reactive environment so as to avoid the possibility of any premature reactions taking place. Therefore, sample vaporisation occurs away from the site of detection, requiring only the furnace to withstand high temperatures. The matrix mixture consists of the sample diluted in the matrix gas at a ratio of ~ 1:500 (> 1:1000 in the pyrolysis experiments). The matrix gas needs to be inert to prevent reaction with the isolated species and pure, so as to ensure a uniform matrix. As the sample is trapped inside a matrix cage, species are unable to rotate (with a few exceptions) and so the resultant spectrum is greatly simplified, as no rotational bands are observed. The vibrational bands are seen to be sharper and narrower than those generally obtained in the gas phase. Electrostatic interactions between the sample and the matrix gas inevitably still exist, which result in vibrational matrix shifts between, differing matrix gases. Argon or nitrogen was used as the matrix gas throughout this work. The deposition window is composed of caesium iodide and is maintained at a temperature of ~12 K. Caesium iodide windows were chosen for these experiments, as they transmit between 4000 – 200 cm^{-1}, which is the frequency range expected for the majority of the species used in this work. At these low temperatures, vibrational transitions occur from the ground vibrational states. The lack of transitions from thermally excited states again ensures that the infrared spectrum is not greatly complicated.

3. Pyrolysis Experiments

For the high temperature matrix isolation pyrolyis experiments, a PE 983 infrared spectrometer was used, together with a PE 3600 data station.

3.1. Apparatus

The vapour pressures of the siloxane samples are such that they do not need any heating for vapourisation to occur. The sample is pyrolysed in a silica pyrolysis tube at temperatures of between 700 – 720 °C and is then deposited onto the caesium iodide deposition window. The matrix gas entered the system at an alternative point. Initially, the matrix gas is sprayed onto the deposition window alone, in order to allow matrix cages to form. The sample is then sprayed on at the same time as the matrix gas and is trapped within the frozen matrix cages. A schematic diagram of the apparatus can be seen in Figure 6.

Figure 6. Pyrolysis set-up for the matrix isolation infrared spectroscopy experiments

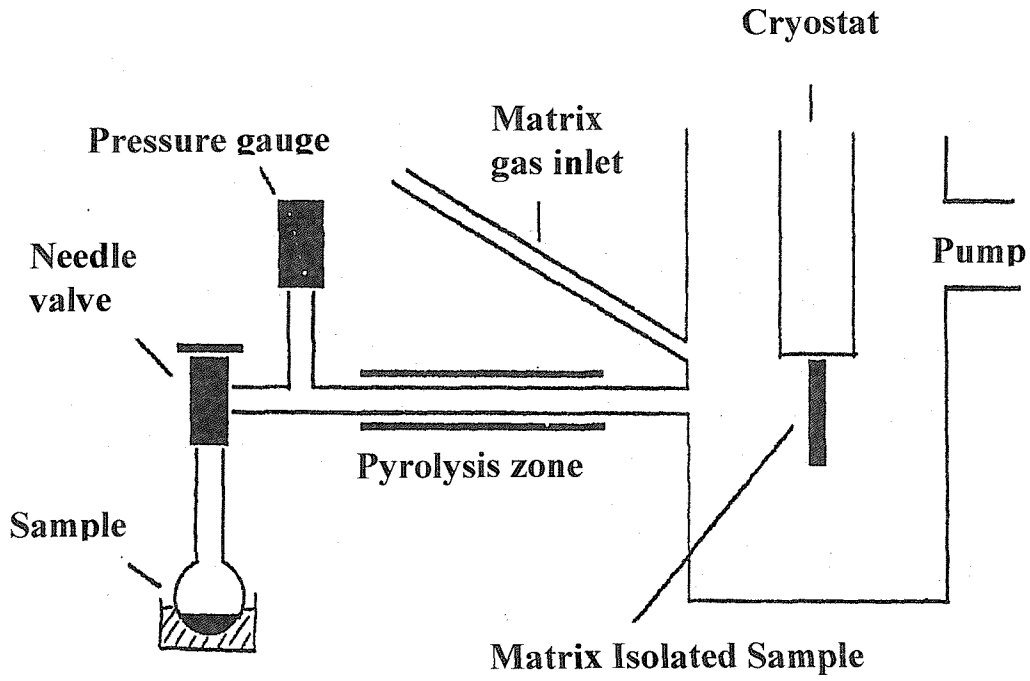

The pumping system enables a vacuum to be sustained within the source housing. The deposition window was kept at a constant temperature of approximately 12 K, with the aid of the displex cooling system. The cooling system can be seen in greater detail in Figure 7. The diagram below shows a cross section of the displex unit, which consists of the vacuum shroud, pumping system and refrigerator expander.

Figure 7. A cross-section of a displex unit

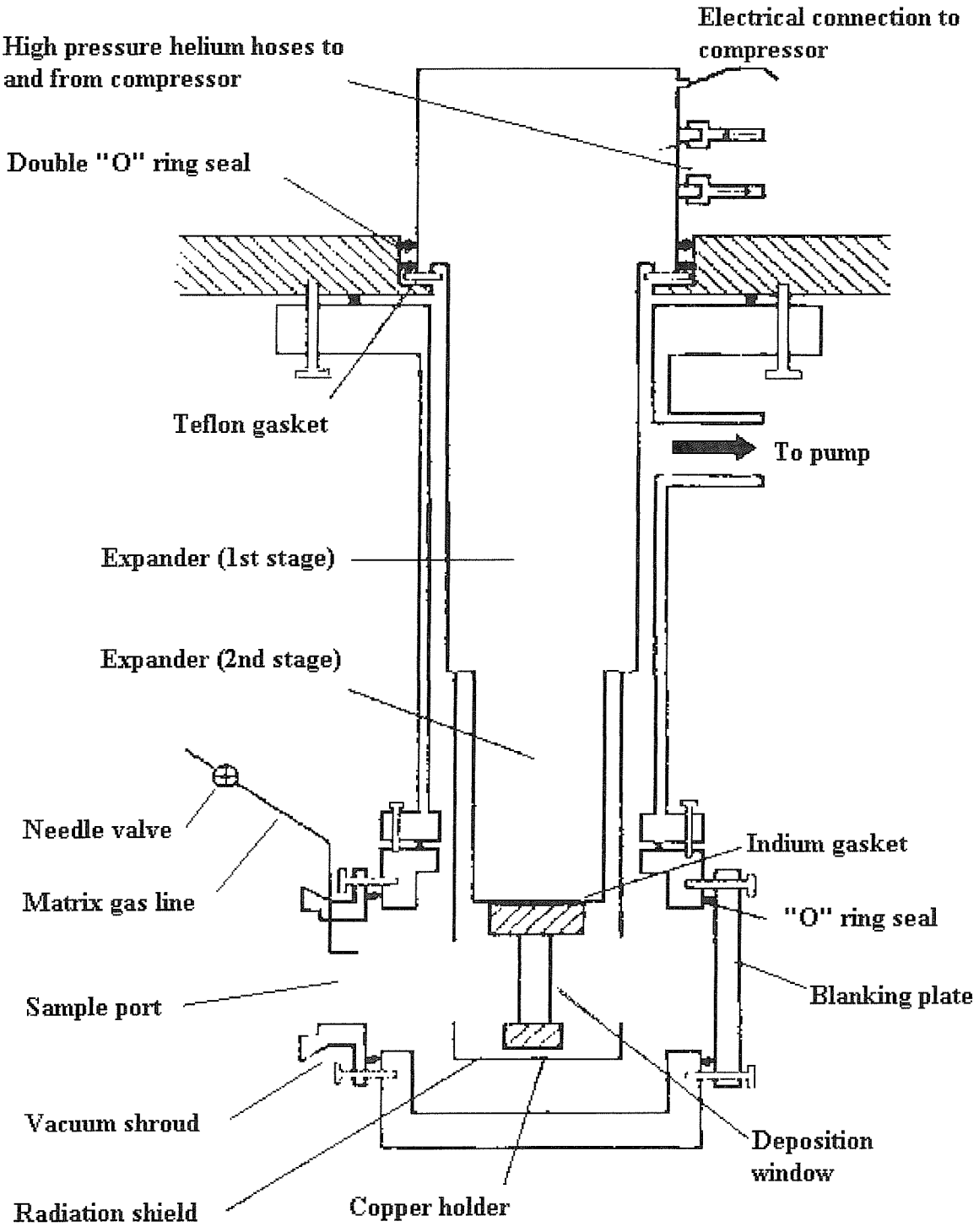

The diffusion pump, together with the liquid nitrogen trap, which is backed by the rotary pump, maintains the pressure within the vacuum shroud at approximately 10^{-6} mbar. The refrigerant, indicated in Figure 7, is high pressure helium and is transported to and from the compressor. As

the helium expands and compresses against the piston, the deposition window is able to be kept at a cool temperature, as the refrigerant goes through the continual process of losing heat as it is doing work and then conducting heat from the window.

A small furnace is used to vaporise the solid sample. This consists of a sample holder with coiled resistance wire placed around the outside of the silica tube. A variac transformer controls potential applied across the two ends of the coiled wire and a cooling jacket surrounds the furnace. Any gaseous samples used are deposited onto the window from a vacuum line. An IR beam is shone through the deposition window, when the latter was aligned to the "scanning" position. As the IR beam passes through the sample chamber, a purger is required to minimise the absorptions of water vapour.

3.2. Experimental

Once the sample is loaded into the furnace, a vacuum is created within the sample chamber, with the aid of the pumping system. A process known as degassing is then carried out. This process not only establishes suitable vaporisation conditions, but also removes any desorbed materials from the sample. This is achieved by heating the sample to an estimated temperature of sublimation. The end temperature is recorded and used as the starting temperature during the "spraying-on" process. The pressure of the vacuum shroud is noted.

The system is then cooled by switching on the displex refrigerator unit, (Figure 7) until the deposition window reaches ~12 K. Once the window has reached the desired temperature, it is rotated, together with the expander unit, through an angle of 90°, into the "spraying-on" position. The matrix mixture is sprayed onto the deposition window initially for ~5 minutes, but can then be anything up to 1 hour. The window and expander unit are then rotated back to the "scanning position" and a spectrum is recorded in the required region between 4000-400 cm^{-1}. This process of "spraying-on" and "scanning" is repeated at increasing temperatures, until desired bands are observed in the spectrum.

By switching off the displex refrigerator unit and allowing the deposition window to warm to ~ 27 K, diffusion experiments can be carried out. As the matrix cages relax, previously trapped

species are able to reorient and react further. Upon recooling the window, different resultant species will this time be trapped within the matrix cages.

4. Laser Kinetics

4.1. Apparatus

The apparatus[6] used for the flash photolysis experiments consists of a Coherent Compex 100 argon-fluoride excimer laser, lasing at 193 nm and a continuous wave dye laser (Coherent 699-21), which is pumped by an argon ion laser (Coherent Inc. Innova 90-5). The beam of the argon ion laser is focused directly into the dye beam laser within the reaction vessel. The latter is known as the probe beam and is used to monitor the intermediates produced. However, part of the incident beam is split from the main beam and focused onto a photodiode. The probe beam is then channelled to multipass ~36 times through a photolysis cell, producing a path length of ~144 cm. The probe beam enters the cell perpendicular to the photolysis beam, produced by the excimer laser and passes through the cell axially. A good overlap of the probe beam by the photolysis beam from the excimer laser is necessary for optimal signal detection and minimises the risk of losing absorbed species due to diffusion. After passing through the cell, the probe beam is then re-focused onto a second photodiode. A differential amplifier (Max.gain = 10.91) is used to feed in the outputs of these two photodiodes and a voltmeter measures the light incident on each photodiode. A Cokin photographic[7] polarising filter is required to ensure a balanced system between the two photodiodes and this is placed in the path of the reference beam. A transient recorder (Digilab 910) is set-up to collect the data, which is activated by the firing of the excimer laser. A schematic diagram of the apparatus used for the laser kinetic experiments can be seen in Figure 8.

The required wavelength (580nm) is achieved with the presence of an iodine vapour calibration tube. The probe beam is focused down the calibration tube and onto another photodiode. It is then possible to be able to lock the dye laser at a specific wavelength, which was found by stopping a scan of the sample at the desired wavelength.

The photolysis cell, which is pumped to a pressure of below 10^{-4} Torr before each run, is connected to a glass vacuum line. An Edward's model 102A oil diffusion pump is used together with an Edward's single stage oil rotary pump. Two MKS baratron gauges are also used, of 0-10

Torr and 0-1000 Torr, for pressure measurements. The background levels are recorded with the aid of a Penning gauge.

Figure 8. Schematic diagram of the apparatus used for the laser kinetic experiments.

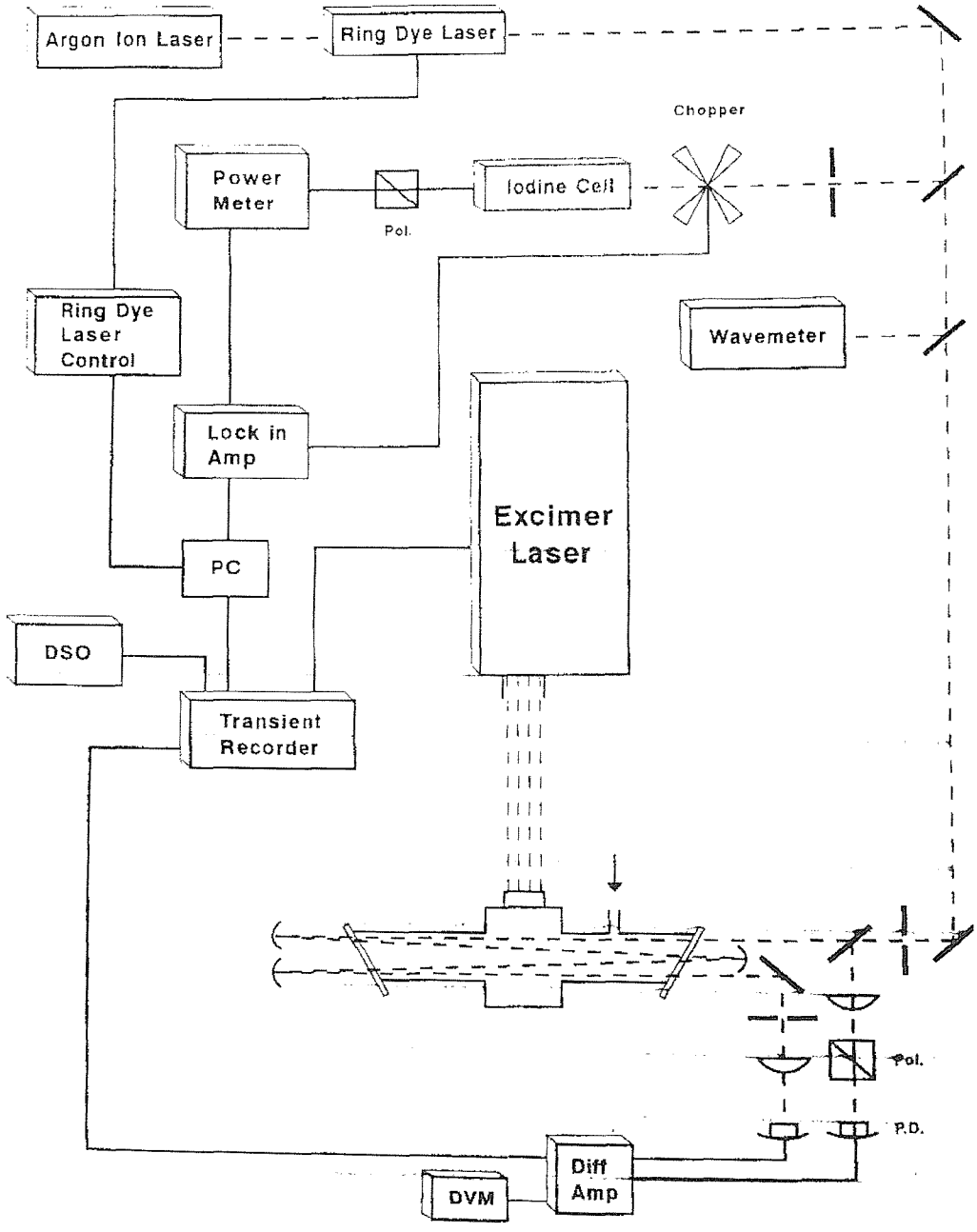

4.2. Experimental

The quality of the traces obtained during the photolysis experiments are determined by the signal-to-noise ratio. Therefore it is necessary to optimise[6] the energy output from the dye laser at the beginning of the experiments. The control box is required to be switched to 'Free Run' and 'Manual' before any tuning of the laser takes place. After tuning the position of the mirrors within the dye laser, the control box is then switched to 'Lock' and 'External', which places the laser under the control of the microcomputer. A procedure is then carried out, of locking the laser to the required wavelength, by stopping the scan of the observed iodine spectrum obtained from the calibration tube, at the desired peak corresponding to the correct wavelength. The energy of the excimer laser also needs to be checked at the beginning of the experiments. Energy of between 40-50 MJ per pulse over a period of 10 ns is required.

The mixture now needs to be prepared in the photolysis cell, using the vacuum line. Reaction mixtures are prepared at suitable partial pressures of precursor and substrate. During these experiments, the precursor used is phenylsilane and the substrates are oxygen, nitric oxide and oxetane. Once a mixture of these substances have been prepared, the mixture is topped up with the buffer gas, to pressures of 1, 3, 10, 30 and 100 Torr total pressure. The buffer gas used during these experiments is SF_6. Requirements of a buffer gas are that it is inert with reasonably high collisional efficiency and freezing point. It is necessary to have a high freezing point, in order to undergo purification by degassing after freezing in liquid nitrogen. When using nitric oxide as the substrate, it is found to be necessary to pass it through a pentane slush[8] at $-130°$ to remove the impurity of ~1% SO_2.

Before firing the excimer laser at the mixture contained within the photolysis cell, there is a need to ensure that the incident probe beam is balanced with the transmitted beam. This is achieved by checking that the digital voltmeter readings for each potential difference are within $\pm$ 5 %. The transient recorder records a number of shots. Usually groups of 5 shots are taken at a time, unless excess dust formation inside the cell is observed. If this occurs, then shots are taken individually. Decay traces are then observed simultaneously on an oscilloscope. The cell is heated to temperatures of approximately $60°$, $120°$, $200°$ and $300°$, as well as studying reactions at room temperature. At each temperature, the partial pressure of the substrate is varied and the partial pressure of the precursor is kept constant. Analysis of the traces observed takes place with a programme called "Scanset", on a BBC computer. Decays followed an exponential time dependence to a good approximation. The number of points chosen to fit the signal were

usually enough to cover 80-90 % of the decay. This number can be reviewed if necessary, until a reasonable agreement is reached between the experimental and the simulation. The decays are then fitted by a Linear-Least-Squares program and second order rate constants are obtained.

A Perkin Elmer 8310 chromatograph is used to determine[7] the purity of the initial samples. The sample injected into the G.C, filled the evacuated sampling loop for a few seconds, before the sampling valve was opened, allowing the nitrogen carrier gas to flow through the sample loop, taking the sample into the column. The sampling valve remained open for a couple of minutes before being closed. The re-evacuation of the sampling loop then took place in preparation for another sample injection. The data was plotted on a Hewlett Packard 3380 A integrator.

The purity and the source of the compounds used throughout this work can be seen below:

Compound	**% Purity**	**Molecular Formula**	**Source**
Phenylsilane	≥ 97.0	C_6H_8Si	Sigma-Aldrich
Oxygen	≥ 99.998	O_2	Sigma-Aldrich
Nitric Oxide	98.5	NO	Sigma-Aldrich
Oxetane	97	C_3H_6O	Sigma-Aldrich
Hexamethylcyclotrisiloxane	98	$C_6H_{18}O_3Si_3$	Sigma-Aldrich
Octamethylcyclotetrasiloxane	≥ 99.0	$C_8H_{24}O_4Si_4$	Sigma-Aldrich
Decamethylcyclopentasiloxane	97	$C_{10}H_{30}O_5Si_5$	Sigma-Aldrich
1,1,3,3-Tetramethyldisiloxane	97	$C_4H_{14}OSi_2$	Sigma-Aldrich
1,1,3,3,5,5-Hexamethyltrisiloxane	≥ 97.0	$C_6H_{20}O_2Si_3$	Sigma-Aldrich
3H, 5H-Octamethyltetrasiloxane	≥ 95	$C_8H_{26}O_3Si_4$	Sigma-Aldrich

5. References

1). E. A. V. Ebsworth, D. W. H. Rankin & S. Cradock, Structural Methods in Inorganic Chemistry, Blackwell scientific publications, second edition, **(1994)**, 182

2). J. M. Hollas, Modern Spectroscopy, John Wiley & sons, third edition, **(1998)**, 35

3). J. E. Stewart, Infrared Spectroscopy , Marcel Dekker, Inc., New York, **(1970)**, 13

4). I. Norman & G. Porter, Proc. Roy. Soc., A230, **(1955)**, 399

5). M. J. Almond & A. J. Downs, Spectroscopy of matrix isolated species, Advances in spectroscopy, 17, John Wiley & sons, **(1989)**, 15

6). R. Becerra, P Cannady and R. Walsh, unpublished work

7). J. M. Jasinski, J. Phys. Chem, 90, **(1986)**, 555

8). J. Chem., D. Beach, R. Estes & J. M. Jasinski, Chem. Phys. Lett., 143, **(1988)**, 135

CHAPTER THREE

VIBRATIONAL SPECTROSCOPY

1. Introduction

There are two main vibrational spectroscopy techniques; Raman spectroscopy and Infrared spectroscopy. The technique of Infrared spectroscopy was chosen for the work carried out here.

Infrared spectroscopy is a technique used for studying molecular vibrations that can lead to the determination of chemical structures. As a result of absorbing energy, molecular vibrations occur in the infrared region of the *electromagnetic spectrum*[1], with functional groups having characteristic absorption frequencies. For molecules in the gas phase, vibrational transitions are accompanied by a change in rotational energy and spectra typically show an envelope of absorption. In condensed phases and in low temperature matrices, molecules are generally non-rotating and as a result, vibrational spectra are generally simpler, with the observed bands corresponding to simple vibrational transitions. In general however, the more complicated a species, the more difficult the vibrational spectra are to interpret. Both simple diatomic and more complicated polyatomic species are discussed below.

2. Diatomic Molecules

A *diatomic* molecule A-B, is bonded together as the result of a balance of forces. A repulsive force between the two positively charged nuclei and the two negative electron clouds of the atoms, is balanced by the attraction between the nucleus of one atom and the electron clouds of the other. This balance of forces results in the bond length, or the equilibrium distance. In order to overcome these forces and distort the bond length, an input of energy is needed. When energy is put into the system, the atoms A-B will vibrate as to compress and extend the bond.

$$\text{Total energy} = \text{Potential energy} + \text{Kinetic energy.}$$

2. (a). Harmonic Oscillator

The motion of a bond being compressed and extended can be compared to that of a spring[2]. It can then be further assumed that a bond obeys *Hookes Law*.

Equation 1. Hookes Law

$$f = - k \ (r - r_{eq})$$

f = Restoring force

k = Force constant

r = Internuclear distance

In the case of diatomic molecules, the above expression yields a parabolic curve for the potential energy, in terms of the displacement from the equilibrium.

Equation 2.

$$E_v = \tfrac{1}{2} k (r - r_{eq})^2$$

E_v = Potential energy

The diagram in Figure 1 of potential energy plotted against internuclear distance[2], indicates the amount of energy required to distort the bond length of a molecule A-B. The equilibrium distance r_{eq}, is where the potential energy is at a minimum.

Figure 1. An energy diagram of a molecule A-B as the bond is compressed or extended

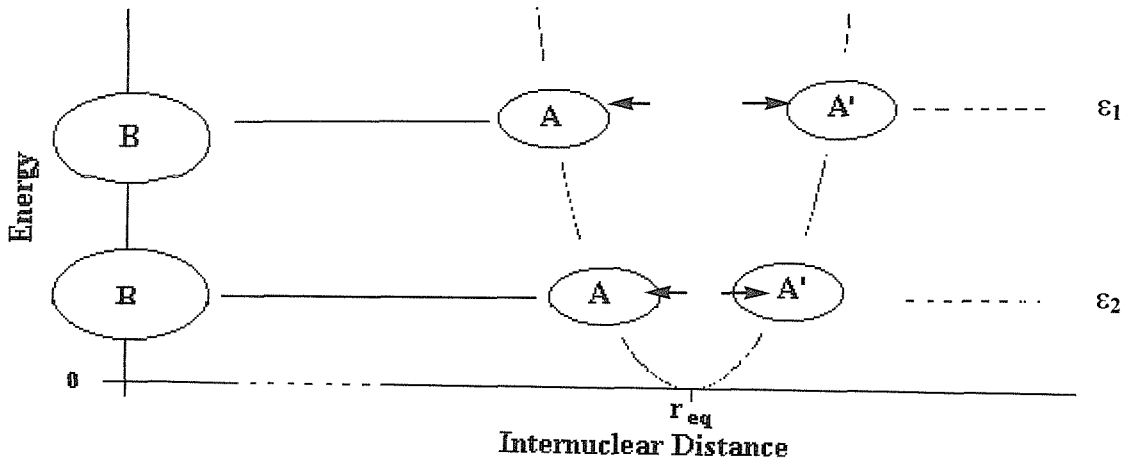

The energy diagram in Figure 1, is known as the *simple-harmonic oscillator* model. This model shows that as the energy input increases, the amplitude of oscillation of an atom between A and

A' becomes greater. However, the vibrational frequency does not change, but is dependent on the reduced mass of the molecule and the force constant. This is demonstrated by the following equation:

Equation 3.

$$\omega = 1/(2\pi c)\sqrt{(k/\mu)}$$

ω = Vibrational wavenumber

c = Velocity of light[3]

μ = Reduced mass

k = Force constant

The above expression includes the velocity of light in order to convert the frequency to wavenumbers, which is the most commonly used unit of 'frequency' in vibrational spectroscopy. The reduced mass has been used in the above expression to account for the dynamical properties of the relative motion of atoms A and B of mass m_1 and m_2 respectively. The reduced mass is defined as follows:

Equation 4. Reduced mass equation

$$1/\mu = 1/m_1 + 1/m_2$$

The allowed vibrational energies of the system can be calculated from the *Schrödinger equation*. In the case of a harmonic oscillator, the vibrational energy levels, E_v are given by the following equation[3]:

Equation 5.

$$E_v = (v + \tfrac{1}{2})\, h\omega$$

v = Vibrational quantum number (= 0, 1, 2, ...)

In the above equation, $h\omega$ represents the uniform separation between the energy levels. This can be seen in the diagram below.

Figure 2. The vibrational energy levels for a simple harmonic motion of a diatomic molecule

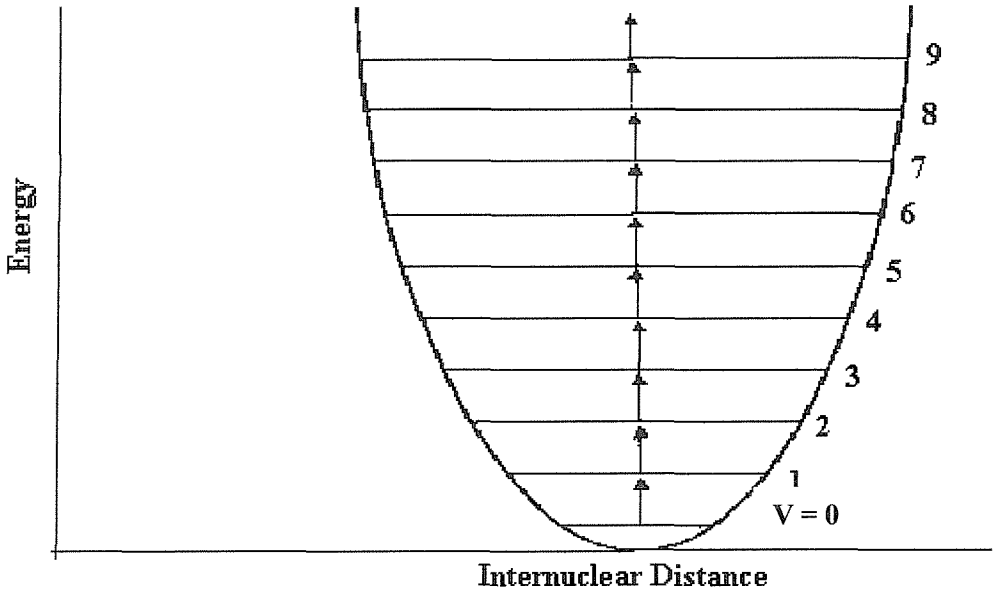

A molecule can never possess zero vibrational energy. That is to say that the bond must always vibrate. The quantity of $\frac{1}{2} h\omega$ cm^{-1} has become known as the zero-point energy and is dependent on the strength of the bond and on the atomic mass of the atoms.

The Schrödinger equation may be used further to obtain the fundamental selection rule for the harmonic oscillator:

$$\Delta v = +1, -1$$

However, in reality molecules do not behave like springs, since if stretched too far, a bond will break and dissociation will occur. This is demonstrated with the *anharmonic oscillator* model[1]. (See Figure 3).

(b). Anharmonic Oscillator

Although it is the case that a bond will distort if a small amount of energy is applied to cause mild compressions and extensions, if too much energy is put into a system, a greater magnitude of motion on the bond will eventually lead to dissociation of the molecule, to form atoms. As the molecule approaches this stage the motion then becomes increasingly anharmonic, as the force applied is no longer proportional to the displacement. A function is then required which is closer to the true situation. One such function is called the *Morse potential energy* and the equation can be seen in Equation 6.

Equation 6.

$$E = D_{eq} \{1-e^{-a(r-re)}\}^2$$

D_e = Depth of the potential minimum
a = Constant

The diagram below shows the potential energy curves for a typical diatomic molecule, for both a harmonic oscillator and an anharmonic oscillator. The latter is closer in practice to a real molecule.

Figure 3. The Morse curve potential energy diagram of a diatomic molecule

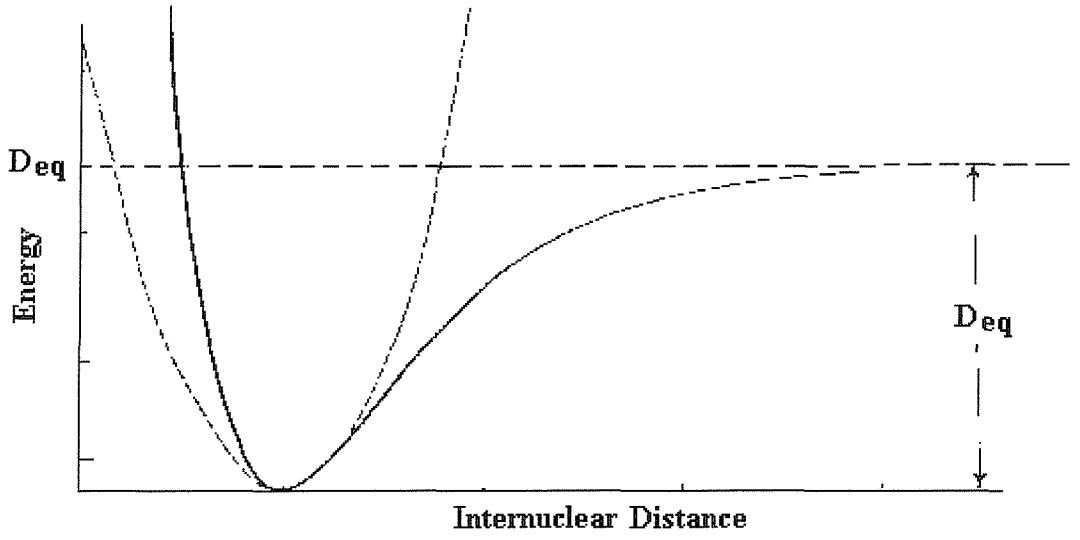

With the Morse potential energy, the Schrödinger equation can again be used to calculate the energy levels for an anharmonic oscillation:

Equation 7.

$$E_v = h\omega_e \{ 1-x_e (v + \tfrac{1}{2}) \} (v + \tfrac{1}{2})$$

x_e = Anharmonicity constant

Equation 7 can be re-written (see Equation 8) and compared to the energy levels for the harmonic oscillator.

Equation 8.

$$\omega_{osc} = \omega_e \{ 1-x_e (v + \tfrac{1}{2}) \}$$

From this above equation it can be seen that both the harmonic and the anharmonic oscillators behave similarly: the main difference being that with an anharmonic oscillator, the spacing between energy levels decreases steadily with increasing v. This can be seen more clearly with the aid of a diagram shown in Figure 4.

Figure 4. <u>The vibrational energy levels for a simple anharmonic motion of a diatomic molecule</u>

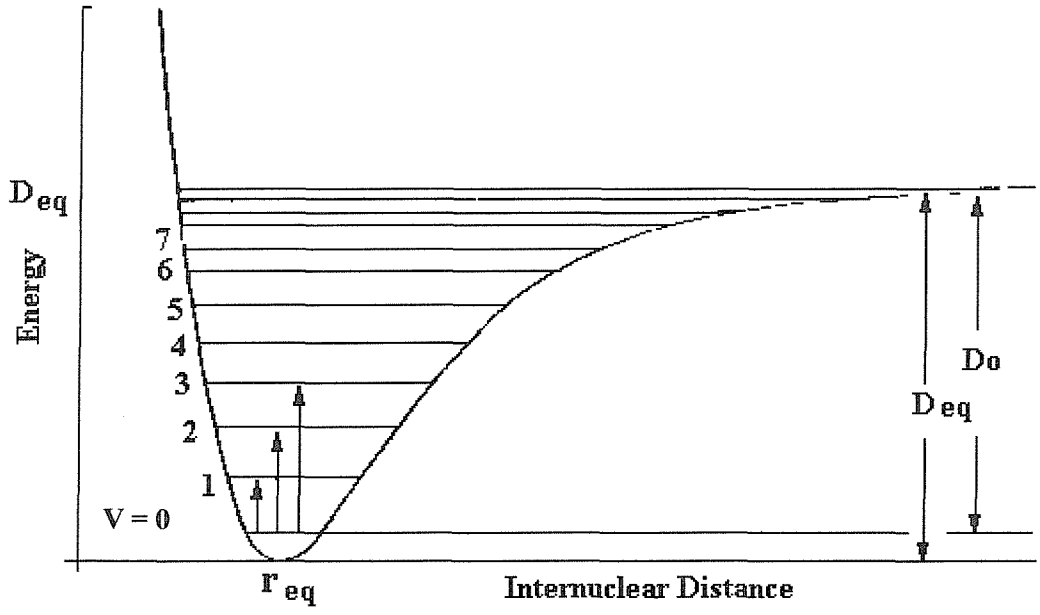

Since the value for x_e is always a small positive number, the energy levels are seen to become closer together with increasing v.

Vibrational spectra consist of narrow peaks resulting from transitions between vibrational quantum levels. The quantified vibrational energies (v = 0,1,2...), are able to be calculated with the aid of the equation shown in Equation 7. In the presence of anharmonicity, the spectrum is further complicated by the appearance of overtones, combination bands and difference bands. It is found that the selection rule for the *anharmonic* oscillator is:

$$\Delta v = \pm 1, \pm 2, \pm 3 \ldots$$

An overtone is a vibrational transition where Δv is greater than 1. For example, the first overtone corresponds to $\Delta v = 2$ and occurs at a frequency of $\sim 2\nu$ and without the restriction of harmonic motion, there is a possibility that this and higher overtones may also be present.

Combination bands occur at energies close to $\nu_a + \nu_b$, where ν_a and ν_b are vibrational fundamentals, and may also occur for anharmonic vibrations.

3. Degrees of Freedom

A diatomic molecule has only one mode of vibration, that is the stretching and the compression of the bond. In *polyatomic* molecules, vibrations generally involve both stretching and bending motion.

The location of the molecule in space can in general be defined by three co-ordinates relating to the position of its centre of gravity[3] and three which establish its orientation. A polyatomic molecule containing N atoms each with the Cartesian co-ordinates of x, y and z, has a total of 3N degrees of freedom. The position[4] of the molecule thus accounts for three of these degrees of freedom, by which the location of the centre of mass of the molecule can be specified and for a non-linear molecule, a further three degrees of freedom define the orientation of a molecule about each of the axes, x, y and z. Therefore, for a non-linear polyatomic molecule, when the translational and rotational degrees of freedom have been taken into account, the molecule has *3N-6 vibrational degrees of freedom.* Water is an example of a non-linear molecule with 3N-6 degrees of freedom.

Figure 5. Vibrational modes of water

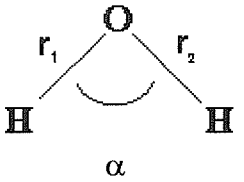

Since water is a triatomic molecule, it has 3 modes of vibration. These are two **O-H** bond stretching modes and one **H-O-H** angle bending mode. The symmetric stretching mode (ν_1) is found in the infrared spectrum at 3651.7 cm^{-1} and the anti-symmetric stretching mode (ν_3) is found at 3755.8 cm^{-1}. The symmetric bend (ν_2), however, is found at 1595 cm^{-1}, reflecting a general result that bending modes occur at significantly lower energies than the stretching modes.

With a linear polyatomic molecule, since there is no rotational movement about the bond axis, *3N-5 vibrational degrees of freedom* result.

3.1. Complex Molecules

For complex molecules, as well as dividing the vibrations into stretching and bending modes, the vibrations may also be divided into two different classes: the *skeletal vibrations* and the *characteristic group vibrations*[12]. In the case of skeletal vibrations, all of the atoms are affected to much the same extent. These vibrations are usually seen in the fingerprint region, below 1500 cm^{-1}. These vibrations result from either linear or branched chain structures in the molecule and are usually highly characteristic of the overall molecular structure. In contrast, characteristic group vibrations are often largely independent of the structure as a whole as they reflect only a small portion of the molecule. They can often be found either significantly above or below the region of the skeletal vibrations, but are usually seen in the region between 1500 – 3700 cm^{-1}.

From this it can be deduced that complex molecules, such as those found here in silicon chemistry, are most likely to show a large number of vibrations. For example, the cyclic siloxane, D5 will have 144 modes of vibration.

Figure 6. A structure of a D5 molecule

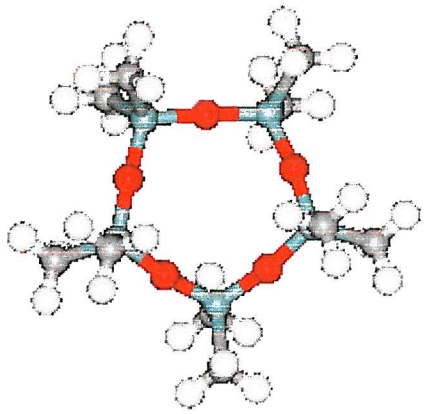

4. Molecular Vibrations and Symmetry

A vibrational mode of a species results in a particular pattern of atomic displacements, known as a normal mode of vibration. During a normal mode of vibration, all of the nuclei undergo (an) harmonic motion at the same frequency. The oscillations occur in phase, but may vary in amplitude. Water can again be used as an example. The normal modes of vibration of H_2O are ν_1, ν_2 and ν_3. These are shown below, together with the resultant vibrational frequencies:

Figure 7. Normal modes of vibration of a water molecule

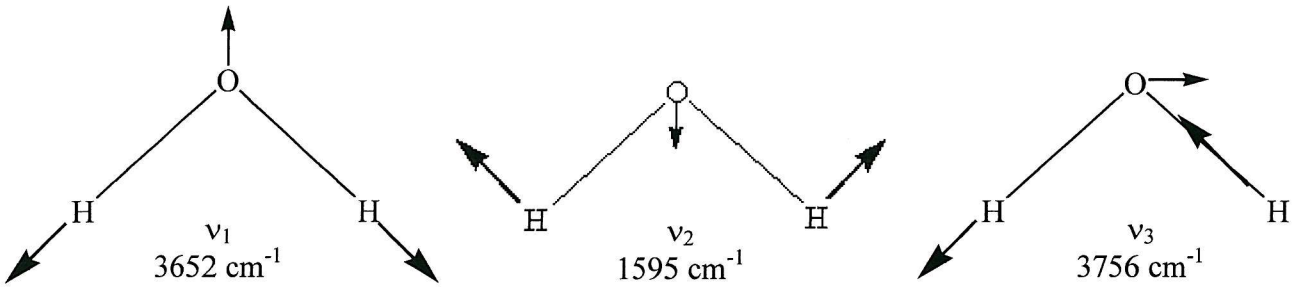

4.1. Symmetry Selection Rule

These normal modes of vibration are able to be classified according to their symmetries and this gives rise to a *symmetry selection rule*, which states that during the course of a vibration there must be a change in dipole moment. This can sometimes be established by inspection, but is more usually determined by group theory. Before group theory can be used to determine

whether a vibrational mode is infrared active or not, the point group of a species needs to be identified. A reducible representation can then be obtained. The symmetry operations of a system correspond to a particular point group. A symmetry operation can be defined as a movement of a system that terminates with each atom in an equivalent position. A list of possible symmetry operations[5] can be seen below:

1). E = Identity;

This operation leaves a molecule unchanged. Every molecule possesses this symmetry operation, which is a necessary operation in group theory.

2). C_n = *n*-fold rotation;

A molecule is rotated through 360°/*n*. The rotation axis possessing the greatest value for *n* is the principal axis.

3). σ_v = Reflection;

This operation reflects a molecule through a vertical plane.

σ_h = Reflection;

This operation reflects a molecule through the horizontal plane.

σ_d = Reflection;

This operation reflects a molecule through a dihedral plane.

4). *i* = Centre of inversion;

A specific point in a molecule through which it is possible to project every other point to an equivalent position on the opposite side of the centre.

5). S_n = Improper rotation;

This consists of an *n*-fold rotation, followed by a reflection in a horizontal plane.

Ethene is used in the example shown below to demonstrate how group theory can be used to determine the number of infrared active vibrations in a system.

Figure 8. Structure of ethene

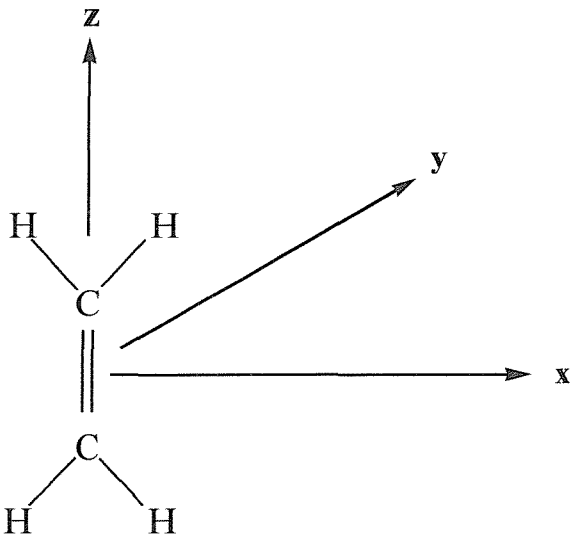

From the above list of symmetry operations, it may be deduced that ethene has eight symmetry elements. It is a non-linear molecule and so it can be expected to have 3N-6 vibrational modes of freedom. It has a principal axis of $C_2(z)$ and another two C_2 axes, ($C_2(x)$ and $C_2(y)$) as well as three horizontal planes of symmetry which lie perpendicular to the $C_2(z)$ axis. From these symmetry operations, it may be concluded that ethene has a point group of D_{2h}. The character table of D_{2h} can be seen below, together with the remaining symmetry elements.

Table 1. Character table for the D_{2h} point group

D_{2h}	E	$C_2(z)$	$C_2(y)$	$C_2(x)$	i	σ (xy)	σ (xz)	σ (yz)		
A_g	1	1	1	1	1	1	1	1		x^2, y^2, z^2
B_{1g}	1	1	-1	-1	1	1	-1	-1	R_z	xy
B_{2g}	1	-1	1	-1	1	-1	1	-1	R_y	xz
B_{3g}	1	-1	-1	1	1	-1	-1	1	R_x	yz
A_u	1	1	1	1	-1	-1	-1	-1		
B_{1u}	1	1	-1	-1	-1	-1	1	1	z	
B_{2u}	1	-1	1	-1	-1	1	-1	1	y	
B_{3u}	1	-1	-1	1	-1	1	1	-1	x	

In order to obtain the irreducible representations, χ_I for the ethene molecule, the characters of the reducible representation for molecular motion must first be established. This may be achieved by carrying out the symmetry operation on each of the atoms and noting which of the atoms

remained in the same position after the operation had been completed. That is to say, the atoms that remained unmoved. The whole molecule is considered while carrying out these operations.

Table 2. Tabulated reducible representations of ethene

	E	C_2 (z)	C_2 (y)	C_2 (x)	i	σ (xy)	σ (xz)	σ (yz)
$\Gamma_{Cartesians}$	3	-1	-1	-1	-3	1	1	1
$\Gamma_{Unmoved\ atoms}$	6	2	0	0	0	0	2	6
$\Gamma_{Total\ molecular\ motion}$	18	-2	0	0	0	0	2	6

The top row of Table 2, labelled $\Gamma_{Cartesians}$ refers to the contribution to the character for each unshifted atom upon carrying out the symmetry operations.

This representation can then be reduced to its simplest form with the aid of the reduction formula[6] shown below:

Equation 9. Reduction formula

$$n = 1/h \, \Sigma \, \chi_R \times \chi_I \times N$$

n = The number of times the irreducible representation occurs in the reducible representation

h = The number of symmetry operations

χ_R = The character of the reducible representation

χ_I = The character of the irreducible representation

N = The number of symmetry operations in the class

Using the reduction formula, the irreducible representations and the reducible representations have been reduced to:

$$\Gamma_{Total\ molecular\ motion} = 3A_g + B_{1g} + 2B_{2g} + 3B_{3g} + A_u + 3B_{1u} + 3B_{2u} + 2B_{3u}$$

In order to obtain $\Gamma_{vibrations}$ the rotational and translational irreducible representations must be subtracted.

The rotational irreducible representations are:

$$\Gamma_{Rotational} = B_{1g} + B_{2g} + B_{3g}$$

The translational irreducible representations are:

$$\Gamma_{Translational} = B_{3u} + B_{2u} + B_{1u}$$

When subtracted from $\Gamma_{Total\ molecular\ motion}$, the vibrational reducible representation is obtained:

$$\Gamma_{Vibrations} = 3A_g + B_{2g} + 2B_{3g} + Au + 2B_{1u} + 2B_{2u} + B_{3u}$$

This agrees with the calculation of the number of degrees of freedom, (see section 3), in that there are 3N-6 = 12 vibrational modes of freedom. It can be seen from the character table of D_{2h} that B_{1u}, B_{2u} and B_{3u} representations in the above expression are infrared active, since these modes belong to the same symmetry species as the component of dipole moment, x, y and z.

It was decided to use NH_3 as another illustration of the use of group theory.

Figure 9. NH_3 molecule

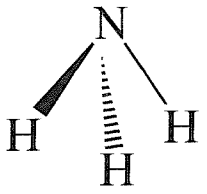

Ammonia has a pyramidal geometry and a point group of C_{3v}. The character table for a C_{3v} point group is shown below.

Table 3. Character table for the C_{3v} point group

C_{3v}	E	$2C_3$	$3\sigma_v$		
A_1	1	1	1	Z	$x^2 + y^2, z^2$
A_2	1	1	-1	R_z	
E	2	-1	0	(x, y) (R_x, R_y)	(x^2-y^2, xy) (xz, yz)

The reducible representation for Γ_{NH3} is then obtained below:

Table 5. Tabulated reducible representations for the NH_3 molecule

C_{3v}	E	$2C_3$	$3\sigma_v$
Γ Cartesians	3	0	1
Γ Unmoved atoms	4	1	2
Γ Total molecular motion	12	0	2

In total, the expression for the molecular motion of NH_3 is:

$$\Gamma_{(NH3)\text{Total molecular motion}} = 3A_1 + A_2 + 4E$$

In order to obtain the vibrational reducible representation, it is necessary to subtract the irreducible representations due to the translations and rotations.

$$\Gamma_{\text{Translations}} = A_1 + E$$

$$\Gamma_{\text{Rotations}} = A_2 + E$$

This gives:

$$\Gamma_{\text{Vibrations}} = 2A_1 + 2E$$

For the above expression, it is observed after consulting the C_{3V} character table, that both types of mode are infrared active. The A_1 mode belongs to the same symmetry species as z and the E mode belongs to the same symmetry as x and y.

These may be shown to break down into:

$$\Gamma_{\text{Stretch}} = A_1 + E$$

$$\Gamma_{\text{Bend}} = A_1 + E$$

5. The 'Sotonvib' Program

The program called 'Sotonvib' was used to model the vibrations of molecules of interest and to obtain computer simulated spectra. Data was fed into the program, such as the cartesian co-ordinates, atom charges, masses and force constants, together with data on internal co-ordinates, including bond angles. The output generated from this program included data on estimated vibrational frequencies and relative band intensities. This program was used in conjunction with experimental data in order to aid the identification of molecular structure. Modelling using the 'Sotonvib' program can also be conducted in order to predict vibrational isotope patterns.

6. References

1). J. M. Hollas, Modern Spectroscopy, third edition, John Wiley & Sons Ltd, **(1998)**

2). C. N. Banwell & E. M. McCash, Fundamentals of Molecular Spectroscopy, fourth edition, Mcgraw-Hill Book Company, **(1994)**

3). P. W. Atkins, Physical Chemistry, fourth edition, Oxford University Press, **(1992)**

4). E. A. V. Ebsworth, D. W. H. Rankin & S. Cradock, Structural Methods in Inorganic Chemistry, second edition, Blackwell Scientific Publications, **(1994)**

5). G. Davidson, Group Theory for Chemists, McMillan Physical science series, **(1991)**

6). A. Vincent, Molecular Symmetry and Group Theory, John Wiley & Sons Ltd., **(1997)**

CHAPTER FOUR

MOLECULAR MODELLING

1. Introduction

Molecular modelling calculations were carried out at Dow Corning sites in Midland, Michigan, U.S.A and in Barry, South Wales. The work carried out at Dow Corning can be divided into two parts. Initially, a series of energy calculations, using the Cerius 2 package and the Gaussian 94 program[1] were conducted on both the reactants and the possible products formed. The purpose of these calculations was to first obtain the energies of the individual species in order to deduce the energy of the overall reactions. The reaction that produced the lowest overall energy, was the most favourable reaction. Once the geometry of a species was established, further calculations were carried out to obtain vibrational frequencies and infrared intensities. After energies were known for all the reactants and the possible products of the systems under investigation, a second package known as Spartan was used in order to attempt to generate possible pathways, with a series of transition state calculations.

2. Potential Energy Surfaces

Geometry optimisation calculations were initially carried out on all of the reactants and the possible products of the experiments in chapters 5, 6 and 7. A geometry of a particular species is obtained once a minimum on the potential energy surface is found. This equates to the equilibrium structure within the constraints of the Born-Oppenheimer approximation[3]. A potential energy surface is a mathematical representation of molecular energy on the geometrical parameters of a molecular species. This energy is a combination of total electronic energy and total nuclear repulsion energy[2], which are separated within the context of the Born-Oppenheimer approximation.

A global minimum on a potential energy surface is the lowest point on the surface where any structural change can only result in a higher energy. At a global minimum the first derivative of the energy with respect to molecular co-ordinates is zero[2].

A global minimum is often surrounded by local minima, especially those potential energy surfaces of weakly bound complexes. A local minimum is a lowest point within a stated region and there may be numerous local minima on a surface.

An area on a surface where it is possible to go 'down-hill' in some directions and 'up-hill' in others is called a saddle point[4]. A first order saddle point has a maximum in only one direction and a minimum in all others and this represents the formation of a transition state. Like for that of a global minimum, both a local minima and a saddle point are as a result of a zero first derivative. This first derivative is equal to the gradient. Since the gradient is the negative of the forces on a system, all the forces are zero at these points. These are known as stationary points[4].

Also located on a potential energy surface are peaks and ridges[4]. These are known as maxima, where the energy is at a maximum in all directions.

2.1. Optimising an Equilibrium Structure

In order to optimise a structure, a pathway is needed to be identified that corresponds to the least amount of potential energy[2]. To achieve this, an estimated geometry has first to be inputted into the program. The potential energy surface is then 'scanned', by carrying out small geometric perturbations, with the intention of locating the point of lowest energy. The energy and the gradient at each point are computed. After each step, a decision is taken automatically as to how far and in which direction the parameters of the next point are to be computed. By computing the gradient, an indication of the steepness of a slope and the declines are gained, aiding the decision as to which direction is needed to be taken next. Computing the Hessian[2], [5], a matrix of force constants, which is the second derivative of the energy with respect to molecular co-ordinates, provides additional information in mapping out the surface. A structure is fully optimised once the optimisation has converged. Essentially this is when all the forces are zero. Once a calculation has successfully optimised a structure, then a stationary point has been located. In order to characterise a stationary point of a transition state, the correct number of imaginary frequencies should have been found as well as the normal modes corresponding to them. An imaginary frequency results from a negative force constant. However, there is always a chance that a local minimum may have been identified as opposed to a true global minimum and so the structure produced may not be that which was intended. This would require a slight alteration in the original inputted geometry and a new calculation.

Once a potential energy surface has been mapped out, information can be extracted, such as the extent of deformation of a species with increased internal energy. Further parameters and

constants may also be produced and compared to those obtained experimentally in the analysis of vibrational spectra.

2.2. Imaginary Frequencies

Imaginary frequencies can be explained by studying the definitions of a saddle point. It is known that a saddle point has a gradient of zero. Upon displacement of the system, the energy increases along all internal co-ordinates except one, along which the energy decreases. This is known as the reaction co-ordinate and corresponds to a stable point. At a saddle point, if the system is displaced along the reaction co-ordinate, the energy will pass through a maximum. At this point, the system experiences a reacting force, which for a harmonic oscillator model, is described in terms[4] of:

Equation 1.

$$V = \tfrac{1}{2} Fx^2$$

V = Potential energy
F = Force constant
x = Displacement

Equation 1 links together the reacting force associated with a harmonic oscillation and the force constant. When at an energy minimum, the force constant is negative. The following equation can then be applied:

Equation 2.

$$\nu = 1 / (2\pi) (k / \mu)^{1/2}$$

μ = Reduced mass

The square root of a negative number gives an imaginary number. The resultant frequency is therefore imaginary.

The force constant increases with increasing strength of the bond and can be given directionality with the aid of a sign. The total energy is the sum of both the kinetic and the potential energies.

At a saddle point, as the internuclear distance is increased, the energy decreases. The above equation can then be integrated to produce the first order derivative as shown below:

Equation 3.

$$\delta V / \delta x = Fx = 0$$

V = Molecular potential energy

This shows that a saddle point has a zero first order derivative. The second derivative is shown to have a negative value.

Equation 4

$$\delta^2 V / \delta^2 x = F = - ve$$

When the restoring energy is put into the equation below, the square root of a negative frequency results, which gives an imaginary number and therefore, an imaginary frequency.

Equation 5

$$4\pi^2\nu^2 = F / \mu$$

ν = Frequency

μ = Reduced mass

However, when a minimum is found, the graph below is produced:

Figure 1. A representation of a minimum on a potential energy curve

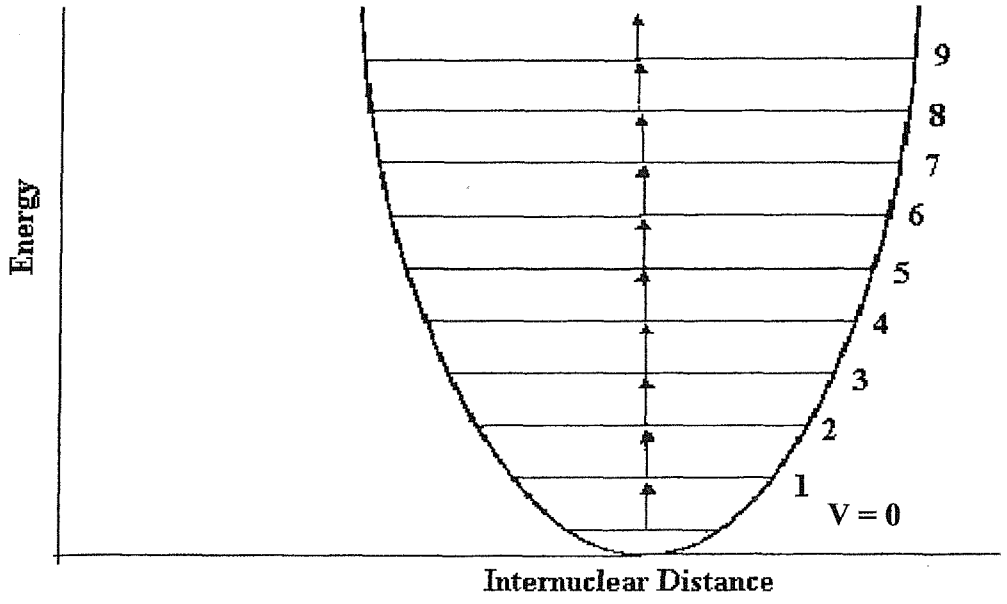

In the above diagram it can be seen that as the internuclear distance increases, the energy also increases. The second derivative will this time be positive. The first and second derivatives are shown below:

Equation 6.

$$\text{First derivative:} \quad \delta V / \delta x = Fx = 0$$

Equation 7.

$$\text{Second derivative:} \quad \delta^2 V / \delta^2 x = F = +ve$$

2.3. Optimising a Transition State Structure

Optimised transition state structures are found in first order saddle points on the potential energy surface. They are more difficult to locate, since the surface of a saddle point tends to be flatter than for a local minimum. This results in the mathematics for calculating the energies being more complicated, as the energy surface will be less well defined by a simple quadratic function.

A program called Spartan was used for the transition state calculations carried out here. Initially, an estimated geometry was inputted for both the reactants and the products. These geometries were then optimised. The program is then requested to generate a guess for a possible transition state structure. This guess is usually midway between the reactant and the product in terms of redundant internal co-ordinates, that is those co-ordinates that were specified.

When the formation of a transition state is as a result of breaking and forming new bonds, a higher level of theory may be required than for locating geometries for equilibrium structures. After the calculation has converged[2], if the energy values and the geometry obtained does not agree with previous knowledge or literature findings, then it is possible to fix parameters, such as known bond lengths and angles in order to increase the chances of the formation of the correct transition state geometry.

2.4. Supporting Data to Confirm Calculated Geometries for a Transition State

Once a geometry has been optimised for either an equilibrium structure or a transition state, there are a small number of values that can be checked in the generated output.

By conducting a normal mode analysis[2], [6] at the same level of theory, the values in the Hessian can be verified. For a transition state structure, it is important to ensure that only one imaginary frequency has been produced in the Hessian, since a structure which has *n* imaginary numbers is an n^{th} order saddle point. However, even if the correct number of imaginary frequencies are found, it does not necessarily mean that the correct structure has been produced. A saddle point is as a result of the joining together of two minima. These minima must belong to the reactant and the product.

The normal mode analysis will also produce displacements of the nuclei in the form of xyz co-ordinates. The co-ordinates can be animated in order to ensure that the imaginary frequencies correspond to the correct co-ordinates.

Although a low-level of theory is necessary initially to obtain the geometry of the species, it is advisable to follow this with a calculation of a higher level of theory[2] in order to obtain the most accurate values possible.

2.5. Frequency Calculations

The main reason for conducting frequency calculations was to predict infrared spectra which could then be compared to spectra obtained experimentally. These calculations can be performed after a geometry has been established. Frequency calculations can be carried out in order to identify a stationary point of an optimised geometry. It is often the case that optimised geometries have actually located local minima or saddle points and not the desired surface minimum. As it has already been seen, identifying the number of imaginary frequencies and the corresponding normal modes from the normal mode analysis of the Hessian, will aid the pursuit for the correct stationary point. Force constants can also be obtained from frequency calculations as well as thermodynamic properties.

3. Methods and Basis Sets – model chemistries

Electronic structure *methods*[2] involve calculating certain properties using the laws of quantum mechanics as opposed to the traditional laws of physics. The desired properties are all obtained by solving the Schrödinger equation. There are three main classes of electronic structure

methods. These are *semi-empirical* methods, *ab initio* methods and *density functional theory* methods. These methods are later described in more detail.

The available *methods* represent a hierarchy of calculations able to be performed. The more accurate a method is, the more expensive it will be in computer time. However, the amount of computer time needed also increases with the size of the molecule.

Basis sets[2] are descriptions of orbitals in a system. The larger a basis set, the more accurate the calculation will be, as less restrictions are imposed on the location of the electrons in space. However, a greater length of computer time will also be used. There are four main classes of basis sets. These are the *minimal*, the *split-level valence*, the *polarised* and the *diffuse* basis sets. The combination of *method* and *basis set* is known as a *model chemistry*[2].

4. Model Chemistries Used to Calculate Overall Reaction Energies

For these first sets of energy calculations, the molecular modelling package used was Cerius 2. Using the Gaussian 94 programme[1], the most accurate energies possible in the given time period were attempted. These included both reactants and possible products of the systems studied in the pyrolysis experiments at Southampton University and the laser kinetics experiments at Reading University. Gaussian is capable of calculating various properties[2] of molecules and reactions, including the desired properties in this case, which were:

Molecular energies and equilibrium geometries

Energies and structure of transition states

Bond and reaction energies

Vibrational frequencies

IR and Raman intensities

Reaction pathways

Initially, a series of geometry optimisation and frequency calculations were performed.

5. Geometry and Frequency Task Calculations

(a). HF / 3-21G

A geometry optimisation and frequency calculation works by initially obtaining an optimised geometry and then by performing the frequency calculations on this optimised structure. The Hartree-Fock (HF) method was first employed together with a 3-21G basis set. The Hartree-Fock method is the least expensive of the *ab initio* methods and enables calculations to be completed quickly, yet at a limited accuracy. *Ab initio* methods contain no experimental parameters in their computations and are based solely on the laws of quantum mechanics. The basis set which was used here, was also a little cruder than those which followed. The name of the 3-21G basis set was derived as follows: firstly it uses three functions in the inner shell. It also uses a split-level valence, which means that there are two sets of Gaussian functions in the valence shell of different sizes. This accounts for the 21G part of the basis set. By using a split-level valence, the basis set is able to provide a reasonably accurate representation of the orbitals relatively quickly. This combination (HF / 3-21G) of method and basis set, is usually performed on larger molecules. It may also be used on smaller molecules to gain the initial basic geometry. When the basic geometry is obtained, then more accurate calculations may be performed on these results.

(b). B3LYP / 6-31G (d)

After this first set of calculations were completed, a second set of calculations were often performed on these results, in order to further optimise the given structure. This time a more accurate, yet more expensive method was used with a larger basis set. The method used was the B3LYP method. This is a Density Functional Theory (D.F.T) method. Density Functional Theory methods are similar to *ab initio* methods, but they also include the effects of electron correlation, by accounting for instantaneous interactions of pairs of electrons with opposite spins. This increases their desirability, by behaving like a more expensive *ab initio* method, but at a much lower cost.

The B3LYP method was derived as follows: it uses Becke's three-parameter formulation, together with the gradient-corrected correlation functional of LYP, developed by Lee, Yang and Parr. Together with the 6-31G (d) basis set, reasonably accurate calculations are able to be carried out on medium-sized molecules. This basis set uses six functions in the inner shell. Again, it uses a split-level valence and two Gaussian functions of different sizes. However, it removes a further restriction in that the basis set adds polarisation functions to heavy atoms.

This accounts for the (d) term. By adding polarisation functions to heavy atoms, the orbitals are in effect being allowed to change shape as well as size. By removing a restriction, more accurate calculations are being performed, but at a greater expense.

(c). HF / 6-31G (d)

It is often the case that an alternative combination is used of HF / 6-31G (d). These calculations are completed quickly and at a higher level of theory than the HF / 3-21G model chemistry is capable of. However, a greater amount of computer time is needed.

(d). B3LYP / 6-311 + (2d, p)

A third combination of method and basis set could then be used if it was found that similar values were obtained for the overall reactions at the end of calculating the energies for the reactants and products. A possible combination would be B3LYP / 6-311 + G (2d, p). A Density Functional Theory method is used here as previously described and a new basis set is introduced. As with the previous basis set, six functions are used in the inner shell. However, this time a triple split-level valence is used. This means that there are three Gaussian functions of different sizes in the valence shell. This adds to the accuracy in the way in which the orbitals will be portrayed. The term (2d, p) refers to the changability of the shape of both the d and the p orbitals. Here, two polarisation functions are added to the larger atoms and one polarisation function is added to the orbitals of the hydrogen atoms. An additional restriction is removed, by adding the term +, which symbolises that diffuse functions have also been added. One plus sign indicates that diffuse functions have been added to d orbital, and two plus signs indicates adding diffuse functions to p orbitals. A diffuse function enables an orbital to occupy a larger area of space. These functions further aid the accuracy of orbital representation. Basis sets containing diffuse functions are particularly important for species where the electrons are a long way from the nucleus, for example, species with lone pairs or anions. Many of the possible products described in chapter seven as a result of the pyrolysis of the linear siloxanes contain lone pairs and therefore diffuse functions would be of particular importance for these systems.

(e). MP2 / 6-31G (d)

This combination of method and basis set is in wide use and is often used to obtain the basic geometry when the HF / 3-21G combination fails. It was especially popular prior to the introduction of Density Functional Theory methods, as it is an inexpensive alternative to the Hartree-Fock method and was the first applied electron correlation method. MP2 stands for

second order Møllet-Plesset (after the people who developed it) perturbation theory. The term 2, indicates that optimisations occur through analytic gradients for second-order. There are other Møllet-Plesset methods of higher levels of theory, e.g. MP3, MP4 and MP5.

6. Singlepoint Energy Task Calculations

Singlepoint energy calculations are an alternative approach, but can only be performed once the basic geometry has already been found and optimised. Therefore they are never used as the first step of a calculation. Once the geometry has been predicted and optimised at a lower level of theory, either using for example, the HF / 3-21G or the B3LYP / 6-31G (d) combination for a geometry optimisation, then the singlepoint energy task can be used to obtain a very accurate energy value. The reason that a specified structure has first to be obtained, is that the calculation is performed at a fixed point on the potential energy curve. However, any combination of method and basis set can be used with this task.

7. Frequency Calculations

As can be seen from chapters 5, 6 and 7, various energy calculations have been carried out using both the Cerius 2 and the Spartan packages. However, these packages can also be used to calculate the expected frequencies of various species. The Cerius 2 package has been used here to obtain the frequencies of reactants and possible products for the siloxane experiments. The results of these calculations can be seen in more detail in chapters 6 and 7, however, an insight will be given here into how these calculations can be used to support experimentally obtained data.

The main focus here will be on the frequencies obtained for the parent compounds. Initially, frequency calculations were carried out on the cyclic siloxanes. Below is a spectrum of the calculated values compared to an experimental spectrum for hexamethylcyclotrisiloxane (D3).

Figure 2. Spectra of hexamethylcyclotrisiloxane

A). Experimentally obtained spectrum of D3 / N_2

B). A spectrum of calculated frequencies of D3

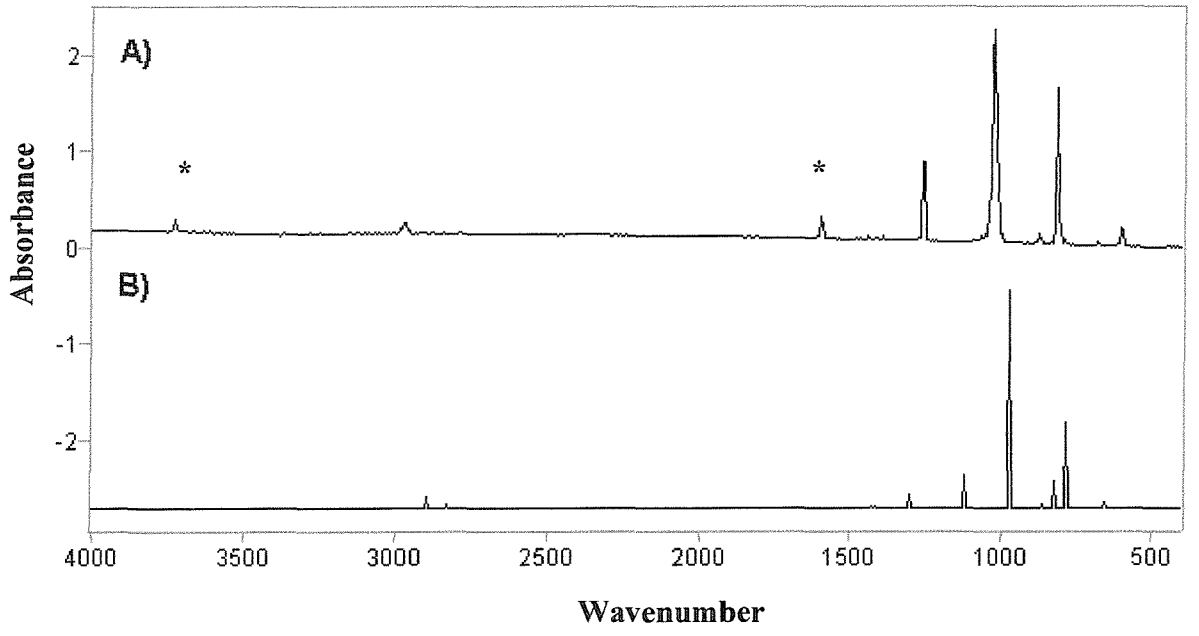

The spectra above demonstrate how accurate the frequency calculations can be. The spectrum of the calculated frequencies is in very good agreement with the spectrum obtained experimentally. Even the calculated infrared intensities agree well with true experimental values.

It was then decided to compare the results of the frequency calculations for the cyclic siloxanes, with the results for the linear siloxanes. The first linear siloxane to be pyrolysed was chosen to be used here as an example. Below is a comparison of the two spectra obtained for 1,1,3,3-tetramethyldisiloxane.

Figure 3. Spectra of 1,1,3,3-tetramethyldisiloxane

A). Experimentally obtained spectrum of L1 / N_2

B). A spectrum of calculated frequencies of L1

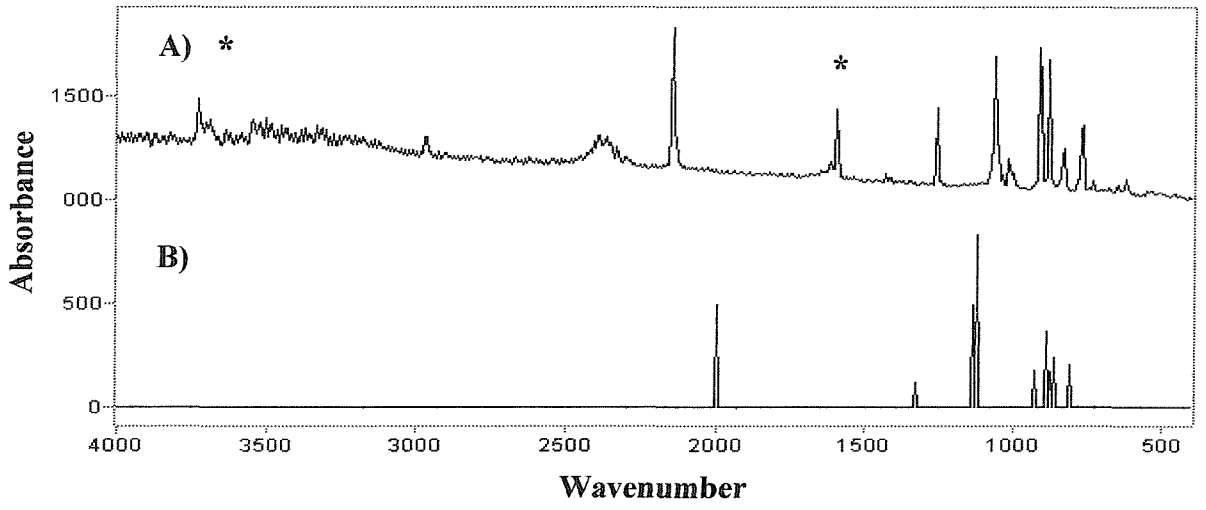

It was found that the linear siloxanes produced more complicated spectra than those of the cyclic siloxanes. In the above spectra (Figure 3), although below 1000 cm^{-1} the two spectra are seen to agree well, this was not the case around the 2000 cm^{-1} mark. This region contains bands due to Si-H bonds. It appears that the calculated spectrum has produced bands that are much lower in frequency than the bands produced in the experimental spectrum. It would appear that *ab initio* methods may not be relied upon for accurate frequency values for the Si-H bond in molecules such as these.

8. References

1). Gaussian 94, Revision E.2, M. J. Frisch, G. W. Trucks, H. B. Schlegel, P. M. W. Gill, B. G. Johnson, M. A. Robb, J. R. Cheeseman, T. Keith, G. A. Petersson, J. A. Montgomery, K. Raghavachari, M. A. Al-Laham, V. G. Zakrzewski, J. V. Ortiz, J. B. Foresman, J. Cioslowski, B. B. Stefanov, A. Nanayakkara, M. Challacombe, C. Y. Peng, P. Y. Ayala, W. Chen, M. W. Wong, J. L. Andres, E. S. Replogle, R. Gomperts, R. L. Martin, D. J. Fox, J. S. Binkley, D. J. Defrees, J. Baker, J. P. Stewart, M. Head-Gordon, C. Gonzalez, and J. A. Pople, Gaussian, Inc., Pittsburgh PA, 1995.

2). J. R. Foresman & A. Frisch, Exploring Chemistry with Electronic Structure, second edition, Gaussian Inc. Pittsburgh, PA, **(1996)**

3). A. Hinchliffe, Ab Initio Determination of Molecular Properties, IOP Publishing Ltd., **(1987)**

4). P. W. Atkins, Physical Chemistry, fourth edition, Oxford University Press, **(1992)**

5). C. E. Dykstra, Ab Initio Calculation of the Structures and Properties of Molecules, second edition, Elsevier Science Publishers, **(1990)**

6). P. Carsky & M. Urban, Ab Initio Calculations – Methods and Applications in Chemistry, Springer-Verlag, **(1980)**

CHAPTER FIVE

LASER KINETICS

1. Introduction

A series of gas kinetics experiments were carried out at the University of Reading. The silicon containing species, silylene (SiH_2) was chosen as the subject for these experiments as it is known to be a key intermediate in many organosilane compound breakdown processes. SiH_2 is known to readily insert into both Si-H and Si-O bonds[1]. Other characteristic reactions of SiH_2 include π-type addition, both to double and triple bonds and also to lone pair containing compounds.

It was decided to study the reactions of silylene and oxygen lone pair containing compounds, since these reactions possess the potential to yield species containing either Si-O or Si=O bonds. The substrates chosen for these experiments were oxygen, nitric oxide and oxetane.

In these experiments SiH_2 was produced from the flash photolysis of phenylsilane[2] ($PhSiH_3$).

Figure1. Photolysis of phenylsilane

$$PhSiH_3 + h\nu \longrightarrow PhH + SiH_2$$

The orbital diagrams of the lowest states of silylene can be seen below.

Figure 2. Orbital diagrams of the lowest states of silylene[1]

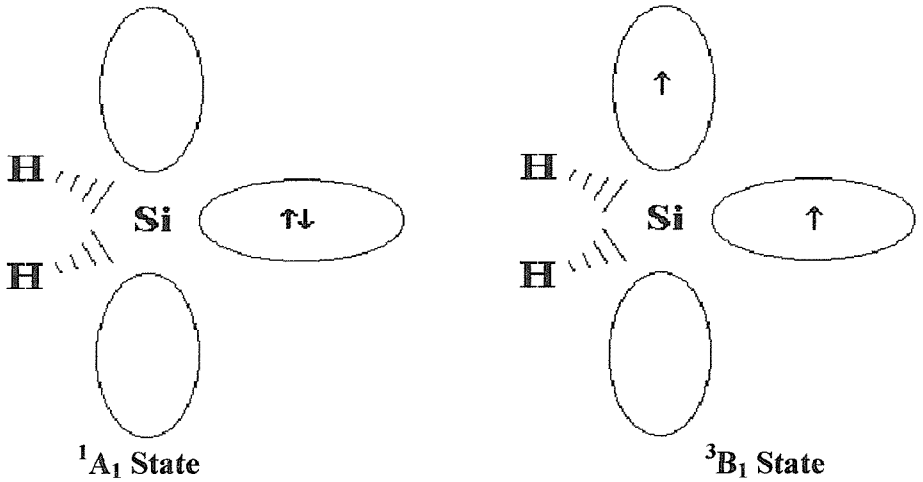

$^1A_1$ State — Closed Shell – Singlet State

$^3B_1$ State — Higher Energy – Triplet State

Inoue and Suzuki[2] were the first to measure the rate constants directly for silylene, using the method of photolysis of phenylsilane. The SiH_2 was detected by the technique of laser induced fluorescence, the emission being detected with the aid of a photomultiplier. Although sensitive,

this method required a restricted range of pressures due to the signal of the excited state fluorescence being quenched[3] at greater pressure ranges.

Jasinski[3] used an alternative method of Laser Resonance Absorption Flash Kinetics Spectroscopy (LRAFKS), which has been used throughout this research, in order to study the kinetics of silylene. This technique was found to be less affected by pressure quenching of the signal, although overall it is a slightly less sensitive method.

In 1995, Jasinski[3] obtained rate constants for the reactions of $SiH_2 + O_2$ at total pressures of 9.5, 5 and 1 Torr (He). However, these experiments were only conducted at a single temperature of 298 K. In 1988, Chu *et al.*[4] conducted experiments in order to obtain the rate constants for SiH_2 + NO at these same total pressures. Again, these experiments were conducted only at 298 K. Both sets of experiments have been repeated here using SF_6 as the buffer gas and the rate constants have been obtained over a range of temperatures and pressures.

2. Third Body Association Reactions

The three reactions that are discussed in this chapter are classed as association reactions. An association reaction is the joining together of two chemical species to form a single molecule[5].

If species **A** and **B** are reacted together, energy is released into the system as a new bond is formed. Since energy is conserved, the resultant species is a vibrationally excited molecule (**AB** *).

Third body association reactions involve an additional species that acts as an energy quencher, **M**. The reactions below show third body association reactions for the reactions studied here, where the substrate is represented by **X** = oxygen, nitric oxide or oxetane. The schematic diagram can be used to explain the degree of pressure dependency associated with each of these reactions.

Figure 3. Reactions showing the quenching of an excited species

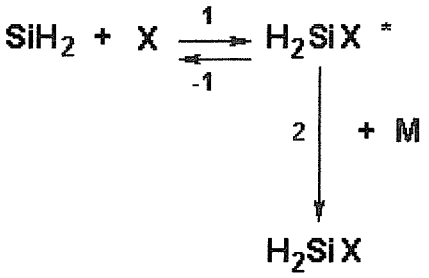

In step 1, silylene reacts with the substrate **X**, to form a vibrationally excited species, SiH_2X^*. If the reaction is pressure independent, then the excited species will be quenched by the buffer gas, **M**, so as to deactivate it and then proceed to form products, thereby following the route of step 2. This will depend on the binding strengths of the excited species but the reaction will be non-reversible. However, if the reaction is pressure dependent, then step 1 will be reversed so as to follow step –1 that is, before collision with **M**, all of the energy within SiH_2X will flow back to the bond, resulting in unimolecular redissociation. This is most likely to occur at low pressures. At higher pressures, there is a greater chance of collision and therefore, a greater possibility that the vibrationally excited species will be stabilised and thereby form products as shown in step 2.

The effectiveness of the buffer gas, M, will depend on its molecular weight and complexity. The graph below demonstrates the efficiency of various buffer gases.

Figure 4. Graph showing the order of effectiveness of third body colliders

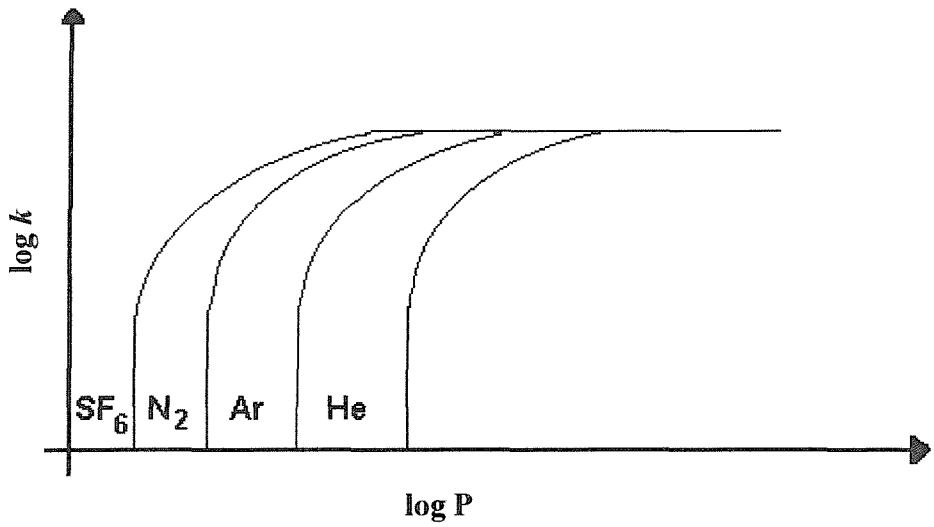

SF_6 has been used as the buffer gas for all the work carried out within this chapter. In comparing SF_6 to other buffer gases, such as helium, it has been found experimentally that SF_6 is a more effective collider[6]. The graph above shows that SF_6 will quench a vibrationally excited species at a much lower pressure than the other buffer gases shown.

Third body associations may be fully interpreted with the aid of the RRKM theory. However, this was beyond the time limit and scope of the work conducted here.

3. Silylene & Oxygen

3.1. Results

Silylene (SiH_2) has been prepared for this set of experiments by the flash photolysis[7] of phenylsilane at 193 nm. The technique of LRAFKS is the most commonly used for the study of kinetics of SiH_2 species. Here, silylene has been reacted with oxygen. This reaction occurs rapidly, due to the presence of a divalent silicon atom within silylene, which results in a highly reactive transient species. Experiments were carried out at temperatures of 296 K, 340 K, 398 K, 477 K and 594 K and at total pressures of 1, 3, 10, 30 and 100 Torr. For each run, the partial pressure of the precursor remained constant, while the partial pressure of the substrate, varied. Below in Figure 5 are plots showing the dependence of the rate constants k_{obs} on the concentration of the substrate, O_2.

Figure 5. Second-order plots of the dependence of k_{obs} on O_2 pressure at 297 K

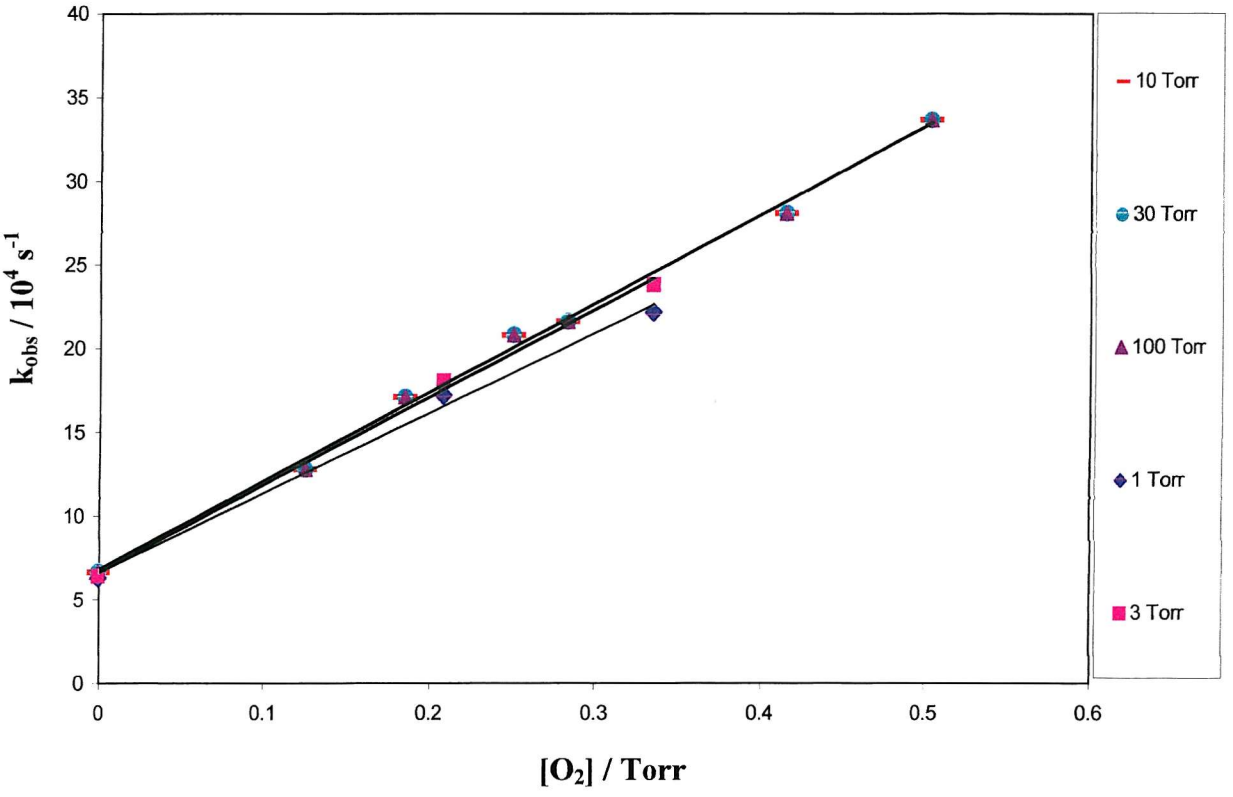

The rate constants are obtained using the Least-Linear-Squares fittings to these plots. The error limits associated with these rate constants are single standard deviations. It can be seen above that there is no pressure dependence.

3.1.(a). Pressure Dependence

The second order rate constants obtained by Linear-Least-Squares fittings can be seen in the table below, for a temperature of 297 K. From Table 1, it can be seen that the rate constants initially increase as the pressure increases. Therefore, it can be said that a very weak pressure dependence is observed.

Table 1. Tabulated values of total pressures and rate constants for $SiH_2 + O_2$ at 297 K

Total pressure / Torr	Rate constant (k) ($\times 10^{-11}$) / cm^3 $molecule^{-1}$ s^{-1}
100	1.64 ± 0.03
30	1.64 ± 0.03
10	1.64 ± 0.03
3	1.62 ± 0.06
1	1.48 ± 0.07

Upon varying the total pressure, a series of pressure dependent plots were produced. In Figure 6, $\log_{10} k$ has been plotted against $\log_{10}$ P.

Figure 6. Pressure dependent plots for the reactions of $SiH_2 + O_2$ at five temperatures.

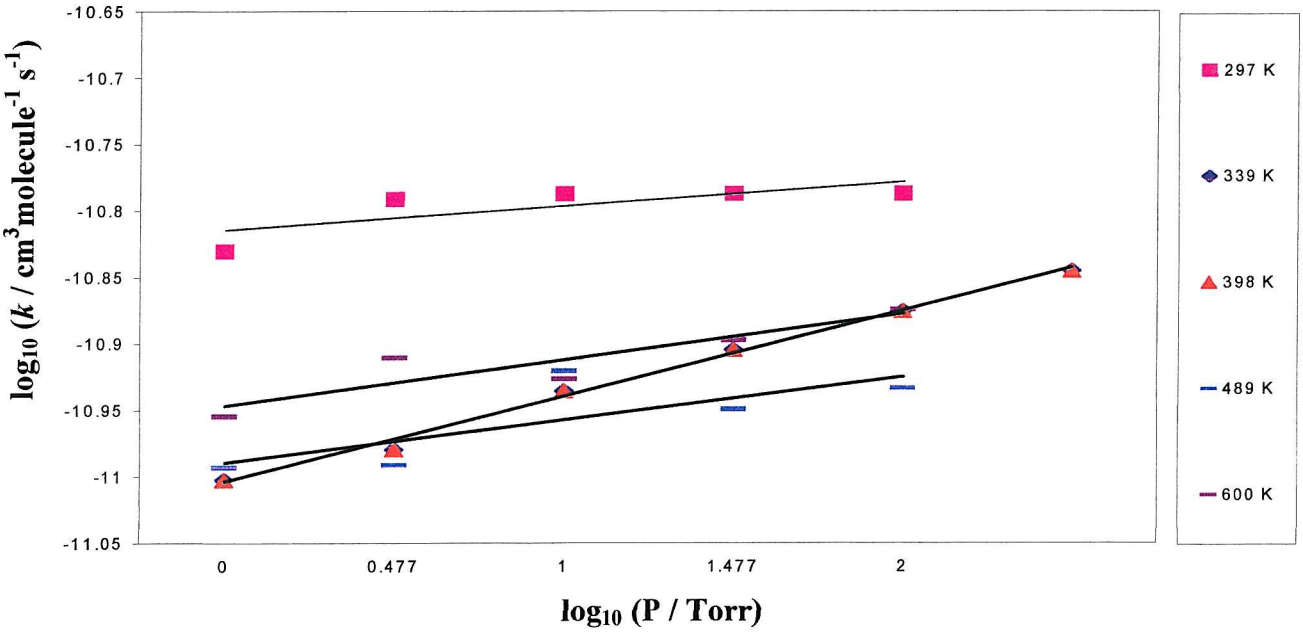

3.1.(b). Temperature Dependence

The rate constants obtained at 10 Torr for various pressures are tabulated below. Again, only a very slight change in the values of the rate constants is seen when the temperature is varied.

Table 2. Tabulated rate constant values obtained at various temperatures and at a total pressure of 10 Torr for the reaction of $SiH_2 + O_2$

T/K	Rate constant (*k*) ($\times 10^{-11}$/ cm^3 $molecule^{-1}$ s^{-1})
297	1.64 ± 0.03
339	1.43 ± 0.02
398	1.25 ± 0.02
489	1.20 ± 0.03
600	1.19 ± 0.04

The $\log_{10}$ of these rate constants are then plotted against 1/T in an Arrhenius plot in order to obtain the activation energy **(Ea)** and the **A** factor. Below can be seen the graph of 10^3 K / *T* against $\log_{10} k$:

Figure 7. An Arrhenius plot for the reaction of $SiH_2 + O_2$ at 10 Torr total pressure and at five temperatures

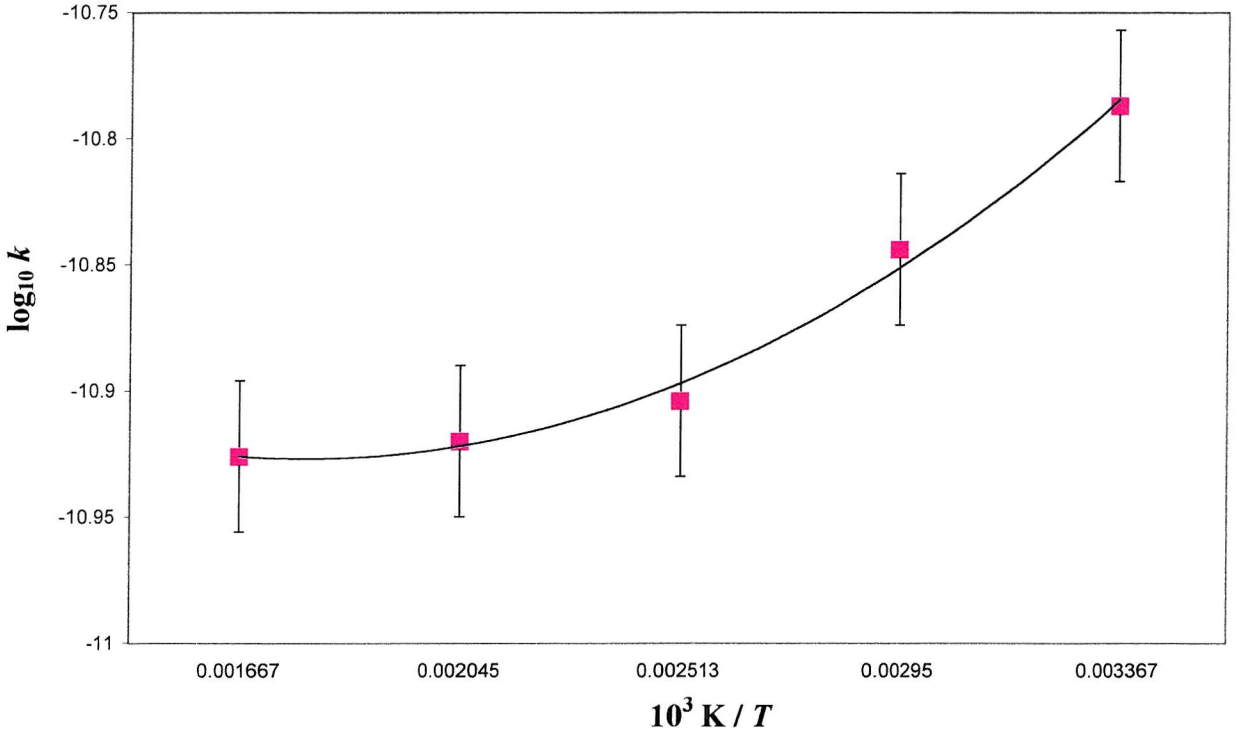

From the graph it can be seen clearly that the difference between the first and last point is very small. This indicates that the reaction of $SiH_2 + O_2$ shows only a very weak temperature dependence.

From the Linear-Least-Squares program, the average activation energy is calculated from the gradient obtained. The average **A** factor is calculated from the antilog of the intercept.

$$\textbf{Intercept} = \log_{10}(A / \text{cm}^3\,\text{molecule}^{-1}\,\text{s}^{-1}) = -11.08 \pm 0.04$$

$$\therefore \quad A = 8.32 \times 10^{-12}\ \text{cm}^3\,\text{molecule}^{-1}\,\text{s}^{-1}$$

$$\textbf{Gradient} = 8.210 \pm 0.1 \times 10^{-2}$$

$$\therefore \quad E_a = -1.572 \pm 0.32 \times 10^3\ \text{J mol}^{-1}$$

The activation energy of the reaction is found to be very close to zero. This suggests that the reaction has no barrier. It was reported by Chu[4] *et al.* that there was a weak pressure dependence at room temperature and at 9.5 Torr (He) for the reaction of silylene and oxygen. The rate constant that was recorded was of a value of $1.40 \pm 0.20 \times 10^{-11}$ cm^3 molecule^{-1} s^{-1}. This literature value compares with the experimental value that was obtained here of $1.64 \pm 0.03 \times 10^{-11}$ cm^3 molecule^{-1} s^{-1} at 10 Torr (SF_6) at room temperature. From this comparison, it might be deduced that the results obtained with SF_6 as the buffer gas gave a faster rate constant but since the reaction is almost pressure independent, this difference may be due to experimental scatter.

3.1.(c). Energy and Pathway Calculations

Molecular modelling calculations were conducted in an attempt to identify the most favourable pathway for the reaction. These calculations were carried out using the Gaussian 94 program[8] and the Cerius 2 package, in order to identify the most energetically stable species with the least positive value of ΔE. The highest theory combination of basis set and method were used in each case to produce the most accurate model chemistry[9]. A molecular modelling program called Spartan was also used in order to calculate the most energetically feasible transition state. When using Spartan to obtain the most favourable transition state for $SiH_2 + O_2$ only one of the attempts proved successful. The reaction that resulted is shown below:

Figure 8. Calculated reaction pathway and transition state for the reaction of $SiH_2 + O_2$

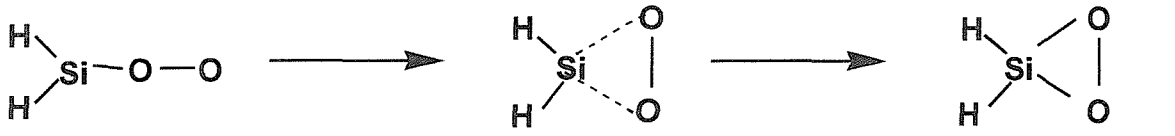

Reactant
-439.700 Hartrees

Transition State
-439.296 Hartrees

Product
-439.707 Hartrees

The initial adduct was calculated to have an almost linear geometry. The above calculations were carried out at the HF / 6-31G (d) level of theory. General energy calculations were then carried out using Cerius 2 in order to aid the identification of the possible products formed. The table below shows energy values obtained for the formation of possible intermediates and products

Table 3. Tabulated energy values of possible products for the reaction of silylene and oxygen

	Geometry Optimisation and Frequency Calculations E / Hartrees		Singlepoint Energy Calculations E / Hartrees			
Reaction Products	**HF / 3-21G**	**B3LYP / 6-31G (d)**	**HF / 3-21G**	**B3LYP / 6-31G (d)**	**ΔE * / Hartrees**	**ΔE / kcal mol^{-1}**
$H_2Si + O_2$	-437.171	-440.871	-	-	0	0
H_2SiO_2	-437.329	-440.955	-	-	-0.084	-52.7
H_2SiO_2 (cyclic)	-437.356	-441.057	-	-	-0.186	-116.7
HSiO(OH)	-437.460	-441.173	-	-	-0.302	-189.5
$SiO + H_2O$	-437.432	-441.129	-	-	-0.258	-161.9
$SiO_2 + H_2$	-	-	-437.345	-441.102	-	-

* ΔE values for the B3LYP / 6-31G (d) level of theory.

The highest level of theory from the above table (B3LYP / 6-31G (d)) was used to calculate the ΔE values. These energy values are represented more clearly in the form of an energy diagram seen below:

Figure 9. An energy diagram (kcal mol^{-1}) for the possible products for the reaction of silylene and oxygen

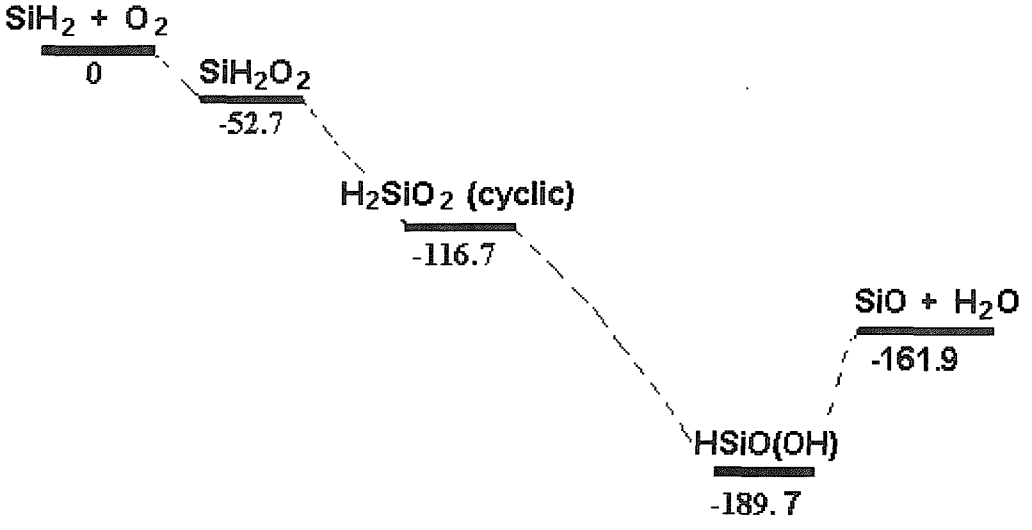

The resultant reaction that is thought to occur can be seen below:

Figure 10. Suggested reaction sequence from the results of the molecular modelling calculations

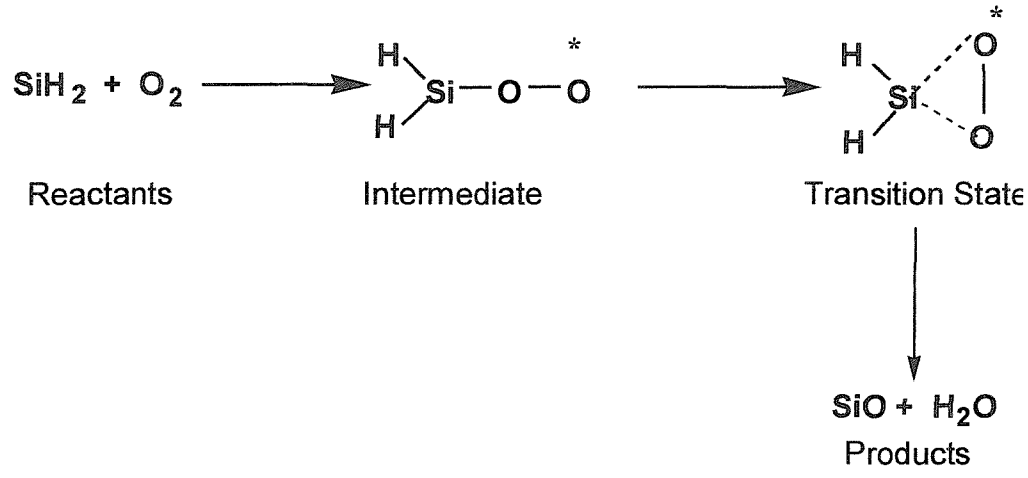

3.2. Discussion and Conclusion

To conclude, it can be seen from the pressure dependent plots (see Figure 6) that the reaction of $SiH_2 + O_2$ shows only a weak pressure dependence. The Arrhenius plot in Figure 7 also shows the presence of only a very weak temperature dependence.

Since the reaction is shown not to be very pressure dependent, the reverse of any intermediates cannot be very significant. Therefore, it is likely that the reaction is going to completion to form a product[5]. The following equation demonstrates a weak pressure dependence:

Figure 11. Reaction of $SiH_2 + O_2$ showing a weak pressure dependence

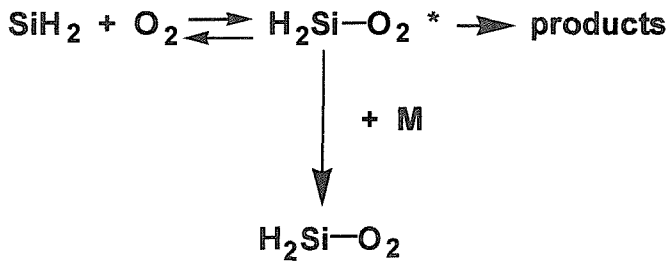

The fact that the reaction of $SiH_2 + O_2$ is shown to be almost pressure and temperature independent increases the difficulty of interpreting the pathway and therefore identifying the products formed. However, with the aid of the molecular modelling calculations, the resultant energy diagram shown in Figure 9 suggests that the reaction proceeds via a linear intermediate species and a cyclic transition state to produce the final products of SiO and H_2O.

In Figure 9, because the first three steps are so exothermic, all intermediates are likely to be produced with high vibrational energy. This will mean that any barriers in the last step (leading to SiO formation) will probably be easily overcome. There was not time in this project to undertake calculations of these barriers.

From the Arrhenius plot, it can be seen that the reaction proceeds with a negative activation energy. A situation where a negative activation energy results, indicates that a collision between the vibrationally excited species (SiH_2X^*) and the collider, (M), would result in an energy transfer from M to SiH_2X^*. This excess energy would be distributed within the internal coordinates of SiH_2X^*, resulting in dissociation to form further complexes or products.

4. Silylene & Nitric Oxide

4.1. Results

The second system to be investigated using the technique of LRAFKS was silylene and nitric oxide. These experiments were carried out at temperatures of 299 K, 337 K, 397 K, 479 K and 592 K and at total pressures of 1, 3, 10, 30 and 100 Torr. For each run, the partial pressure of the precursor remained constant, while the partial pressure of the substrate, varied. Below in Figure 12 are plots showing the dependence of the rate constant, k_{obs} on the concentration of the substrate, NO.

Figure 12. Second-order plots of the dependence of k_{obs} on NO pressure at 299 K

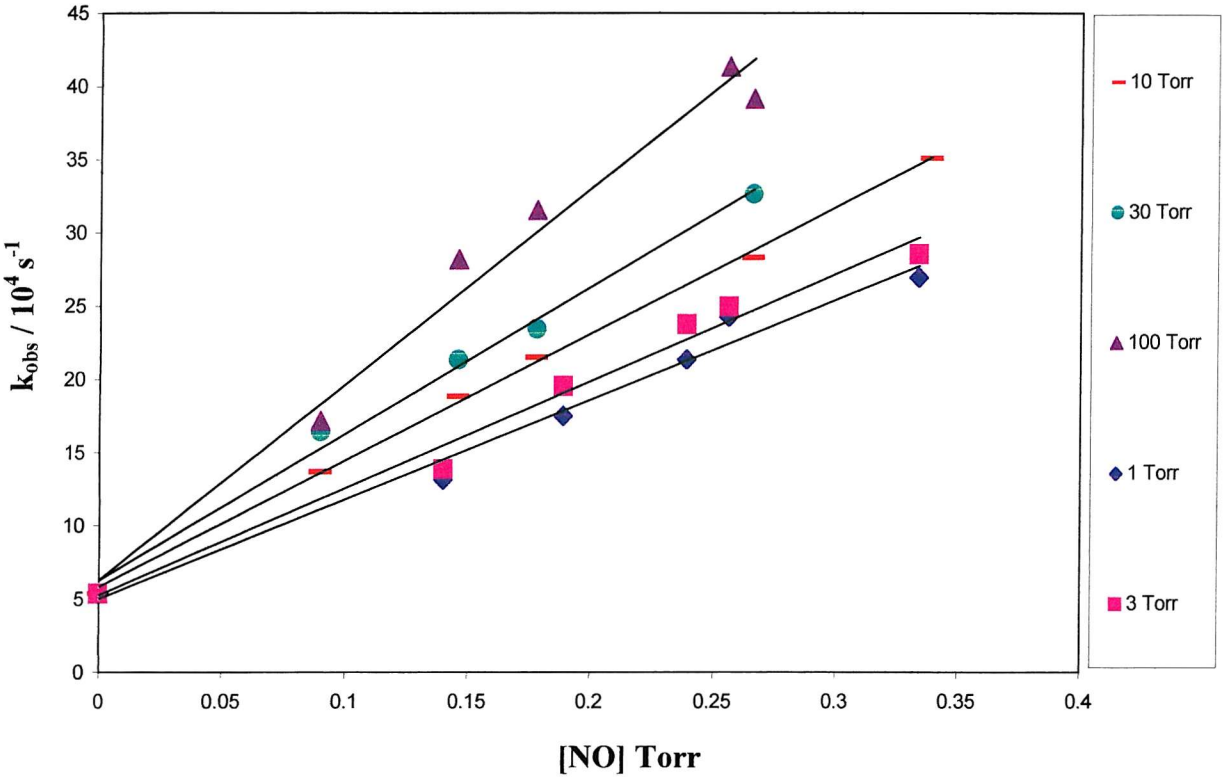

4.1.(a). Pressure Dependence

Upon varying the total pressure, a series of linear plots were produced, showing a pressure dependence. The second order rate constants obtained by Linear-Least-Squares fittings can be seen in Table 4, for a temperature of 299 K. Log_{10} *k* has been plotted against log_{10} P in Figure 12.

Table 4. Tabulated rate constant values obtained upon varying the pressure at a temperature of 299 K for the reaction of SiH_2 + NO

Total pressure / Torr	Rate constant (k) ($\times 10^{-11}$) / cm^3 $molecule^{-1}$ s^{-1}
100	3.98 ± 0.20
30	3.21 ± 0.08
10	2.71 ± 0.03
3	2.07 ± 0.07
1	2.25 ± 0.07

From the above table and Figure 13, it can be seen that a moderate pressure dependence is observed, as the rate constants obtained increase slightly in value as the pressure is increased.

Figure 13. Pressure dependent plots for the reaction of SiH_2 + NO at five temperatures

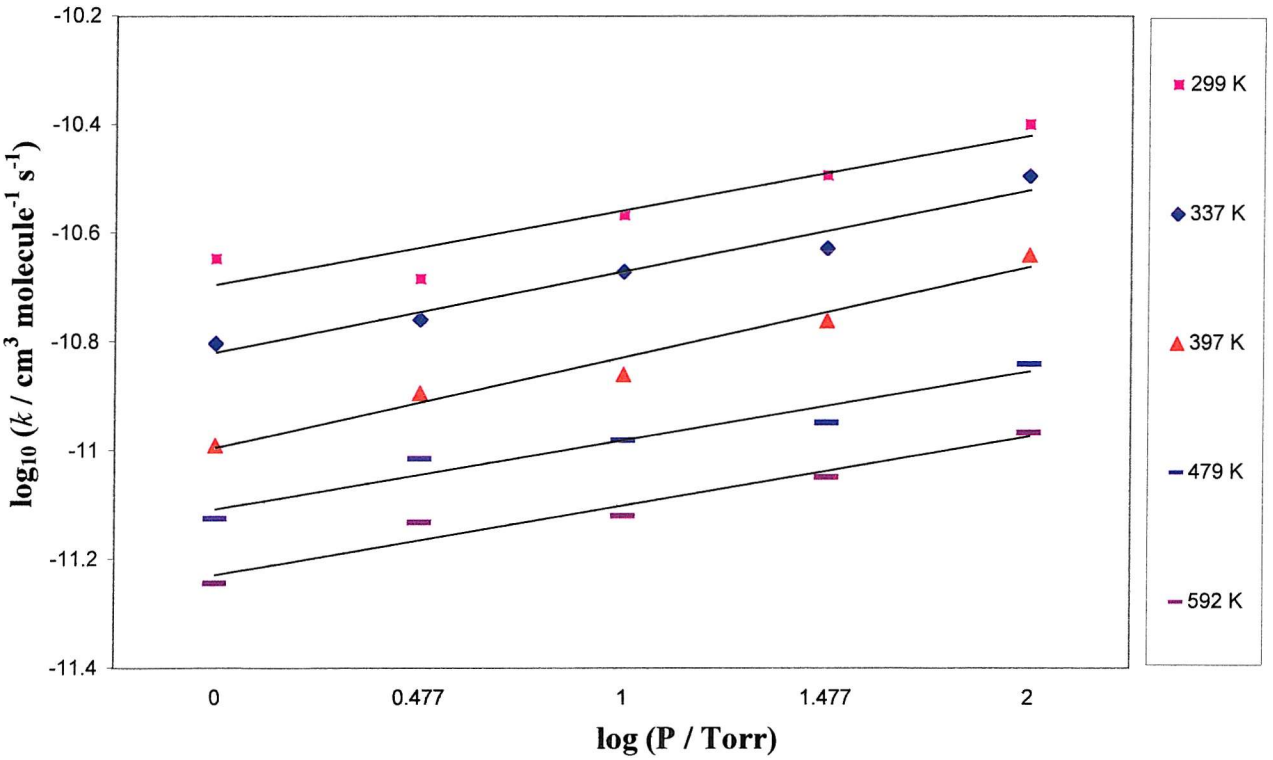

4.1.(b). Temperature Dependence

The rate constants were then studied to see if there was an effect on increasing the temperature.

Table 5. Tabulated rate constant values obtained upon varying the temperature at a total pressure of 10 Torr for the reaction of SiH_2 + NO

T/K	Rate constant (k) (x 10^{-11}) / cm^3 $molecule^{-1}$ s^{-1} SiH_2 + NO
299	2.71 ± 0.03
337	2.13 ± 0.22
397	1.38 ± 0.03
479	1.05 ± 0.02
592	0.76 ± 0.21

The $\log_{10}$ of these rate constants were then plotted against 1/T in an Arrhenius plot (see Figure 14), in order to obtain the activation energy (E_a) and the **A** factor.

Figure 14. An Arrhenius plot for the reaction of SiH_2 + NO at 10 Torr total pressure and at five temperatures

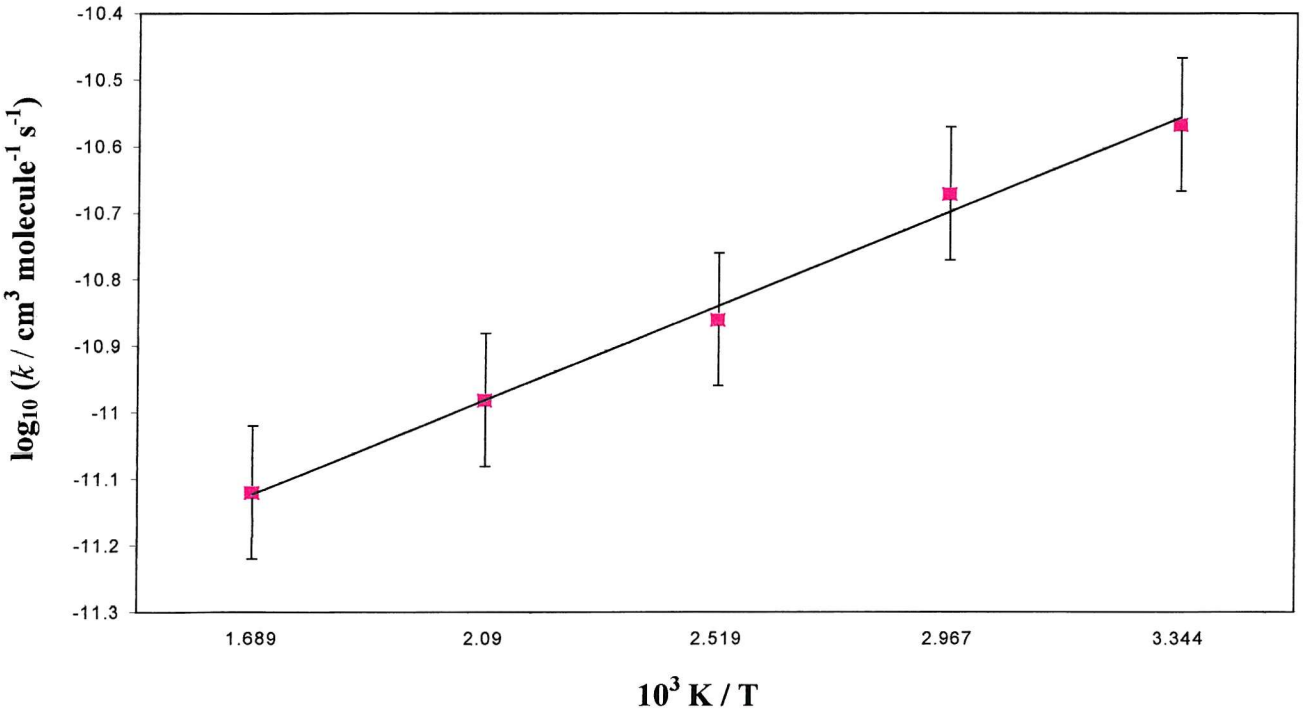

The Arrhenius plot shows that a significant temperature dependence exists, as the rate constant is seen to decrease as the temperature increases.

From the Linear-Least-Squares program, the average activation energy was calculated from the gradient obtained, and the average **A** factor was calculated from the antilog of the intercept. From the Arrhenius plot, the following values were obtained for the reaction of SiH_2 + NO at 10 Torr total pressure:

$$\textbf{Intercept} = \log_{10}(A / \text{cm}^3\ \text{molecule}^{-1}\ \text{s}^{-1}) = -11.69 \pm 0.03$$

$$\therefore \quad A = 2.04 \times 10^{-12}\ \text{cm}^3\ \text{molecule}^{-1}\ \text{s}^{-1}$$

$$\textbf{Gradient} = 3.39 \pm 0.12 \times 10^{-2}$$

$$\therefore \quad E_a = -6.49 \pm 0.22 \times 10^3\ \text{J mol}^{-1}$$

From the results obtained, the reaction of silylene and nitric oxide is seen to proceed with a significant negative activation energy. This means that the reaction has no barrier and there maybe an important intermediate complex.

Chu *et al*[4] studied the reaction of silylene and nitric oxide by LRAFKS. However, helium was used as the buffer gas. Chu reported that this reaction produced a rate constant of $1.5 \pm 0.2 \times 10^{-11}$ cm^3 $molecule^{-1}$ s^{-1} at room temperature for 1 Torr total pressure. This compares with a value obtained here (using SF_6 as the buffer gas) of $2.25 \pm 0.73 \times 10^{-11}$ cm^3 $molecule^{-1}$ s^{-1}. The difference between these two values can be attributed to the difference in collisional efficiencies between the two buffer gases used. The reaction is shown to be faster when SF_6 is used as the buffer gas. This is because SF_6 is more complicated a molecule than He and therefore has more internal modes in which the excess energy can be distributed. This situation is different here than for $SiH_2 + O_2$, because the reaction of SiH_2 + NO is pressure dependent. On further comparing the two sets of rate constants obtained at a total pressure of approximately 10 Torr, a difference is again observed of ~ 0.6×10^{-11} cm^3 $molecule^{-1}$ s^{-1}.

Literature Value[4]: $2.1 \pm 0.2 \times 10^{-11}$ cm^3 $molecule^{-1}$ s^{-1} at 9.5 Torr (He)

Experimental Value: $2.7 \pm 0.03 \times 10^{-11}$ cm^3 $molecule^{-1}$ s^{-1} at 10 Torr (SF_6)

Both sets of data indicate that the reaction of silylene and nitric oxide is weakly pressure dependent.

As an additional comparison, the data for the carbon analogue[10] [11] to the SiH_2 reaction is also cited here:

Figure 15. Analogue reaction to SiH_2

$CH_2 + NO \rightarrow$ product

The reaction of methylene ($^1A_1$) and nitric oxide has been carried out in this example also with helium as the buffer gas. This reaction proceeds at a rate of $1.6 \pm 0.10 \times 10^{-11}$ cm^3 $molecule^{-1}$ s^{-1}. This reaction however, appears to be pressure independent. Although the silylene reaction is slightly faster at higher pressures, the results are comparable. The products of the methylene reaction are not reported.

4.1.(c). Energy and Pathway Calculations

It is reasonable to assume that one of the following reactions may occur during the reaction of SiH_2 with NO.

Figure 16. Schematic diagram of possible intermediates formed for the reaction of SiH_2 + NO

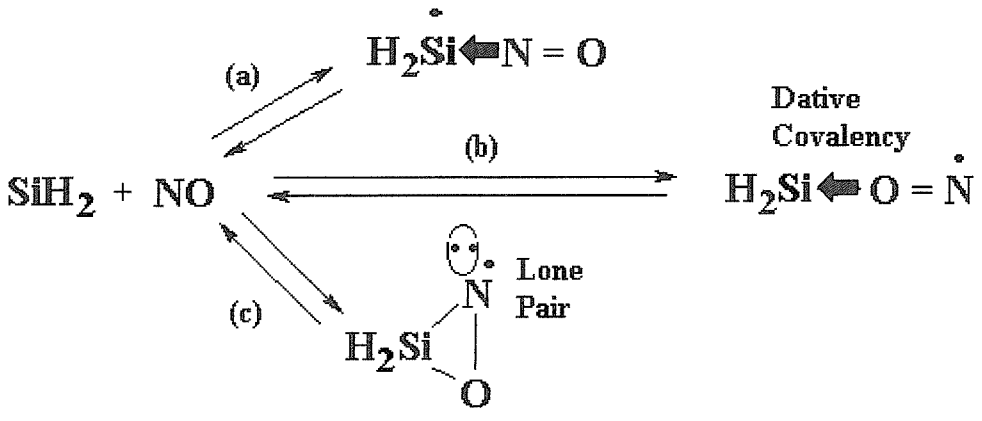

The suggested schematic diagram in Figure 16 was used to aid the search for a low energy intermediate. Figure 17 (a)–(c) shows three possible initial complexes. The deciding factor in each case is the unknown strength of the H_2Si-NO bond. Using the Cerius 2 package and the Gaussian 94 program[8], a set of values were derived:

Figure 17. (a)–(c). Calculated energies for the structure of a reaction intermediate

-290.0772 Hartrees -129.5645 Hartrees -419.6689 Hartrees

ΔE = -0.2725 Hartrees ≡ -17.1 kcal / mol

-290.6131 Hartrees -129.8882 Hartrees -420.5226 Hartrees

ΔE = -0.0213 Hartrees ≡ -13.4 kcal / mol

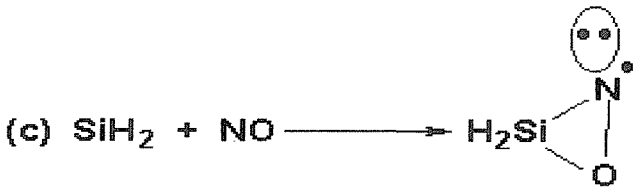

-290.6131 Hartrees -129.8882 Hartrees -420.5656 Hartrees

ΔE = -0.0643 Hartrees ≡ -40.3 kcal / mol

In each case, the highest level calculation possible was undertaken. In general, this was the B3LYP method and the 6-31G (d) basis set[9]. However, for the product of Figure 17 (a) **(H_2Si←N=O)**, the MP2 method and the 6-31G (d) basis set was employed, as this model chemistry was found to produce the most accurate values in the given time period.

From these calculations, the following reaction is the most likely to occur, producing the most feasible complex with the most negative value of ΔE:

18. **Reaction producing the most feasible intermediate**

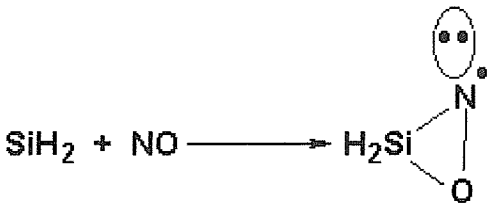

Since it is not clear as to whether a second complex is also produced, a further molecular modelling package known as Spartan was used to carry out additional *ab initio* calculations at the HF / 6-31G (d) level of theory.

Figure 19. Possible intermediate of the reaction of SiH_2 + NO

However, these calculations were this time carried out with the intent of calculating the reaction pathway of the formation of the complex formed. Therefore, the aim was identify whether the linear intermediate contained a Si-N bond or a Si-O bond, as suggested in Figure 19. This involved the formation of a transition state. The calculated values obtained from the two molecular modelling packages differ slightly due to the different programs used.

Figure 20. (a)-(b). Pathway calculations for the reaction of SiH_2 + NO

a).

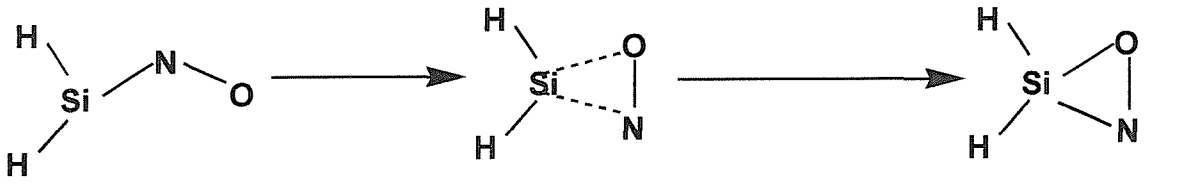

Reactant	Transition State	Product
-419.2860 Hartrees	-419.2116 Hartrees	-419.2912 Hartrees

b).

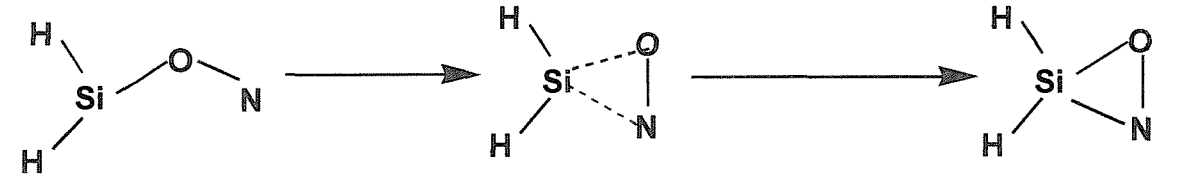

Reactant
-419.2112 Hartrees

Transition State
-419.2440 Hartrees

Product
-419.2912 Hartrees

Of the two reactions shown above, the most feasible reaction pathway producing the transition state that possessed the least positive value of ΔE is seen in equation 20 (b). This suggests that the oxygen atom end of NO is the most likely end to join to the silicon atom of silylene, since it has the least positive value of ΔE. From the formation of these complexes, further reactions are thought to take place resulting in dissociation of the intermediate. A similar reaction may occur for SiH_2 + NO as for the possible reactions of NH_2 + NO.

Figure 21. (a)-(c). Possible reactions of NH_2 + NO

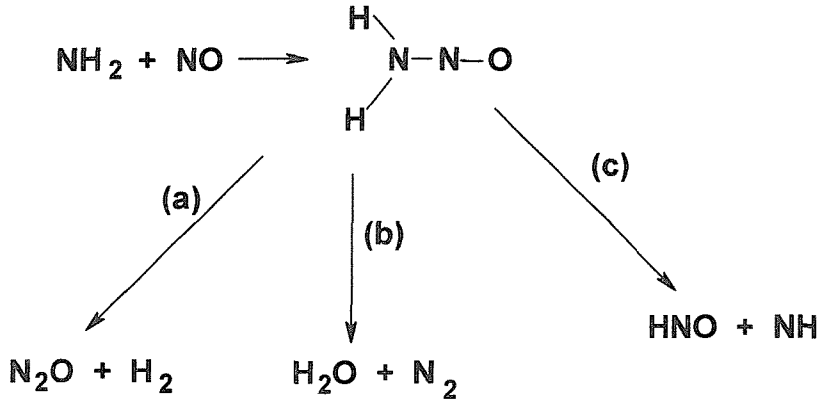

From the possible reactions of NH_2 + NO, a series of dissociation reactions and products have been suggested for SiH_2 + NO and molecular modelling calculations were carried out for many of these reactions in order to obtain energies to attempt to identify the most feasible of these reactions. Possible reactions of SiH_2 + NO and the calculated energies for the overall reactions are tabulated below:

Table 6. Calculated energies for possible reaction of SiH_2 + NO

Reactions of silylene and nitric oxide	Geometry Optimisation and Frequency Calculations E / Hartrees		
	HF / 3-21G	B3LYP / 6-31G (d)	ΔE / kcal mol^{-1}
(a). SiH_2 + NO → H_2 + SiNO	-0.012	-0.042	-26.36
(b). SiH_2 + NO → H_2O + SiN	0.013	-0.001	-0.63
(c). SiH_2 + NO → SiO + NH_2	0.101	0.070	43.93
(d). SiH_2 + NO → HSiO + NH	-	-	-
(e). SiH_2 + NO → OH + (HSiN) (HNSi)	-	-	- -

Calculations for the energies of reactions (d) and (e) were not able to be completed within the given time period. From the above energy calculation results, it was found that reaction (a) is the most favourable of these reactions, producing an energy value of: -26.36 kcal / mol.

Figure 22. Reaction producing most energetically favourable energy value

$$SiH_2 + NO \rightarrow H_2 + SiNO$$

A mechanism for this reaction has been investigated and a possible solution has been suggested:

Figure 23. Suggested mechanism for the most energetically favourable reaction

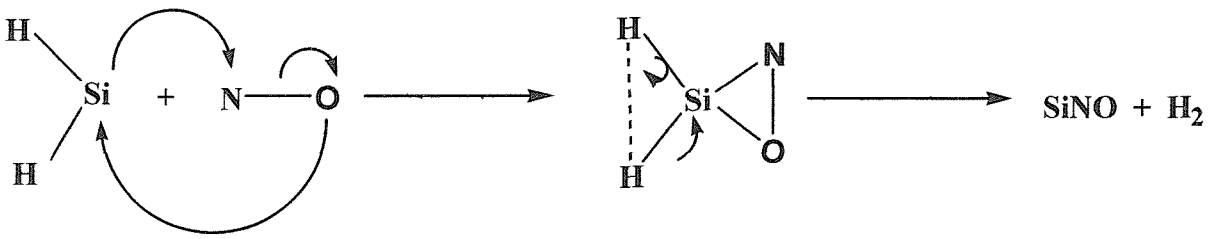

Table 7. Tabulated calculated energies of possible products of the reaction of SiH_2 + NO

	Geometry and Frequency Optimisation Calculations E / Hartrees					
Reaction Products	**HF / 3-21G**	**B3LYP / 6-31G (d)**	**HF / 6-31G (d)**	**MP2 / 6-31G (d)**	**ΔE * / Hartrees**	**ΔE / kcal mol^{-1}**
H_2Si + NO	-416.985	-420.501	-419.2477	-419.6417	0	0
H_2SiNO	-	-	-419.2693	-419.6689	-	-
H_2SiON	-417.064	-420.523	-419.2917	-419.6565	-0.022	-13.4
H_2SiON (cyclic)	-417.041	-420.566	-419.2912	-419.7084	-0.065	-40.3
H_2 + SiNO	-416.997	-420.543	-	-	-0.042	-26.4
H_2O + SiN	-416.972	-420.502	-	-	-0.001	-0.60
SiO + NH_2	-416.884	-420.432	-	-	0.069	43.3
OH+(HSiN) (NHSi)	-	-	-	-	-	-

* ΔE values for the B3LYP / 6-31G (d) level of theory.

The results from the energy values seen tabulated in Table 7 have been further interpreted in the form of an energy diagram in Figure 24:

Figure 24. Energy (kcal mol^{-1}) diagram for the reaction of SiH_2 + NO

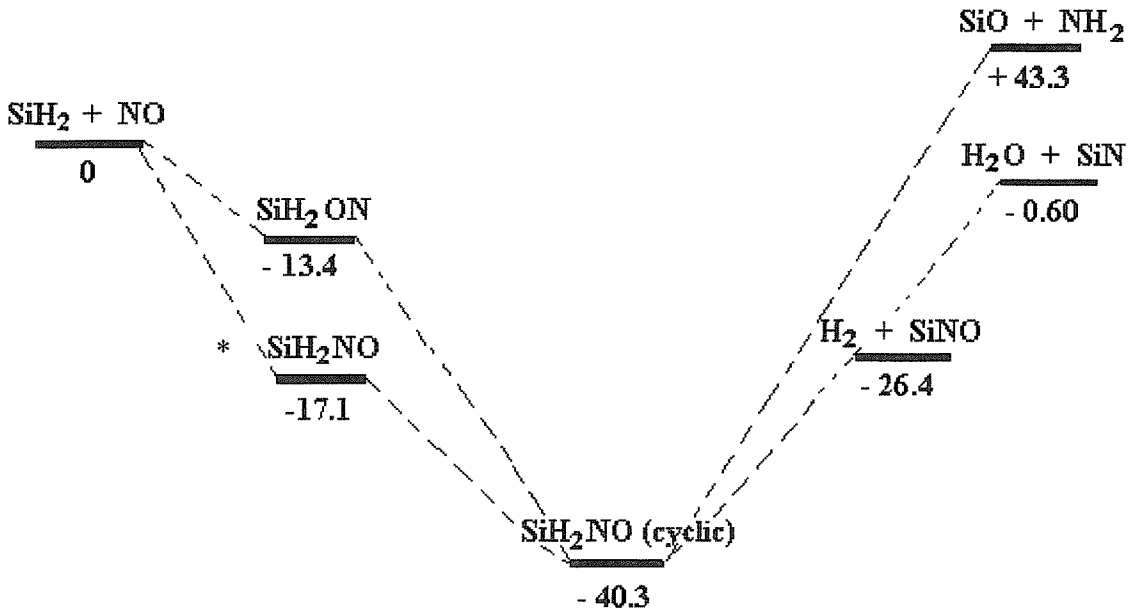

* Calculation conducted with the MP2 / 6-31G (d) level of theory.

From this energy diagram, it would appear that the reaction proceeds via the lowest energy intermediate, SiH_2ON (cyclic) and it then reacts further to produce the products also of the lowest energy, SiNO and H_2. These findings agree with the energy calculations that were carried out previously.

4.2. Conclusion

For the reaction of SiH_2 and NO, the resultant pressure dependence plots (Figure 13), reveal that this reaction proceeds with a moderate pressure dependence. The Arrhenius plots (Figure 14), show that a weak temperature dependence is also observed.

The third body association theory[5] can again be used to explain the pressure dependence observed.

Figure 25. Reaction of SiH_2 + NO showing moderate pressure dependence

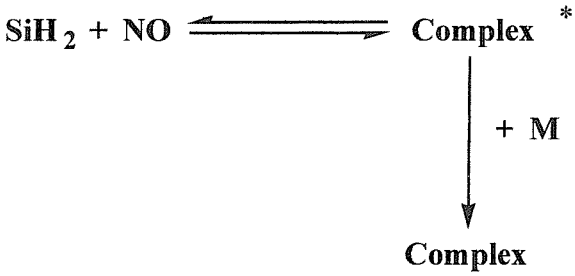

The molecular modelling calculations indicate that there are four stages to the reaction of SiH_2 + NO which were able to be deduced using both the Cerius 2 and the Spartan programs. The overall reaction that is thought to occur can be seen below:

Figure 26. Overall reaction of SiH_2 + NO

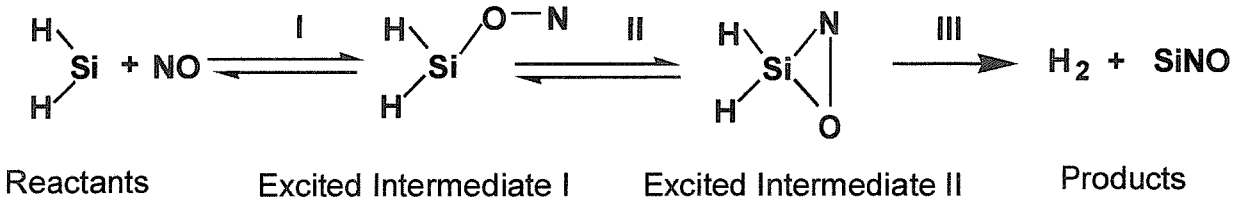

However, as it has already been seen, this reaction is pressure dependent and therefore highly reversible. It would therefore require the barrier to product formation to be low enough to permit competition.

5. Silylene & Oxetane

5.1. Results

These experiments were repeated for a new system. The reaction of silylene and oxetane was next to be investigated. The same total pressures were employed as for the previous system. For the silylene and oxetane experiments, there were slight differences in the average temperatures used. The temperatures recorded were 296 K, 340 K, 398 K, 477 K and 594 K.

The structure of oxetane is seen in Figure 27.

Figure 27. Structure of oxetane

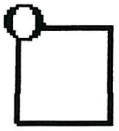

Below in Figure 28 are plots showing the dependence of the rate constant, k_{obs} on the concentration of the substrate, oxetane.

Figure 28. Second-order plots of the dependence of k_{obs} on oxetane pressure at 296 K

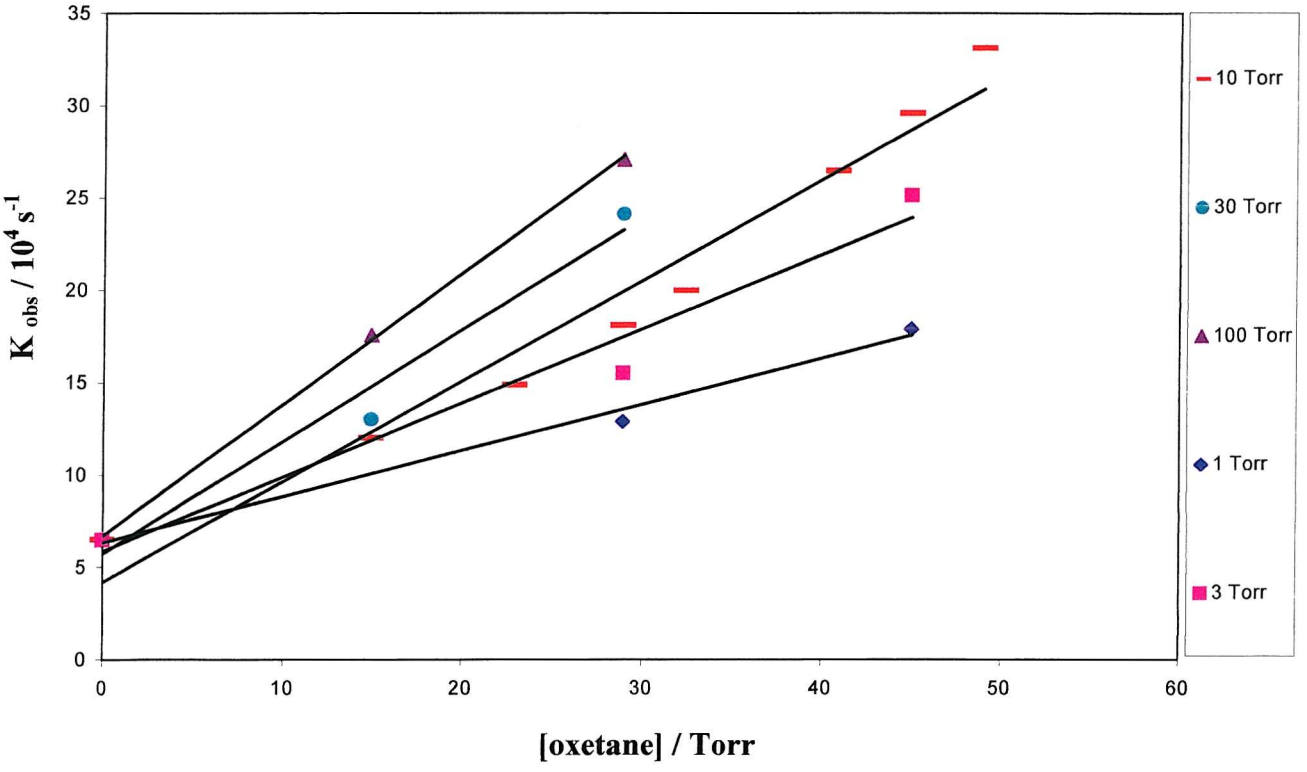

5.1.(a). Pressure Dependence

Upon varying the total pressure a moderate pressure dependence was again observed and is seen only slightly in excess of that for SiH_2 + NO. However, this pressure dependence was seen to decrease as the temperature increased. The pressures used, together with the second order rate constants obtained from the Linear-Least-Squares fittings, are tabulated below in Table 8.

Table 8. Tabulated rate constant values obtained at various pressures and at a temperature of 296 K for the reaction of SiH_2 + oxetane

Total pressure / Torr	Rate constant (k) ($\times 10^{-10}$) / cm^3 $molecule^{-1}$ s^{-1}
100	2.19 ± 0.03
30	1.80 ± 0.10
10	1.57 ± 0.10
3	1.20 ± 0.10
1	0.75 ± 0.36

The $\log_{10}$ of these rate constants ($\log_{10} k$), were then plotted against the $\log_{10}$ of the partial pressures of the substrate ($\log_{10} P$) in a second order plot. Figure 29 indicates how the pressure dependency varies with temperature. The graph shows clearly that there is a greater pressure dependence at lower temperatures, producing steeper plots.

Figure 29. Pressure dependent plots for the reaction of SiH_2 + oxetane at five temperatures

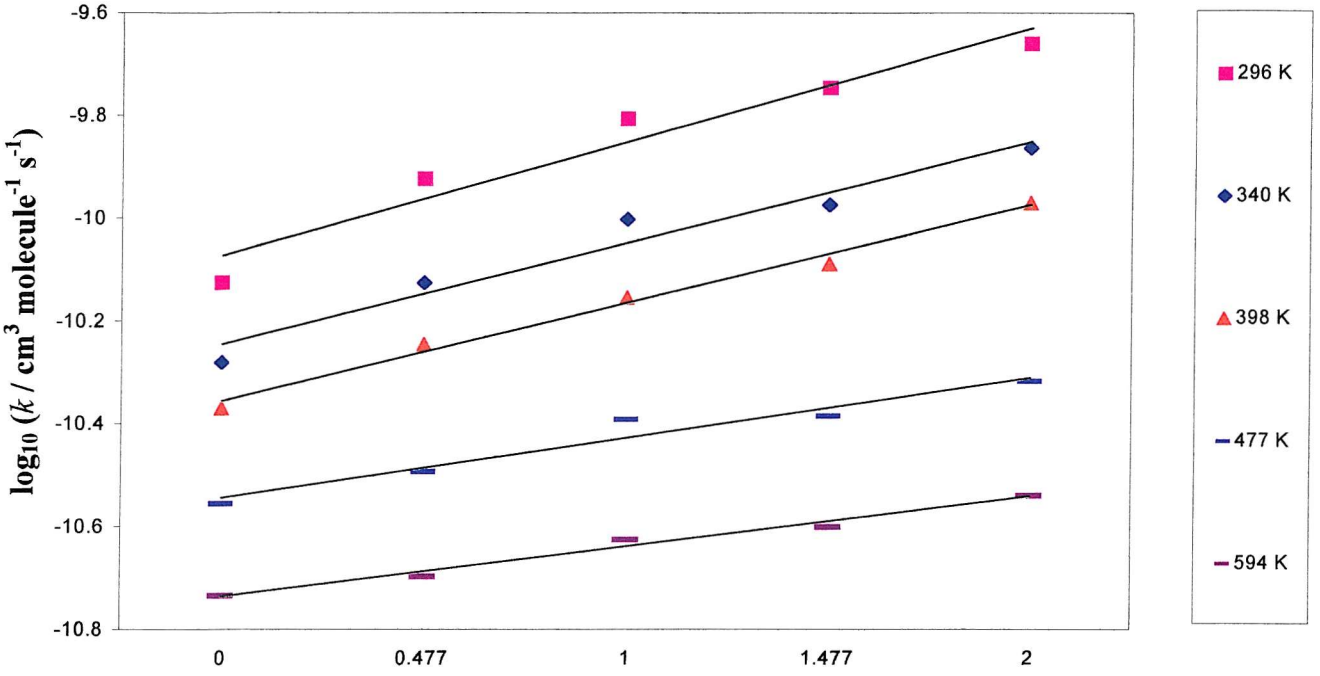

5.1.(b). Temperature Dependence

An Arrhenius graph was then plotted of $\log_{10} k$ against 1/T at five temperatures. The result was a reasonably steep slope as seen in Figure 30, showing a temperature dependence.

Figure 30. An Arrhenius plot for the reaction of SiH_2 + oxetane at 10 Torr total pressure and at five temperatures

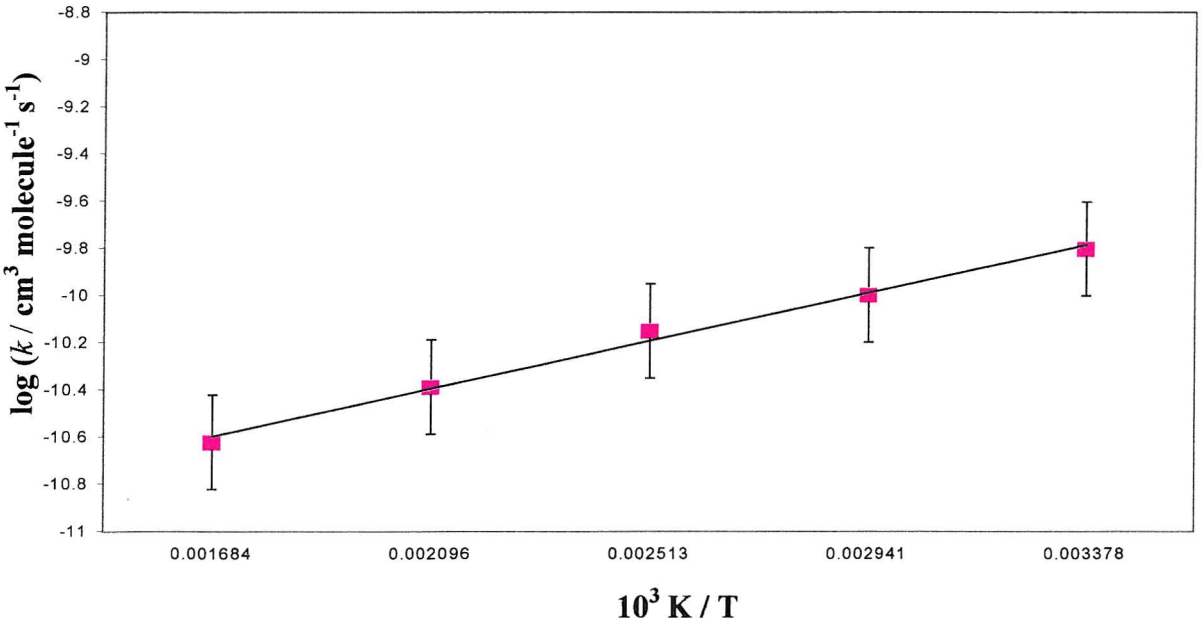

The Arrhenius equation was obtained from this graph. The **A** factor and the activation energy ($\mathbf{E_a}$), were calculated in the same way as previously described. The following values resulted at a total pressure of 10 Torr:

$$\textbf{Intercept} = \log_{10}(\mathbf{A} / \mathbf{cm^3\ molecule^{-1}\ s^{-1}}) = \mathbf{-11.14 \pm 0.07}$$

$$\therefore \quad \mathbf{A = 7.24 \times 10^{-12}\ cm^3\ molecule^{-1}\ s^{-1}}$$

$$\textbf{Gradient} = \mathbf{4.78 \pm 0.25 \times 10^2}$$

$$\therefore \quad \mathbf{E_a = -9.14 \pm 0.49 \times 10^3\ J\ mol^{-1}}$$

These values show that the reaction of silylene and oxetane proceeds at a fast rate and the negative activation energy suggests that there is no reaction barrier. Gu and Weber[12] investigated a similar reaction, reacting dimethylsilylene with oxetane. It was found that two products were produced. Allyloxydimethylsilane and 2,2-dimethyl-1-oxa-2-2-silacyclopentane were formed in yields of 38 % and 41 % respectively. The equation can be seen below:

Figure 31. The reaction of dimethylsilylene and oxetane

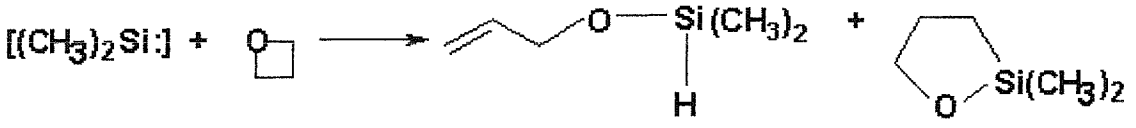

On the basis of this and the fact that the silylene is strongly attracted to the oxygen lone pairs, the mechanism for reaction of SiH_2 with oxetane is proposed in Figure 32.

Figure 32. Possible mechanisms for the reaction of silylene and oxetane

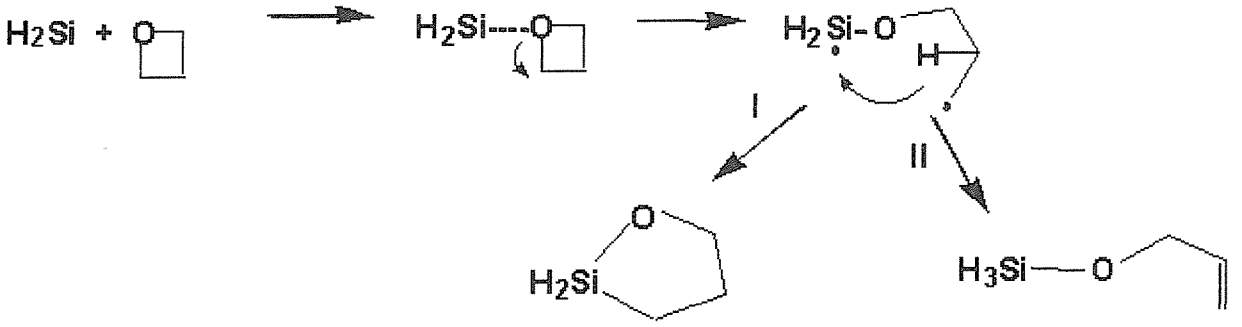

5.1.(c). Oxetane vs Oxirane

This work has also been compared to unpublished data by Becerra *et al.*[13] for silylene reacting with oxirane. For 10 Torr total pressure at a temperature of 294 K, Becerra *et al.* reported the rate constant to be $9.27 \pm 0.21 \times 10^{-11}$ cm^3 $molecule^{-1}$ s^{-1}. At 296 K, for the same total pressure the higher value of $1.57 \pm 0.10 \times 10^{-10}$ cm^3 $molecule^{-1}$ s^{-1} was obtained here for silylene reacting with oxetane. The full comparison is shown in Table 9.

Figure 33. Structure of oxirane

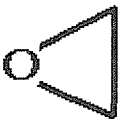

Both systems used SF_6 as the buffer gas. Tabulated rate constant values can be seen below for the two systems obtained at a total pressure of 10 Torr:

Table 9. A comparison of rate constant values of oxetane and oxirane obtained upon varying the temperature at a total pressure of 10 Torr

T / K	Rate constant (*k*) (x 10^{-11}) / cm^3 $molecule^{-1}$ s^{-1} SiH_2 + oxetane	*T* / K	Rate constant (*k*) (x 10^{-11}) / cm^3 $molecule^{-1}$ s^{-1} SiH_2 + oxirane
296	15.70 ± 0.10	294	9.27 ± 0.21
340	9.97 ± 0.30	357	6.54 ± 0.29
398	7.04 ± 0.21	398	4.31 ± 0.17
477	4.08 ± 0.19	478	2.82 ± 0.08
594	2.38 ± 0.09	603	2.08 ± 0.13

It can be seen from the above table, that both sets of systems were temperature dependent. It also shows that the reaction involving oxirane proceeds slightly slower than for those experiments with oxetane, although it should be noted that both systems are pressure dependent.

5.1.(d). Energy and Pathway Calculations

As a result of these experiments, it is thought that the reaction producing the intermediate shown below is likely to occur from the photolysis of SiH_2 + oxetane:

Figure 34. Schematic diagram of the formation of the intermediate for SiH_2 + Oxetane

Possible products and intermediates have been calculated and tabulated below. The level of theory used was B3LYP / 6-31G (d) except in the case of the linear product, where HF / 3-21G[9] was used.

Table 10. Tabulated energy values for possible products and intermediates

	Geometry Optimisation and Frequency Calculations E / Hartrees			
Reaction Products	**HF / 3-21G**	**B3LYP / 6-31G (d)**	**ΔE * / Hartrees**	**ΔE / kcal mol^{-1}**
H_2Si + Oxetane	**-479.323**	**-483.718**	**0**	**0**
$H_2SiOC_3H_6$ (intermediate)	**-479.378**	**-483.757**	**-0.039**	**-24.5**
$H_2SiOC_3H_6$ (cyclic)	**-479.491**	**-483.880**	**-0.162**	**-101.7**
$H_2SiOC_3H_6$ (linear)	**-479.394**	-	-	-

* ΔE values for the B3LYP / 6-31G (d) level of theory.

The energy calculations from the above values show that pathway **I** in Figure 32 was the most feasible reaction, with the most negative value of ΔE. Although pathway **II** was not calculated at the B3LYP / 6-31G (d) level of theory, at the HF / 3-21G (d) level of theory pathway **I** was seen to be more favourable than pathway **II**. This agrees with the experimental findings of Gu and Weber[12], who reported that pathway **I** produced the greater yield.

GC analytical experiments were attempted to try to find support for this mechanism. Product peaks were observed at the approximately expected retention times (ca. 15 minutes), but in the absence of authentic samples of the likely products, these could not be identified. It was verified that these peaks did not arise for photolysis of oxetane alone.

5.2. Conclusion

For the reaction of SiH_2 with oxetane, the resultant pressure dependent plots (Figure 29) show that the reaction was pressure dependent. The pressure dependence was seen to decrease with increasing temperature. The Arrhenius plots (Figure 30) also show a negative temperature dependence for the reaction. However, the oxirane reaction proceeds at a slightly slower rate than the oxetane reaction. Both reactions have negative activation energies and both are interpreted as occurring via donor-acceptor intermediate complexes. It is clear that these complexes must react further, otherwise the pressure dependences would become more pronounced as the temperature increased.

The fact that the pressure dependence decreases at higher temperatures, suggests that a product channel exists (see Figure 35). The third body association theory has been used below to explain the pressure dependence of the reactions of SiH_2 +  .

Figure 35. Reaction of SiH_2 + oxetane showing product channel

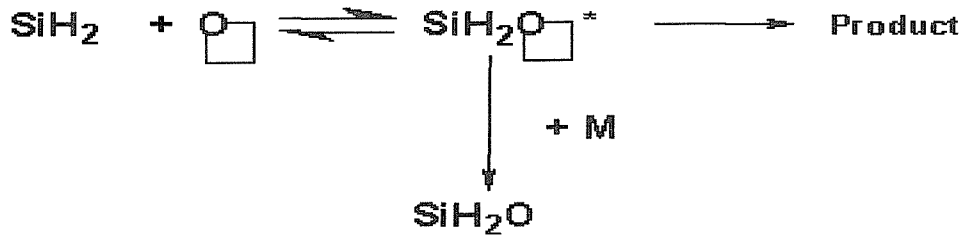

The molecular modelling calculations show that the following pathway is likely to occur:

Figure 36. Possible mechanism for the reaction of silylene and oxetane

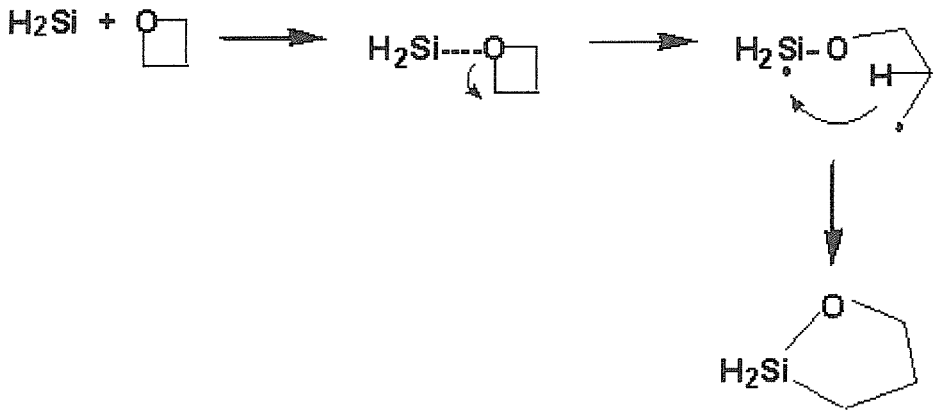

6. References

1). R. Becerra and R. Walsh, Kinetics and Mechanisms of Silylene Reactions: A Prototype for Gas-Phase Acid / Base Chemistry, Elsevier Science, **(1995)**, 263-326

2). G. Inoue and M. Suzuki, Chem., Phys., Lett., 105, **(1984)**, 641-644

3). J. M. Jasinski, J. Phys. Chem., 90, **(1986)**, 555-556

4). J. Chu, D. Beach, R. Estes and J. M. Jasinski, Chem. Phys. Lett., 143, **(1988)**, 135-139

5). M. J. Pilling and P. W. Seakins, Reaction Kinetics, Oxford Science Publications, Oxford University Press, **(1995)**

6). K. J. Laidler, Chemical Kinetics, Third edition, Harper & Row publishers, New York, **(1987)**

7). J.M. Jasinski, R.Becerra and R.Walsh, Chem. Rev., 95, **(1995)**, 1203-1228

8). Gaussian 94, Revision E.2, M. J. Frisch, G. W. Trucks, H. B. Schlegel, P. M. W. Gill, B. G. Johnson, M. A. Robb, J. R. Cheeseman, T. Keith, G. A. Petersson, J. A. Montgomery, K. Raghavachari, M. A. Al-Laham, V. G. Zakrzewski, J. V. Ortiz, J. B. Foresman, J. Cioslowski, B. B. Stefanov, A. Nanayakkara, M. Challacombe, C. Y. Peng, P. Y. Ayala, W. Chen, M. W. Wong, J. L. Andres, E. S. Replogle, R. Gomperts, R. L. Martin, D. J. Fox, J. S. Binkley, D. J. Defrees, J. Baker, J. P. Stewart, M. Head-Gordon, C. Gonzalez, and J. A. Pople, Gaussian, Inc., Pittsburgh PA, **(1995)**.

9). J. B. Foresman and A. Frisch, Exploring Chemistry with Electronic Structure Methods, second edition, Gaussian, Inc., Pittsburgh, PA, **(1996)**

10). A. H. Laufer and A. M. Bass, J. Phys. Chem., 78, **(1974)**, 1344 - 1248

11). A. O. Langford, H. Petek and C. B. Moore, J. Chem. Phys., 78, **(1983)**, 11-12

12). T-Y.Y. Gu and W. P. Weber, J Am. Chem. Soc., 102:5, **(1980)**, 1641-1644

13). R. Becerra, P. Cannady, R. Walsh, unpublished work

CHAPTER SIX

PYROLYSIS OF CYCLIC SILOXANES

1. Introduction

Siloxanes are important species in silicon chemistry within the chemical company, Dow Corning. A transient intermediate formed through the reactions of siloxanes and frequently used at Dow Corning, is dimethylsilanone, ($Me_2Si{=}O$). However, its production is a costly process. It was hoped that the pyrolysis of various siloxanes would lead to the discovery of a novel method for the formation of this molecule. Initially a number of cyclic siloxanes were pyrolysed. If the pyrolysis of the parent cyclic siloxane compounds and the isolation of any reactive intermediate products proved successful, then the intention was to carry out further siloxane investigations, by pyrolysing various linear siloxanes. (See chapter seven).

In 1989, Khabashesku *et al.*[1] attempted to produce dimethylsilanone through the pyrolysis of octamethylcyclotetrasiloxane (D4) and isolate the pyrolysis products in an argon matrix. From these experiments, they observed that a number of small hydrocarbons and radical species were being produced. However, the assignment of these species in many cases, relied solely on the appearance of a single band, since spectra were only published between 1400 - 400 cm^{-1}. It was therefore decided to start this investigation by attempting to reproduce the results obtained by Khabashesku *et al.* and then take the investigation further by pyrolysing other cyclic siloxanes.

In addition to octamethylcyclotetrasiloxane (D4), two other easily accessible and inexpensive cyclic siloxane compounds were chosen for these sets of experiments. These compounds were hexamethylcyclotrisiloxane (D3) and decamethylcyclopentasiloxane (D5). The abbreviations in brackets are official Dow Corning abbreviations for these compounds. All spectra obtained have been collected in both argon and nitrogen matrices.

1.1. Nitrogen Matrix vs Argon Matrix

Below can be seen two spectra of the smallest of the three cyclic siloxanes, hexamethylcyclotrisiloxane obtained in both argon and nitrogen matrices.

Figure 1. A comparison between hexamethylcyclotrisiloxane in an argon matrix and a nitrogen matrix

A) D3 / Ar
B) D3 / N_2

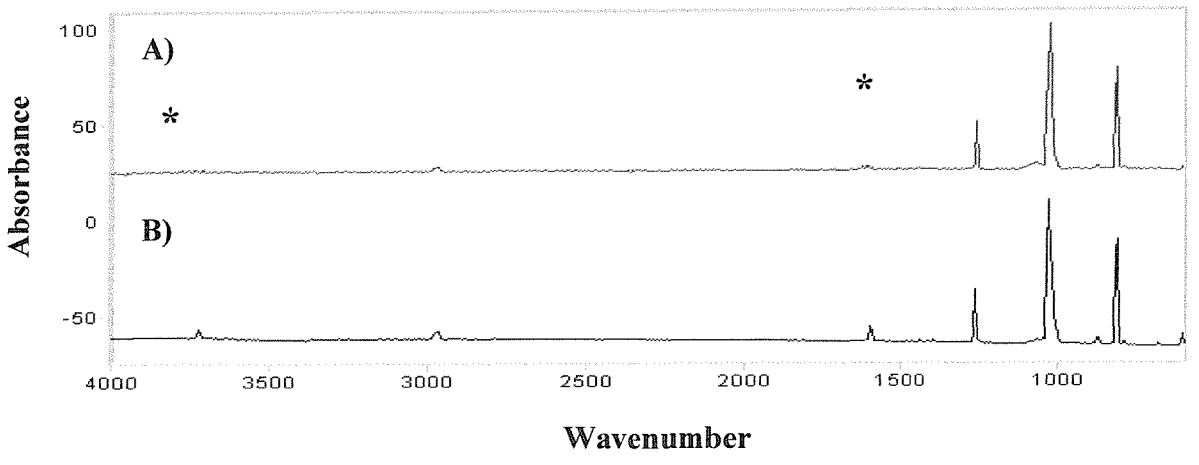

As expected, it was found that the bands produced in spectrum **B)** were sharper than those found in spectrum **A)**. Therefore, only spectra obtained in a nitrogen matrix will be presented and discussed in this chapter. The asterisks show bands due to water.

1.2. General Procedure

Below is a flow diagram for the experimental and theoretical procedures of the cyclic siloxane experiments.

Figure 2. A flow diagram below summarises links between experimental and theoretical procedures

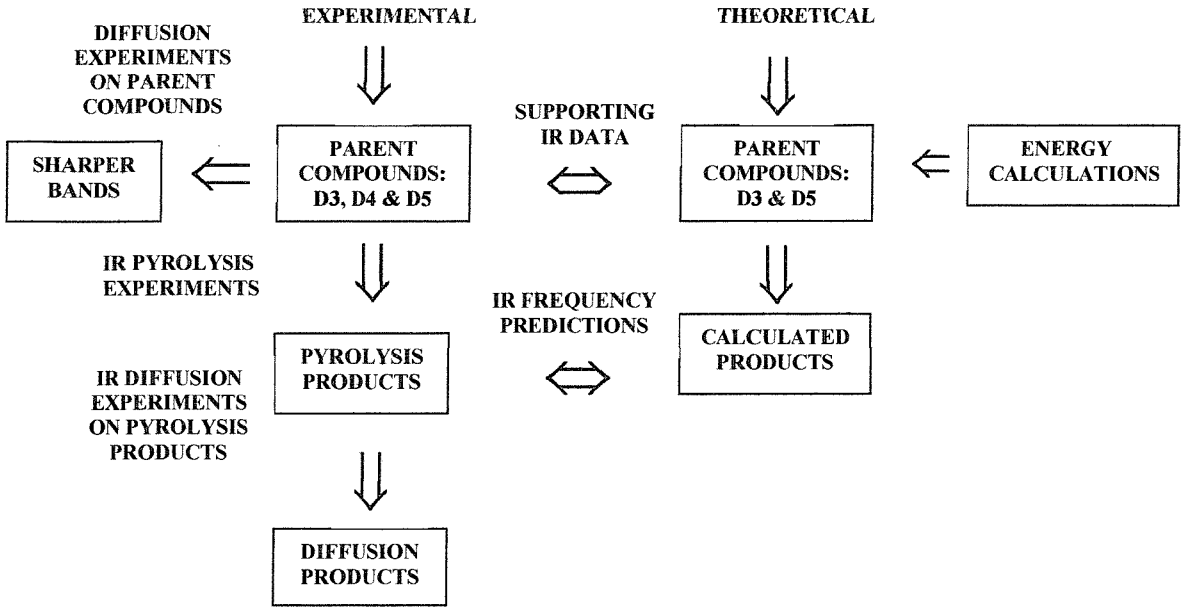

Spectra were initially obtained of the parent compounds immediately after deposition. Experiments were then conducted which involved pyrolysing the sample vapour at temperatures up to 700-720 °C. As a result, the parent compounds dissociated to produce potentially reactive intermediates, which were then trapped within the matrix on the deposition window. Diffusion experiments of the pyrolysis products were then carried out. These took place to investigate whether reactive species produced on pyrolysis underwent further reaction. The experiments involved warming the matrix window to 27 K, which loosened the matrix cages that had formed. This allowed species that had been trapped within the cages the chance to reorient. Finally, diffusion experiments were conducted on the parent compounds to find out the effects of diffusion on the parent bands. All spectra shown are as a result of the subtraction of the background spectrum.

After spectra had been collected and analysed, it was found that there were a number of unknown bands that had been formed upon pyrolysis. Molecular modelling calculations were conducted of a number of possible products in order to produce the minimum energies of these species to find the most favourable products. This was followed by frequency calculations of pyrolysis products and of parent compounds. These calculated frequencies were then compared to the frequencies of the unknown bands to assist in the identification of the unknown products.

1.3. Previous Studies

After producing a number of bands that could be assigned to either known products or to unknown species, molecular modelling calculations were conducted in order to support the identification of the pyrolysis products. In carrying out these calculations, the energies, geometries and the frequencies of suspected novel products were obtained and compared with experimental results.

Recent publications have shown that this method of supporting experimental data with theoretical results is successful in identifying new products from IR spectra. In particular, Khabashesku *et al.*[2] has confirmed the original assignments for the IR spectra of matrix isolated transient silenes ($R_2Si{=}CR_2$), using *ab initio* or density functional theory computational methods and have subsequently carried out the vacuum pyrolysis of the cyclic species, 3,3-dimethoxy-6-oxa-3-silabicyclo[3.1.0]hexane and its 3,3-diphenyl derivative[3]. Computational methods were this time used to aid the identification of the matrix isolated transient organic silanone pyrolysis products. For these spectra, two bands at 697 and 1202 cm^{-1} were observed in the spectra assigned to the SiH_2 in-plane rock and Si=O stretch respectively of the parent silanone ($H_2Si{=}O$). Using the computational method and the B3LYP / 6-311 (d,p) level of theory these two bands were produced at 705 and 1216 cm^{-1} along with additional bands at 710, 1022, 2229 and 2245 cm^{-1}. These bands may not have been observed in the experimental spectra due to their low intensity. Dimethylsilanone ($(CH_3)_2Si{=}O$) is also reported to have been produced during pyrolysis with bands at 657 (Si-C asymmetric stretch) and 770, 798, 822, 1210, 1240 and 1244 cm^{-1} due to stretches of the CH_3 units. The computationally obtained bands were produced at 686, 800, 810, 863, 1227, 1290 and 1296 cm^{-1} again using the B3LYP / 6-311 (d,p) level of theory. Although the agreement here between experimental and theory is not exact, this strategy is very encouraging.

Khabashesku *et al.*[4] also published the results of the identification of silicon containing species from the reactions of silicon atoms with small organic species. These findings were also based on the comparison between experimental and theoretical data. This time a number of silylene compounds were produced as well as silanones. From the reaction of silicon atoms with methanol (CH_3OH), methyl(methoxy)silylene (CH_3SiOCH_3) was formed. Three bands were observed in the spectra of matrix isolated silylene. These were found at 1084 (C-O stretch), 1218 (HCO rock) and 1262 cm^{-1} (HCSi deformation rock). The computational equivalent bands were calculated at 1098, 1200 and 1265 cm^{-1}. These bands are again seen to be in satisfactory

agreement. Bands were also observed at 749 (Si-O stretch), 859 (Si-H in-plane rock), 1086 (C-O stretch) and 1925 cm^{-1} (Si-H stretch). The computational method using the B3LYP / 6-311G (d,p) level of theory calculated the corresponding bands at 742, 864, 1101 and 1995 cm^{-1}. The observed spectra of matrix isolated methyl(hydroxy)silylene produced three bands. These were at 789 (HCSi in-plane rock), 831 (Si-O stretch) and 881 cm^{-1} (O-H in-plane rock).

For these systems above, the calculations would also seem to provide useful support for experimental interpretation, but it should be noted that there was a significant difference between the observed and calculated frequency for the Si-H stretch.

2. Preliminary Results

Spectra were initially produced of octamethylcyclotetrasiloxane and compared to the results obtained by Khabashesku *et al.*[1]. These experiments were followed by the pyrolysis of additional cyclic siloxanes, namely hexamethylcyclotrisiloxane and decamethylcyclopentasiloxane. The investigation into the products produced from the pyrolysis of the above cyclic siloxanes, started by examining the pyrolysis products reported by Khabashesku *et al.*. These included a series of small hydrocarbons and radical species. The investigation was then expanded to include other possible hydrocarbon species. The spectra obtained for each of the three cyclic siloxanes can be seen below.

2.1. Spectra of Cyclic Siloxanes

(a). Octamethylcyclotetrasiloxane (D4) / N_2

Octamethylcyclotetrasiloxane was the first of the cyclic siloxanes to be pyrolysed and its structure is seen below. D4 is an eight-membered ring, consisting of alternate silicon and oxygen atoms. Two methyl groups are attached to each silicon atom.

Figure 3. Octamethylcyclotetrasiloxane

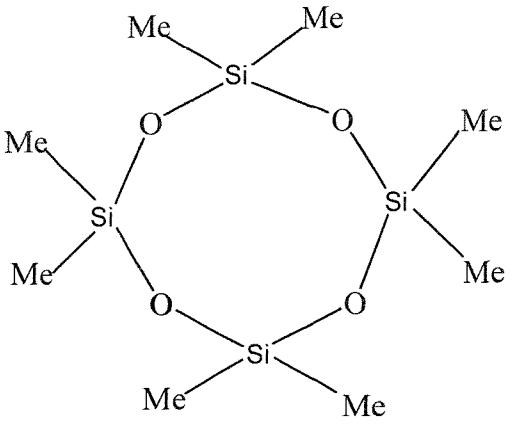

Spectra were obtained after each experiment. These experiments were carried out in a nitrogen matrix and the spectra were analysed after each stage.

Figure 4. Spectra of octamethylcyclotetrasiloxane / N_2 - 4000 – 400 cm^{-1}

A). D4 / N_2
B). D4 / N_2 after diffusion
C). D4 / N_2 after pyrolysis
D). D4 / N_2 after pyrolysis & diffusion

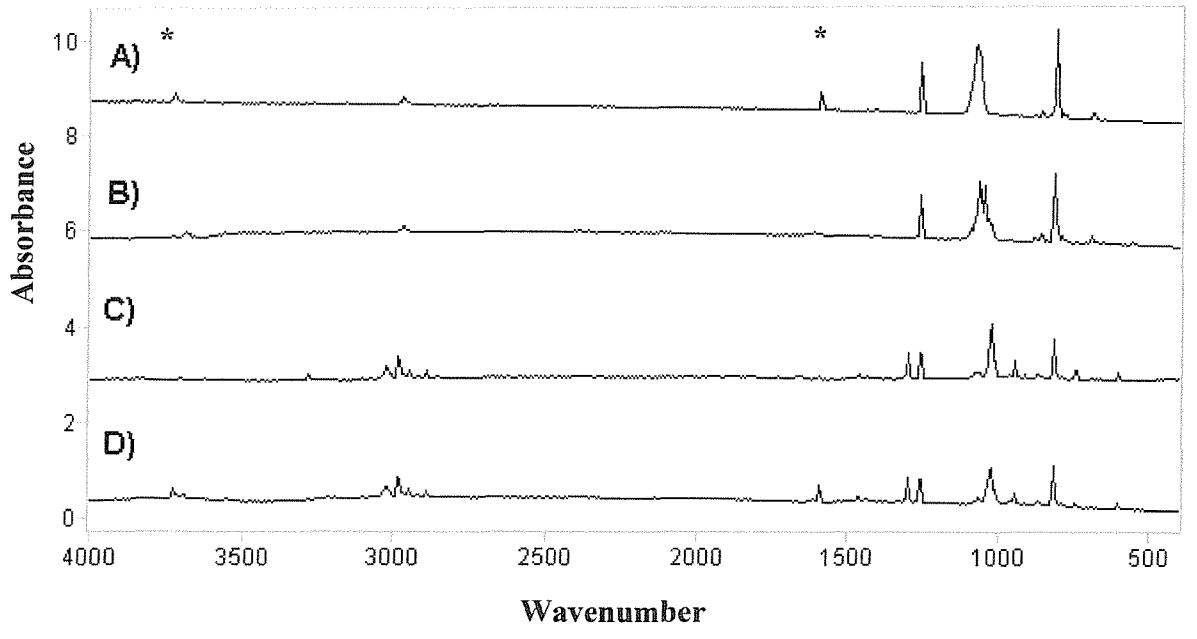

It was noticed from the above spectra that the majority of new bands produced after pyrolysis appeared below 1500 cm^{-1}. Therefore this region was expanded.

Figure 5. Spectra of octamethylcyclotetrasiloxane / N_2 - 1500 – 400 cm^{-1}

A). D4 / N_2
B). D4 / N_2 after pyrolysis
C). D4 / N_2 after pyrolysis – D4 / N_2

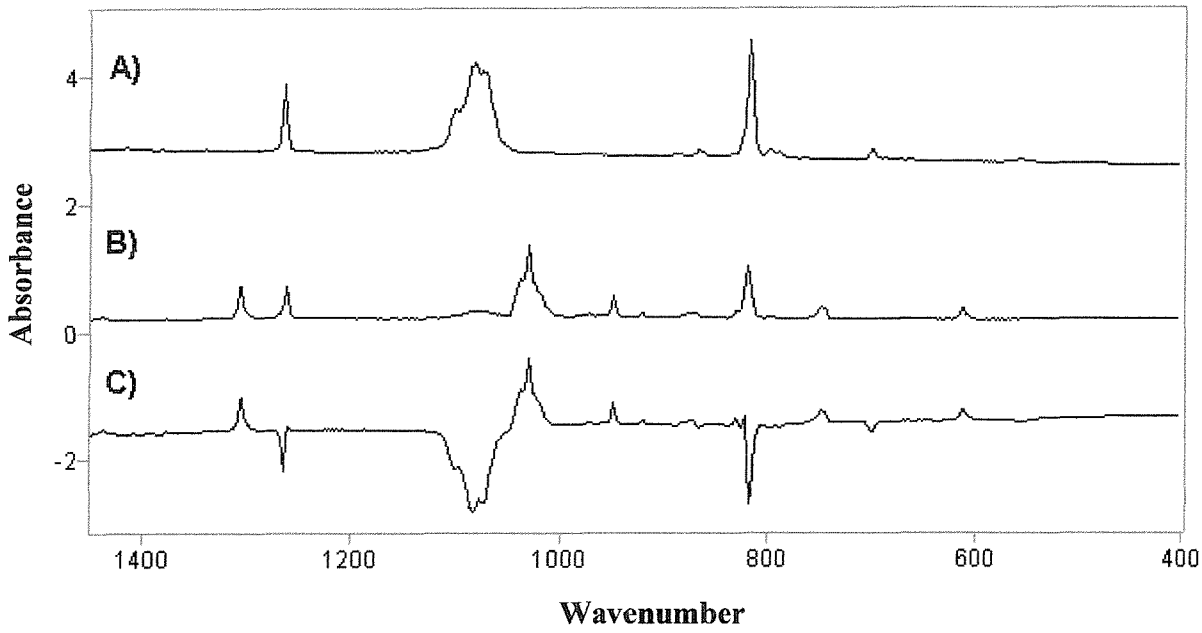

All positive bands shown in spectrum **C)** are due to pyrolysis products and all negative bands are due to the original parent compound. All the bands found in the above spectra have been tabulated and analysed in order to identify the formation of any pyrolysis products.

Table 1. Tabulated bands obtained for octamethylcyclotetrasiloxane / N_2

D4	D4 after diffusion	D4 after pyrolysis	D4 after pyrolysis & after diffusion
-	-	610 (w)	610 (w)
697 (w)	699 (w)	-	-
-	-	746 (w)	-
786 (vw)	786 (vw)	-	-
797 (vw)	797 (vw)	797 (vw)	797 (vw)
816 (m)	817 (s)	817 (s)	819 (s)
-	-	828 (sh)	828 (sh)
-	-	865 (vw)	865 (vw)
888 (vw)	888 (vw)	-	-
-	-	919 (vw)	919 (vw)
-	-	946 (m)	-
-	-	1029 (s)	1029 (s)
-	1036 (sh)	1036 (sh)	1036 (sh)
-	1052 (sh)	-	-
-	1065 (sh)	-	-
1072 (sh)	-	-	-
-	1075 (sh)	-	1075 (sh)
1083 (sh)	-	-	-
1099 (sh)	-	-	-
-	1101 (sh)	-	-
1263 (s)	1263 (s)	1262 (s)	1262 (s)
-	-	1305 (s)	1305 (s)
-	-	1437 (vw)	1437 (vw)
-	-	1464 (vw)	1464 (vw)
1597 (m)	-	1597 (vw)	1597 (m)
-	-	2140 (vw)	2140 (vw)
-	-	2891 (w)	2891 (w)
-	-	2950 (w)	2950 (w)
-	-	2975 (m)	2975 (m)
-	-	2986 (m)	2986 (m)
-	-	3280 (w)	-
-	-	3632 (vw)	3632 (vw)
-	3691 (vw)	-	3691 (vw)
3724 (w)	-	3724 (w)	3724 (w)

(b). **Hexamethylcyclotrisiloxane (D3) / N_2**

Below is the structure of hexamethylcyclotrisiloxane. It consists of a six-membered ring of silicon and oxygen atoms. Two methyl groups are joined to each of the silicon atoms.

Figure 6. Hexamethylcyclotrisiloxane

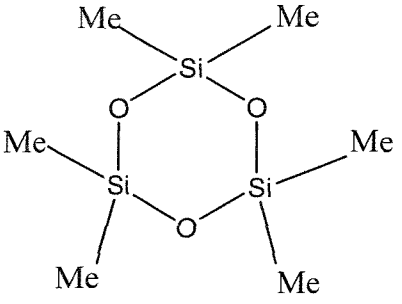

Spectra were again obtained after each of the four experimental stages involving hexamethylcyclotrisiloxane. These spectra are shown below.

Figure 7. Spectra of hexamethylcyclotrisiloxane / N_2 - 4000 – 400 cm^{-1}

A). D3 / N_2
B). D3 / N_2 after diffusion
C). D3 / N_2 after pyrolysis
D). D3 / N_2 after pyrolysis & diffusion

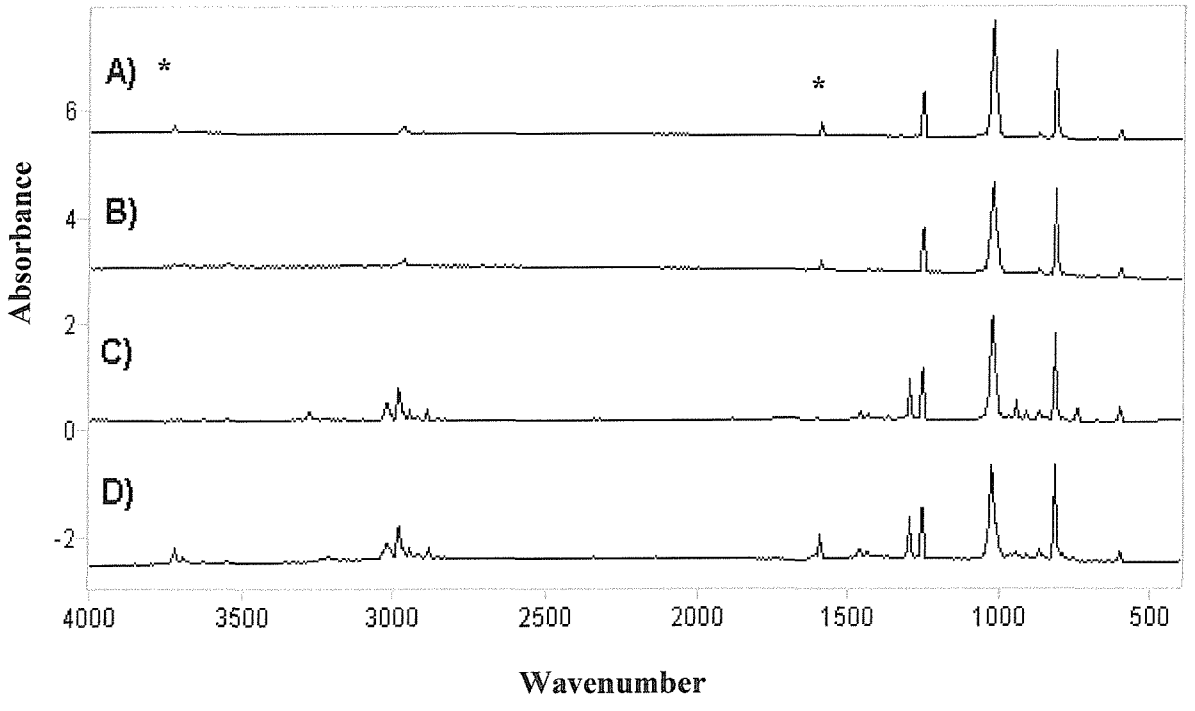

After studying each spectrum carefully, it was observed that the majority of the changes that occurred after each stage were in the region between 1500-400 cm^{-1}. This region was then expanded and studied in greater detail.

Figure 8. Spectra of hexamethylcyclotrisiloxane / N_2 - 1500 – 400 cm^{-1}

A). D3 / N_2
B). D3 / N_2 after pyrolysis
C). D3 / N_2 after pyrolysis – D3 / N_2

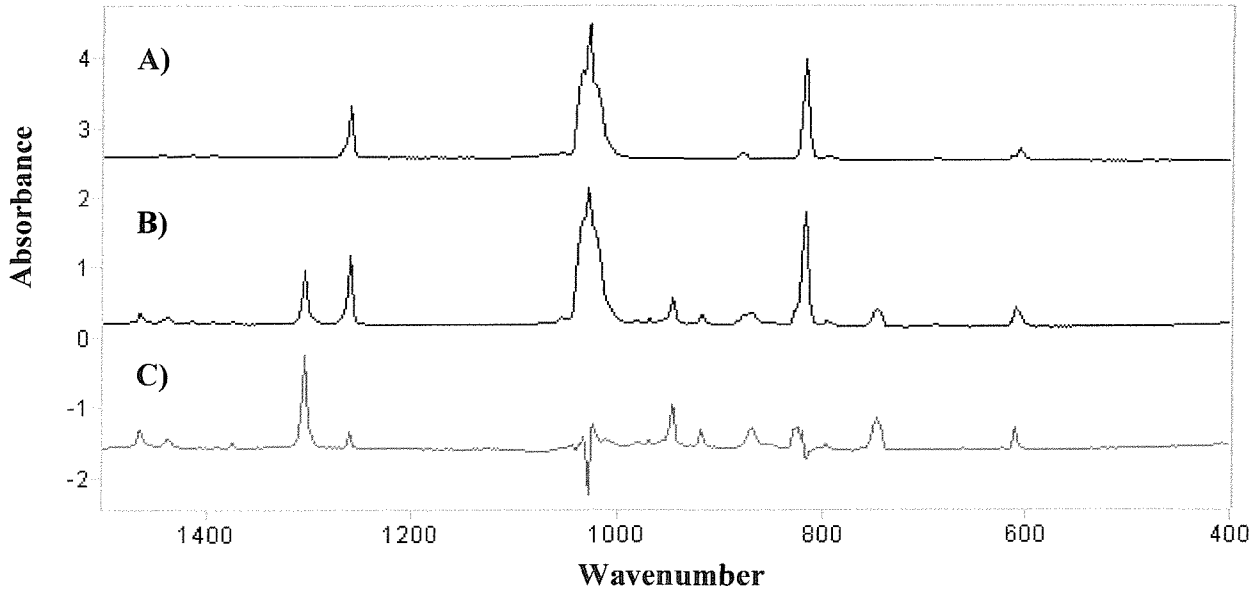

Each spectrum was analysed and the bands were tabulated and can be seen below. (See Table 2).

Table 2. Tabulated bands obtained for hexamethylcyclotrisiloxane / N_2

D3	D3 after diffusion	D3 after pyrolysis	D3 after pyrolysis & after diffusion
606 (w)	606 (w)	609 (w)	607 (w)
-	-	746 (w)	-
818 (s)	818 (s)	818 (s)	818 (s)
-	-	870(vw)	870(vw)
878 (w)	878 (w)	878 (w)	878 (w)
-	-	919 (vw)	919 (vw)
-	-	-	940 (m)
-	-	947 (m)	-
-	-	1016 (sh)	-
1022 (sh)	1022 (sh)	1022 (sh)	-
1028 (sh)	1028 (sh)	1028 (sh)	1028 (sh)
1036 (sh)	1036 (sh)	1036 (sh)	1036 (sh)
1262 (m)	1262 (m)	1262 (m)	1262 (m)
-	-	1305 (m)	1305 (m)
-	-	1436 (w)	1436 (w)
-	-	1464 (w)	1464 (w)
1597 (w)	1597 (w)	1597 (w)	1597 (w)
-	-	2986 (m)	2983 (m)
-	-	2950 (w)	2950 (w)
-	-	2890 (w)	2890 (w)
-	-	3281 (w)	-
-	-	-	3220 (vw)
-	-	3107 (vw)	-
3024 (m)	3024 (m)	-	-
3724 (vw)	3724 (vw)	3724 (w)	3724 (w)

(c). Decamethylcyclopentasiloxane

The final cyclic siloxane to be pyrolysed was decamethylcyclopentasiloxane. The structure of D5 can be seen below. It is a ten-membered ring consisting of alternate silicon and oxygen atoms. Two methyl groups are attached to each silicon atom.

Figure 9. Decamethylcyclopentasiloxane

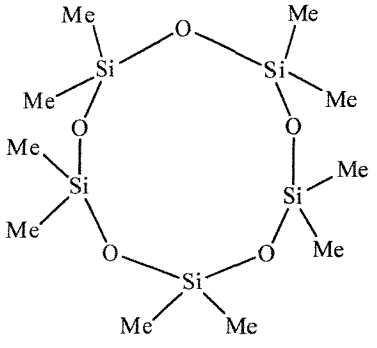

Four spectra are shown below. These were obtained after each of the four experiments.

Figure 10. Spectra of decamethylcyclopentasiloxane / N_2 - 4000 – 400 cm^{-1}

A). D5 / N_2
B). D5 / N_2 after diffusion
C). D5 / N_2 after pyrolysis
D). D5 / N_2 after pyrolysis & diffusion

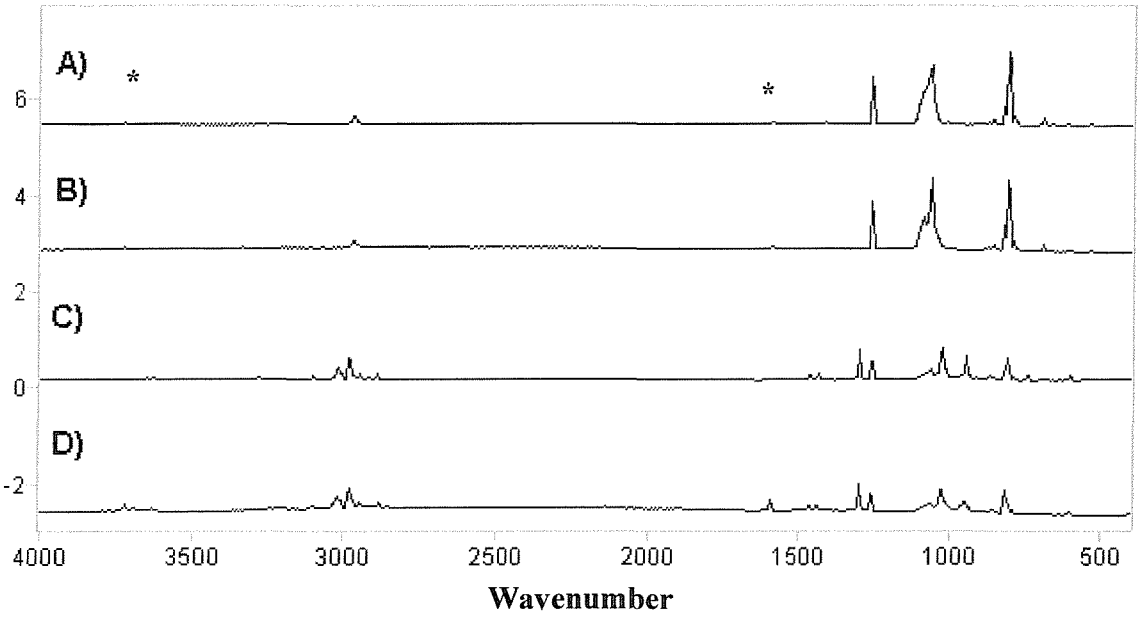

As before, on studying the spectra it appeared that the majority of the new bands produced after pyrolysis were in the region between 1500-400 cm^{-1}.

Figure 11. Spectra of decamethylcyclopentasiloxane / N_2 - 1500 – 400 cm^{-1}

A). D5 / N_2
B). D5 / N_2 after pyrolysis
C). D5 / N_2 after pyrolysis – D5 / N_2

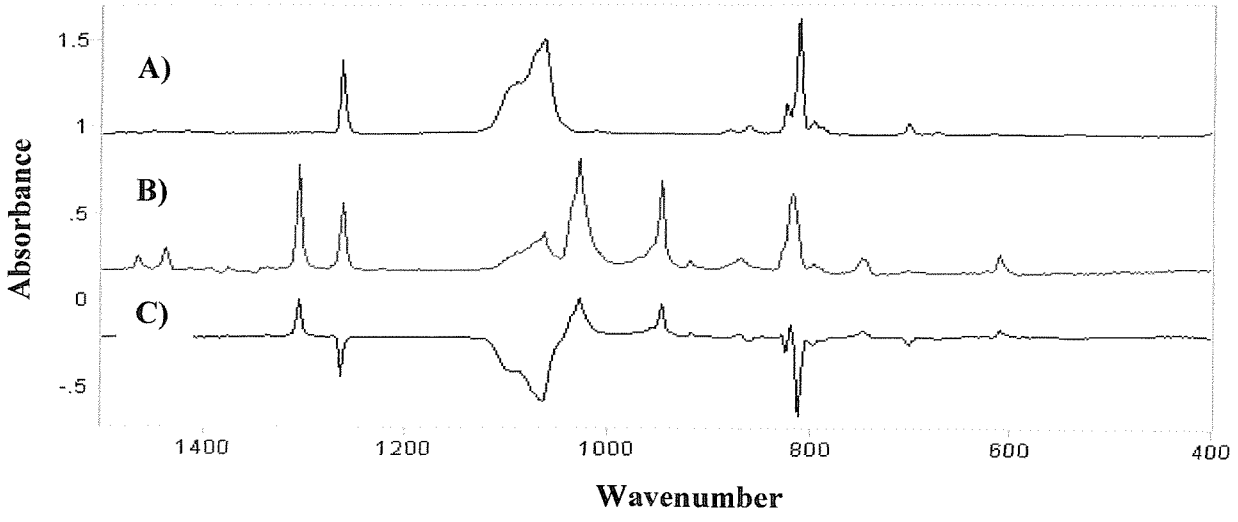

The above two sets of spectra were carefully examined and all the bands found present were tabulated in order to identify any new bands that are formed.

Table 3. Tabulated bands obtained for decamethylcyclopentasiloxane / N_2

D5	D5 after diffusion	D5 after pyrolysis	D5 after pyrolysis and diffusion
-	-	610 (w)	610 (w)
702 (w)	702 (w)	-	-
-	-	747 (w)	747 (w)
797 (w)	797 (w)	797 (w)	797 (w)
812 (s)	812 (s)	812 (s)	812 (s)
825 (w)	825 (w)	818 (sh)	818 (sh)
862 (vw)	862 (vw)	869 (vw)	869 (vw)
882 (vw)	882 (vw)	-	-
-	-	919 (vw)	-
-	-	947 (s)	-
-	-	-	940 (m)
-	-	-	956 (sh)
-	-	-	1015 (sh)
-	-	1029 (sh)	1029 (sh)
-	-	1035 (sh)	-
1064 (s)	1064 (m)	1064 (m)	1064 (m)
1075 (sh)	1075 (sh)	-	-
1092 (sh)	1092 (sh)	-	-
1101 (sh)	1101 (sh)	-	-
1262 (s)	1262 (s)	1262 (s)	1262 (s)
-	-	1305 (s)	1305 (s)
-	-	1438 (w)	1438 (w)
-	-	1465 (m)	1465 (m)
1597 (vw)	1597 (vw)	1597 (vw)	1597 (m)
-	-	2140 (vw)	2140 (vw)
-	-	2890 (m)	2888 (m)
-	-	2949 (m)	2949 (m)
2970 (w)	2970 (w)	-	-
-	-	2985 (s)	2981 (s)
-	-	3019 (m)	3019 (m)
-	-	3105 (vw)	3098 (vw)
-	-	3279 (vw)	-
-	-	3723 (w)	3723 (w)

3. Preliminary Conclusions

Experiments were conducted by Khabashesku *et al.*[1] involving the pyrolysis of the cyclic siloxane, octamethylcyclotetrasiloxane. Spectra were obtained in an argon matrix at 1030 °C. This led to pyrolysis experiments of D4 being carried out here, in order to attempt to reproduce

the previous results. A comparison and analysis of both sets of spectra can be seen below. A number of bands and regions in the spectra were immediately identified due to previous knowledge. It is known that bands due to water are found at ~ 3600 and 1600 cm^{-1}. Small amounts of carbon dioxide and carbon monoxide were also identified at 2343 and 2138 cm^{-1} respectively. The Si-O[1] region is known to be between 1000-600 cm^{-1}, the Si-Me region lies between 1275 – 1260 cm^{-1} and the Si-H region is found between 2250-2090 cm^{-1}. These regions are focussed on when carrying out the analysis of the spectra in both chapters in order to aid the identification of the pyrolysis products.

Figure 12. **A matrix infrared (Ar, 12 K) spectrum of the vacuum pyrolysis products of octamethylcyclotetrasiloxane at 1030 °C[1]**

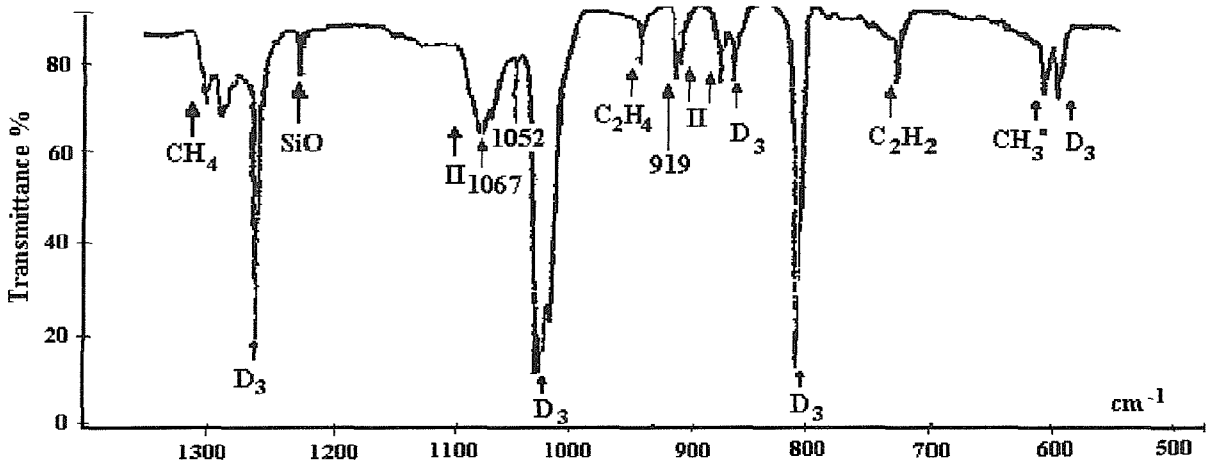

Figure 13. **A spectrum of octamethylcyclotetrasiloxane / Ar after pyrolysis**
Negative bands – Parent compound
Positive bands – Pyrolysis products

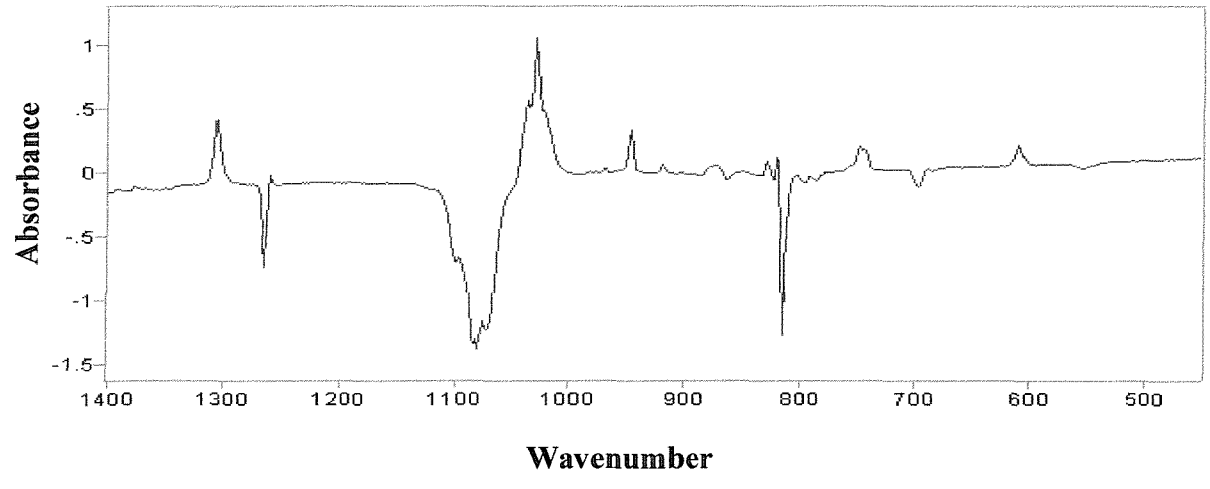

As can be seen from Figure 12, the published spectrum is only shown in a narrow range. He speculated on the assignments of the pyrolysis products on many occasions, with the presence of only one band. With spectra collected here of a broader frequency range, it is hoped that more accurate judgements can be made on the products formed, since more than one band is likely to be present for any given species. As well as collecting spectra of the three cyclic siloxanes, a number of spectra were also obtained here of possible pyrolysis products that were previously suggested by Khabashesku *et al.*. In addition, further spectra of other logical small hydrocarbons have also been obtained.

3.1. An Investigation into the Formation of the Methyl Radical

Khabashesku *et al.*[1] report that the methyl radical is being produced when octamethylcyclotetrasiloxane is pyrolysed. However, as they only published spectra between 1500 – 400 cm^{-1}, only one CH_3 band is reported as being present. Therefore, an in-depth literature search into the bands produced from the methyl radical in infrared spectra was required.

Spectra were obtained by Khabashesku *et al.* initially at 12 K and then at 1030 °C after heating. One of the bands that they identified and that was of particular interest here, was a band at 611 cm^{-1}, which was present in both of the above mentioned spectra. Khabashesku *et al.* recorded this band as being due to the out-of-plane bending mode of ν_2, due to CH_3. However, no stretching modes of CH_3 were observed in these papers and so the identification of this band can not be conclusive.

This led to a wide literature search to establish the frequency of the stretching mode of the methyl radical and to therefore hopefully confirm the presence of CH_3 in the spectra produced here. In 1954, Mador[5] first stabilised methyl radicals in a matrix cage, produced by the photolysis and *x*-ray radiation of CH_3I and the pyrolysis of $Pb(CH_3)_4$. It was found that one of the first papers to publish frequencies of the methyl radical was by Andrews[6] in 1966. Andrews condensed methyl iodide (CH_3I) with a stream of lithium atoms and the spectra were obtained at 15 K in argon at a ratio of Ar / CH_3I = 200 / 600. A band was produced at 730 cm^{-1} and was reported as being due to the CH_3 radical out-of-plane bending mode of ν_2. An almost planar structure and a point group of D_{3h} was assigned to the radical by Herzberg[7], which was concluded from an electronic spectrum and supported by an ESR spectrum. Andrews[6] provided

evidence from normal co-ordinate analysis to confirm these findings. Normal co-ordinate analysis allows possible frequencies to be calculated for a species with a given structure, based on calculated force constants. An agreement between the calculated and experimental values helped to confirm the assignment.

A second paper by Andrews and Pimentel[8] in 1967 confirmed these findings and further identified the ν_4 in-plane bending mode at 1383 cm^{-1}. Again, there was excellent agreement between the observed and the calculated frequencies obtained from normal co-ordinate analysis.

However, this same year, an additional paper in this area was published by Milligan and Jacox[9]. Milligan and Jacox produced methyl radicals through the vacuum ultraviolet pyrolysis of methane in both argon and nitrogen matrices at 14 K. (See Figure 14). An agreement was met on the point group of the CH_3 radical. However, the ν_2 mode was found at the much lower frequency of 611 cm^{-1}. Evidence for this modified frequency value came from a series of isotopic substitution studies with deuterium and carbon-13.

Figure 14. Infrared spectrum of photolysis of N_2:CH_4 at 14 K in a nitrogen matrix[9]

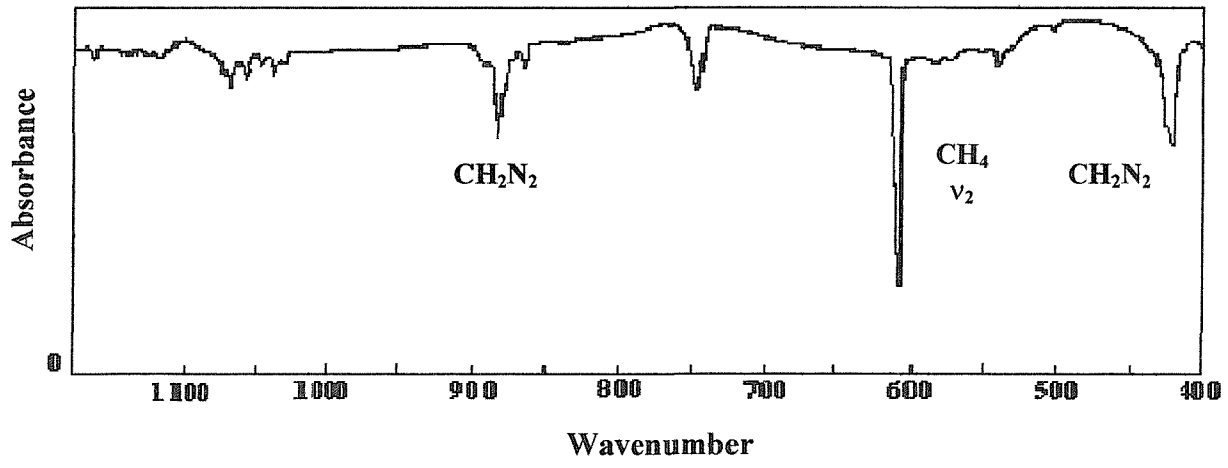

The dispute of the out-of-plane bending mode of ν_2 was finally summarised and concluded by Tan and Pimentel[10] (see Figure 15) in 1968 using a similar experimental procedure as that used by Andrews and Pimentel[8]. However, this time sodium atoms as well as lithium atoms were used to reduce the methyl halides, in order to identify whether the lithium atoms had had any influence over the reported new features. Again, bands were found to be present at 730.1 and 729.6 cm^{-1} as well as a weak and diffuse band at 611 cm^{-1}. It was revealed that this band was

also present in the original Andrews and Pimentel[8] spectra, only to be dismissed and assigned to impurities, due to a similar, though weaker band being present in the spectrum of the parent molecule before pyrolysis. It was concluded that the original band at 730 cm^{-1} that had been assigned to the ν_2 mode was actually as a result of interaction by lithium. It was discovered that the CH_3 radical was interacting with a MX species. This had resulted in the formation of a new species, which was named a methyl alkali halide.

Figure 15. Infrared spectrum of methyl halides reacting with metal atoms at 15 K in an argon matrix[10]

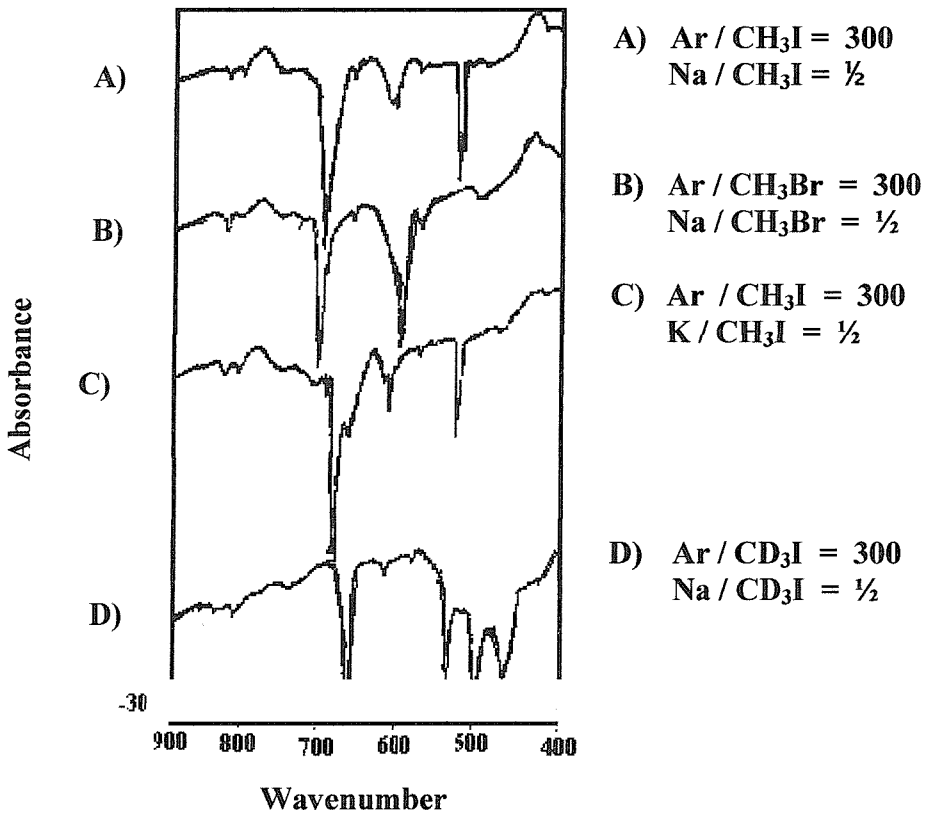

Snelson[11] suggests that since Andrews and Pimentel had assigned an incorrect frequency to the ν_2 mode, that it may also be possible that the value reported for the ν_4 was unreliable. In an attempt to obtain the true frequency of this vibrational mode and to demonstrate the ease of trapping the methyl radical using the technique of matrix isolation, Snelson pyrolysed both methyl iodide and dimethyl mercury. Upon pyrolysis of methyl iodide in a neon matrix at 1300 °C, three bands were obtained and assigned to the CH_3 radical. These were found at frequencies of 617, 1398 and 3162 cm^{-1}. When dimethyl mercury was pyrolysed under the same conditions, three CH_3 bands of similar frequencies and relative intensities were again observed at 614, 1396

and 3162 cm^{-1}. The most intense band found at 617 / 614 cm^{-1}, is in close agreement with the band produced by Milligan and Jacox[9] at 611 cm^{-1}. Slight discrepancies are seen due to different matrix gases. As with previous reports, Snelson also agreed on the structure being planar and the point group of the methyl radical being D_{3h}. Tan, Winer and Pimentel[12] reported a frequency comparable to the findings of both Milligan and Jacox and Snelson, by carrying out a series of flash photolysis experiments of CH_3I, with argon as the matrix gas. A band was observed at 607 cm^{-1}, together with a less prominent band at 603 cm^{-1}. These experiments were then repeated using CH_2DI and CD_3I and the positive results served as evidence. The less prominent band was thought to be due to the CH_3 out-of-plane bending mode of ν_2.

Allen, Kennedy and Pritchard[13] have also attempted to locate the ν_4 in-plane bending mode of the methyl radical, by pyrolysing di-*t*-butyl peroxide vapour to ~ 700 K and then isolating the products in a CF_2Cl_2 matrix. Allen *et al.*, claimed that a band produced at 2878 cm^{-1} was in part due to the CH_3 radical. Evidence for these findings was demonstrated by changing the carrier gas from CF_2Cl_2 to SF_6. By doing this, the deposition temperature was also changed, which resulted in an environment that was either more or less likely to trap reactive intermediates. Snelson[11] had overturned this idea by concluding that a molecule with such a point group should possess two infrared-active vibrational modes. These modes were attributed to the two higher frequencies of 1398 / 1396 and 3162 cm^{-1}. These frequencies have been assigned to the modes of ν_4 and ν_3 respectively. Isotopic labelling was used to confirm these findings.

In 1977, Jacox[14] re-investigated the regions which had been assigned to the modes of ν_2 and ν_4 through the photolysis of methane in argon. The bands at 603, 611 and 1398 cm^{-1} were again observed, as well as an additional band observed for ν_2 at 639 cm^{-1}. Jacox later reproduced these findings by reacting fluorine atoms, (which were produced by passing a microwave discharge through a sample of CF_4 or NF_3), with methane in an argon matrix. However, the bands produced were less intense than those produced by previous methods.

Klabunde and co-workers[15], [16], [17] conducted a series of co-deposition experiments of methane with elements such as; aluminium, boron, gallium and indium, run at ~ 10 K in an argon matrix. The results agreed with previous reports. Burczyk and Downs[18] also identified CH_3 bands around 600 cm^{-1}, due to the ν_2 out-of-plane bending mode. In an attempt to isolate either CH_3Na or CH_3K by co-condensing CH_3I with sodium or potassium vapour, the methyl radical was

produced. Finally, the rocking mode of CH_3 was identified by Ault[19] in 1992, by producing a band at 733 cm^{-1} as a result of reacting $(CH_3)_3Al$ with NH_3 in an argon matrix.

To summarise, it was found that the most intense band produced by CH_3 was the ν_2 out-of-plane bending mode at ~ 611 cm^{-1}. The results of this search are in agreement with the experimental findings, as this band was the only band that has been observed experimentally. As can be seen from Table 4 below, Snelson found the bands of ν_1, ν_3 and ν_4 to be much weaker than the band due to ν_2.

Table 4. Tabulated summary of CH_3 vibrations

Matrix Gas	Frequency of CH_3 ν_1 / cm^{-1}	Frequency of CH_3 ν_2 / cm^{-1}	Frequency of CH_3 ν_3 / cm^{-1}	Frequency of CH_3 ν_4 / cm^{-1}
Argon[8]	-	607	-	1383
Nitrogen[9]	-	611	-	-
Neon[10]	3044*	617 (vs)	3162 (w)	1398 (w)

* Calculated value

Published work reported carrying out these experiments in different matrix gases. Slight discrepancies were noted as the matrix gas was changed, resulting in an overall difference of approximately 5 cm^{-1}.

The bands that have been reported as being due to the methyl radical were then looked for in the spectra shown above of the three cyclic siloxanes. All three cyclic siloxane spectra were seen to produce a band at ~ 611 cm^{-1}. The exact frequency of this band was observed at 610, 607 and 610 cm^{-1} for D4, D3 and D5 respectively. However, no stretching modes were found. This was as expected, as the result of the literature search, seen summarised in Table 4, shows that the stretching and bending modes at 3162 and 1398 cm^{-1} are very weak. Therefore, they may well have been produced in the cyclic siloxane spectra but not seen because they are low in abundance.

A set of diffusion experiments were then carried out where the deposition window was warmed to 27 K. As the matrix cages relax, the molecules are able to reorient and are therefore given the chance to react further. When studying the spectra obtained of the three cyclic siloxanes after diffusion, it was observed that in all three sets of spectra, the band at ~ 610 cm^{-1} was seen to disappear. It is likely that the methyl radicals reacted further when the cages loosened.

3.2. An Investigation into the Formation of Acetylene

Acetylene was another possible by-product for the pyrolysis of the three cyclic siloxanes. A possible route for the formation of acetylene would be through the combination of two methyl radicals and then the elimination of two hydrogen molecules. Independent experiments were carried out here in order to obtain spectra of acetylene. These spectra were then compared with the spectra obtained after the pyrolysis of the cyclic siloxanes. The positive bands in the siloxane spectra are those formed after pyrolysis. The negative bands are due to the parent compound.

Figure 16. A comparison between spectra of the three cyclic siloxanes and acetylene in nitrogen matrices

A). D4 / N_2 after pyrolysis – D4 / N_2
B). D3 / N_2 after pyrolysis – D3 / N_2
C). D5 / N_2 after pyrolysis – D5 / N_2
D). Acetylene / N_2

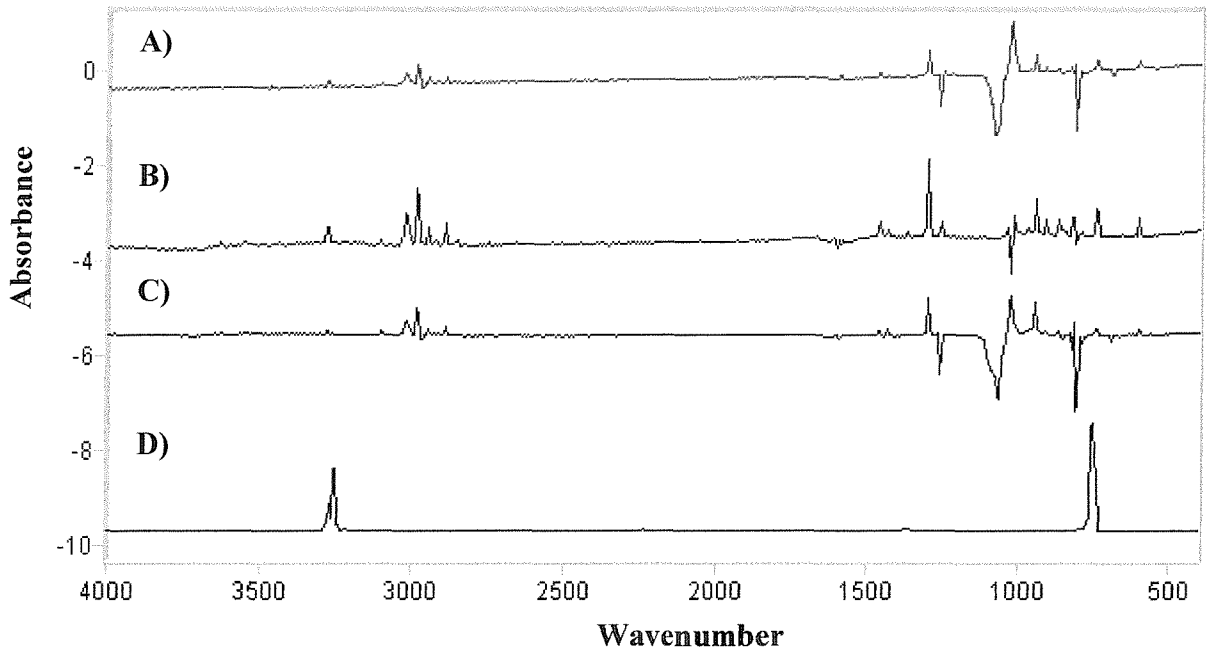

From spectrum **D)** of acetylene, it is seen that there are two main bands produced at 3280 and 746 cm^{-1}. After bands obtained in the three spectra of the cyclic siloxanes after pyrolysis were compared to the bands observed in the spectra of acetylene, it was observed that both acetylene bands were present in the siloxane spectra.

Diffusion experiments were carried out and the bands were required to change in size at the same relative intensity, in order to confirm that they were due to the same species. Below can be seen the results of the diffusion experiments for the regions containing bands belonging to acetylene, for spectra obtained after the pyrolysis of D3.

Figure 17. Spectra of hexamethylcyclotrisiloxane / N_2 produced after pyrolysis and both before and after diffusion

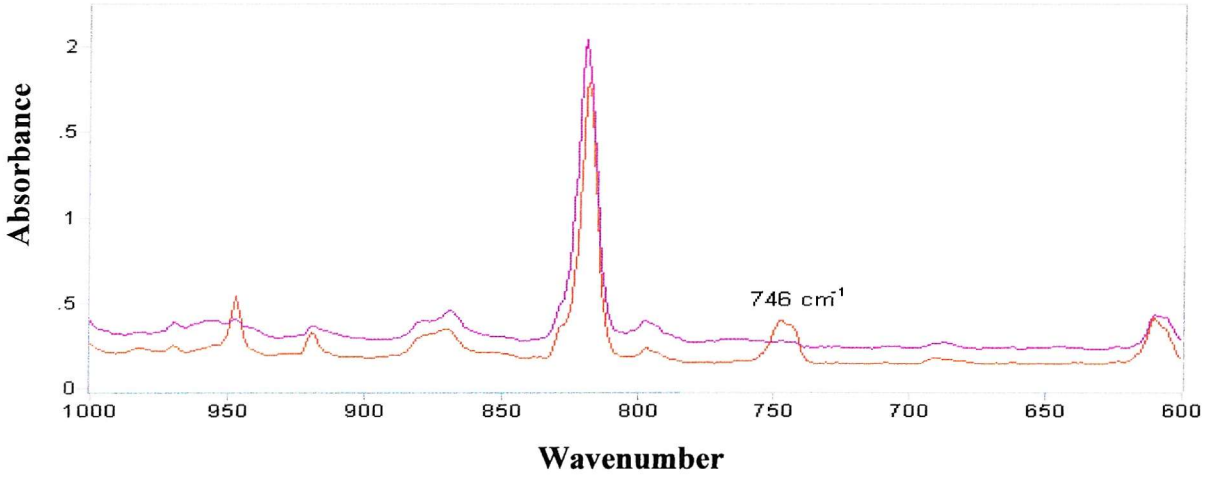

Red Line = D3 after pyrolysis

Purple Line = D3 after pyrolysis and after diffusion

Figure 18. Spectra of hexamethylcyclotrisiloxane / N_2 produced after pyrolysis and both before and after diffusion

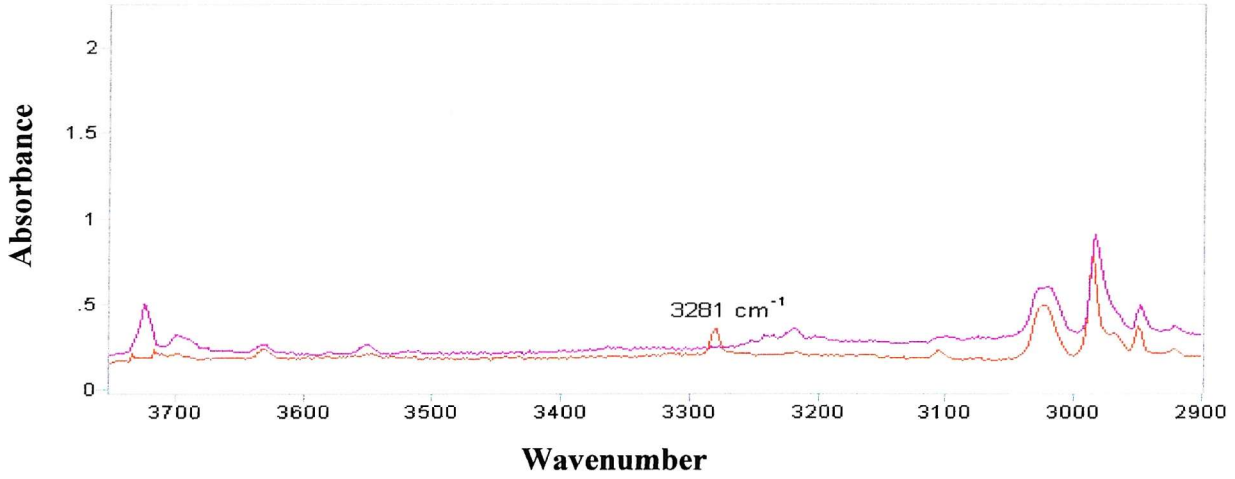

Purple Line = D3 after pyrolysis

Red Line = D3 after pyrolysis and after diffusion

It can be seen from the spectra above that after diffusion, the two bands that had been produced after pyrolysis, both completely disappear. As the bands change with the same relative intensity, it is likely that they are due to the same species, therefore confirming that acetylene is produced.

3.3. An Investigation into the Formation of Ethene

Khabashesku *et al.*[1] only show one band thought to be due to the formation of ethene in their spectra, obtained after the pyrolysis of octamethylcyclotetrasiloxane (Ar). This band is reported to be present at 1436 cm^{-1}. However, this is not to say that the pyrolysis of D4 only produces one ethene band, as only the region between 1500 – 400 cm^{-1} are shown in the spectra published by Khabashesku *et al.*. A paper by Frei *et al.*[20] reports that a band at 947.2 cm^{-1} (Ar) or 947.0 cm^{-1} (N_2) is produced as a result of reacting C_2H_4 with F_2 under cryogenic conditions. However, all of the infrared active vibrational modes obtained in the gas phase are published in the Tables of Molecular Vibrational Frequencies[21]. These bands are at 826.0 (ν_{10}), 949.3 (ν_7), 1443.5 (ν_{12}), 2988.6 (ν_{11}) and 3105.5 (ν_9) cm^{-1}. Below are spectra of the three cyclic siloxanes obtained after pyrolysis together with a spectrum of ethene.

Figure 19. A comparison between spectra of the three cyclic siloxanes and ethene in nitrogen matrices

A). D4 / N_2 after pyrolysis – D4 / N_2
B). D3 / N_2 after pyrolysis – D3 / N_2
C). D5 / N_2 after pyrolysis – D5 / N_2
D). Ethene / N_2

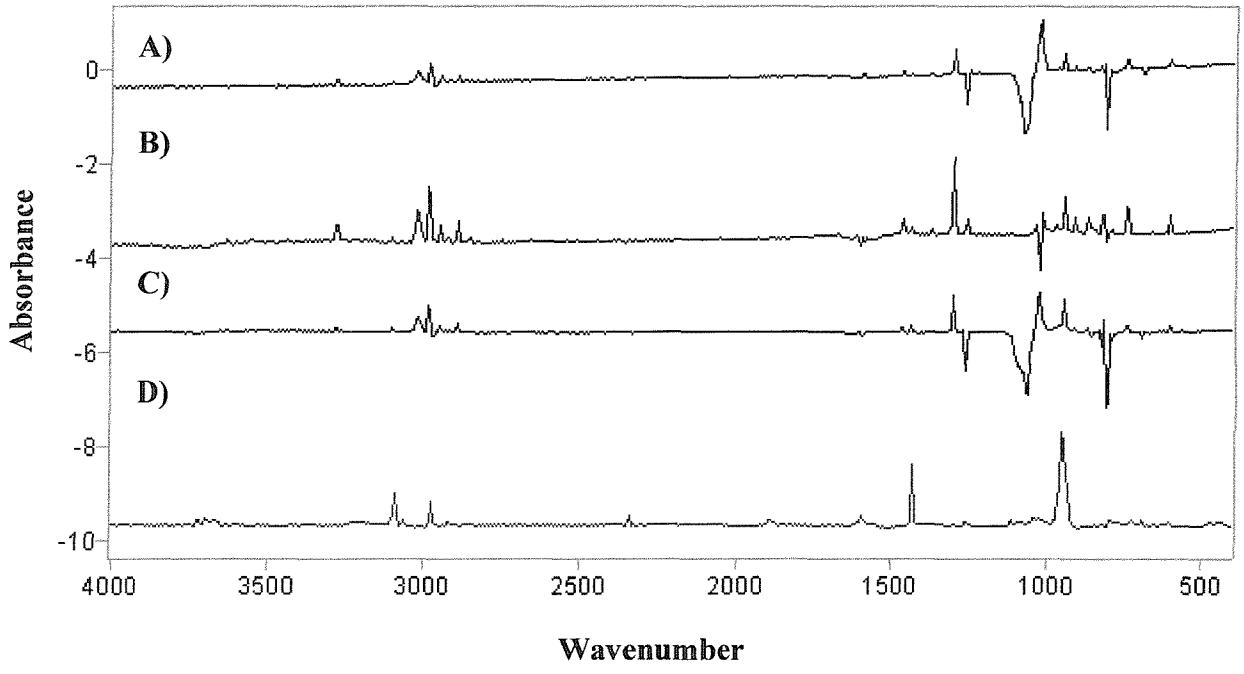

It appears that D4 produces four bands thought to be due to the formation of ethene. These bands were found at 2986, 1437, 946 and 828 cm^{-1}. Upon analysing the results obtained from the pyrolysis of hexamethylcyclotrisiloxane, four bands were again produced that were thought to be due to ethene. These bands were found at 3107, 2986, 1436 and 947 cm^{-1}. D5 produces five bands found at 3105, 2985, 1438, 947 and 829 cm^{-1}. In order to confirm that these bands were in-fact due to the formation of ethene, an investigation was needed into the effects on the bands during diffusion.

Diffusion experiments were then carried out where the deposition window was warmed to 27 K. Spectra were obtained, paying particular attention to the regions containing bands thought to be due to ethene. Initially, the bands reported to be in the fingerprint region of the spectrum were analysed. Below are expanded spectra of octamethylcyclotetrasiloxane obtained both after pyrolysis and then after diffusion.

Figure 20. Spectra of octamethylcyclotetrasiloxane / N_2 produced after pyrolysis and both before and after diffusion

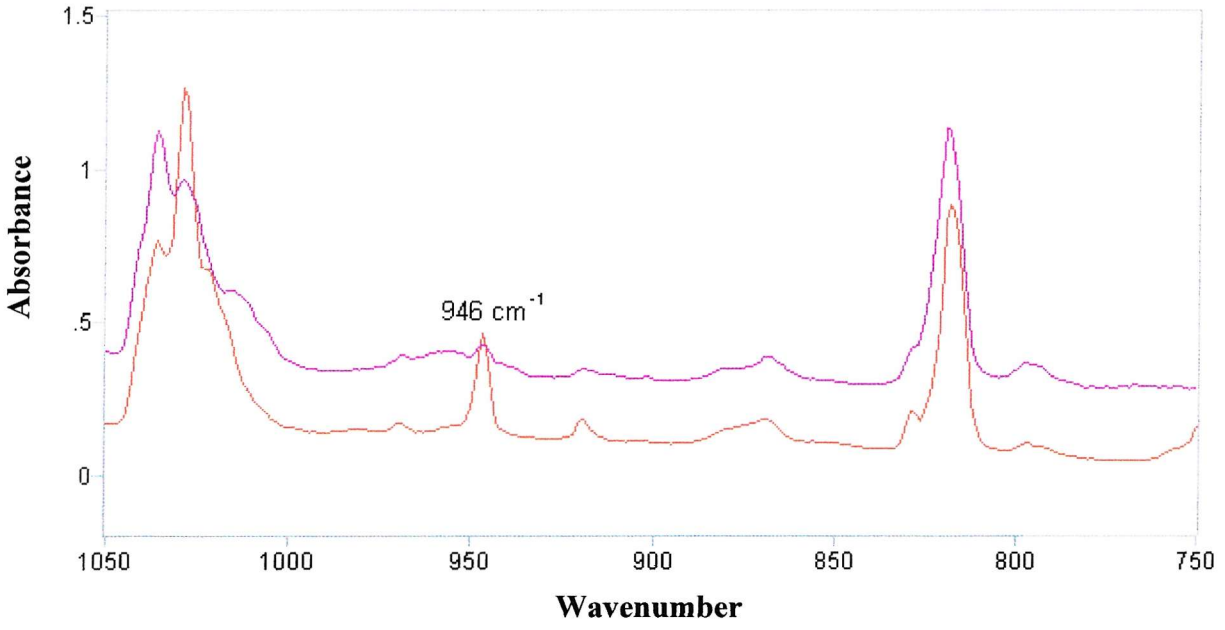

Red Line = D4 after pyrolysis

Purple Line = D4 after pyrolysis and diffusion

Figure 21. Spectra of octamethylcyclotetrasiloxane / N_2 produced after pyrolysis and both before and after diffusion

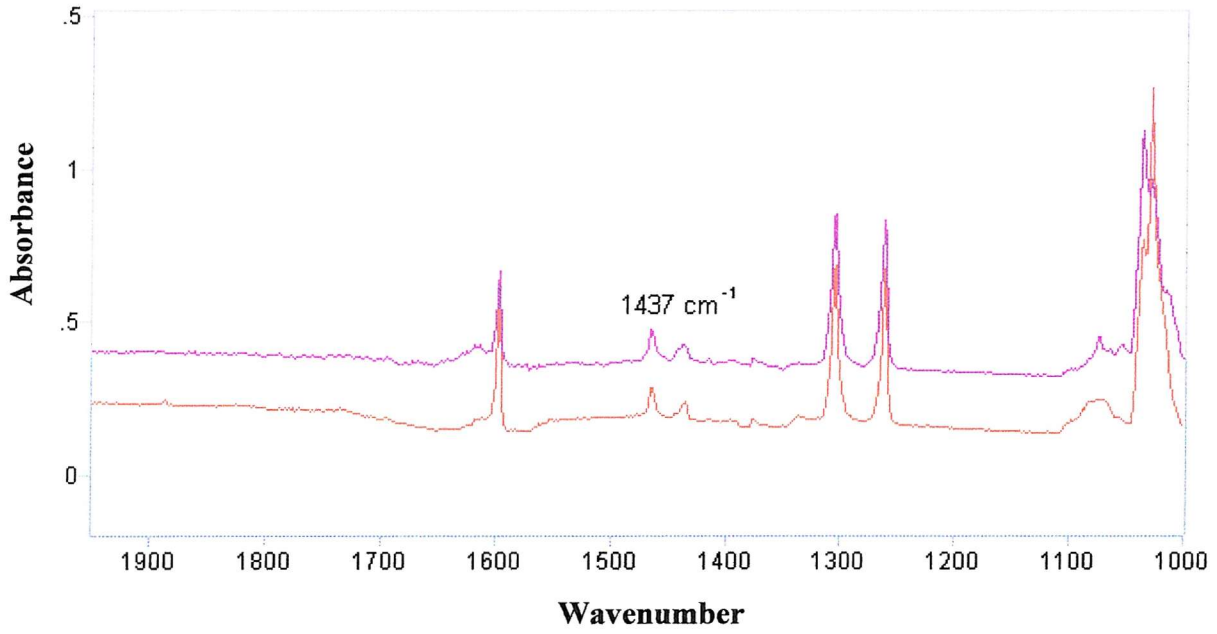

Red Line = D4 after pyrolysis
Purple Line = D4 after pyrolysis and diffusion

However, interestingly, in spectra collected for both D4 and D5, only one of the bands of ethene was seen to disappear, this was the band at 946 cm^{-1}. No change was seen in the ethene region of the spectra obtained for D3. It is not know why these changes occur with differing relative intensities. It would suggest that ethene is not actually produced and that these bands are due to different species. However, the formation of ethene was not entirely ruled out, since there were many bands produced which were thought to be due to ethene. Therefore, the region containing the stretching modes was expanded and studied

Figure 22. Spectra of octamethylcyclotetrasiloxane / N_2 produced after pyrolysis and both before and after diffusion

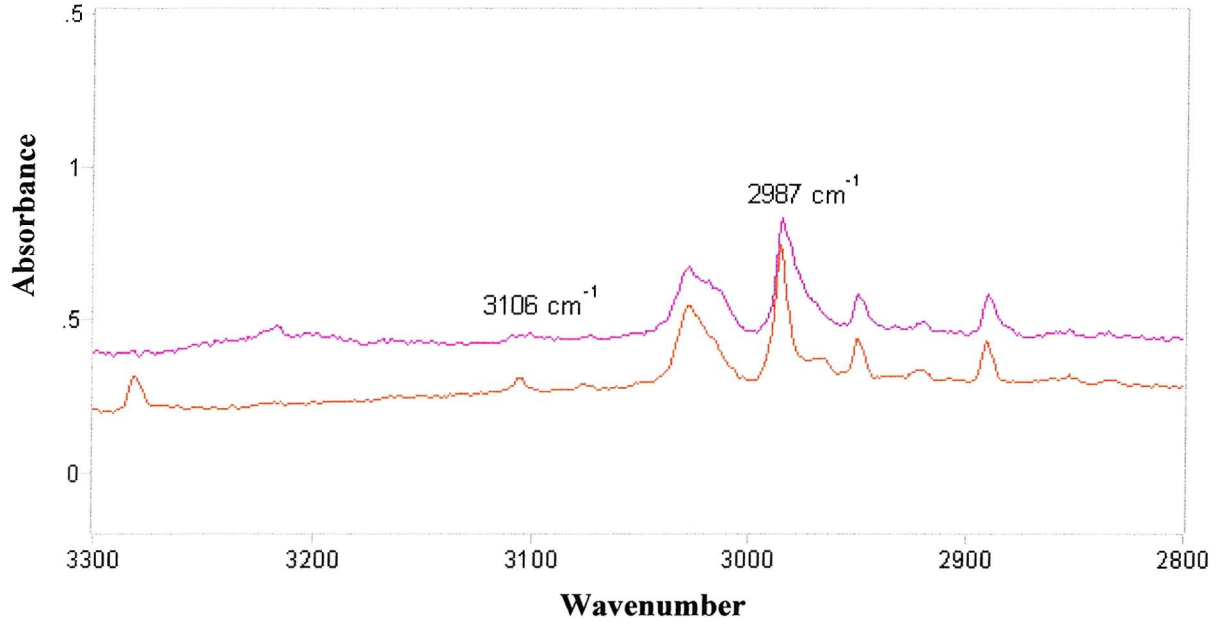

Red Line = D4 after pyrolsis

Purple Line = D4 after pyrolysis and diffusion

Although no band was initially reported as being produced from the pyrolysis of D4 at 3106 cm^{-1}, on expansion of the region, a very weak band is seen to be present. This band becomes sharper after diffusion. The band at 2987 cm^{-1} also sharpens after diffusion. These bands therefore behave with the same relative intensities. This adds to the argument that ethene is produced after the pyrolysis of D4, despite the previous discrepancies. D5 behaves very similarly to D4. However, when analysing the results of D3, it was seen that the band at 3107 cm^{-1} disappears after diffusion. It is unknown why the bands thought to be due to ethene behave so differently after diffusion.

3.4. An Investigation into the Formation of Methane

As can be seen from the structures of the cyclic siloxanes (section 2.1.), each silicon atom is joined to two methyl groups. Therefore, the formation of methane is a logical pyrolysis product. Below is a table of both Nakomoto's [22] published gas-phase frequencies of methane and the matrix isolated frequencies in nitrogen obtained here.

Table 5. Tabulated bands obtained for methane in a nitrogen matrix and compared to bands obtained in the gas phase

Methane / N_2 – Matrix isolated / cm^{-1}	Methane – Gas phase[22] / cm^{-1}	Vibrational modes
1305	1306	ν_4
-	1534	ν_2
-	2917	ν_1
3026	3019	ν_3

After studying the spectra of D4, D3 and D5 after pyrolysis, it was seen that a band due to the bending vibration of methane is present at ~ 1306 cm^{-1} in all cases and the stretching modes are found at 3029, 3025 and 3020 cm^{-1} in D4, D3 and D5 respectively. All bands produced after the pyrolysis of the three cyclic siloxanes remained present after diffusion, confirming the presence of methane. The spectra of the cyclic siloxanes are shown in Figure 23 together with a spectrum of methane.

Figure 23. A comparison between spectra of the three cyclic siloxanes and methane in nitrogen matrices

A). D4 / N_2 after pyrolysis – D4 / N_2
B). D3 / N_2 after pyrolysis – D3 / N_2
C). D5 / N_2 after pyrolysis – D3 / N_2
D). Methane / N_2

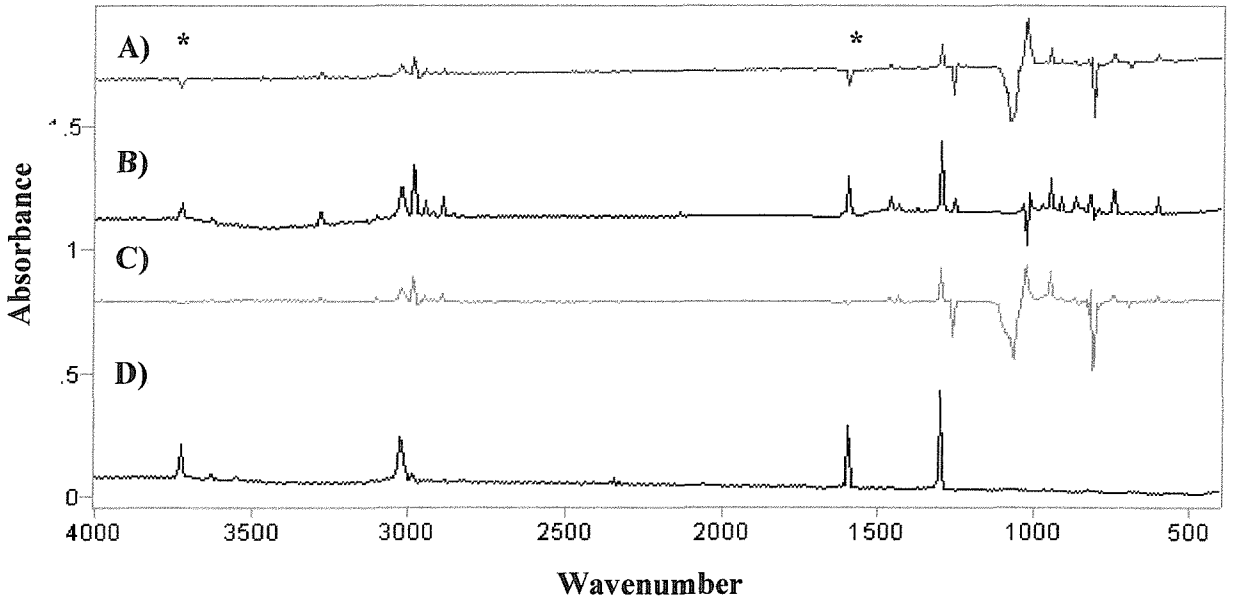

Khabashesku *et al.*[1] claim that methane is produced from the pyrolysis of D4. It is reported by these authors that the bending mode of methane, when isolated in an argon matrix is present at 1306 cm^{-1}, however, no stretching mode is shown. A report by Ogawara *et al.*[23] describes the use of the technique of matrix isolation Fourier-transform infrared spectroscopy to confirm that the bending mode of methane is present at 1306.1 cm^{-1} in an argon matrix. It is further reported that this band is due to the degenerate deformation of ν_4. This finding is also reported by Mielke *et al.*[24]. However, Ogawara *et al.* state that when methane is isolated in nitrogen, two bands are seen at 1306.1 and 3030 cm^{-1}. The latter band is due to the ν_3 degenerate stretching mode.

3.5. An Investigation into the Formation of Ethane

Ethane is the next logical pyrolysis product to investigate. It could be formed from the recombination of two eliminated methyl radicals. Bands that are produced in the spectrum of ethane isolated in a nitrogen matrix, seen in Figure 14. **D)**, have been tabulated and compared to Nakamoto's gas phase frequencies.

Table 6. Tabulated bands obtained for ethane in a nitrogen matrix and compared to bands obtained in the gas phase

Ethane / N_2 – Matrix isolated / cm^{-1}	Ethane – Gas phase[18] / cm^{-1}
829	821
-	1155
1376	1375
1465	1460
-	1486
-	1534
2235	-
2891	2899
2921	2917
2950	2954
-	2963
2985	-
-	2994
-	3019
3546	-

Many of the bands tabulated above, produced both in a nitrogen matrix and in the gas phase, appear at similar frequencies. However, expected discrepancies exist due to the differing

techniques of gas phase infrared spectroscopy compared to matrix isolation infrared spectroscopy. Below are spectra of the three cyclic siloxanes and ethane.

Figure 24. A comparison between spectra of the three cyclic siloxanes and ethane in nitrogen matrices

A). D4 / N_2 after pyrolysis – D4 / N_2
B). D3 / N_2 after pyrolysis – D3 / N_2
C). D5 / N_2 after pyrolysis – D3 / N_2
D). Ethane / N_2

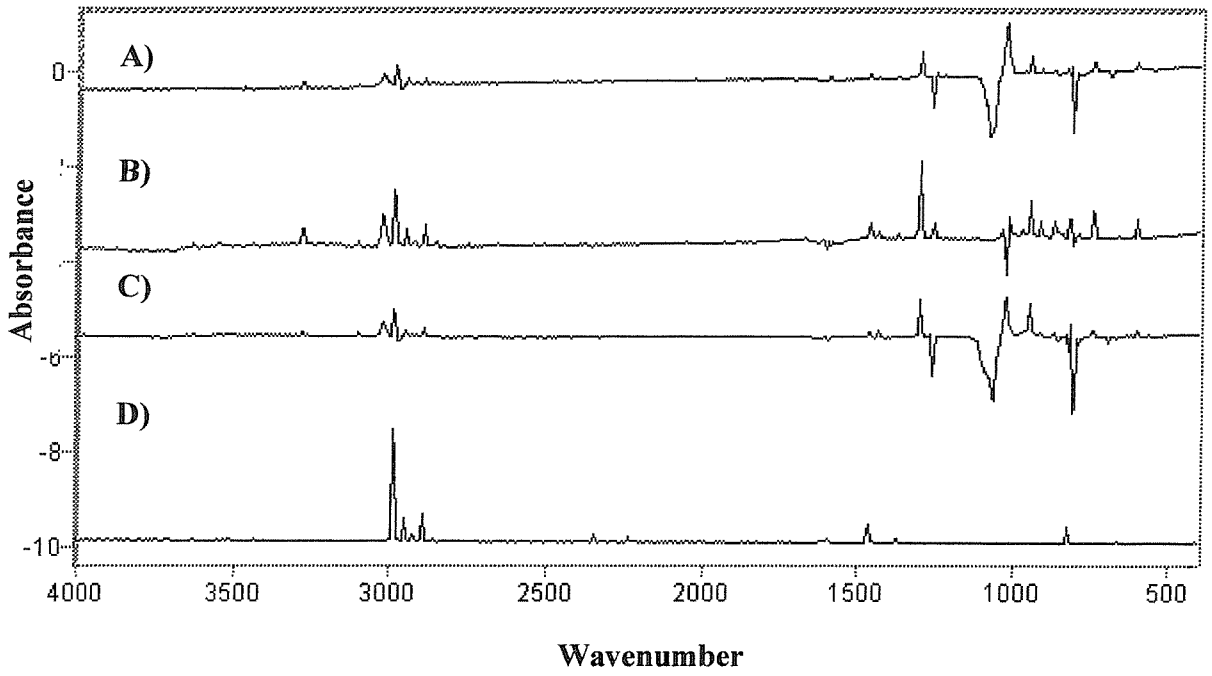

Many ethane bands are produced in the above siloxane spectra. From the spectra obtained after the pyrolysis of D4, five of the nine tabulated ethane bands (see Table 5), were found to be present. It is likely that the remaining four bands are of low abundance and therefore not seen. The five bands seen were found at 2986, 2950, 2891, 1464 and 828 cm^{-1}. The first three of these bands are due to the stretching vibrations and the remaining two bands are due to the bending vibrational modes. When analysing the spectra obtained after the pyrolysis of D3, it was found that four of the tabulated ethane bands were present. These bands were found at 2986, 2950, 2890 and 1464 cm^{-1}. The latter band is due to the bending vibrational mode and the remaining bands are due to the stretching modes. Upon analysing the spectra obtained for the pyrolysis of D5 it was seen that four ethane bands were again produced. These bands were found at 2985, 2949, 1465 and 829 cm^{-1}. After diffusion, it was seen that all of the observed ethane bands, produced as a result of the pyrolysis of D4, D3 and D5, remained present. This indicates that ethane did not react further upon diffusion

3.6. An Investigation into Cyclic Siloxanes Produced as Pyrolysis Products

After analysing the spectra produced from the pyrolysis and diffusion of the three parent compounds, a number of unknown compounds still exist. It is important at this stage to investigate a theory suggested by Khabashesku *et al.*[1] which has been supported by energy calculations produced here. Khabashesku *et al.* state that upon the pyrolysis of the cyclic siloxane, D4, a D unit (dimethylsilanone) is eliminated from the D4 ring and re-inserted back into another D4 ring, therefore producing both D3 and D5. The pathway for this reaction is shown below.

Figure 25. Reaction pathway of Khabashesku *et al.*[1]

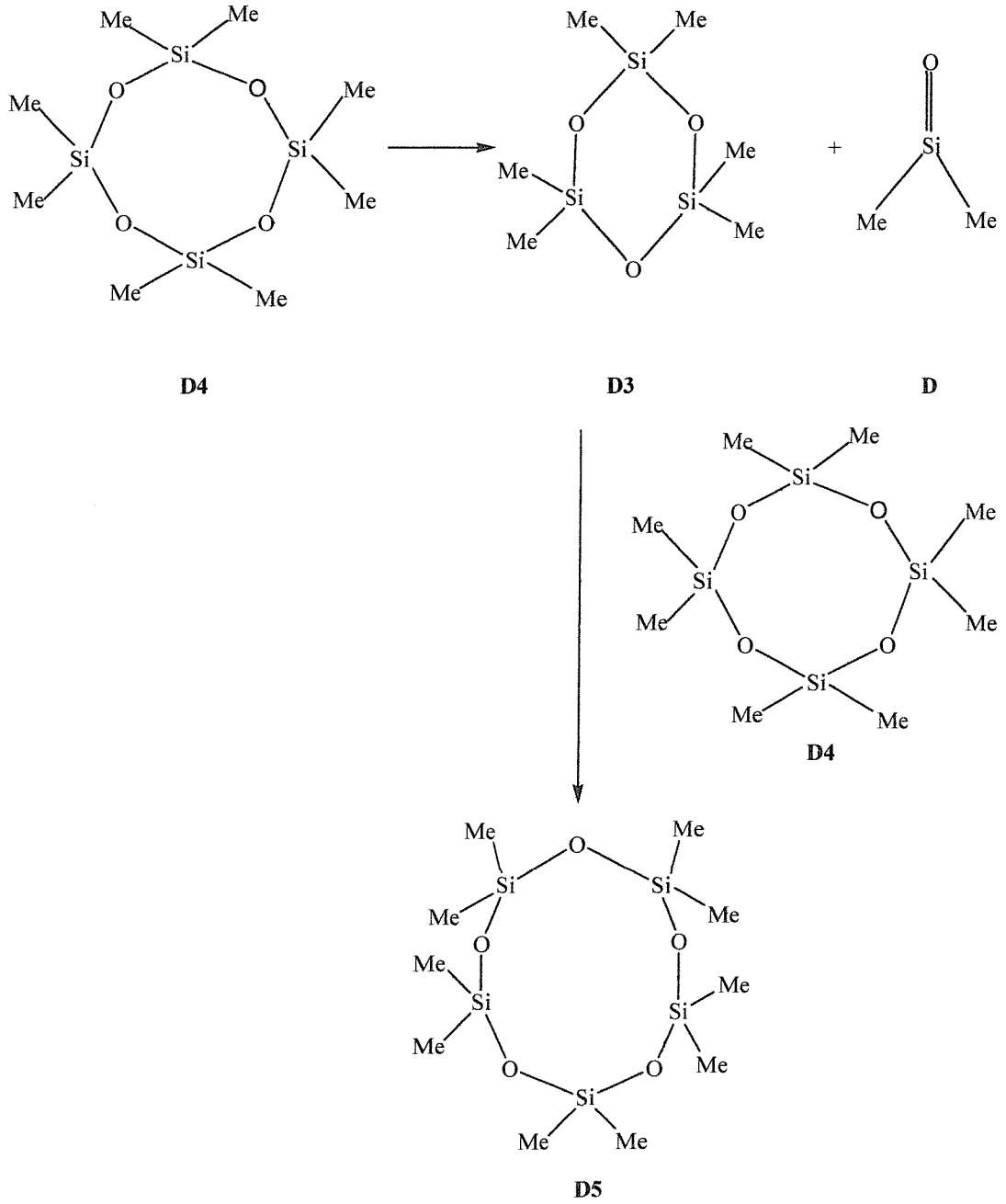

This is known as an interconversion reaction and it is thought to occur for each of the cyclic siloxanes after pyrolysis, therefore producing other cyclic siloxane compounds. The remaining unknown bands produced as a result of the pyrolysis of all three cyclic siloxanes are tabulated below, together with the known bands of the parent compounds before pyrolysis. A comparison of the two sets of data was then made, in order to determine whether any secondary cyclic siloxanes are produced as a result of the pyrolysis of the primary siloxanes.

Table 7. A summary of the bands produced after pyrolysis compared with the bands belonging to known compounds of the cyclic siloxanes

Bands due to D3 / cm^{-1}	Bands due to D4 / cm^{-1}	Bands due to D5 / cm^{-1}	Unknown bands of D3 from pyrolysis / cm^{-1}	Unknown bands of D4 from pyrolysis / cm^{-1}	Unknown bands of D5 from Pyrolysis / cm^{-1}
606	-	-	-	-	-
-	697 (w)	702	-	-	-
-	786	-	-	-	-
-	797 (w)	797	-	-	-
818	816	812	-	-	-
-	-	862 (vw)	-	-	-
-	-	-	870 (w)	-	-
878	888	882 (vw)	-	-	-
-	-	-	1016	-	-
1022	-	-	-	-	-
1028	-	-	-	-	-
1036	-	-	-	1036	1035
-	-	1064	-	-	-
-	1072	1075	-	-	-
-	1083	-	-	-	-
-	-	1092	-	-	-
-	1099	-	-	-	-
-	-	1101	-	-	-
1262	1263	1262	-	-	-
-	-	-	2890	2890	2890
-	-	2970	-	-	-
-	-	-	-	2975	-
-	-	-	-	-	3019
3024	-	-	-	-	-

From the above table, it was deduced that both D4 and D5 appear to produce D3. However, no D5 appears to be produced from the pyrolysis of D4, as was reported in Khabashesku's paper. The frequencies of the bands due to the parent compounds of the three cyclic siloxanes are often

seen to be very close together. Therefore, overlapping of the bands may occur making it difficult to determine which of the three siloxanes are being produced

The formation of D3 from the pyrolysis of both D4 and D5, suggests the initial production of dimethylsilanone, as shown in Figure 25. However, no bands due to the formation of dimethylsilanone were observed.

4. A comparison of the Unknown Bands Produced as a Result of the Pyrolysis of the Three Cyclic Siloxanes: D4, D3 and D5

(a). Unknown Bands Produced After Pyrolysis

Although there were many unknown bands produced after pyrolysis, none were common to all of the three cyclic siloxanes. In order to establish which of these new bands were due to the same species, diffusion experiments were carried out on the pyrolysis products and the results have been tabulated below.

Table 8. Tabulated effects on the new bands of the three cyclic siloxanes after diffusion experiments on the pyrolysis products

Frequency / cm^{-1}	Species	Effect on new band Upon diffusion
870	D3	Increase
2975	D4	Increase
2890	D3	No change
1016	D3	Decrease
3019	D5	Decrease

The unknown bands produced can be put into three groups as shown in the above table. Members of each of the three groups, corresponds to the observed effects on the bands with the same relative intensity, after the diffusion experiments. Therefore suggesting the formation of three new species.

(b). Significant Changes in Intensity of Bands of all Three of the Cyclic Siloxanes After Diffusion Experiments were Carried out on the Pyrolysis Products

After the diffusion experiments were carried out on the pyrolysis products of D4, D3 and D5 changes to the spectrum were again seen and these changes have been tabulated below.

Table 9. Tabulated effects on the new bands of the three cyclic siloxanes as the parent compounds undergo diffusion experiments after pyrolysis

Frequency / cm^{-1}	Species	Effect on new band After diffusion
940	D5	Appear
956	D5	Appear
1016	D5	Appear
1035	D5	Disappear
1075 (vw)	D4	Appear
3279	D5	Disappear
3691 (vw)	D4	Appear

Two bands were seen to appear after the diffusion of the pyrolysis products of D4. These were at frequencies of 3691 and 1075 cm^{-1}. Both bands have been quoted as being very weak and they had also appeared after the diffusion experiments of the parent compound. Therefore, it is likely that these bands were actually due to the sharpening of the baseline.

Spectra were also obtained after the diffusion of pyrolysed D5. A band at 1016 cm^{-1} was produced after pyrolysis and then disappeared after diffusion. It is thought that this band must be due to unstable species that react further once the deposition window is warmed and the matrix cages are relaxed. In addition, two more bands were seen to appear after diffusion. These bands were seen at 956 and 940 cm^{-1}. One band was also seen to disappear. This band was at 3279 cm^{-1} and was thought to be due to an unstable species.

Below are spectra of D4, D3 and D5. The spectra obtained after pyrolysis has been subtracted from spectra of the parent compounds. Any new bands that have been formed after pyrolysis are shown by positive bands and the negative bands are due to the original parent compound bands. Bands that have yet to be identified have been labelled with a cross (X). (See Table 8).

Figure 26. Spectra of D3, D4 and D5 showing the bands still to be identified.

A). D3 / N_2 after pyrolysis – D3 / N_2
B). D4 / N_2 after pyrolysis – D4 / N_2
C). D5 / N_2 after pyrolysis – D5 / N_2

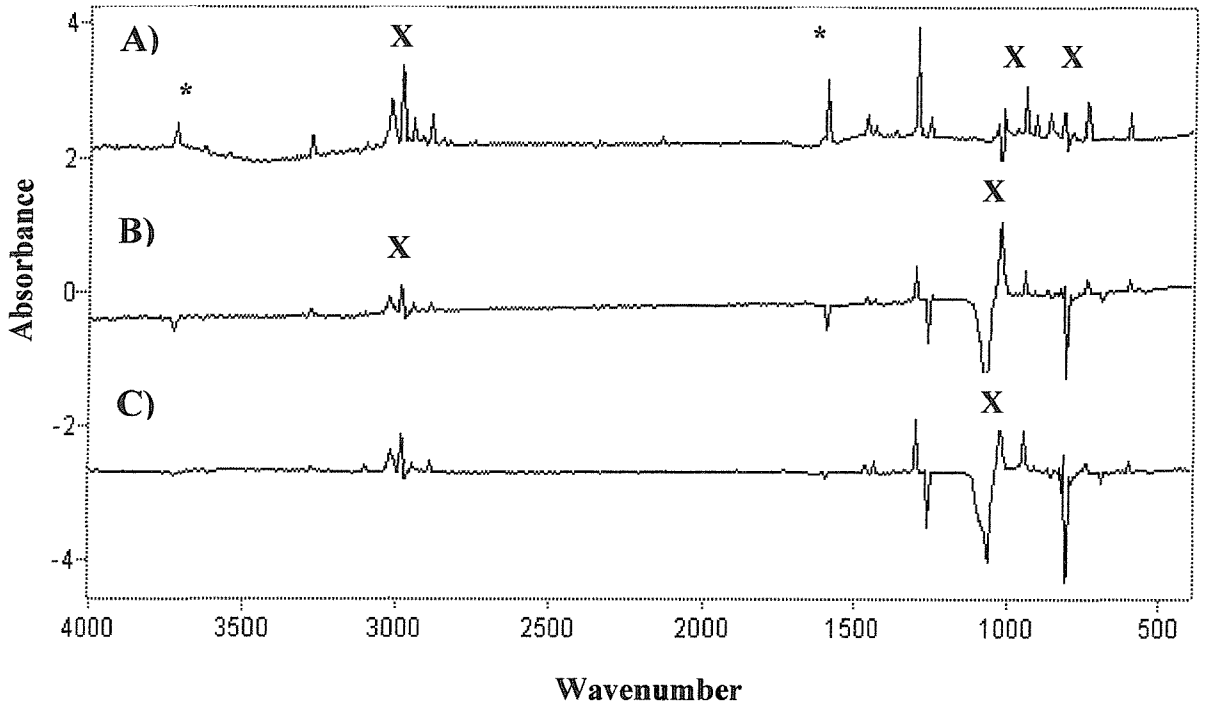

5. Minimum Energy Calculations

The analysis of the results of D4, D3 and D5 were supported by a number of molecular modelling calculations. Initially, a number of energy calculations were carried out with the intention of obtaining the geometry of the reactants and possible products of the reactions. The lowest theory of model chemistry[25] was used and then the calculations were repeated using a higher level of theory on the results of the first set of energy values.

However, there were some species where the geometry optimisation and frequency calculations were not able to be completed. In these cases, singlepoint energy calculations were conducted. The results can be seen below.

Table 10. Tabulated energy values in units of Hartrees

Species	HF / 3-21G Geom. & Freq. Optimisation / Hartrees	B3LYP / 6-31G(d) Geom. & Freq. Optimisation / Hartrees
CO_2	-186.1176	-188.5800
CO	-112.0933	-113.3095
H_2O	-75.5860	-76.4090
H_2	-1.1230	-1.1755
O_2	-148.6872	-150.1574
SiH_2	-288.4843	-290.6131
C_2H_6	-78.7939	-79.8304
C_2H_4	-77.6010	-78.5875
C_2H_2	-288.4843	-290.6131
CH_4	-39.9769	-40.5184
CH_3	-39.3426	-39.8383
D	-440.6558	-444.5662
D_2	-881.5302	-889.2962
D_3	-1322.4255	/
D_4	-1763.2683	/
D_5	-2204.0916	/
$Si(Me)_2(H)OH$	-441.8718	-445.8033
SiH_2O	-362.9559	-365.8977
SiMeH	-327.3255	-329.9418
Si(H)OH	-362.9977	-365.8974
SiMe(H)O	-401.8063	-405.2330

From the above table it can be seen that initially all calculations were carried out using a low level of theory in the form of the HF / 3-21G model chemistry (described in detail in Chapter 4). These calculations were then repeated using a higher level of theory of B3LYP / 6-31G (d). These values were calculated on the results of the first set of values. However, for the parent compounds of D4, D3 and D5, the energy values were not able to be achieved using the higher level of theory within the given time period.

Table 11. Tabulated energy values of singlepoint energy calculation in units of Hartrees

Species	HF / 3-21G Geom. & Freq. Optimisation / Hartrees	B3LYP / 6-31G(d) Singlepoint Energy Calculation / Hartrees
D4	-1763.2683	-1778.6861
D3	-1322.4255	-1329.4310
D5	-2204.0916	-2223.3584

Singlepoint energy calculations allowed the energies of the species to be calculated more quickly and relatively accurately, but it was necessary to first input the geometry that was originally calculated from a lower level of theory. The results tabulated in both Table 10 and Table 11 were then used to devise possible reaction schemes.

(a). Octamethylcyclotetrasiloxane Reaction Schemes

Possible by-products for the pyrolysis of D4, included CH_3, CH_4 and C_2H_6. Therefore, reaction schemes were devised around these pyrolysis products.

Figure 27. (A) – (D). Reaction schemes for the pyrolysis of D4

A)

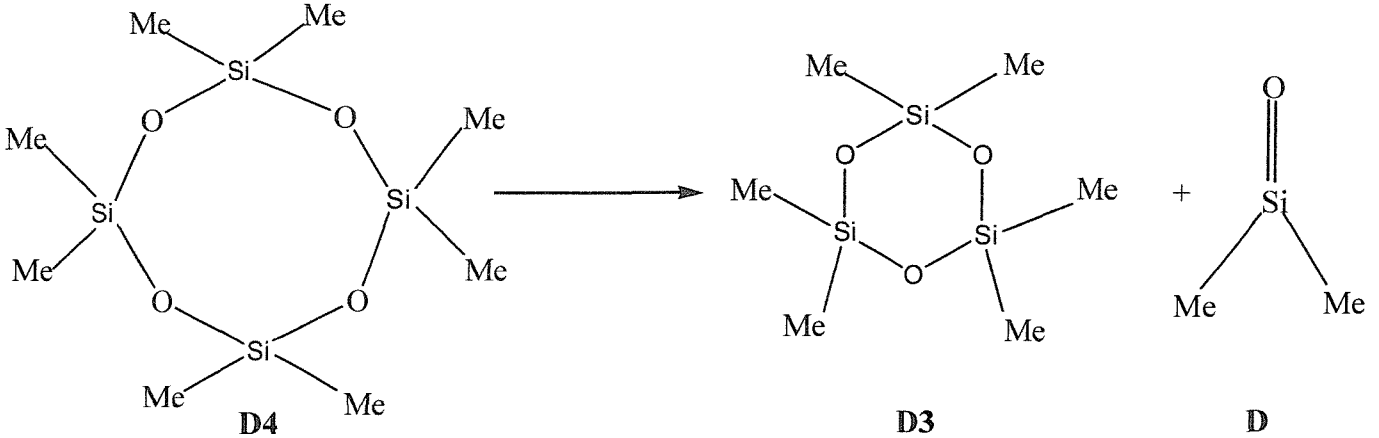

D4
-1778.6861 Hartrees

D3
-1329.4310 Hartrees

D
-444.5662 Hartrees

⟹ **4.6889 Hartrees ≡ ΔE = 2942.3316 kcal / mol**

B)

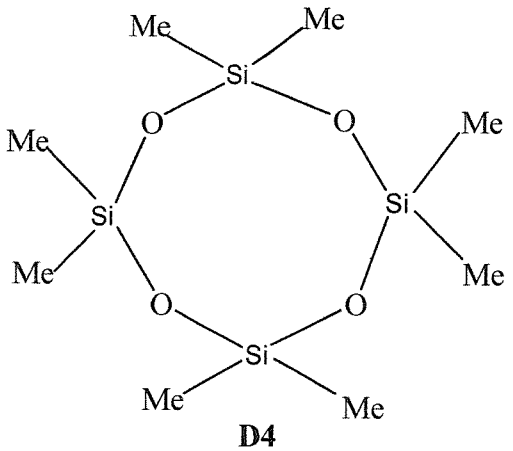

D4
-1778.6861 Hartrees

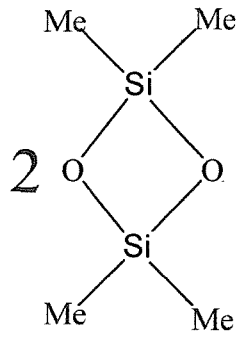

D2
-889.2962 (2x) Hartrees

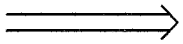

0.0937 Hartrees ≡ ΔE = 58.7977 kcal / mol

C)

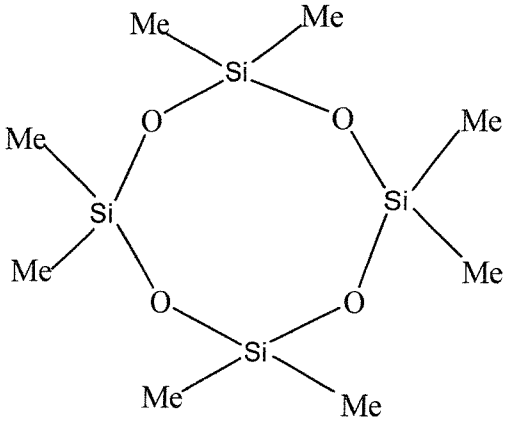

D4
-1778.6861 Hartrees

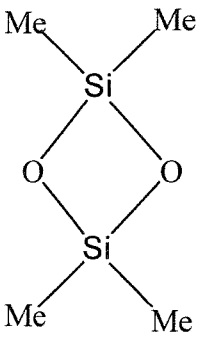

+ 2 SiO + C_2H_6

D2
-889.2962 Hartrees -79.8304 Hartrees
-364.7200 (x2) Hartrees

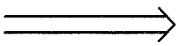

80.1195 Hartrees ≡ ΔE = 50275.7874 kcal / mol

D)

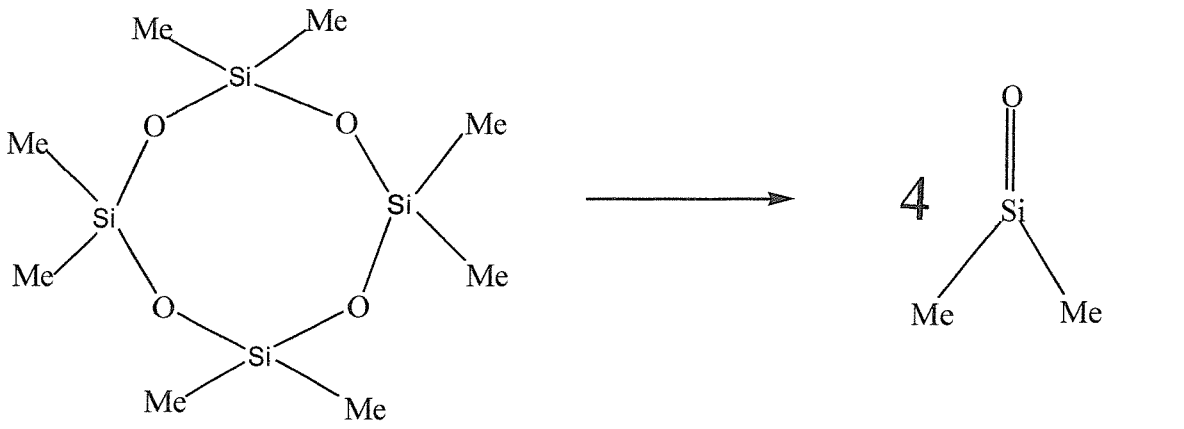

D4
-1778.6861 Hartrees

D
-444.5662 (4x) Hartrees

0.4213 Hartrees ≡ ΔE = 264.3700 kcal / mol

As it can be seen, each of the above energy values were calculated in units of Hartrees and then converted to kcal / mol. It should be noted that 1 Hartree = 627.510 kcal / mol. From the above possible reaction schemes, the reaction with the least positive value of ΔE, is equation **B)** where D4 dissociates to produce D2. It is know the paper of Khabashesku *et al.*[1] that the bands of D2 are found at 1067, 1052 and 919 cm^{-1}. From Table 1 it can be seen that only one of these bands is produced from the pyrolysis of D4 and this band is at 919 cm^{-1}. However, since this band is reported as being the strongest of the three bands, it could be that the other bands are not seen as they are of low abundance. The second most feasible equation from the above reaction schemes, is reaction **D)** to produce the cyclo dimer. However, the latter species is known to be very reactive and would therefore almost certainly dissociate further, possibly to produce SiO and small hydrocarbons. However, if any SiO is produced from these pyrolysis experiments, then it is likely to be produced in low abundance since no SiO bands are observed.

(b). Hexamethylcyclotrisiloxane Reaction Schemes

With the knowledge of the possible pyrolysis products produced from the pyrolysis of D3, various reaction schemes were devised.

Figure 28. A) – C). Reaction schemes showing possible pyrolysis products of D3

A)

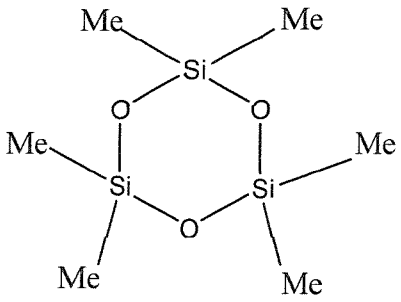

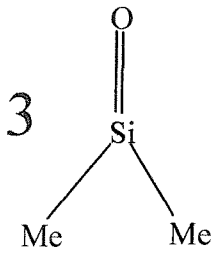

D3
-1329.4310 Hartrees

D
-444.5662 (3x) Hartrees

⟹

-4.2676 Hartrees ≡ ΔE = -2677.9617 kcal / mol

B)

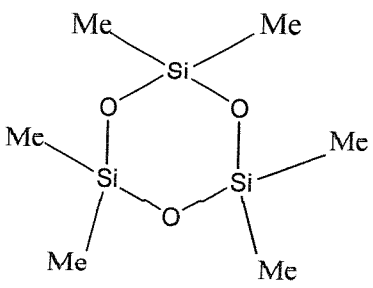

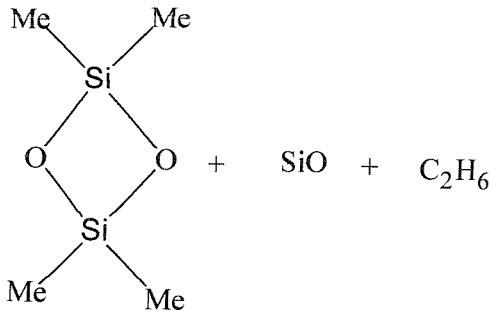

D3
-1329.4310 Hartrees

D2
-444.5662 Hartrees -364.7200 Hartrees -79.8304 Hartrees

⟹

-4.4156 Hartrees ≡ ΔE = -2770.8332 kcal / mol

C)

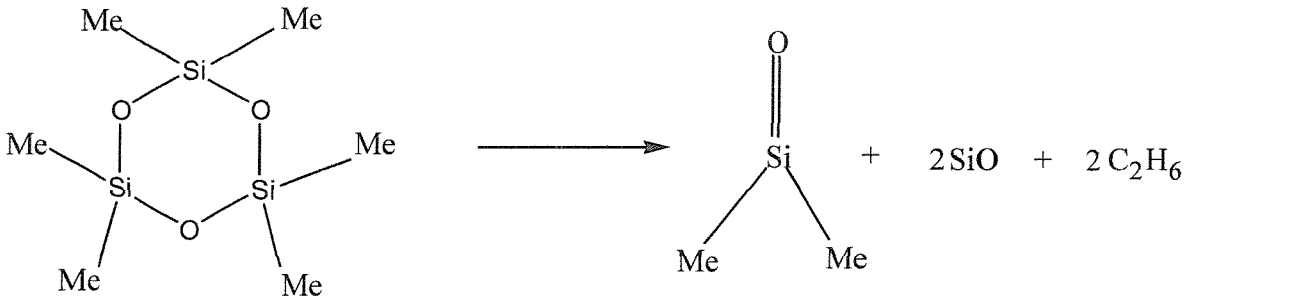

D3
-1329.4310 Hartrees

D
-444.5662 Hartrees
-79.8304 (2x) Hartrees
-364.7200 (2x) Hartrees

$\Longrightarrow$

-4.1995 Hartrees ≡ ΔE = -2635.2282 kcal / mol

From these possible schematic diagrams, the reaction scheme with the least positive value of ΔE is equation **B)** to produce D2, silicon monoxide and ethane. In work of Khabashesku *et al.*[1] of the pyrolysis of D4, bands were reported to be produced due to D2 at 1067, 1052 and 919 cm^{-1}. Looking back at the tabulated bands produced from the pyrolysis of D3 in Table 2, a band was produced at 919 cm^{-1} in the experiments carried out here after the pyrolysis of D3. However the other two bands are not observed. It has also already been seen that ethane is produced as a result of pyrolysis. It is possible that acetylene may also be further produced with the elimination of hydrogen from ethane. However, this is not say that the other two possible reaction schemes to not occur. They may well occur, but to a lesser extent.

(c). Decamethylcyclopentasiloxane Reaction Schemes

The energy values obtained for the parent compound and the possible products tabulated in Tables 10 and 11, together with the knowledge acquired of possible species produced, mainly in the form of hydrocarbons, were used to devise various reaction schemes. These schemes are shown below.

Figure 29. (A)-(C). Reaction schemes for the pyrolysis of D5

A)

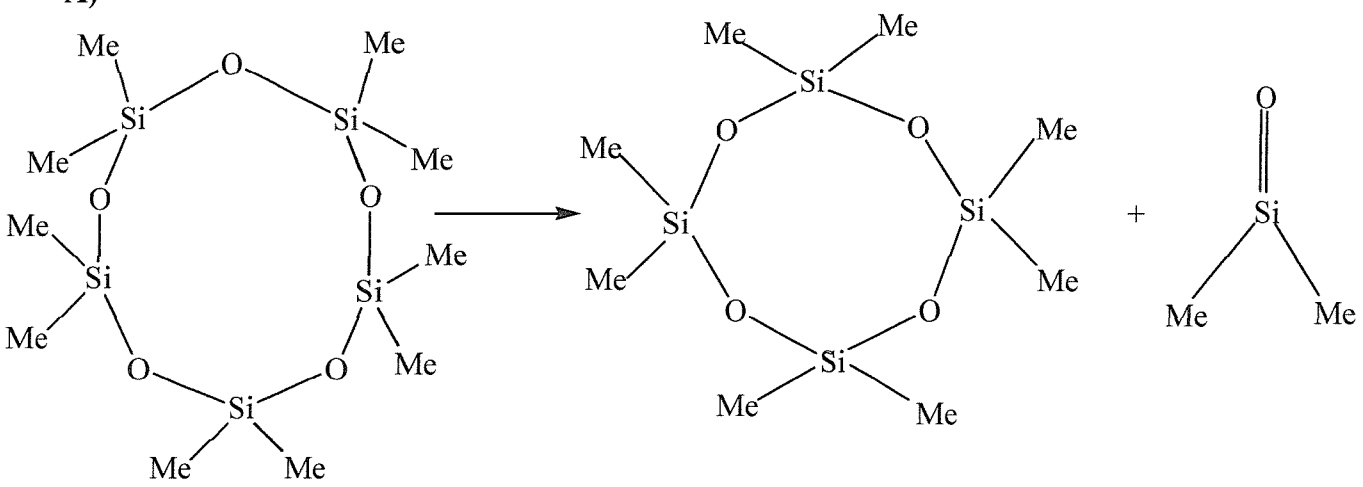

D5
-2223.3584 Hartrees

D4
-1778.6861 Hartrees

D
-444.5662 Hartrees

⟹ **0.1061 Hartrees ≡ ΔE = 66.5788 kcal / mol**

B)

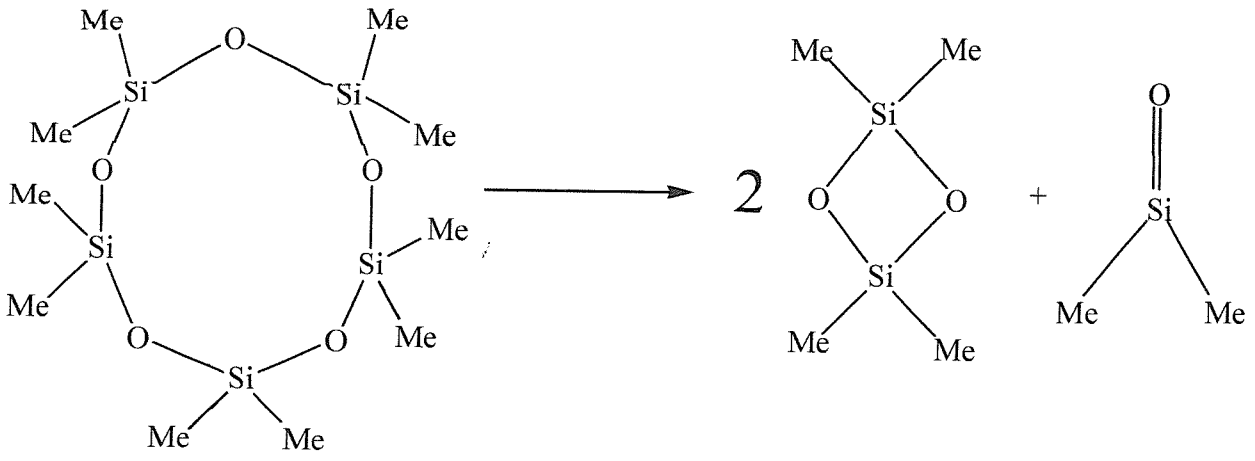

D5
-2223.3584 Hartrees

D2
-889.2962 (2x) Hartrees

D
-444.5662 Hartrees

⟹ **0.1998 Hartrees ≡ ΔE = 125.3765 kcal / mol**

C)

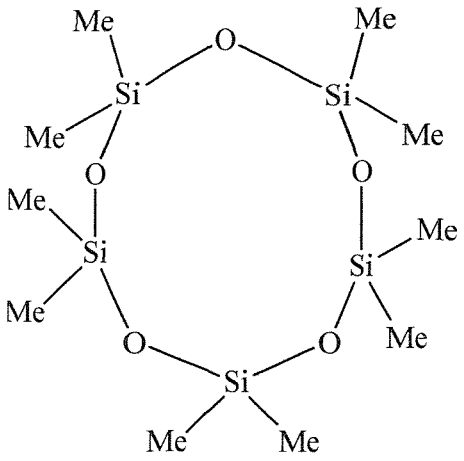

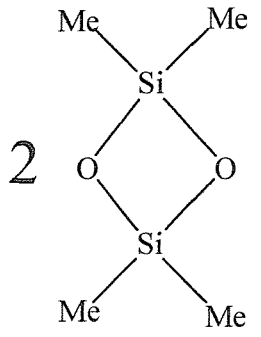

2 + SiO + C_2H_6

D5
-2223.3584 Hartrees

D2
-889.2962 (2x) Hartrees -79.8304 Hartrees
-364.7200 Hartrees

$\Longrightarrow$

0.2156 Hartrees ≡ ΔE = 135.2912 kcal / mol

D)

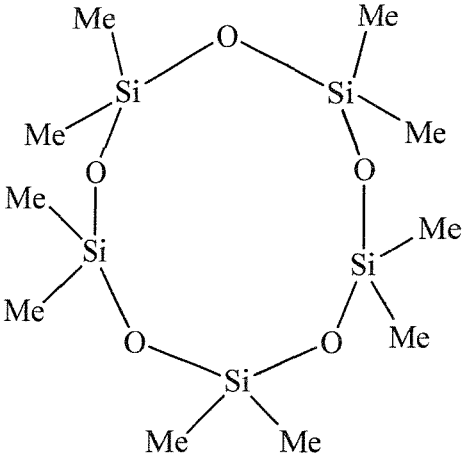

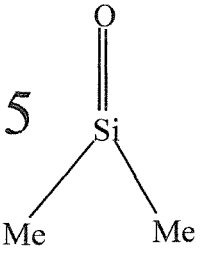

5

D5
-2223.3584 Hartrees

D
-444.5662 (5x) Hartrees

$\Longrightarrow$

-0.5274 Hartrees ≡ ΔE = -330.9488 kcal / mol

As can be seen from the above reaction schemes, the reaction with the least positive value of ΔE, and therefore the most favourable reaction is equation **D)** with a overall energy value for the formation of D4 and D of –330.9488 kcal / mol.

6. Frequency Calculations

(a). Hexamethylcyclotrisiloxane

Frequency calculations were then carried out on the parent compound, D3. It was important to establish whether these calculations could be relied upon to produce an accurate calculated spectrum.

Figure 30. Spectra of hexamethylcyclotrisiloxane

A). Experimentally obtained spectrum of D3 / N_2
B). A spectrum of calculated frequencies of D3 – (HF / 3-21G)

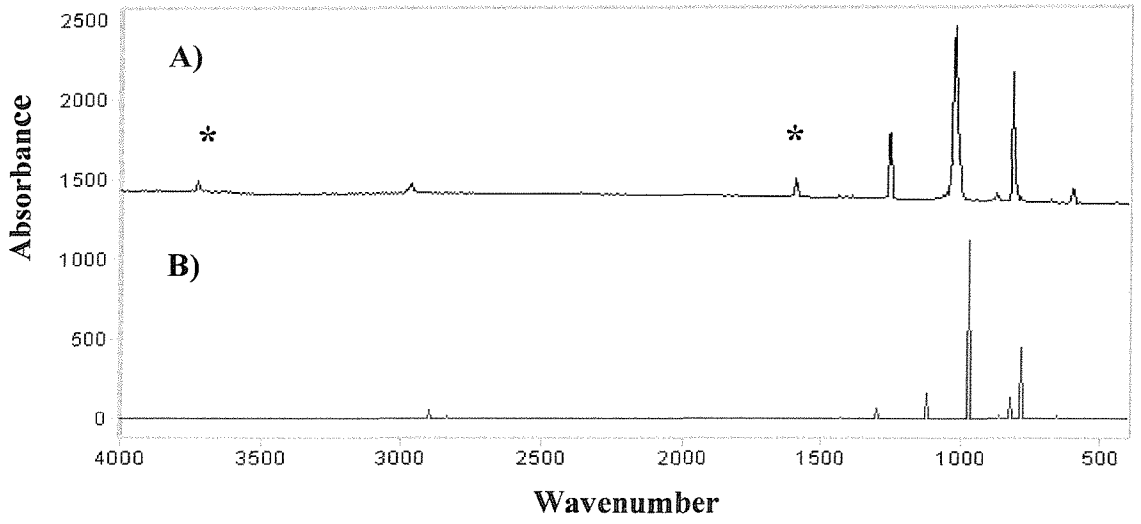

The two spectra shown above demonstrate the accuracy of the frequency calculations. The spectra are in good agreement with each other, both in terms of the intensities of the bands (shown in the spectra) and the frequencies of the bands tabulated below.

Figure 12. A comparison of frequencies in both experimental and calculated spectra

Frequencies obtained from experimental spectrum of D3 / N_2	Frequencies obtained from calculated spectrum of D3 – (HF / 3-21G)
606 (w)	664 (vw)
689 (vw)	796 (m)
817 (s)	824 (w)
880 (vw)	871 (vw)
1021 (sh)	-
1028 (s)	977 (s)
1035 (sh)	-
1261 (m)	1129 (m)
-	1301 (w)
1597 (w)	-
-	1432 (vw)
2972 (vw)	2839 (vw)
3724 (vw)	2902 (w)

(b). Decamethylcyclopentasiloxane

As with D3, frequency calculations were carried out for D5. As before, the purpose of these calculations was to establish the reliability of the Gaussian program for calculating the frequencies of the species used here. These calculations are observed to be of fundamental importance when analysing the cyclic siloxanes but are later seen to be far more significant when analysing the linear siloxanes (see chapter seven).

Below are two spectra demonstrating the accuracy of the Gaussian program for calculating the frequencies of the parent compounds.

Figure 31. Spectra of decamethylcyclopentasiloxane

A). Experimentally obtained spectrum of D5 / N_2
B). A spectrum of calculated frequencies of D5 – (HF / 3-21G)

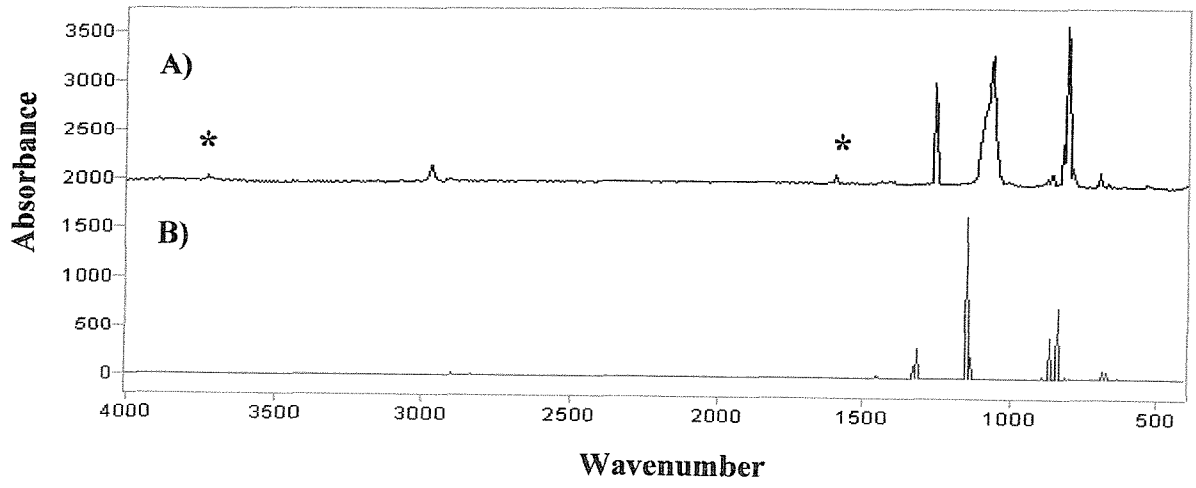

Again, as with the results from the frequency calculations of D3, the results of the calculations of D5 show a very close fit to the spectrum obtained experimentally. (See Table 11).

Figure 13. A comparison of frequencies in both experimental and calculated spectra

Frequencies obtained from experimental spectrum of D5 / N_2	Frequencies obtained from calculated spectrum of D5 – (HF / 3-21G)
702 (vw)	673 (vw)
812 (s)	688 (vw)
824 (sh)	841 (m)
862 (sh)	863 (w)
881 (sh)	867 (w)
-	983 (vw)
1064 (s)	1137 (w)
-	1147 (s)
1262 (s)	1319 (vw)
-	1322 (w)
-	1325 (vw)
-	1453 (vw)
1597 (vw)	-
-	2834 (vw)
2971 (vw)	2895 (vw)
3723 (vw)	-

(c). Dimethylsilanone

Dimethylsilanone is known to be an important species in silicon chemistry at Dow Corning. As a result, this species was greatly featured in the reaction schemes in section 4, as a possible product of the pyrolysis of various cyclic siloxanes. Khabashesku *et al.*[1] are reported to have produced dimethylsilanone from the pyrolysis of allyloxydimethylsilane with the production of a band at 798 cm^{-1}. In order to confirm that this band does belong to dimethylsilanone and to therefore eliminate this species from the suspected possible products for these reactions, a frequency calculation was carried out and a spectrum was obtained of the calculated frequencies.

Figure 32. A calculated spectrum of dimethylsilanone – (B3LYP / 6-31G (d))

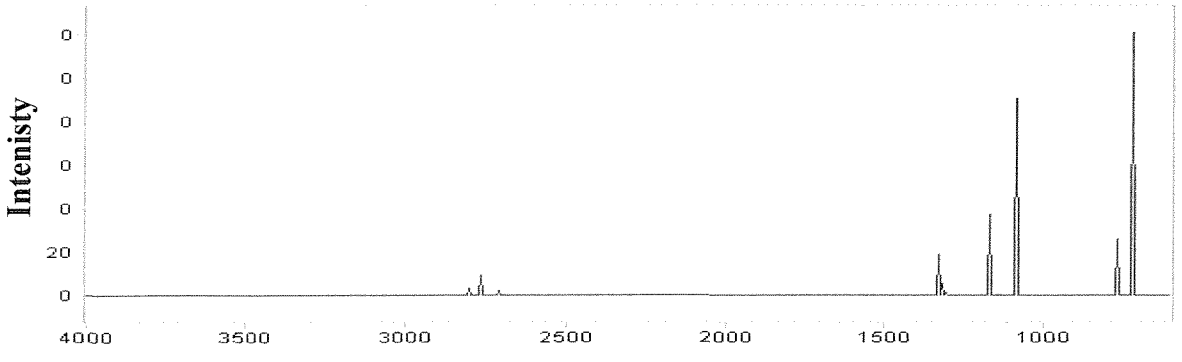

Khabashesku *et al.* claim that bands were present in their spectra at 1067, 1052 and 919 cm^{-1} due to the formation of the cyclic dimer, D2. This suggests the involvement of dimethylsilanone within these pyrolysis reactions.

On referring back to Table 7, which contains all of the remaining unknown bands, it can be seen that none of these unknown bands match those bands observed in the spectrum of dimethylsilanone. Therefore, it can be deduced that no dimethylsilanone is produced from the pyrolysis of D4, D3 or D5.

7. Conclusion

The initial pyrolysis experiments carried out here on octamethylcyclotetrasiloxane agree in part with the findings of Khabashesku *et al.*[1]. However, their spectra were only published in the region between 1500-400 cm^{-1} and so since no stretching modes were observed, the reported results could not be taken as conclusive. Full range spectra were recorded for the work carried out here, which enabled confirmation of the formation of the small hydrocarbons in the previously published spectra of CH_3, CH_4 and C_2H_2. However, the formation of C_2H_4 has been questioned.

This area of research was continued and further expanded to include the investigation of other cyclic siloxanes, namely hexamethylcyclotrisiloxane and decamethylcyclopentasiloxane. It can be concluded that CH_3, CH_4, C_2H_2 and also C_2H_6 were found present in each of the spectra of D4, D3 and D5 after pyrolysis. Although there is some unambiguity, it is also likely that C_2H_4 is produced.

Evidence of interconversion reactions taking place was also found. Khabshesku *et al.* report that D4 produces both D3 and D5 upon pyrolysis, via the elimination of the reactive intermediate, dimethylsilanone. It was found from work conducted here that both D4 and D5 produces D3 upon pyrolysis. This result agrees with the suggestion of the formation of dimethylsilanone and its participation within these pyrolysis reactions. However, no evidence of additional cyclic siloxane pyrolysis products was found.

A number of energy and frequency calculations carried out here support the claim that pyrolysis reactions are occurring via the production of dimethylsilanone. The energy calculations gave the following reactions as being the most favourable for the cyclic siloxanes during pyrolysis:

Figure 33.

D4 ⟶ **2D2**

D3 ⟶ **D2 + SiO + C_2H_6**

D5 ⟶ **5D**

Each of these reactions support the elimination of dimethylsilanone, however, only the calculation of *D5* actually produces the reactive intermediate, indicating that either fragmentation or dimerisation readily occurs, resulting in no dimethylsilanone being isolated.

8. References

1). V. N. Khabashesku, Z. A. Kerzina, A. K. Maltsev and O. M. Nefedov, J. Organomet. Chem., 364, **(1989)**, 301 – 312

2). V. N. Khabashesku, N. K. Konstantin and J. L. Margrave, J. Mol. Struc., 443, **(1998)**, 175 – 189

3). V. N. Khabashesku, N. K. Konstantin and O. M. Nefedov, J. Organomet. Chem., 566, **(1998)**, 45 – 59

4). V. N. Khabashesku, N. K. Konstantin , J. L. Margrave and L. Fredin, J. Organomet. Chem., 595, **(2000)**, 248 - 260

5). I. L. Mador, J. Chem. Phys., 22, **(1954)**, 1617-1618

6). W. L. S. Andrews, J. Chem. Phys., 44, **(1966)**, 2527 – 2528

7). G. Herzberg, Proc. Roy. Soc., A262, **(1961)**, 291 – 305

8). L. Andrews and G. C. Pimentel, J. Chem. Phys., 47, **(1967)**, 3637 – 3644

9). D. E. Milligan and M. E. Jacox, J. Chem. Phys, 47, **(1967)**, 5146 – 5156

10). L. Y. Tan and G. C. Pimentel, J. Chem. Phys., 48, **(1968)**, 5202 – 5204

11). A. Snelson, J. Phys. Chem., 74, **(1970)**, 537 – 544

12). L. Y. Tan, A. M. Winer and G. C. Pimentel, J. Chem. Phys. 57, **(1972)**, 4028 – 4037

13). G. Allen, A. D. Kennedy and H. O. Pritchard, J. Phys. Chem., 65, **(1961)**, 885 – 886

14). M. E. Jacox, J. Mol. Spec. , 66, **(1977)**, 272 – 287

15). K. J. Klabunde and Y. Tanaka, J. Am. Chem. Soc., 105, **(1982)**, 3544 – 3546

16). G. Jeong and K. J. Klabunde, J. Am. Chem. Soc., 108, **(1986)**, 7103 – 7104

17). G. H. Jeong, R. Boucher and K. J. Klabunde, J. Am. Chem. Soc., 112, **(1990)**, 3332 – 3337

18). K. Burczyk and A. J. Downs, J. Chem. Soc., Dalton Trans., **(1990)**, 2351 – 2357

19). B. S. Ault, J. Phys. Chem., 96, **(1992)**, 7908 - 7912

20). H. Frei, L. Fredin and G. C. Pimentel, J. Chem. Phys., 74, **(1981)**, 397-410

21). Tables of Molecular Vibrational Frequencies, Consolidated Volume 1, **(1972)**, by the secretary of commerce on behalf of the United States Government

22). K. Nakamoto, Infrared and Raman Spectra of Inorganic and Co-ordination Compounds, volume 2, 5th edition, Wiley – Interscience, **(1997)**

23). Y. Ogawara, A. Bruneau and T. Kimura, Anal. Chem., **(1994)**, 66, 4354-4358

24). Z. Mielke, K. G. Tokhadze, M. Hulkiewicz, L. Schriver-Muzzuoli, A. Schriver and F. Roux, J. Phys. Chem., **(1995)**, 99, 10498-10505

25). J. R. Foresman & A. Frisch, Exploring Chemistry with Electronic Structure, second edition, Gaussian Inc. Pittsburgh, PA, **(1996)**

CHAPTER SEVEN

PYROLYSIS OF LINEAR SILOXANES

1. Introduction

After successfully pyrolysing various cyclic siloxanes and isolating the products, it was then decided to attempt to isolate the products of various linear siloxanes. The linear siloxanes that were decided upon to pyrolyse were 1,1,3,3-tetramethyldisiloxane (L1), 1,1,3,3,5,5-hexamethyltrisiloxane (L2) and 3H, 5H-octamethyltetrasiloxane (L3). The abbreviations in brackets have been used for simplicity.

1.1. Nitrogen Matrix vs Argon Matrix

As with the previous experiments involving the cyclic siloxanes, the pyrolysis of the linear siloxanes were again carried out in both argon and nitrogen matrices. The spectra obtained in a nitrogen matrix were again found to produce the sharpest bands.

Figure 1. A comparison between 1,1,3,3-tetramethyldisiloxane in an argon matrix and a nitrogen matrix

A). L1 / Ar
B). L1 / N_2

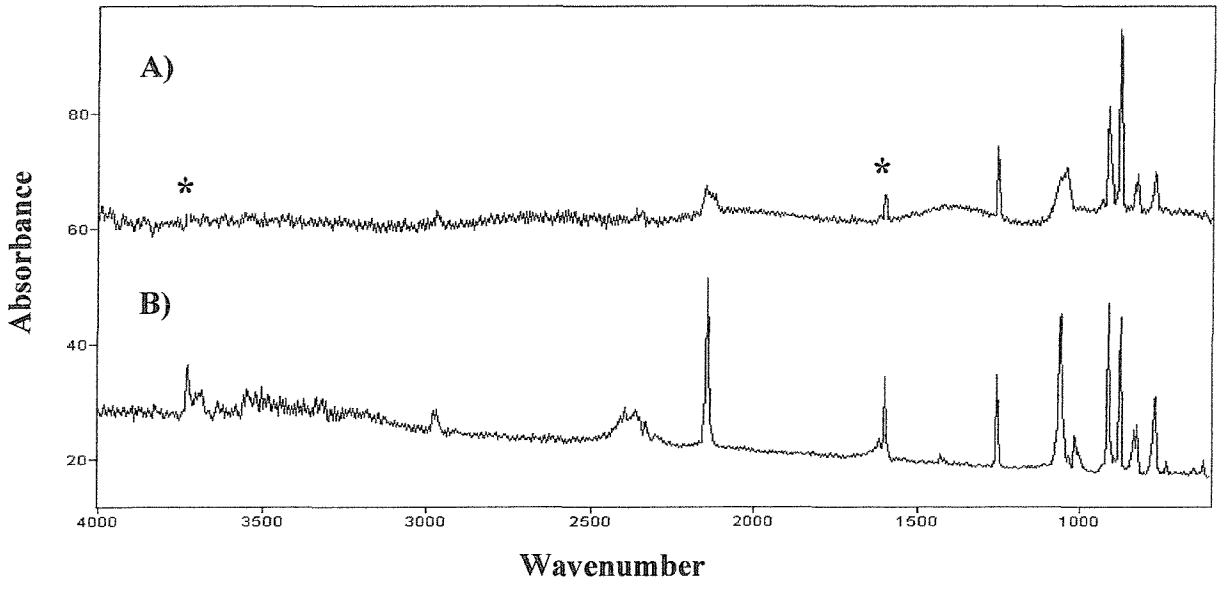

The bands in spectrum **B)** are sharper than those observed in spectrum **A)**, therefore it was decided to present and discuss spectra obtained in a nitrogen matrix throughout this chapter.

1.2. General Procedure

Below is a flow diagram for the experimental procedure of the linear siloxane experiments.

Figure 2. A flow diagram below summarises links between experimental and theoretical procedures

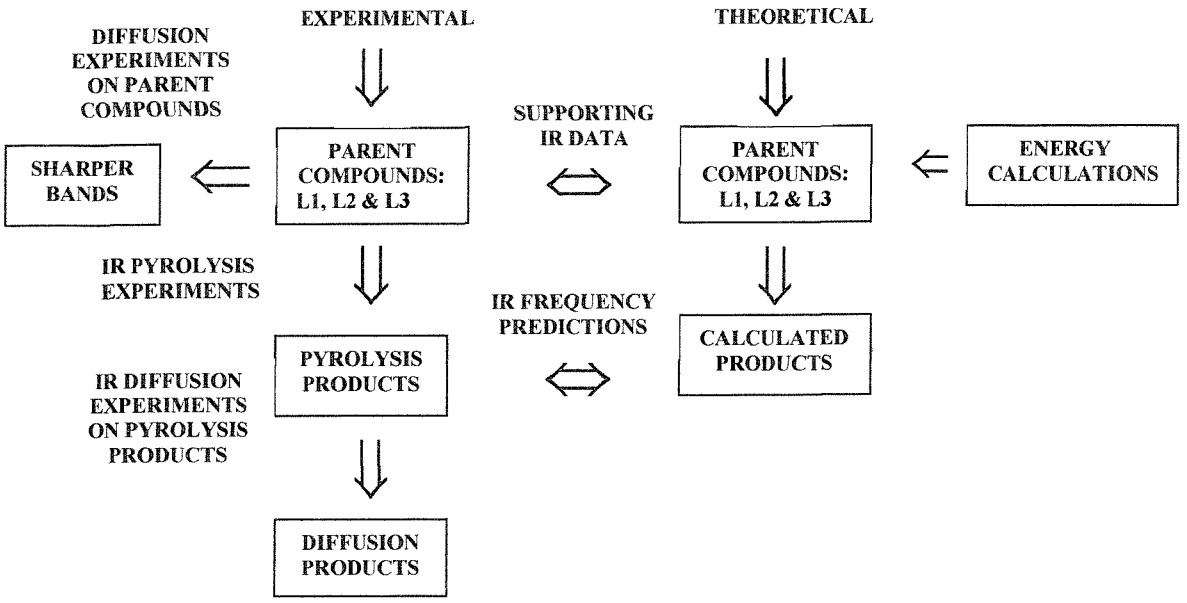

The experimental conditions are the same as those used in chapter six and were described in chapter two. Initial spectra of the three linear siloxane parent compounds were obtained. The sample vapour was then heated to high temperatures of up to 700-720 °C and the reactive intermediates that were formed were isolated within the matrix cages. Diffusion experiments were performed after pyrolysis, where the deposition window was warmed to about 27 K. This allowed the matrix cages to loosen and any trapped species the chance to reorient and the possibility to react further. By carrying out diffusion experiments it was hoped that bands responsible for the same species could be identified, through observed common changes in intensity. Finally, diffusion experiments were then carried out on the parent compounds, as a control to find out the effects of diffusion on the parent bands. Spectra were obtained at each of these four stages. All spectra shown are as a result of the subtraction of the background spectrum.

After spectra had been collected and analysed, it was again found that there were a number of unknown bands that had been formed upon pyrolysis. Molecular modelling calculations were conducted of a number of possible products in order to produce the minimum energies of these

species to therefore find the most favourable products. This was followed by frequency calculations of pyrolysis products and of parent compounds. These calculated frequencies were then compared to the frequencies of the unknown bands in order to further assist in the identification of the unknown bands.

2. Preliminary Results

Spectra were obtained of 1,1,3,3-tetramethyldisiloxane, 1,1,3,3,5,5-hexamethyltrisiloxane and 3H, 5H-octamethyltetrasiloxane. The investigation into the products produced from the pyrolysis of the above linear siloxanes, started by examining the pyrolysis products that were thought to be produced from the pyrolysis of the cyclic siloxanes, shown in the previous chapter. These included a series of small hydrocarbons and radicals species. The spectra obtained for each of the three linear siloxanes can be seen below.

2.1. Spectra of Linear Siloxanes

(a). 1,1,3,3-Tetramethyldisiloxane (L1) / N_2

1,1,3,3-Tetramethyldisiloxane was the first of the linear siloxanes to be pyrolysed and its structure is seen below. L1 is a three-membered chain, consisting of alternate silicon and oxygen atoms. Four methyl groups and two hydrogen atoms are attached to the two silicon atoms.

Figure 3. 1,1,3,3-Tetramethyldisiloxane

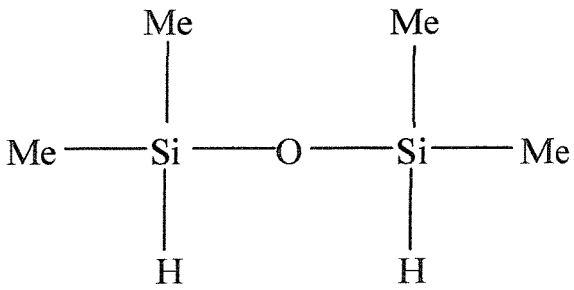

Spectra were obtained after each experiment. These experiments were carried out in a nitrogen matrix and the spectra were analysed after each stage.

Figure 4. Spectra of 1,1,3,3-tetramethyldisiloxane / N_2 - 4000-400 cm^{-1}

A). L1 / N_2
B). L1 / N_2 – after diffusion
C). L1 / N_2 – after pyrolysis
D). L1 / N_2 – after pyrolysis & diffusion

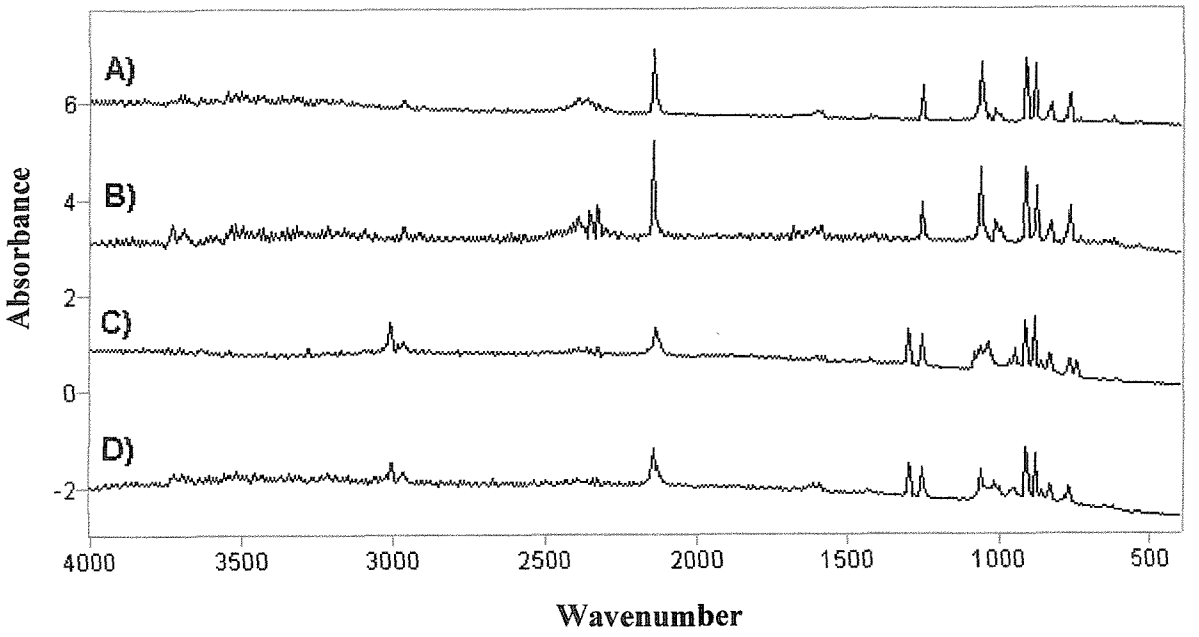

It was observed that many changes occurred in the region between 1500-400 cm^{-1}. This region was therefore expanded and can be seen below.

Figure 5. Spectra of 1,1,3,3-tetramethyldisiloxane / N_2 – 1500– 400 cm^{-1}

A). L1 / N_2
B). L1 / N_2 after pyrolysis
C). L1 / N_2 after pyrolysis – L1 / N_2

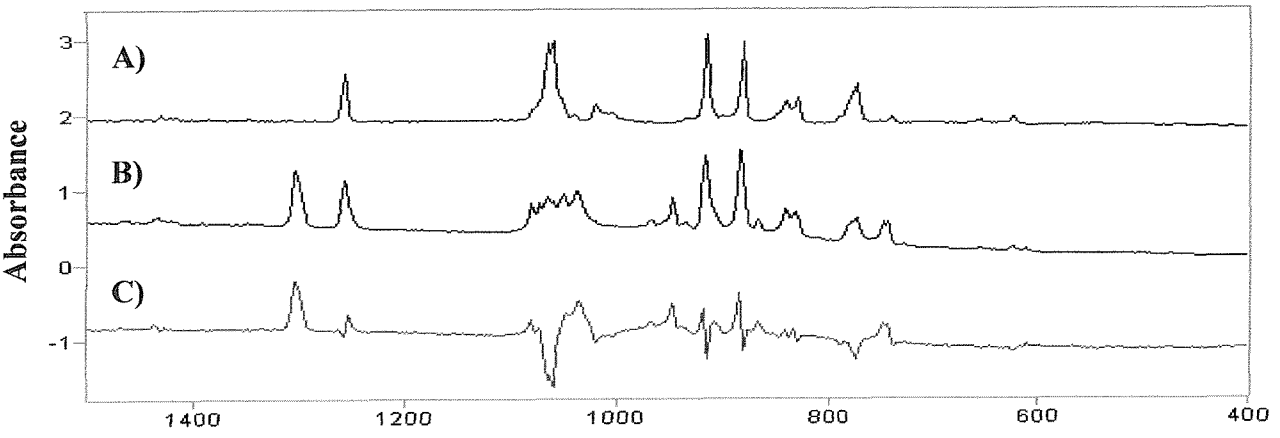

All bands found in Figure 3 have been tabulated in Table 1, in order to aid the analysis of the pyrolysis of 1,1,3,3-tetramethyldisiloxane.

Table 1. Tabulated bands obtained for 1,1,3,3-tetramethyldisiloxane / N_2

L1	L1 after diffusion	L1 after pyrolysis	L1 after pyrolysis & after diffusion
-	-	610 (vw)	-
623 (w)	623 (w)	623 (w)	623 (w)
-	-	726 (w)	-
738 (vw)	738 (vw)	-	-
-	-	742 (m)	-
-	-	746 (m)	-
771 (m)	771 (m)	771 (m)	771 (m)
779 (sh)	779 (sh)	779 (sh)	779 (sh)
830 (m)	830 (m)	830 (m)	830 (m)
839 (m)	839 (m)	839 (m)	839 (m)
-	-	866 (w)	866 (w)
880 (s)	880 (s)	880 (s)	880 (s)
914 (s)	914 (s)	914 (s)	914 (s)
-	-	946 (w)	-
-	-	967 (w)	-
1019 (w)	1019 (w)	1019 (w)	1019 (w)
1037 (w)	-	1037 (w)	-
-	-	1050 (sh)	-
1059 (sh)	1059 (sh)	1059 (sh)	1059 (sh)
1065 (sh)	1065 (sh)	1065 (sh)	1065 (sh)
-	-	1072 (sh)	-
-	-	1081 (sh)	-
1257 (s)	1257 (s)	1257 (s)	1257 (s)
-	-	1302 (s)	1302 (s)
1435 (w)	1435 (w)	1435 (w)	1435 (w)
1597 (vw)	1597 (vw)	1597 (vw)	1597 (vw)
-	1694 (w)	1694 (w)	-
-	-	2127 (sh)	-
-	-	2133 (sh)	2133 (sh)
2142 (sh)	2142 (sh)	2142 (sh)	2142 (sh)
2146 (s)	2146 (s)	2146 (s)	2146 (s)
-	2330 (w)	2330 (w)	2330 (w)
2346 (vw)	2346 (vw)	2346 (vw)	2346 (vw)
-	-	-	3007 (m)
-	-	3010 (m)	-
-	-	3014 (m)	-
-	-	3281 (w)	-
3723 (w)	3723 (w)	3723 (w)	2723 (w)

(b). 1,1,3,3,5,5-Hexamethyltrisiloxane (L2) / N_2

Below is the structure of 1,1,3,3,5,5-hexamethyltrisiloxane. It consists of a five-membered chain of silicon and oxygen atoms. Six methyl groups and two hydrogen atoms are joined to the three silicon atoms.

Figure 6. 1,1,3,3,5,5-hexamethyltrisiloxane

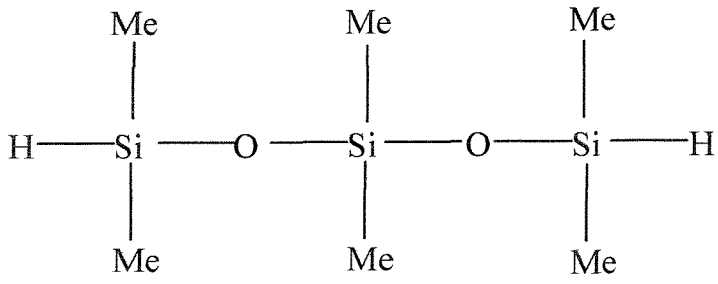

As with 1,1,3,3-tetramethyldisiloxane, initial spectra of 1,1,3,3,5,5-hexamethyltrisiloxane were obtained, as well as spectra of L2 after pyrolysis and diffusion.

Figure 7. Spectra of 1,1,3,3,5,5-hexamethyltrisiloxane / N_2 – 4000-400 cm^{-1}

A). L2 / N_2
B). L2 / N_2 after diffusion
C). L2 / N_2 after pyrolysis
D). L2 / N_2 after pyrolysis & diffusion

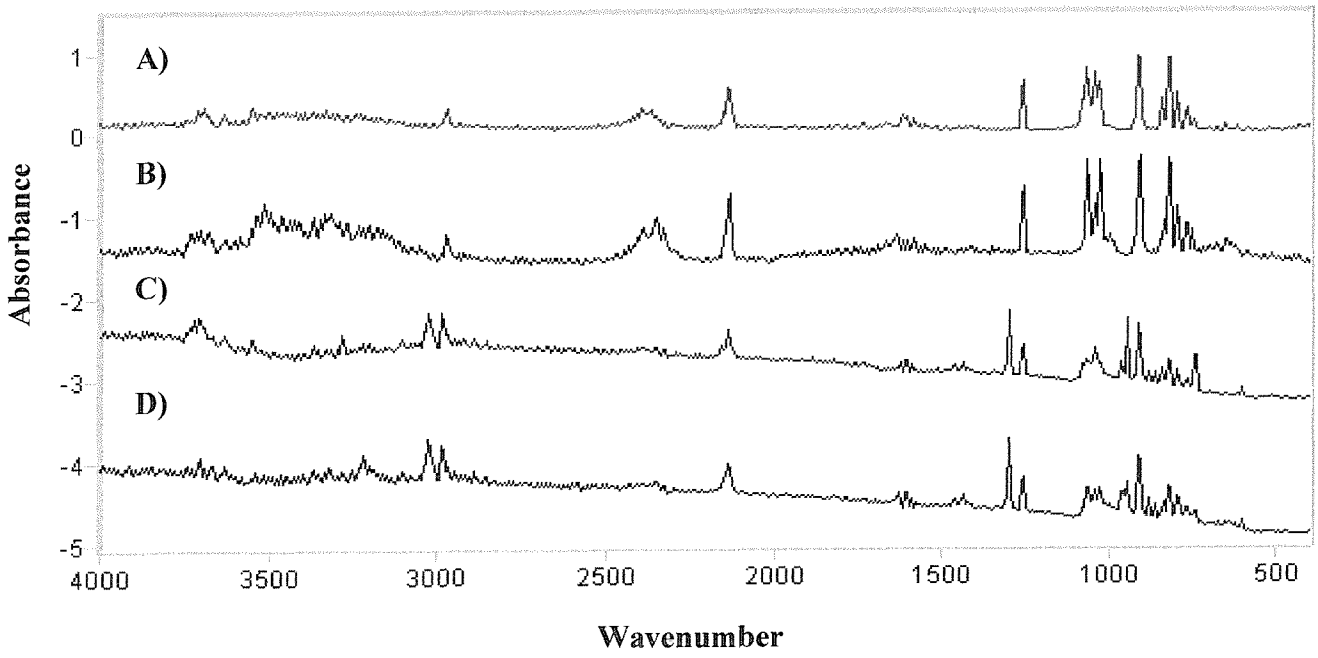

From the above spectra it can be seen that many of these new bands were produced below 1500 cm^{-1}. This region was expanded and can be seen below.

Figure 8. Spectra of 1,1,3,3,5,5-hexamethyltrisiloxane / N_2 – 1500-400 cm^{-1}

A). L2 / N_2
B). L2 / N_2 after pyrolysis
C). L2 / N_2 after pyrolysis – L2 / N_2

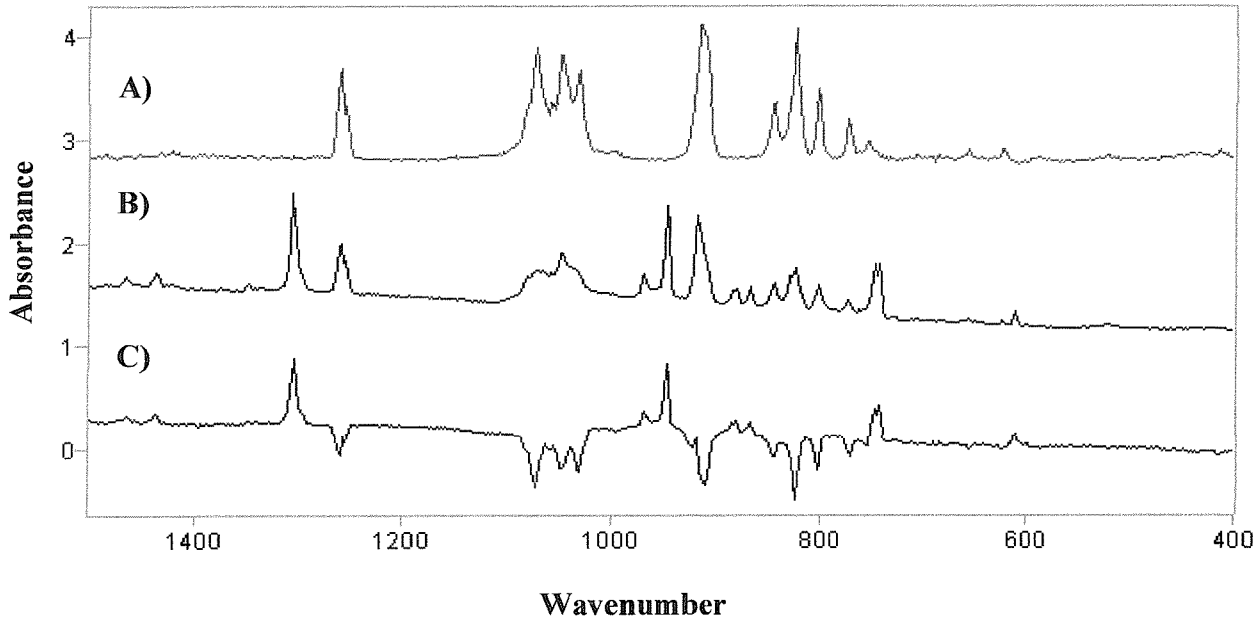

All the bands found in the above two sets of spectra have been tabulated below. Again, many new bands were produced and an investigation into the formation of small hydrocarbons was carried out. An analysis of the spectra took place in order to try and establish the pyrolysis products.

Table 2. Tabulated bands of obtained for 1,1,3,3,5,5-hexamethyltrisiloxane / N_2

L2	L2 after diffusion	L2 after pyrolysis	L2 after pyrolysis & after diffusion
-	-	610 (w)	610 (w)
622 (w)	-	-	-
657 (vw)	657 (vw)	-	-
-	-	742 (m)	-
-	-	747 (m)	-
772 (w)	772 (w)	772 (m)	772 (w)
800 (m)	800 (m)	800 (m)	800 (m)
823 (m)	823 (m)	823 (m)	823 (m)
828 (sh)	828 (sh)	828 (sh)	828 (sh)
843 (w)	843 (w)	843 (w)	843 (w)
-	-	866 (w)	866 (w)
-	-	880 (w)	880 (w)
913 (s)	913 (s)	917 (s)	915 (s)
-	-	947 (s)	947 (s)
-	-	969 (w)	969 (w)
1032 (s)	1032 (s)	1032 (s)	1032 (s)
1048 (m)	1048 (m)	1048 (m)	1048 (m)
1072 (s)	1072 (s)	1072 (s)	1072 (s)
1082 (vw)	-	-	-
1254	1254	1254	1254
1261	1261	1261	1261
-	-	1305	1305
-	-	1436 (w)	1436 (w)
-	-	1464 (w)	1464 (w)
1597	1597	1597	1597
1613 (w)	1613 (w)	1613 (w)	1613 (w)
2123 (w)	-	-	-
2135 (s)	2135 (s)	2135 (s)	2135 (s)
2143 (sh)	2143 (sh)	2143 (sh)	2143 (sh)
-	-	2159 (w)	-
-	-	2890 (w)	2890 (w)
-	2332 (vw)	-	-
-	2347 (vw)	-	-
-	2361 (vw)	-	-
2970 (vw)	2970 (broad / w)	-	-
-	-	2985 (m)	2985 (m)
-	-	-	3006 (vw)
-	-	3011 (sh)	3012 (sh)
-	-	3015 (sh)	-
-	-	3028 (broad)	3028 (broad)
-	-	3106 (w)	
-	-	-	3224 (w)
-	-	3282 (w)	-
3684 (broad)	3684 (broad)	-	3684 (w)

(c). 3H, 5H-Octamethyltetrasiloxane (L3) / N_2

The final linear siloxane to be pyrolysed was 3H, 5H-octamethyltetrasiloxane. The structure of L3 can be seen below. It is a seven-membered ring consisting of alternate silicon and oxygen atoms. Eight methyl groups and two hydrogen atoms are attached to the four silicon atoms.

Figure 9. 3H, 5H-Octamethyltetrasiloxane

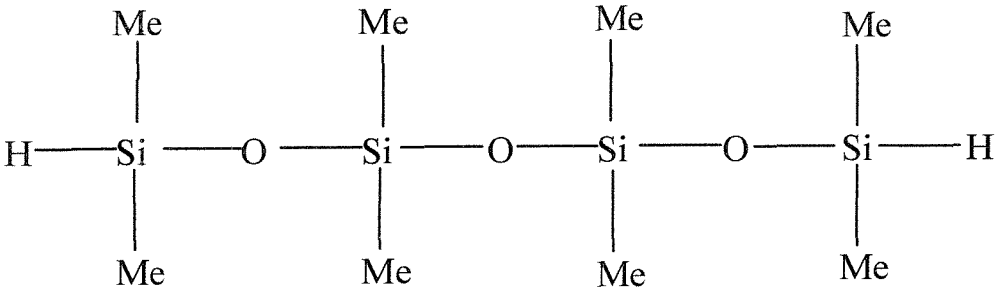

Four spectra were collected, one after each experiment and analysed in order to determine the products formed after pyrolysis.

Figure 10. Spectra of 3H, 5H-octamethyltetrasiloxane / N_2 – 4000-400 cm^{-1}
A). L3 / N_2
B). L3 / N_2 after diffusion
C). L3 / N_2 after pyrolysis
D). L3 / N_2 after pyrolysis and diffusion

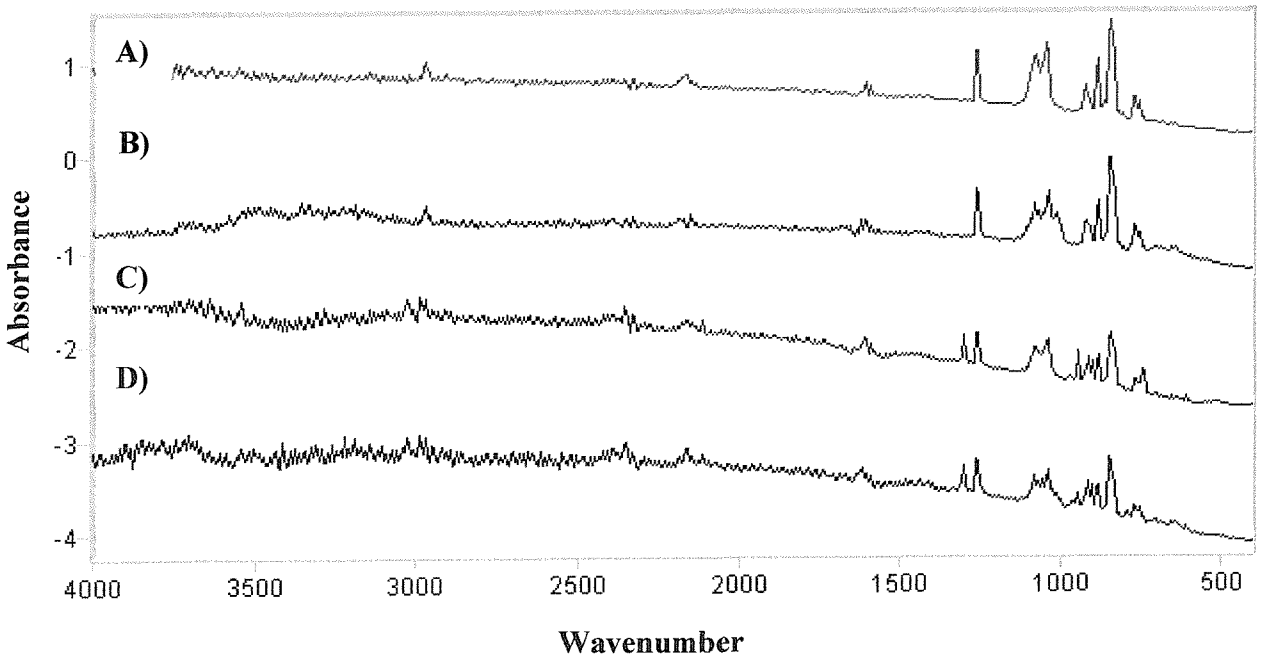

It can be seen that many of these new bands were produced below 1500 cm^{-1} and it has already been shown that a reasonable number of these may be due to the formation of small hydrocarbons.

Figure 11. Spectra of 3H, 5H-octamethyltetrasiloxane / N_2 – 1500-400 cm^{-1}

A). L3 / N_2
B). L3 / N_2 after pyrolysis
C). L3 / N_2 after pyrolysis – L3 / N_2

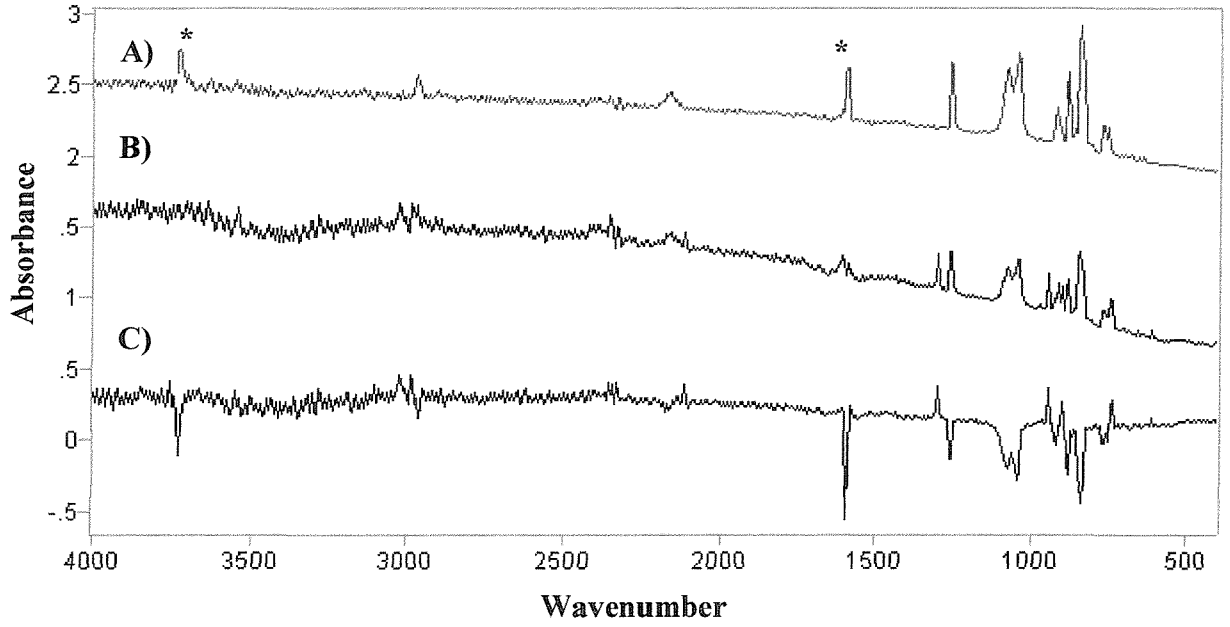

As before, many bands are present in the four spectra above. These bands have been tabulated in Table 3 seen below and analysed.

Table 3. Tabulated bands of spectra obtained for 3H, 5H-octamethyltetrasiloxane / N_2

L3	L3 after diffusion	L3 after pyrolysis	L3 after pyrolysis & diffusion
-	-	607 (w)	607 (w)
-	-	742 (w)	-
-	-	747 (w)	-
755(w)	754 (vw)	-	-
771 (w)	774 (vw)	771 (vw)	-
840 (s)	838 (s)	-	-
846 (sh)	847 (sh)	846 (sh)	848 (sh)
871 (sh)	-	-	853 (sh)
886 (m)	886 (m)	886 (m)	887 (m)
-	-	904 (m)	904 (m)
920 (m)	916 (m)	917 (m)	916 (m)
-	925 (sh)	-	-
-	-	947 (m)	946 (m)
1046 (sh)	1013 (sh)	-	-
-	1040 (m)	1043 (w)	1039 (w)
-	1058 (vw)	-	1058 (vw)
-	1072 (vw)	-	1072 (vw)
1080 (w)	1085 (w)	1079 (w)	1085 (w)
1256 (s)	1256 (s)	1256 (s)	1255 (s)
1262 (sh)	1262 (sh)	1262	1262 (sh)
-	-	1306 (s)	1305 (s)
1597 (s)	1596 (w)	1596 (w)	1596 (w)
2159 (vw)	2159 (vw)	-	2159 (vw)
2332 (vw)	2332 (vw)	-	2332 (vw)
-	2347 (vw)	2347 (vw)	2347 (vw)
-	-	2359 (w)	2361 (w)
-	-	2891 (w)	2893 (w)
2968 (w)	2968 (w)	-	-
-	-	2986(w)	2986(w)
-	-	3027(w)	3027(w)
-	-	3105 (w)	-
-	3686 (w)	-	3684 (w)
3725 (m)	-	3725 (w)	3724 (w)
-	-	3740 (w)	-

3. Preliminary Conclusions

Khabashesku *et al.* carried out the pyrolysis of octamethylcyclotetrasiloxane and reported the formation of many small hydrocarbon compounds and radical species. In chapter six, three cyclic siloxanes were pyrolysed and these species were studied as possible pyrolysis products, together with additional logical species. When analysing the results obtained from the pyrolysis of the linear siloxanes, the possible pyrolysis products investigated for the cyclic siloxanes were studied.

3.1. An Investigation into the Formation of the Methyl Radical

A small band observed by Khabashesku at 610 cm^{-1} in the spectra collected after the pyrolysis of octamethylcyclotetrasiloxane, proved to be very significant as a product in the pyrolysis of the cyclic siloxanes (see chapter six). The formation of this band was therefore investigated when carrying out pyrolysis experiments of the linear siloxanes. The formation of the methyl radical[2][3][4] at 610 cm^{-1} was observed in the spectrum of pyrolysed 1,1,3,3-tetramethyldisiloxane. This was again of particular interest, since it was thought that the pathway of the reactions, which occur upon the pyrolysis of both the linear and the cyclic siloxanes, could be studied by investigating the production of the methyl radical. An in-depth literature search of CH_3 has been conducted in the previous chapter. The methyl radical was again found at 610 cm^{-1}, in the spectra obtained of 1,1,3,3,5,5-hexamethyltrisiloxane and at 607 cm^{-1} in the spectra of 3H, 5H-octamethyltetrasiloxane.

However, on all three occasions, no bands were observed at 3162 and 1398 cm^{-1}. It has already been discussed that these results are as expected, since the literature search showed the bands due to the stretching modes to be present at significantly weaker intensities than the main bending mode at 610 cm^{-1}.

After the diffusion experiments were carried out, where the deposition window was warmed to 27 K, allowing the trapped species the chance to reorient and possibly react further, a change common to all three of the linear siloxanes was observed. The band at ~ 610 cm^{-1} was seen to disappear. This confirms that this band was due to an unstable species that reacted further upon diffusion.

3.2. An Investigation into the Formation of Acetylene

From the results obtained from the analysis of the pyrolysis spectra of the cyclic siloxanes, it was found that two bands are present in a spectrum of acetylene. These bands are found at 3282 and 747 cm^{-1}. Bands were found at 3281 and 726 cm^{-1} in the spectra obtained from the pyrolysis of L1 and at 3282 and 747 cm^{-1} in the spectra of L2. However, although the spectra of L3 after pyrolysis produced a band at 747 cm^{-1}, no band due to the stretching mode was observed. This may well be due to the band being present at a low abundance.

Upon diffusion, all bands produced due to the formation of acetylene were seen to disappear. This confirms that these bands were due to the formation of acetylene, as the bands were seen to change at the same relative intensities.

3.3. An Investigation into the Formation of Ethene

From the investigations that took place into the possible pyrolysis products for the cyclic siloxanes, the bands that are known to be due to ethene are at approximately 3105, 2890, 1438, 947 and 829 cm^{-1}.

L1 produces one new band after pyrolysis due to ethene at 947 cm^{-1}. However, it is possible that two other ethene bands were produced at 1435 and 830 cm^{-1}, but were not seen as new bands, since they were formed at approximately the same frequencies as existing parent compound bands. No bands were seen at 3105 or 2890 cm^{-1}. This could be due to the bands being produced at a low abundance. The pyrolysis of L2 produced four new bands thought to be due to the formation of ethene. These bands were found at 3105, 2890, 1436 and 947 cm^{-1}. L2 produces a parent compound band at 828 cm^{-1} and it therefore can not be confirmed as to whether ethene also produces a band at this frequency. The parent compound of L3 has a broad band at 846 cm^{-1} that could also be obscuring the ethene band formed at ~ 829 cm^{-1}. No band is produced at 1438 cm^{-1}. However, a new band is seen at 947 cm^{-1}, together with two weak bands at 2891 and 3105 cm^{-1}.

It has already been seen for the cyclic siloxanes that after diffusion the ethene bands do not change with the same relative intensities. Diffusion experiments were then conducted for the linear siloxanes.

Figure 12. Spectra of 1,1,3,3,5,5-hexamethyltrisiloxane / N_2 produced after pyrolysis and both before and after diffusion

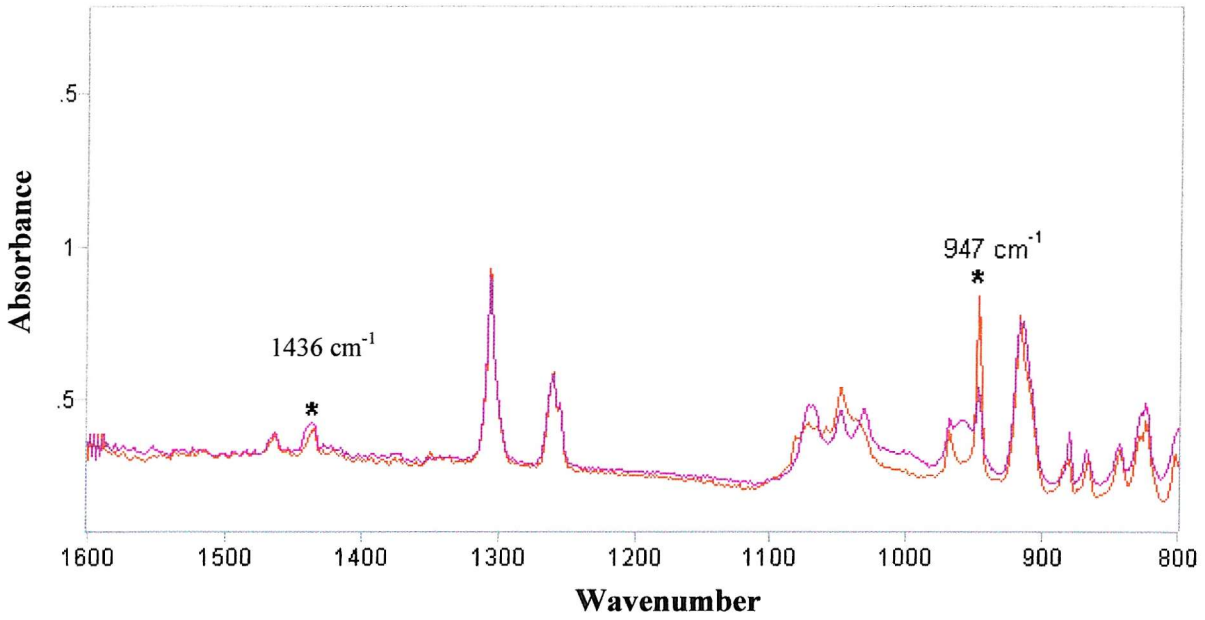

Red line = L2 after pyrolysis

Purple line = L2 after pyrolysis and after diffusion

The two bands marked on the above spectra of L2 after pyrolysis, are the bands thought to belong to the bending modes of ethene. However, it can be seen that after both pyrolysis and diffusion (the purple line), the band at 947 cm^{-1} is seen to decrease in size quite considerably, whereas the band at 1436 cm^{-1} remains almost the same size after the diffusion experiments have been conducted. It is unknown why this occurs and unlikely that ethene is not produced since so many new bands are formed at the same frequencies as ethene bands. The band at ~ 947 cm^{-1} is also seen to decrease significantly or disappear altogether in the spectra of both L1 and L3. The weak bands at approximately 2890 and 3105 cm^{-1} are seen to also decrease in intensity or disappear after diffusion in the spectra of all three linear siloxanes.

3.4. An Investigation into the Formation of Methane

Bands due to the formation of methane are seen to be of principal importance in analysing the results of the pyrolysis of both the cyclic and the linear siloxanes. As the main methane band at 1306 cm^{-1} was of high intensity, the formation of this band was used to measure the degree of dissociation of the parent compound. After pyrolysis, L2 produces two methane bands at 3028

and 1305 cm^{-1} and two bands are also observed in the spectra of L3 at 3028 and 1306 cm^{-1}. However, only one band is seen in the spectra of L1, at 1302 cm^{-1}. This again could be due to the stretching mode band being present in low abundance. 1,1,3,3,5,5-Hexamethyltrisiloxane has been used as an example to show the effects of diffusion on the band due to the bending mode of vibration produced due to methane. Spectra are shown below of L2 after pyrolysis and then after both pyrolysis and diffusion.

Figure 13. Spectra of 1,1,3,3,5,5-hexamethyltrisiloxane / N_2 produced after pyrolysis and both before and after diffusion

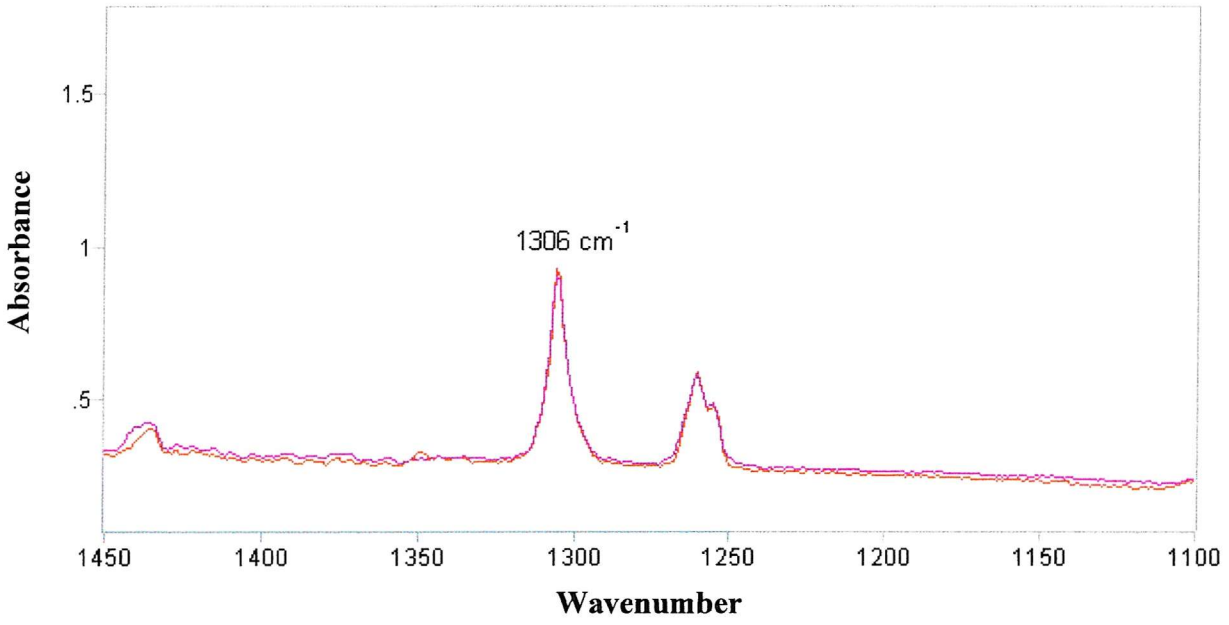

Purple Line = L2 after pyrolysis

Red Line = L2 after pyrolysis and after diffusion

Figure 14. Spectra of 1,1,3,3,5,5-hexamethyltrisiloxane / N_2 produced after Pyrolysis and both before and after diffusion

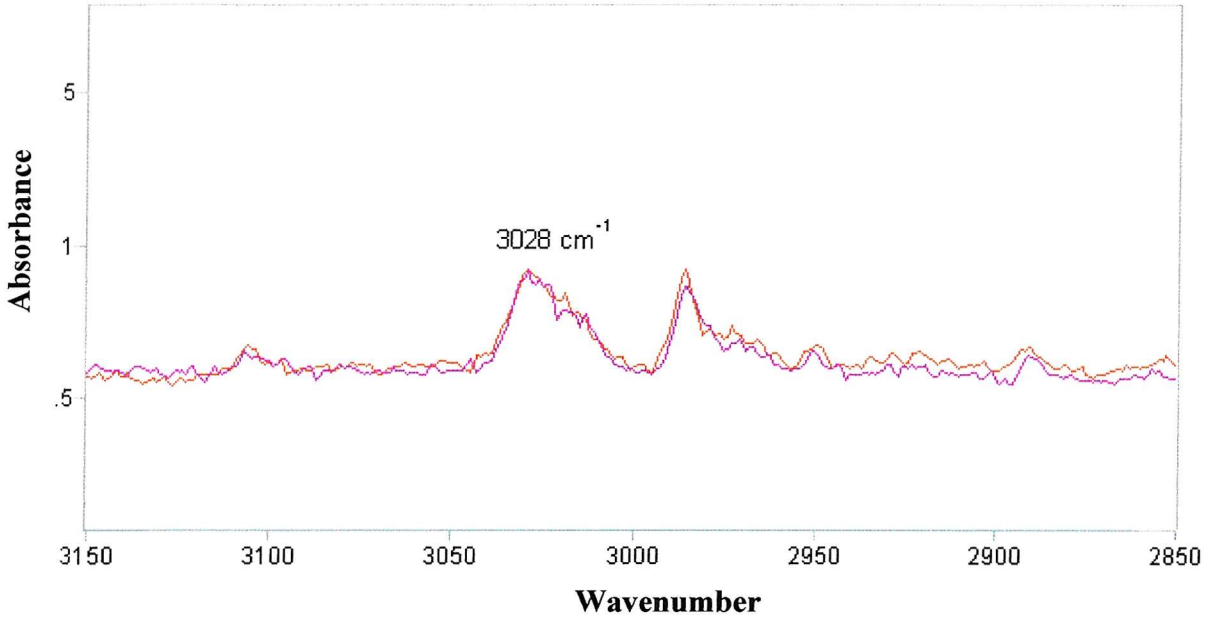

Red Line = L2 after pyrolysis

Purple Line = L2 after pyrolysis and diffusion

Neither bands are seen to decrease in size after diffusion as expected. These results therefore confirm that they are due to small stable species that do not react further upon diffusion.

3.5. An Investigation into the Formation of Ethane

In chapter six, a spectrum of ethane in a nitrogen matrix was obtained and compared to the spectra of the cyclic siloxanes after pyrolysis, in order to establish whether any bands due to ethane were formed. Five ethane bands were in general found to be present in the cyclic siloxane spectra, at 2986, 2950, 2891, 1464 and 828 cm^{-1}. However, no ethane bands were produced as a result of pyrolysing 1,1,3,3-tetramethyldisiloxane. Unlike L1, a number of new bands formed after the pyrolysis of L2 were thought to be due to ethane. These bands were found at 2985 and 1464 cm^{-1}. A spectrum of L2 contains a band at 828 cm^{-1}, therefore it is unknown if ethane also produced a band at this frequency. No bands due to the formation of ethane were seen to be produced for spectra obtained after the pyrolysis of L3.

4. A Comparison of the Results of the Three Linear Siloxanes: L1, L2 and L3

In order to establish a pathway for the reactions of the various linear siloxanes, it is important to identify common bands and try to find common fragments produced from the pyrolysis experiments. This has been attempted with the aid of a number of tables. The bands of interest from the spectra of each linear siloxane have been tabulated after each process.

4.1. Pyrolysis Experiments

It has been shown that a lot of new products were produced as a result of the pyrolysis experiments. Below are tabulated changes that occurred within the spectra of all three linear siloxanes.

Table 4. Changes observed in the original spectra of the parent compounds after pyrolysis

L1 / N_2	L1 / N_2 – after pyrolysis	L2 / N_2	L2 / N_2 – after pyrolysis	L3 / N_2	L3 / N_2 – after pyrolysis
-	610	-	610(w)	-	607
-	726(w)	657 (vw)	-	-	742
738	-	-	742	-	747
-	742	-	747	-	742
-	746	-	866	840	-
-	866	-	880	871	-
-	946	-	947	-	904
-	967	-	969	-	947
-	1050	1082 (vw)	-	1046	-
-	1072	-	1305	-	1043 (w)
-	1081	2123 (w)	-	-	1306
-	1302	-	2159 (w)	2159 (vw)	-
-	1694 (w)	-	2984	2332 (vw)	-
-	2127	-	3006	-	2347 (vw)
-	2133	3011	3012	-	2359
-	2330 (w)	3015	-	2968 (vw)	-
-	3014	-	3028(broad)	-	2986 (w)
-	3281 (w)	-	3106 (w)	-	3027 (w)
-	3010	-	3282 (w)	-	3740
-	3014	-	3699 (sh)	-	-
-	3281 (w)	-	-	-	-

The table above shows that a lot of changes occurred in the spectra upon pyrolysis. These changes are either due to bands being produced or disappearing. The number of bands that disappeared are seen to increase as the linear siloxane is changed from L1 to L2 and then to L3. These bands are likely to be due to parts of the original parent compound that does not exist after pyrolysis, due to the fragmentation that occurs during this process. However, it is difficult to exactly state which of these bands are due to what part of the relevant siloxane compound, since there are no common bands.

There are however, many new bands in common between the three linear siloxanes. The first new band in each case is due to the methyl radical[2][3][4], at ~ 610 cm^{-1}. Acetylene appears to have been produced by both L1 and L2 with two bands at ~ 746 and ~ 3281 cm^{-1}. Acetylene was found only at 747 cm^{-1} in the spectrum of L3 after pyrolysis. Bands due to methane[2] were also produced by the pyrolysis of each of the three linear siloxanes. Bands were produced at 1302, 1305 and 1306 cm^{-1} for L1, L2 and L3 respectively and the stretching vibrations were present at 3014, 3028 and 3027 cm^{-1}. In each case the bands produced from L1 were noticeably lower in value than for L2 and L3. A number of bands due to ethene were also produced for both L2 and L3. The pyrolysis of L2 produced two bands due to ethane at 1464 and 2985 cm^{-1}. However, after accounting for those bands that are due to the hydrocarbons, there are still many bands that have not been assigned. A table of all the remaining bands in the spectra after pyrolysis of all three linear siloxanes can be seen below.

Table 5. Bands remaining in the spectra obtained after the pyrolysis of the three linear siloxanes

L1 / N_2 – after pyrolysis	Species	L2 / N_2 – after pyrolysis	Species	L3 / N_2 – after pyrolysis	Species
623(w)	L1	742	-	742	-
726(w)	-	772	L1	771	L1 / L2
742	-	800	L2	846	L3
771	L1	823	L2	886	L3
779	L1	843	L2	904	-
839	L1	866	-	917	-
866	-	880	L1	947	-
880	L1	917	-	1043(w)	-
914	L1	947	-	1079(w)	L3
946	-	969	-	1256	L1 / L3
967	-	1032	L2	1262	L3
1019	L1	1048	L2	2359	-
1037	-	1072	L2		
1050	-	1254	L1 / L2		
1059	L1	1261	L2		
1065	L1	1436(w)	-		
1072	-	1613(w)	L2		
1081	-	2135(sh)	L2		
1257	L1	2159	-		
1694(w)	-				
2127	-				
2133	-				
2330(w)	-				
3010	-				

As well as accounting for the possible hydrocarbons produced from the pyrolysis experiments, many of the remaining bands are due to the original parent compounds and bands which appear to be as a result of the formation of a second linear siloxane, have now been identified.

Of the bands that have yet to be identified, there are a few common bands between the linear siloxanes. A band at 947 cm^{-1}, thought to be due to ethene, was found to be a product of the pyrolysis of each of the linear siloxanes. L1 and L2 each produced bands at 866 and 967 cm^{-1} and L2 and L3 produced a band at 917 cm^{-1}.

4.2. Diffusion Experiments on the Pyrolysis Products

Finally, the results of the second diffusion experiments, after pyrolysis for each of the linear siloxanes were compared.

Table 6. Changes observed in the spectra obtained after pyrolysis of the parent compounds and after pyrolysis and diffusion

L1 / N_2 – after pyrolysis	L1 / N_2 – after pyrolysis and diffusion	L2 / N_2 – after pyrolysis	L2 / N_2 – after pyrolysis and diffusion	L3 / N_2 – after pyrolysis	L3 / N_2 – after pyrolysis and diffusion
610	-	742	-	742	-
726(w)	-	747	-	747	-
742	-	2159(w)	-	771	-
746	-			-	853
946	-			-	1058(vw)
967	-			-	1072(vw)
1037	-			-	2159(vw)
1050	-			-	2332(vw)
1072	-			-	3684
1081	-			3740	-
1694(w)	-				
2133	-				
-	3007				

It can be seen from the tabulated results above, that the majority of the changes that occurred between the two sets of spectra, were that many of the bands produced after pyrolysis disappeared after the second diffusion experiments were conducted. There is an obvious exception to this with the group of bands in the table of results of L3 between 853 and 3684 cm^{-1}. However, as can be seen from the table of results discussed earlier (Table 3), this group of bands also appeared after the first set of diffusion experiments, suggesting that they are within the boundaries of the baseline, and become more clearly resolved after diffusion. Bands at 742 and ~ 747 cm^{-1} are common to all of the linear siloxanes, and are seen to disappear after diffusion. Whereas a band at 1072 cm^{-1} is common to both L1 and L3 and is also seen to disappear after diffusion for L1, but appears after diffusion for L3. A band at 2159 cm^{-1} is observed to disappear after the diffusion of L2 and appear after the diffusion of L3.

4.3. Diffusion Experiments on the Parent Compounds

Initially, diffusion experiments were carried out at 27 K before the parent compound was pyrolysed. The table below shows the differences between the original spectrum and that obtained after diffusion. (See Figure 3 (A)-(D)).

Table 7. Changes observed in the original spectra of the parent compounds after diffusion

L1 / N_2	L1 / N_2 – after diffusion	L2 / N_2	L2 / N_2 – after diffusion	L3 / N_2	L3 / N_2 – after diffusion
1037(w)	-	622(w)	-	871	-
-	1694 (w)	2123(w)	-	-	925(sh)
-	2330(w)	-	2332(vw)	-	1040
		-	2347(vw)	-	1058(vw)
		-	2361(vw)	-	1072(vw)
		-	3686	-	2347(vw)
				-	3686

It has already been mentioned in the previous sections that the initial diffusion experiments did not change the original spectra obtained of the parent compounds, to any significance. The main observations made after diffusion were that the bands in the spectra appeared sharper. However, there were one or two smaller changes also observed and these are seen in the above table. With the exception of a couple of bands, the majority of these small changes involved the appearance of seemingly new bands. These are likely however, to be due to the sharpening of the baseline to include bands which were once within the boundaries of the baseline.

Common bands included the appearance of new bands at ~ 2330 cm^{-1} for both L1 and L2 and a band at 2347 cm^{-1} for both L2 and L3. Both of these seemingly new bands are weak bands. It is likely that the band at 2347 cm^{-1} is due to CO_2, possibly as a result of a slight leak in the nitrogen supply.

5. Conclusion

Clearly this work is in no way conclusive, but it has attempted to identify new bands produced after pyrolysis, not only of common vibrations throughout a spectrum, but also bands common to spectra of pyrolysed parent compounds, throughout a series of linear siloxanes. This has been achieved with the aid of supporting energy and frequency molecular modelling calculations.

6. Energy Calculations

A number of molecular modelling calculations were then carried out both on the parent compounds of the linear siloxanes and on a number of possible products in order to obtain the geometries and the energies of the structures. After the geometries were established, the aim of these calculations was to attempt to identify the most feasible product with the lowest energy. The formation of small hydrocarbons are particularly featured in the possible reaction schemes shown below. From these reaction schemes, the most energetically feasible pathway was identified.

Table 8. Tabulated energy values in units of Hartrees

Species	HF / 3-21G Geom. & Freq. Optimisation / Hartrees	B3LYP / 6-31G(d) Geom. & Freq. Optimisation / Hartrees
L_1	-808.1710	-815.2021
L_2	-1248.9894	/
L_3	-1689.8014	-1704.5464
CO_2	-186.1176	-188.5800
CO	-112.0933	-113.3095
H_2O	-75.5860	-76.4090
H_2	-1.1230	-1.1755
SiH_2	-288.4843	-290.6131
C_2H_6	-78.7939	-79.8304
C_2H_4	-77.6010	-78.5875
C_2H_2	-288.4843	-290.6131
CH_4	-39.9769	-40.5184
CH_3	-39.3426	-39.8383
I	-729.2956	/
II	-768.1419	/
III	-729.1910	-735.2548
IV	-440.6558	-444.5662
V	-367.3657	-370.5380
VI	-768.0411	-774.5886
VII	-1208.7308	-1219.2969
VIII	-1208.8481	-1219.2550
IX	-1169.8958	-1179.7992
X	-1169.9933	-1179.9190
$SiMe_2$	-366.1663	-369.2701
Si(H)OH	-362.9977	-365.8974
$Si(Me)_2(H)OH$	-441.8718	-445.8033
SiH_2O	-362.9559	-365.8977
Si(H)OH	-362.9977	-365.8974
SiMe(H)O	-401.8063	-405.2330

All of the energy calculations were carried out initially using a low level of theory[151] in the form of the HF / 3-21G model chemistry (described in detail in Chapter 3). These calculations were then repeated using a higher level of theory of B3LYP / 6-31G (d). The second set of calculations were carried out on the results of the first set. In some cases an energy value was not able to be obtained with the above model chemistries in the given time period. In these cases, singlepoint energy calculations were employed, which relied on a specified geometry.

Table 9. Tabulated energy values of singlepoint energy calculation in units of Hartrees

Species	HF / 3-21G Singlepoint Energy Calculation / Hartrees	B3LYP / 6-31G (d) Singlepoint Energy Calculation / Hartrees
L_2	/	-1259.8725
I	/	-774.6217
III	/	-735.2902
VII	/	-1219.2937
IX	/	-1179.9626

From the results of these calculations, a number of reaction schemes have been devised and these are shown below. In each case, the lowest level of theory has been used.

6.1. 1,1,3,3-Tetramethyldisiloxane

Initially, reaction schemes were produced for the elimination of methane from the parent compound, in the form of a hydrogen atom and a methyl group. Product **I** is a possible product as a direct result of the elimination of these two species. Product **II** would be produced if a further step was conducted, involving the rearrangement of product **I**. These schemes are shown below:

Figure 15. A) – B). Reaction schemes showing the elimination of a hydrogen atom and a methyl group from L1

A)

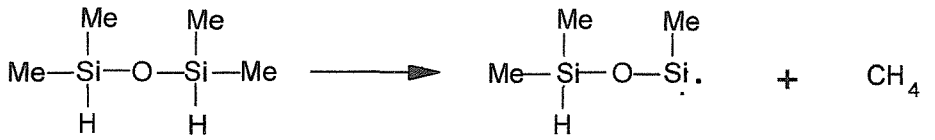

L1 I

-815.2028 Hartrees -774.6217 Hartrees -40.5184 Hartrees

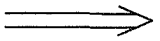

+0.0627 Hartrees ≡ ΔE = + 39.3299 kcal / mol

B)

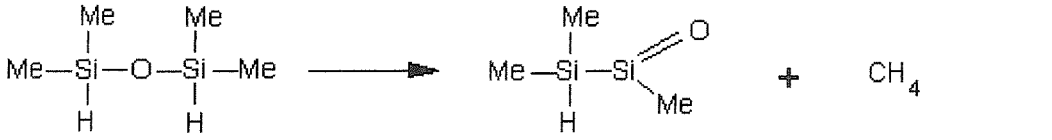

L1 II

-815.2028 Hartrees -774.5886 Hartrees -40.5184 Hartrees

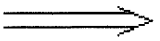

+0.0958 Hartrees ≡ ΔE = + 60.1101 kcal / mol

Each of these energy values were initially calculated in units of Hartrees and then converted to kcal / mol. It should be noted that 1 Hartree is equal to 627.510 kcal / mol. From these energy values it can be seen that the equation with the least positive value of ΔE is equation **A)**, therefore suggesting that compound **I** is the most stable product of the two shown above.

Two methyl radicals could alternatively be eliminated from the parent compound. This process could give rise to a possible method for the formation of ethane. The two most likely reaction schemes for the formation of ethane are shown below:

Figure 16. C) – D). Reaction schemes showing the elimination of two methyl groups

C)

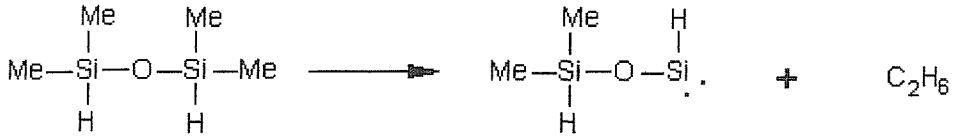

L1
-815.2028 Hartrees

III
-735.2902 Hartrees

-79.8304 Hartrees

+0.0822 Hartrees ≡ ΔE = +51.5806 kcal / mol

D)

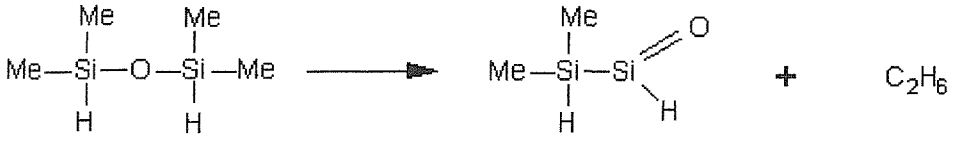

L1
-815.2028 Hartrees

IV
-735.2548 Hartrees

-79.8304 Hartrees

+0.1176 Hartrees ≡ ΔE = +73.7882 kcal / mol

Reaction scheme **A)** is still the most energetically feasible reaction, suggesting that product **I** is the most favourable product. Since the secondary product of the formation of product **I** is methane, this suggests that the formation of methane is more likely than the formation of ethane. This is supported by the spectra obtained, since the main methane band is of high intensity and the bands due to ethane are barely present. However, this is not to say that reaction **C)** does not occur. Reaction **C)** has the second least positive energy value, and although ethane is not present to any significance in the spectrum, the methyl radical is. Therefore, this reaction may still occur to a lesser extent producing methyl radicals.

6.2. 1,1,3,3,5,5-Hexamethyltrisiloxane

The energy values tabulated in Tables 8 and 9 were used to obtain the schematic energy diagrams for L2 upon pyrolysis. Hydrocarbons and radical species of significant intensity were represented in the schematic diagrams.

Figure 17. A) – B). Reaction schemes showing the elimination of a hydrogen atom and a methyl group from L2

A)

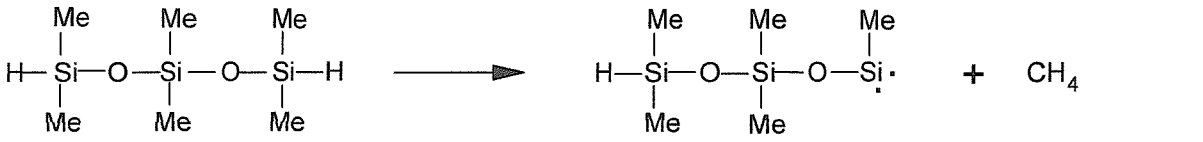

L2 **VII**

-1259.8725 Hartrees -1219.2937 Hartrees -39.9769 Hartrees

⟹

+0.6019 Hartrees ≡ ΔE = +37.6717 kcal / mol

B)

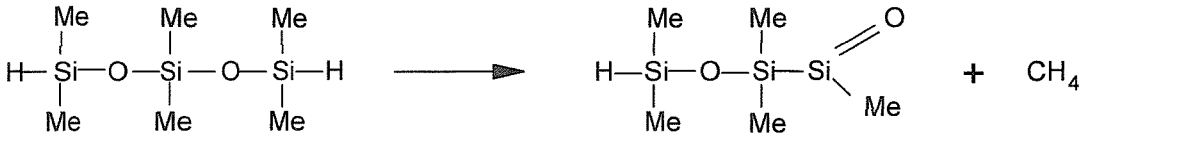

L2 **VIII**

-1259.8725 Hartrees -1219.2550 Hartrees -39.9769 Hartrees

⟹

+0.0991 Hartrees ≡ ΔE = +62.1744 kcal / mol

Figure 18. C) – D). Reaction schemes showing the elimination of a hydrogen atom and a methyl group from L2

C)

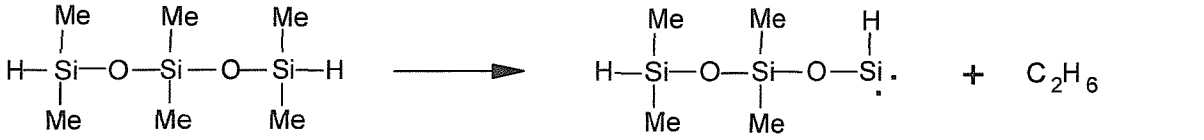

L2
-1259.8725 Hartrees

IX
-1179.9626 Hartrees

-79.8304 Hartrees

+0.0795 Hartrees ≡ ΔE = +49.8823 kcal / mol

D)

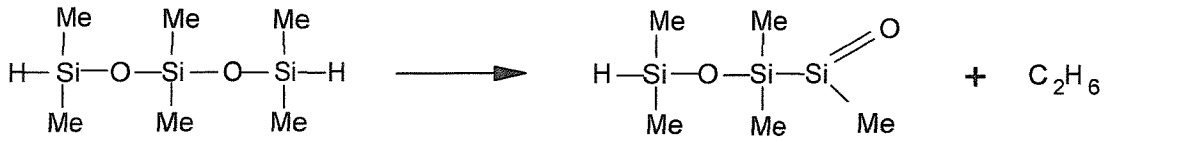

L2
-1259.8725 Hartrees

X
-1179.9190 Hartrees

-79.8304 Hartrees

+0.1231 Hartrees ≡ ΔE = +77.2196 kcal / mol

The results of these energy calculations agree with those obtained for L1. The most energetically favourable product is the equivalent of product **I**, that is product **VII** and methane. However, as previously seen with L1, the second most feasible reaction is reaction **C)**, producing product **IX** and ethane. Unlike L1, the spectrum obtained as a result of the pyrolysis of L2, shows a considerable amount of both methane and ethane being produced. To account for this, the ΔE values need to be studied. It can be seen that although equation **A)** in both cases produces the lowest energy value, the reaction with the second lowest energy value in each case, equation **B)**, has a much lower value of ΔE for L2, than for L1. This suggests that the formation of ethane is much more likely to occur for L2 than it is for L1.

7. Frequency Calculations of the Parent Compounds

It was then decided to carry out a number of molecular modelling calculations in an attempt to identify the calculated frequencies of various possible products and identify the unknown species formed. This would aid the identification of the pathway taken by the eliminated methyl radicals and hydrogen atoms. However, initially it was decided to obtain calculated frequencies of the original parent compounds of L1, L2 and L3 to confirm and satisfy the reliability of the program used. It was seen in chapter seven that the frequencies of the cyclic siloxanes were calculated accurately.

7.1. 1,1,3,3-Tetramethyldisiloxane

Two spectra of L1 are shown below. Spectrum **A)** shows the calculated spectrum of 1,1,3,3-tetramethyldisiloxane, which was produced by inputting the calculated frequencies obtained from the Cerius 2 program into Grams, (a graphics program).

Figure 20. Spectra of 1,1,3,3-tetramethyldisiloxane / N - 4000 – 400 cm^{-1}

A). Calculated spectrum of LI – (B3LYP / 6-31G (d))
B). Experimental spectrum of L1

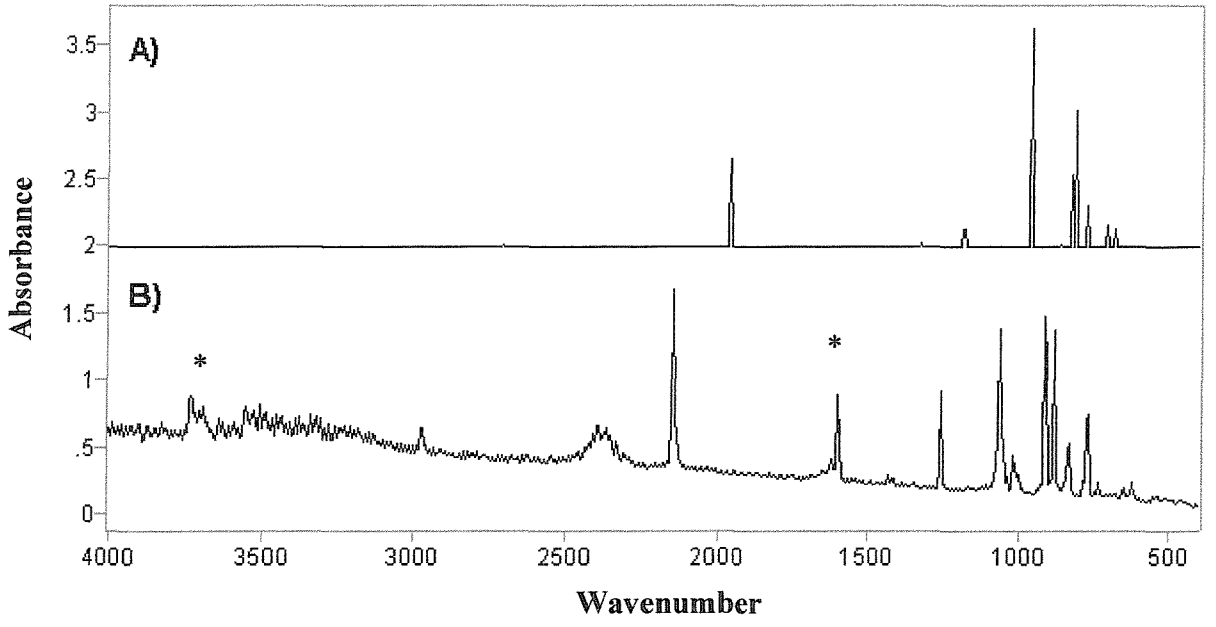

As can be seen from the above spectra, the calculated spectrum shows many similarities to the spectrum obtained experimentally, especially below 1000 cm^{-1}. However, it was noted that in the region of ~ 2000 cm^{-1} (the Si-H bond region), the calculated frequencies appeared lower in value than the experimentally obtained frequencies.

7.2. 1,1,3,3,5,5-Hexamethyltrisiloxane

Below are two spectra of L2. Spectrum **A)** is of the calculated frequencies that have been inputted into the graphics program, Grams. This spectrum has been compared to that obtained experimentally.

Figure 21. Spectra of 1,1,3,3,5,5-hexamethyltrisiloxane / N_2 - 4000 – 400 cm^{-1}

A). Calculated spectrum of L2 – (HF / 3-21G)
B). Experimental spectrum of L2

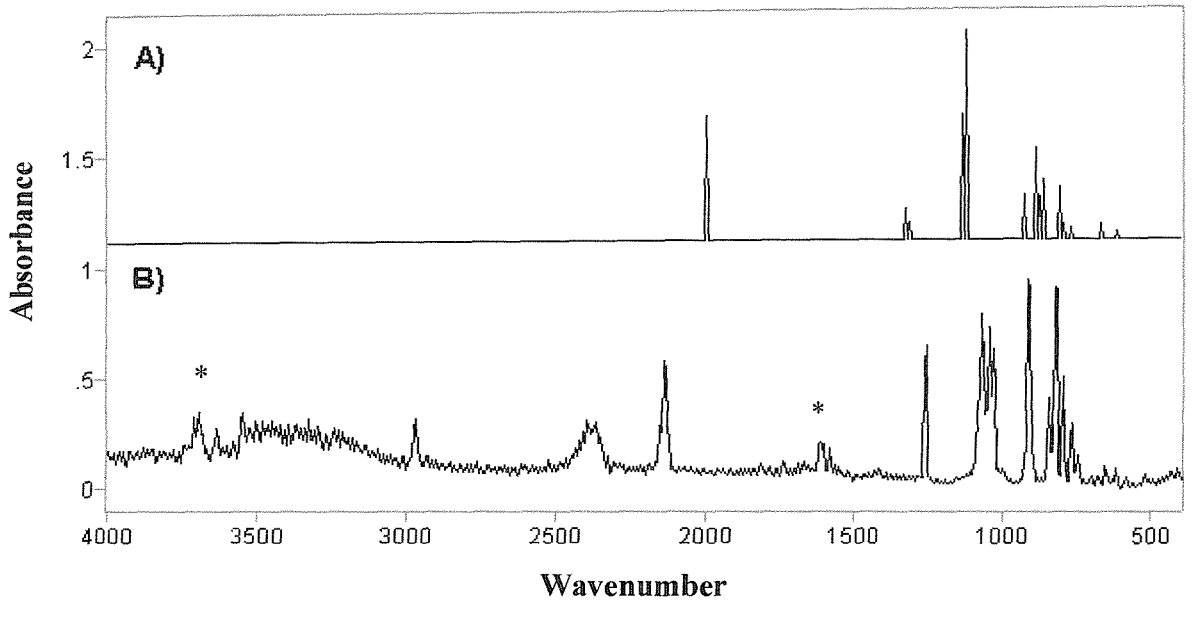

Again, as for L1, the two spectra appear to agree reasonably well, especially below 1000 cm^{-1}. However, the Si-H bonds again are seen to be a problem where the frequency calculations are concerned. The Gaussian program calculated the frequencies of the Si-H bonds as being much lower than they are when obtained experimentally.

7.3. 3H, 5H-Octamethyltetrasiloxane

Below can be seen a comparison of the calculated spectrum of the parent compound to the experimental spectrum. As previously observed, the frequencies calculated for the Si-H bonds appear to be significantly lower than the obtained experimental values.

Figure 22. Spectra of 3H, 5H-octamethyltetrasiloxane

A). Calculated spectrum of L3 – (B3LYP / 6-31G (d))
B). Experimental spectrum of L3

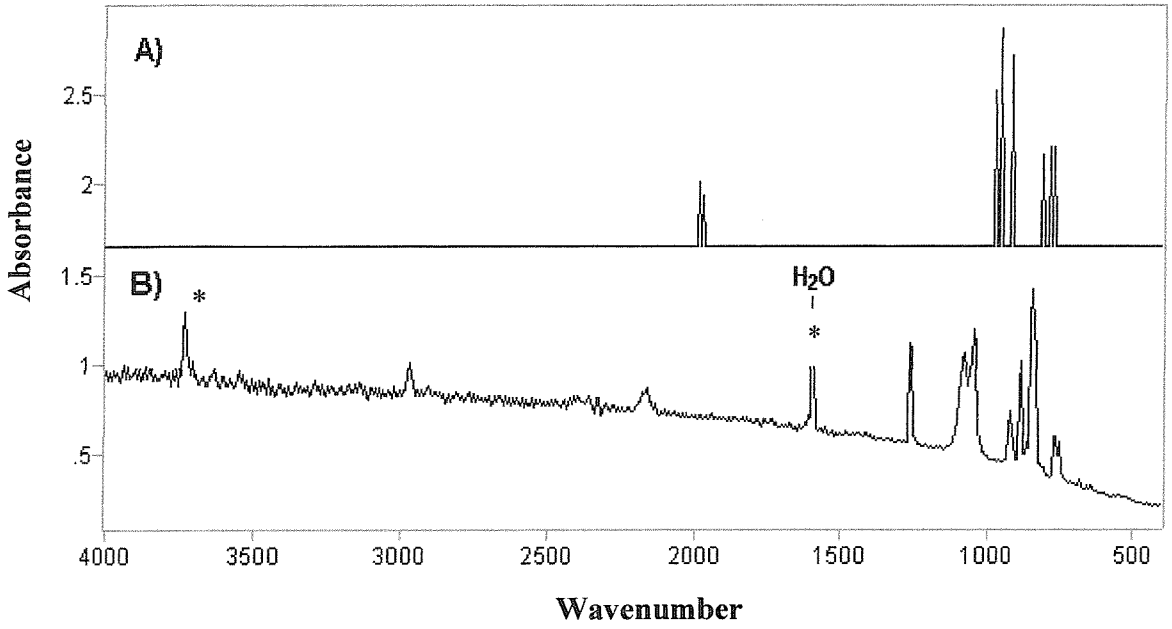

In discussing the results of the pyrolysis of the three linear siloxanes, it appears that there is an error in the Gaussian program in calculating the frequencies of the Si-H bonds. Any possible products from the pyrolysis of L1, L2 and L3 that contain Si-H bonds had yet to be calculated before a conclusion could be reached on the overall reliability of the Gaussian program.

However, apart form this region of the spectra, the calculated frequencies agree reasonably well with the experimental values. Any discrepancies between the calculated and the experimental spectra was seen to increase with an increase in frequency. The fingerprint region was seen to be the most accurate region.

8. Frequency Calculations of the Possible Products

The frequency calculations were then expanded and carried out on all of the possible products of the pyrolysis of the linear siloxanes. The frequencies obtained were then inputted into the Grams program and analysed together with the findings from the energy calculations.

8.1. 1,1,3,3-Tetramethyldisiloxane

It was found that products **I** and **III** were definite possibilities of the pyrolysis of 1,1,3,3-tetramethyldisiloxane. The spectra of both possible products together with the spectrum of the parent compound (L1) are shown below.

Figure 23. A comparison between the experimental spectrum of 1,1,3,3-tetramethyldisiloxane / N_2 and the calculated spectrum of two possible products

A). Calculated values of product III – (B3LYP / 6-31G (d))
B). Calculated values of product I – (B3LYP / 6-31G (d))
C). Full experimental spectrum of parent compound (L1)

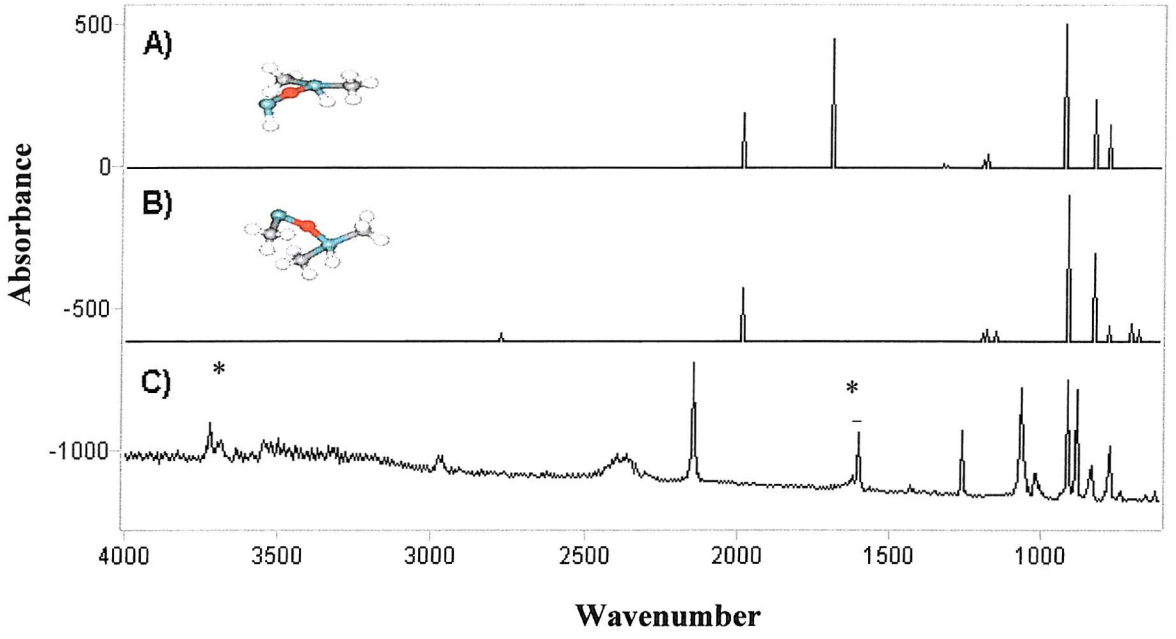

The formation of species **I** and **III** are as a result of the elimination of the secondary products, methane, (in the case of the formation of product **I**) and ethane (in the case of product **III**). The regions below 1000 cm^{-1} agree well.

As previously seen with the spectra of the calculated frequencies of the parent compound, the bands due to the Si-H bonds appear lower in frequency than in the experimental spectrum. This supports the fact that the Gaussian calculations for calculating the frequencies of the Si-H bond contains an error. However, the calculations have managed to predict the correct number of Si-H bonds present in a compound. Calculated spectrum **A)** predicts correctly that product **I** contains one Si-H bond, by producing one band in the region around 2000 cm^{-1}. Although, these bands appear far apart in the spectrum. Calculated spectrum **B)** correctly predicts that product **III** contains two Si-H bonds.

8.2. 1,1,3,3,5,5-Hexamethyltrisiloxane

Since products **I** and **III** are thought to be possible pyrolysis products of 1,1,3,3-tetramethyldisiloxane, the equivalent products for 1,1,3,3,5,5-hexamethyltrisiloxane were investigated. These were products **VII** and **IX**, which were calculated to have lowest energies.

Figure 24. A comparison between the experimental spectrum of 1,1,3,3,5,5-hexamethyltrisiloxane / N_2 and the calculated spectrum of two possible products

A). Spectrum of calculated values of product VII – (HF / 3-21G)
B). Spectrum of calculated values of product VIII – (HF / 3-21G)
C). Experimental spectrum of L2 after pyrolysis

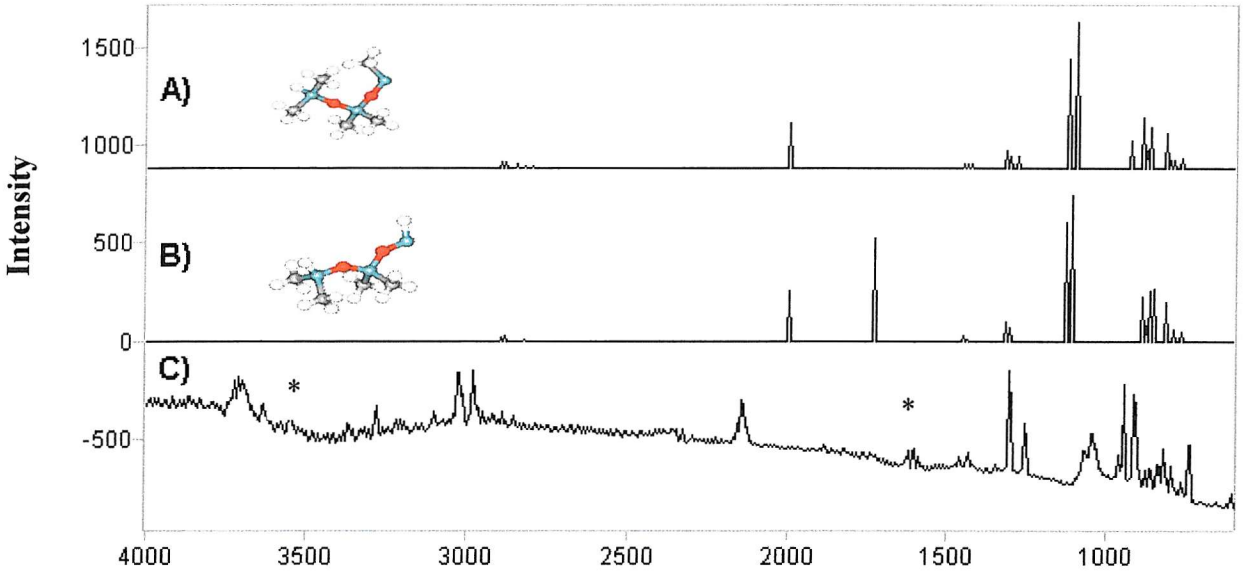

Again, the calculated bands below 1000 cm^{-1} fit the experimental spectrum very well. The bands due to the Si-H bonds, around 2000 cm^{-1}, appear lower in frequency than the bands obtained experimentally, as previously seen with L1. This further supports the theory that the Gaussian program contains an error in calculating the frequencies of the Si-H bonds. However, the correct number of Si-H bonds has once again been calculated accurately.

9. A Comparison of the Frequency Calculations Between the Parent Compound and the Possible Products.

9.1. 1,1,3,3-Tetramethyldisiloxane

From the energy calculations it was concluded that both reaction schemes **A)** and **B)** are likely to occur, producing both methane and the methyl radical, (the latter to a lesser extent). Therefore, the two favourable possible products from the results of the energy calculations and supported by the frequency calculations, are products **I** and **III**.

Therefore the next step was to compare the two spectra obtained experimentally, of both before and after the pyrolysis of L1. Particular attention was paid to the Si-H region of the spectra, in order to identify the number of bonds found in each case and to further aid the identifications of the unknown compounds. These two spectra can be seen below.

Figure 25. Spectra of 1,1,3,3-tetramethyldisiloxane / N_2 – 4000-400 cm^{-1}

A). L1 before pyrolysis
B). L1 after pyrolysis

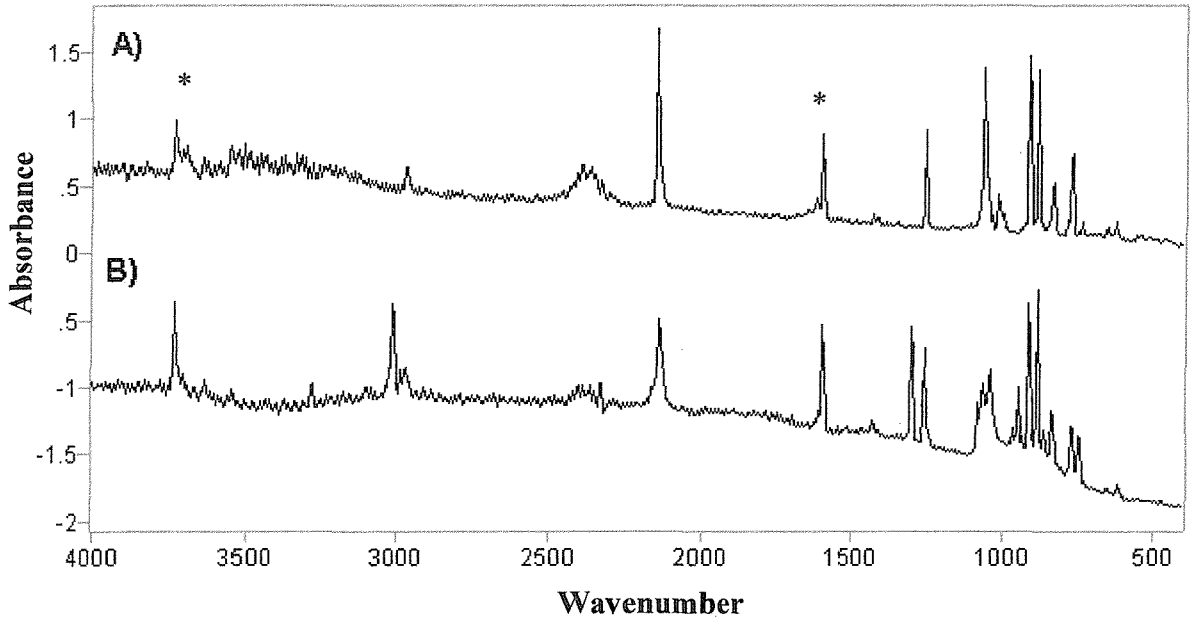

At first, it appears that the initial spectrum of L1 has just one band around the 2000 cm^{-1} mark, whereas L1 contains two Si-H bonds. This region of the spectrum was then expanded to show the Si-H band more closely, (as shown below). It can be seen that there is a shoulder at the left-hand side of the band, which could account to the presence of the two Si-H bonds in the parent compound (L1).

Figure 26. Spectra of 1,1,3,3-tetramethyldisiloxane / N_2 – 2400-1800 cm^{-1}

A). L1 before pyrolysis
B). L1 after pyrolysis

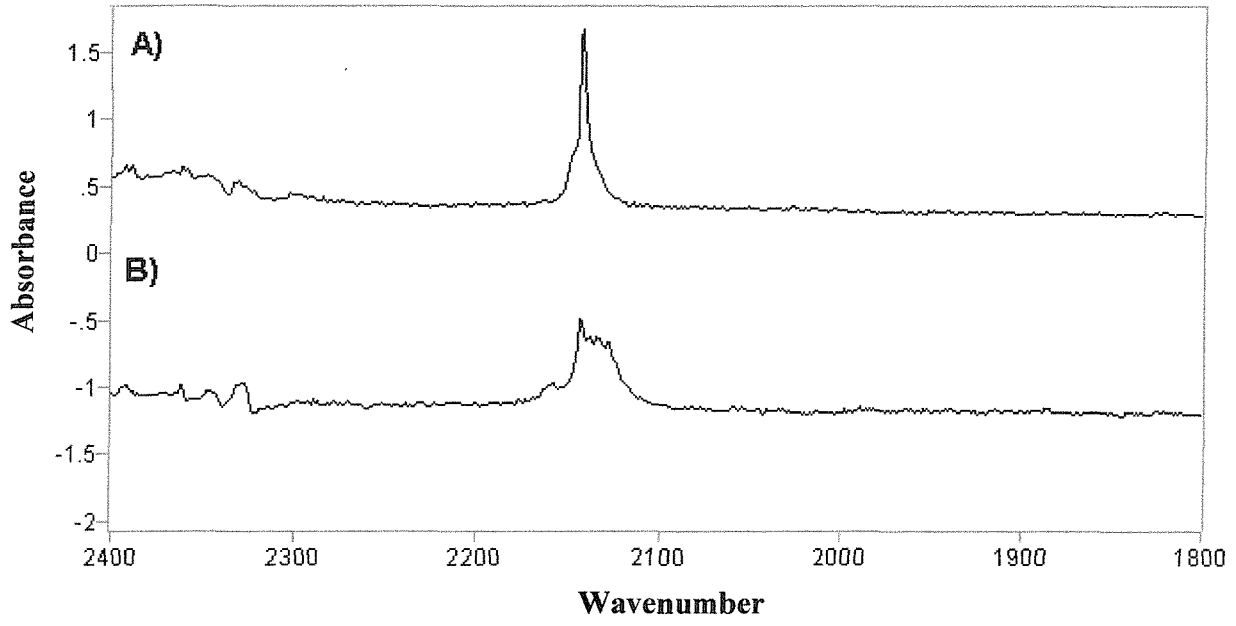

After pyrolysis, the Si-H band looked broader and it became difficult to determine the number of bands present. Therefore it was decided that a subtraction needed to be carried out of the two spectra both before and after diffusion. The result is shown below.

Figure 27. A spectrum of 1,1,3,3-tetramethyldisiloxane / N_2 – 2250-2000 cm^{-1}

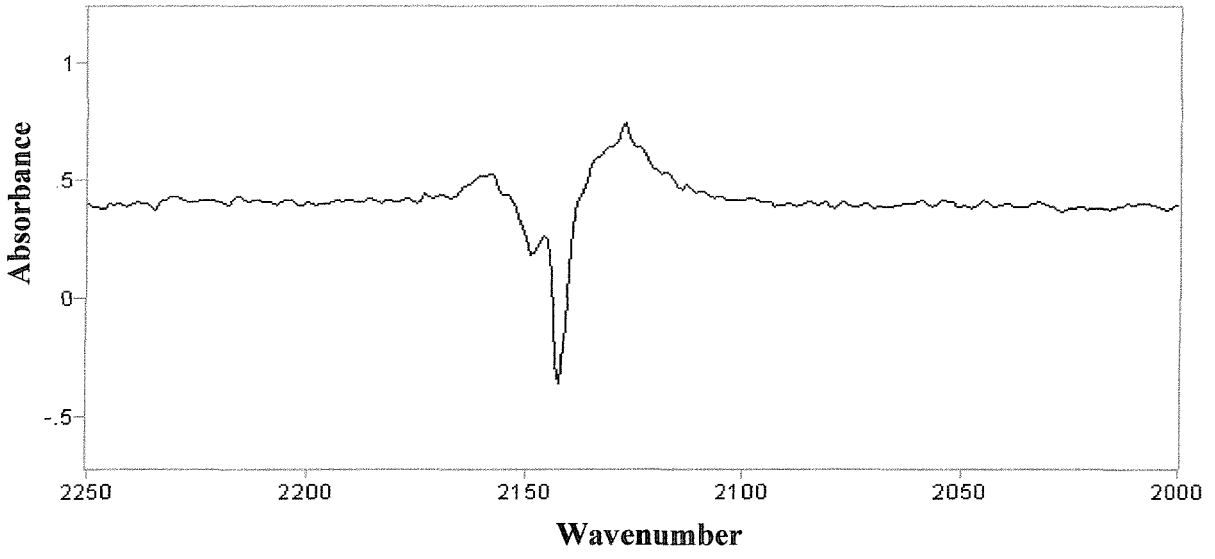

From the above spectrum, it is now clear that the original parent compound before pyrolysis, shown by the peaks in the negative absorbance, had two Si-H bonds. The spectrum also shows a peak in the positive absorbance, representing the main species formed after pyrolysis. From this spectrum, the pyrolysis product clearly has only one Si-H bond.

This therefore further supports the theory for the formation of product **I** as a result of the elimination of a methyl group and a hydrogen atom.

9.2. 1,1,3,3,5,5-Hexamethyltrisiloxane

As a result of both the energy and frequency calculations that were carried out, the favourable possible products are thought to be products **VII** and **IX**. The spectra obtained of L2 were studied closely of both before and after pyrolysis in an attempt to identify which of these two products are formed.

Figure 28. Spectra of 1,1,3,3,5,5-hexamethyltrisiloxane / N_2 – 4000-400 cm^{-1}

A). L2 before pyrolysis
B). L2 after pyrolysis

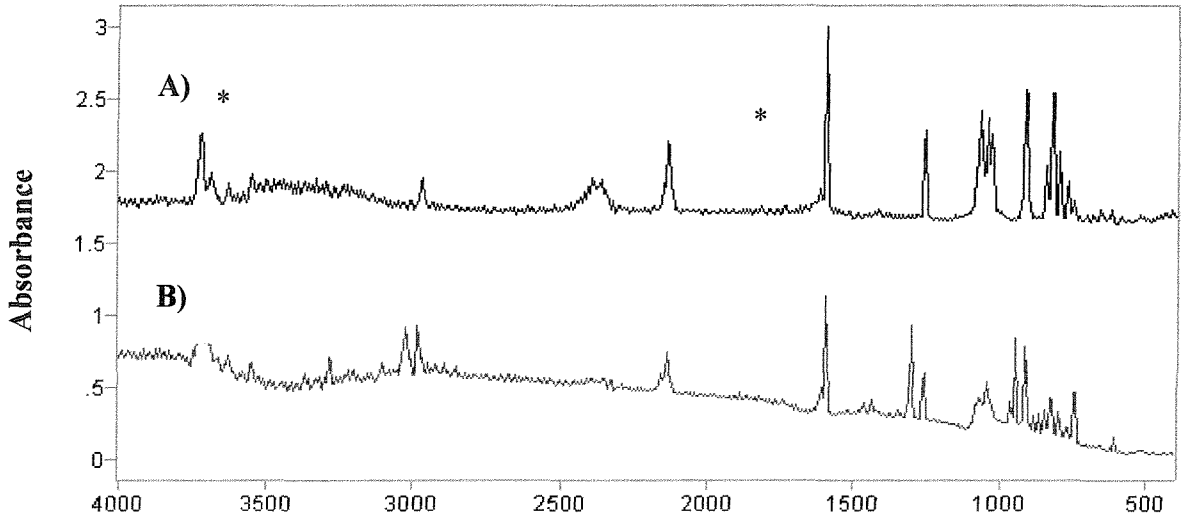

It again appears that there is only one band representing the Si-H bond before pyrolysis and one band after pyrolysis. However, this does not fit the theory that the Gaussian program correctly predicts the number of Si-H bonds in a particular species, since the starting material contains two Si-H bonds. An expansion of the region of the spectrum containing the Si-H bonds was then required.

Figure 29. Spectra of 1,1,3,3,5,5-hexamethyltrisiloxane / N_2 – 2400-1800 cm^{-1}

A). L2 before pyrolysis
B). L2 after pyrolysis

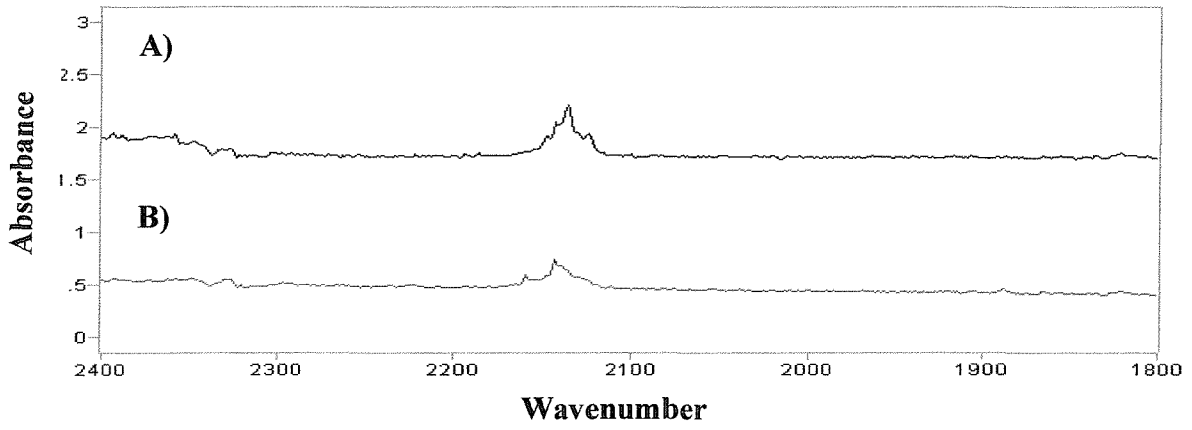

Much ambiguity still remains after expanding the spectra above. However, it does seem less likely that only one band due to the Si-H bond is present, since the band is seen to have a shoulder attached. The two spectra were subtracted from each other in order to reveal more information about the band.

Figure 30. A spectrum of 1,1,3,3,5,5-hexamethyltrisiloxane / N_2 – 2350-1950 cm^{-1}

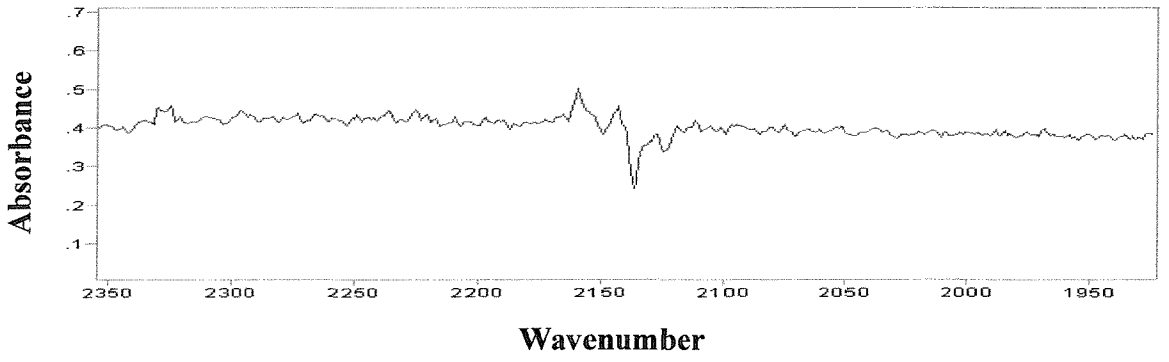

Two positive bands are shown in the above spectrum, representing the bands in the pyrolysis product, and the negative bands represents the number of the bands in the original parent compound. Since there is only one negative band, this suggests that there is only one Si-H band in the resultant main pyrolysis product. This would agree with the energy calculations and the frequency calculations, which claim that product **VII** is the most likely product to be formed, with the elimination of a methyl group and a hydrogen atom.

10. Conclusion

An investigation was conducted to establish whether the same hydrocarbon pyrolysis products produced upon pyrolysing the cyclic siloxanes are also produced for the linear siloxanes. It can be concluded that CH_3, CH_4, C_2H_2 and C_2H_6 were all produced upon the pyrolysis of the linear siloxanes as with the pyrolysis of the cyclic siloxanes.

After assigning a number of the new bands to small hydrocarbon species, an attempt was then made to identify the silicon containing species produced. Due to the size of L3, it was only possible to carry out energy and frequency calculations for L1 and L2 in the given time period. The following reactions are calculated as being the most favourable and therefore the most likely to occur:

Figure 31.

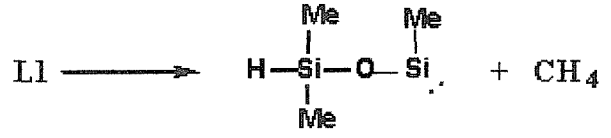

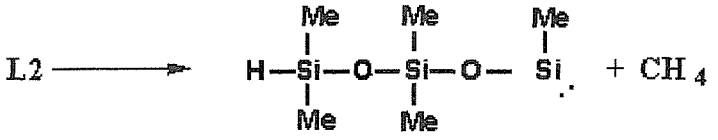

Intense methane bands in spectra of both L1 and L2 supports these findings. The results of the frequency calculations also favour this result. However, it was discovered that although the frequency calculations are generally in agreement with experimental results, they couldn't be relied upon for calculating the frequency of the Si-H bond. The calculated value for the latter was found to be about 300 cm^{-1} below that of the experimentally determined value.

11. Future Work

As a result of the work carried out here, a number of possible products have been suggested for the pyrolysis of both the cyclic and the linear siloxanes. However, this work is in no way conclusive. In order to confirm the formation of the silicon-containing compounds reported here, some additional supporting experiments may be carried out in future work.

Molecular beam mass spectrometry could be used to identify the silicon–containing fragments of the siloxane compounds. The species elucidated from the *m/z* ratio of the fragments produced in the mass spectrometer can be compared to the suggested pyrolysis products and used to confirm their presence.

Molecular modelling calculations were carried out in conjunction with the matrix isolation infrared spectroscopy experiments. However, the choice of method and basis set used was determined by the limited time period allocated to carrying out these calculations. Given more time, more accurate methods and basis sets would increase the efficiency of the calculations. It was also discovered here that there is a fault in the Gaussian program when calculating Si-H infrared frequencies.

12. References

1). D. H. Williams and I. Fleming, Spectroscopic methods in Organic Chemistry, Fifth edition, **(1997)**, The McGraw-Hill Companies

2). V. N. Khabashesku, Z. A. Kerzina, A. K. Maltsev and O. M. Nefedov, J. Organomet. Chem., 364, **(1989)**, 301-312

3). L. Andrews and G. C. Pimentel, J. Chem. Phys., 47, **(1967)**, 3637-3644

4). D. E. Milligan and M. E. Jacox, J. Chem. Phys., 47, **(1967)**, 5146-5156

5). J. B. Foresman and A. Frisch, Exploring Chemistry with Electronic Structure Methods, Second edition, **(1996)**, Gaussian, Inc. Pittsburgh, PA

6). D. E. Milligan and M. E. Jacox, J. Am Chem. Soc., 85, **(1963)**, 278-282